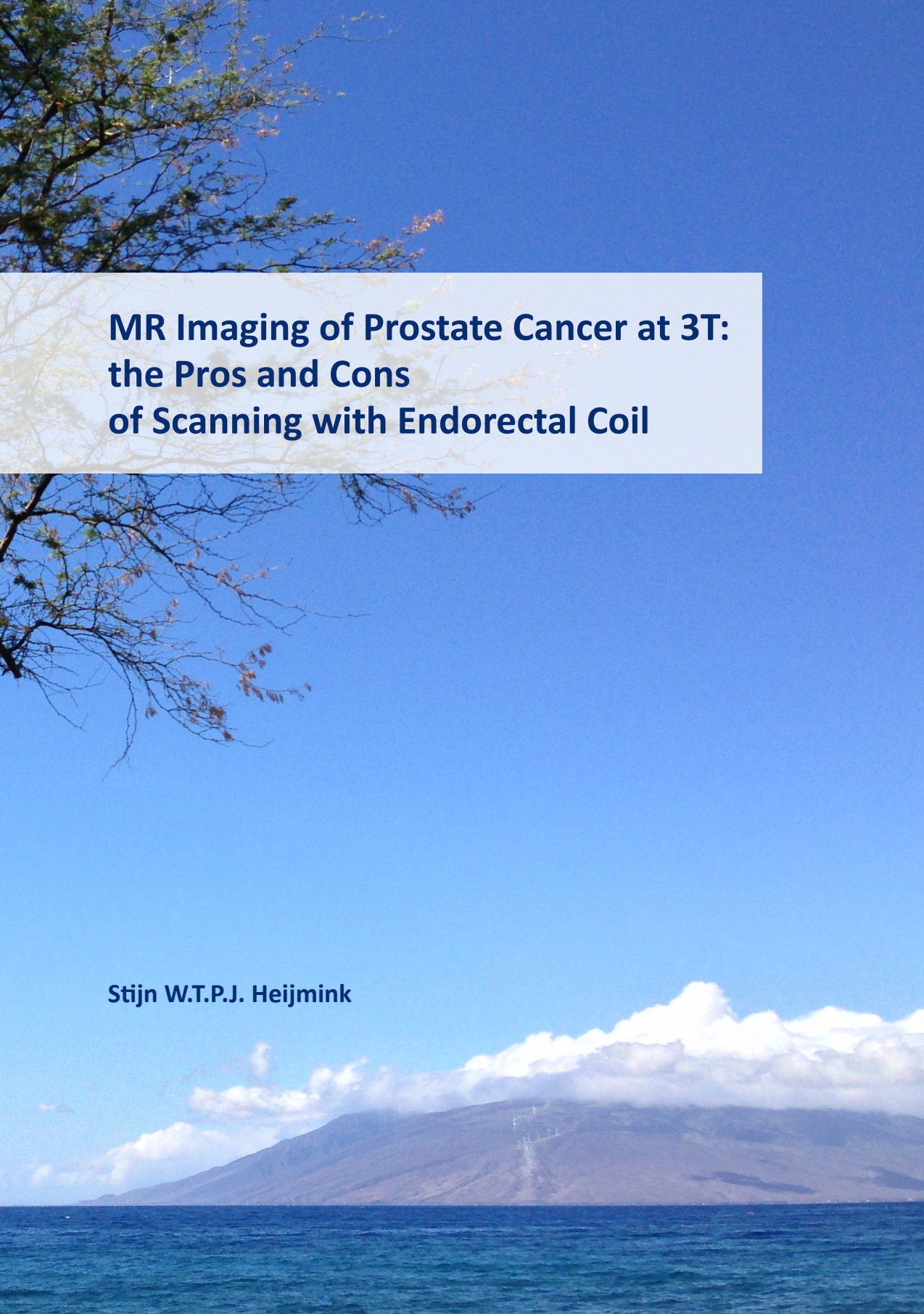

MR Imaging of Prostate Cancer at 3T: the Pros and Cons of Scanning with Endorectal Coil

Stijn W.T.P.J. Heijmink

MR Imaging of Prostate Cancer at 3T: the Pros and Cons of Scanning with Endorectal Coil

Stijn W.T.P.J. Heijmink

MR Imaging of Prostate Cancer at 3T: the Pros and Cons of Scanning with Endorectal Coil

Proefschrift

ter verkrijging van de graad van doctor
aan de Radboud Universiteit Nijmegen
op gezag van de rector magnificus prof. dr. Th.L.M. Engelen,
volgens besluit van het college van decanen
in the openbaar te verdedigen op woensdag 24 juni 2015
om 10.30 uur precies

door

Stijn Wilhelmus Theodorus Petrus Johannes Heijmink
geboren op 15 april 1978
te Nijmegen

Promotores:
Prof. dr. J.O. Barentsz
Prof. dr. J.A. Witjes

Copromotores:
Dr. J.J. Fütterer
Dr. T.W.J. Scheenen

Manuscriptcommissie:
Prof. dr. P.F.A. Mulders (voorzitter)
Prof. dr. J.H.J.M. van Krieken
Dr. J. Veltman (Ziekenhuisgroep Twente)

ISBN/EAN: 978-90-9029032-4

Cover design: Proefschriftmaken.nl || Uitgeverij BOXPress
Printed & Lay Out by: Proefschriftmaken.nl || Uitgeverij BOXPress
Published by: Uitgeverij BOXPress, 's -Hertogenbosch

The research presented in this thesis was supported financially by Grant KUN 2003-2925 from the Dutch Cancer Society (KWF).

CONTENTS

CHAPTER 1

Introduction – Thesis outline

This thesis encompasses an exploration of the state-of-the-art imaging techniques magnetic resonance (MR) imaging and MR spectroscopic imaging in the diagnostic process of men with prostate cancer.

Chapter 2 provides a review of the imaging modalities available for detecting and localizing prostate cancer and determines their comparative strengths and weaknesses. From these, a potential scheme is proposed for prostate cancer detection and localization.

In **Chapter 3**, the imaging modalities for staging prostate cancer are reviewed and a scheme is proposed for their use in patient management.

In **Chapter 4**, the first published prostate cancer patient cohort to undergo MR imaging with an endorectal coil at 3 tesla is presented, using prostatectomy as standard of reference in order to establish the feasibility of accurately staging prostate cancer with this technique.

In **Chapter 5** a prospective study of a patient cohort that underwent both body-array coil and endorectal coil MR imaging at 3 tesla for the purpose of prostate cancer localization and local staging is presented.

Chapter 6 encompasses a study of the changes in prostate diameters and volumes after the introduction of an endorectal coil using MR imaging at 3 tesla in a patient cohort.

In **Chapter 7**, the MR spectroscopic imaging technique using only a body-array coil at 3 tesla to detect recurrent disease within the prostate gland as well as metastatic disease in a lymph node in a patient is outlined.

Chapter 8 presents the feasibility of performing MR spectroscopic imaging at 3 tesla using only a body-array coil in localizing prostate cancer in a patient cohort that underwent radical prostatectomy.

In **Chapter 9**, a direct comparison of the prostate cancer localization performance between body-array and endorectal coil MR spectroscopic imaging at 3 tesla is performed in a patient cohort that subsequently underwent radical prostatectomy.

Chapter 10 reflects a selection from the imaging chapter of the 2007 Dutch comprehensive cancer centres (CBO) guideline regarding the use of imaging in prostate cancer diagnosis.

CHAPTER 2

State-of-the-art uroradiologic imaging in the diagnosis of prostate cancer

Stijn W.T.P.J. Heijmink
Jurgen J. Fütterer
Stephen S. Strum
Wim J.G. Oyen
Ferdinand Frauscher
J. Alfred Witjes
Jelle O. Barentsz

Acta Oncologica 2011; 50(S1):25-38.

In the diagnostic process of prostate cancer, several radiologic imaging modalities significantly contribute to the detection and localization of the disease. These range from transrectal ultrasound (TRUS) and magnetic resonance imaging (MRI) to positron emission tomography (PET). Within this review, after evaluation of the literature, we will discuss the advantages and disadvantages of these imaging modalities in clarifying the patient's clinical status as to whether he has prostate cancer or not and if so, where it is located, so that therapy appropriate to the patient's disease may be administered. TRUS, specifically with the usage of intravenous contrast agents, provides an excellent way of directing biopsy towards suspicious areas within the prostate in the general (screening) population. MRI using functional imaging techniques allows for highly accurate detection and localization, particularly in patients with prior negative ultrasound guided biopsies. A promising new development is the performance of biopsy within the magnetic resonance scanner. Subsequently, a proposal for optimal use of radiologic imaging is presented and compared with the European and American urological guidelines on prostate cancer.

With a total of 217 730 new cases estimated for 2010, prostate cancer (PC) now accounts for 28% of all new male cancers diagnosed in the USA [1]. In their lifetime, one in six men will be clinically diagnosed with having PC, although many more men are found to have histological evidence of PC at autopsy [2–4]. Presently, approximately 1 in 10 men will die of PC [5,6]. The everaging population and wider spread use of the prostate-specific antigen (PSA) test [7,8], as well as the tendency to apply lower cut-off levels for this test [9], will further increase the diagnosis of this disease [10].

An elevated PSA level, abnormal changes in PSA level (i.e. PSA dynamics) such as PSA velocity or doubling time, or an abnormal digital rectal examination are biologic indicators signaling an increased risk of PC. With the improvement and wider range of curative therapies, detection and subsequent exact localization of PC have become increasingly important because of their influence on treatment strategy [11,12]. Two such affected treatments are laparoscopic (robotic) radical prostatectomy and intensity-modulated radiation therapy (IMRT [13]). The urologist's inability to palpate the operating field during laparoscopic surgery makes it even more crucial to know where the cancer is located. Similarly, the urologist must know whether the cancer is near a neurovascular bundle since this affects the decision of whether or not to perform nerve-sparing prostatectomy [14]. IMRT also necessitates accurate PC localization. While giving a standard dose to the prostate, a higher (i.e. boost) dose can be given to any dominant intraprostatic lesion(s) as these lesions regularly appear to be the sites of recurrent disease [15]. Furthermore, precision radiation dosimetry will decrease radiation complications, particularly rectal wall toxicity [16], thereby likely diminishing the development of post-radiation rectal cancer [17].

In order to determine the optimal treatment for the individual patient, it is necessary to evaluate all patient and cancer characteristics. Most often used for this purpose are laboratory values (PSA level and dynamics), the results of digital rectal examination (clinical staging), and histopathological prostatic biopsy findings (Gleason score). However, imaging may play an important role in detecting and localizing areas most reflective of the actual aggressiveness of the cancer. This directly influences the assessment of the patient and may lead to important changes in treatment strategy which can mean the difference between treatment success and failure.

Currently, a spectrum of imaging modalities is available to clinicians for tackling detection- and localization-related problems. To provide optimal and cost efficient patient care, these techniques should be used in the appropriate clinical context to aid clinicians in detecting and localizing PC.

This review 1) presents an overview of the currently available imaging methods to aid in PC detection and localization. 2) Additionally, a scheme is proposed for optimal evidence-

based use of imaging in detecting and localizing prostate cancer and a critical comparison is made between this scheme and the most recent guidelines as put forward by the American Urological Association (AUA) and European Association of Urology (EAU).

LITERATURE SEARCH

Relevant articles were retrieved using combinations of both Medical Subject Headings (MeSH) and free search terms in the MedLine® (WebSPIRS Version 5.12, Build 20060224, Ovid Technologies) and Pubmed (U.S. National Library of Medicine) online search engines. MeSH terms included: "Prostate", "Anatomy", "Prostatic Neoplasms", "Neoplasm Staging", "Ultrasonography", "Tomography, X-Ray Computed", "Magnetic Resonance Imaging", "Magnetic Resonance Spectroscopy", "Diffusion Magnetic Resonance Imaging", "Radionuclide Imaging", and "Positron- Emission Tomography".

Free search terms included: "prost*", "cancer", "detect*", "localization", "localisation", "biops*", "stag*", "capsul*", "extracapsular penetration", "extracapsular extension", "seminal vesicle invasion", "transrectal ultraso*", "TRUS", "computed tomography", "CT", "magnetic resonance imaging", "MRI", "ferumoxtran-10","magnetic resonance spectroscopy", "spectroscopy", "MRS", "bone scan*", "bone scintigraphy", "positron-emission tomography", "PET", and "ProstaScint".

Reference lists of selected articles were further analyzed for relevant articles.

PROSTATE CANCER DETECTION AND LOCALIZATION IN REFERENCE TO PROSTATE ANATOMY AND ESSENTIAL PROSTATE CANCER CHARACTERISTICS

In order to effectively apply the various imaging modalities, it is important to first understand both the normal prostate anatomy and the distribution and intrinsic characteristics of PC.

Normal anatomy as related to PC localization

On the basis of its embryological origins, the prostate is anatomically divided into three zones that are eccentrically located around the urethra: the innermost transition zone (TZ), the central zone, and the outermost peripheral zone (PZ) [18,19]. In older patients, the former two cannot be distinguished radiologically due to compression of the central zone by benign prostatic hyperplasia (BPH) in the TZ and together they are referred to as the central gland; this as opposed to the outer gland, which comprises the PZ. Furthermore, the prostate is craniocaudally divided into apex (the caudal one-third), mid-gland, and base (the cranial one-third).

Anatomical distribution of PC

Up to 70–80% of PC is located in the PZ [20] and overall analysis of these cancers has shown homogeneous distribution across the entire PZ [21], with over half of the prostates

containing two or more distinct cancer foci [22]. Nevertheless, while up to 20–52% of all PC originate in the TZ, only a small (3.6–25%) percentage of these cancers [21,23] occur solely in the TZ as many will have concurrent PZ cancer foci [20,24,25].

Pathological grading of PC aggressiveness

Presently, the most widely used histological scaling system for PC aggressiveness is the Gleason score [26,27], which consists of two numbers: a primary and secondary Gleason grade reflecting the two grades most frequent in the specimen. Each Gleason grade is assigned a value between 1 and 5, the higher numbers indicating a more aggressive cancer. The prognostic value of the Gleason grading system is well-documented [28,29].

PATIENTS CLINICALLY AT RISK FOR PROSTATE CANCER: RADIOLOGICAL IMAGING TO DETECT AND LOCALIZE PRIMARY PC

Transrectal ultrasound (TRUS): Reliable, although not perfect, daily-use modality

Grayscale TRUS. Today, in regular clinical practice, prostate biopsies are performed under TRUS guidance. Even though the traditional ultrasound appearance of PC is a PZ hypoechoic lesion (Figure 1A, B), other conditions such as prostatitis and prostatic intraepithelial neoplasia may also present as hypoechoic lesions [30,31]. It is important to note that over 40% of PC lesions are isoechoic (Figure 1C, D) while only 5% are hyperechoic [32]. Therefore, targeting only hypoechoic areas is not an optimal approach for successful PC detection [33] and various biopsy protocols that sample tissue at standard locations (i.e. systematic biopsy) within the prostate have become the most common biopsy technique [34]. The number of cores taken per session varies across institutions. Recently, however, emphasis has been put on adequate tissue sampling from more laterally located PZ regions [35,36] and on the relative unimportance of biopsying the central gland [37]. Despite the use of extended systematic biopsy protocols, there is still an approximately 20% chance that the Gleason score at prostatectomy will differ from that at biopsy to a clinically relevant degree [38]. Recently, it was observed that biopsies performed with an endfire probe obtained a significantly higher biopsy rate compared with side-fire probes [39]. PC detection rates have varied from 19–40% [40,41] and repeat biopsy sessions are often necessary [42]. Localization sensitivity varied widely between 39–75% (Table).

Doppler TRUS. Because increased blood flow due to neovascularity is one of the characteristics of PC, this is a means of targeting lesions. In a study of 96 patients with lower urinary tract symptoms and PSA levels over 4 ng/ml [43], the degree of Doppler signal correlated with the microvessel density and Gleason score of a lesion. One study achieved Doppler imaging-based detection rates of 40% [44]. Power Doppler TRUS could improve the localization specificity [45]. However, a drawback of Doppler imaging is the high inter-observer variability [46,47], reflected in the widely spread sensitivity and specificity figures in the literature (27–98% and 46–84%, respectively) (Table).

Table: Overview of Studies that Examined the Diagnostic Performance of Localizing Prostate Cancer by Imaging Modality.

Imaging modality	References	Periods of publication, range	Number of patients, range	Accuracy (%)	Sensitivity (%)	Specificity (%)	PPV (%)	NPV (%)
Transrectal ultrasound								
Gray-scale	[47,75,131]	1998-2000	47-265	52-62	39-75	40-82	45-84	36-72
Doppler	[44,132–136]	1997-2004	136-591	54-83	27-98	46-84	16-84	69-99
Contrast-enhanced	[33,49,50,137,138]	2000-2005	59-380	58-91	48-94	46-88	33-88	55-93
Endorectal MR imaging at 1.5 tesla								
T2-weighted MR imaging	[68,74–76,139,140]	1999-2007	24-53	69-82	52-83	46-88	38-80	54-89
Diffusion-weighted imaging	[88]	2010	48	86-89	71-88			
Proton MRSI	[74–76,139,141,142]	1999-2007	24-94	67-87	57-92	57-88	48-83	51-99
Endorectal MR imaging at 3 tesla								
T2-weighted MR imaging	[103]	2007	46	76-80	53-58	83-86	48-56	85-87
PET scanning								
FDG	[108,111]	1999-2001	24-44	N/A	4-64	100	100	25
^{11}C-choline	[116,117]	2005-2006	41-43	71-72	66	81-84	87-88	55-59

Abbreviations: PPV: positive predictive value; NPV: negative predictive value; MRSI: magnetic resonance spectroscopic imaging; PET: positron emission tomography, FDG: 18-fluorine-labelled fluorodeoxyglucose, ^{11}C-choline: carbon-11 labeled choline

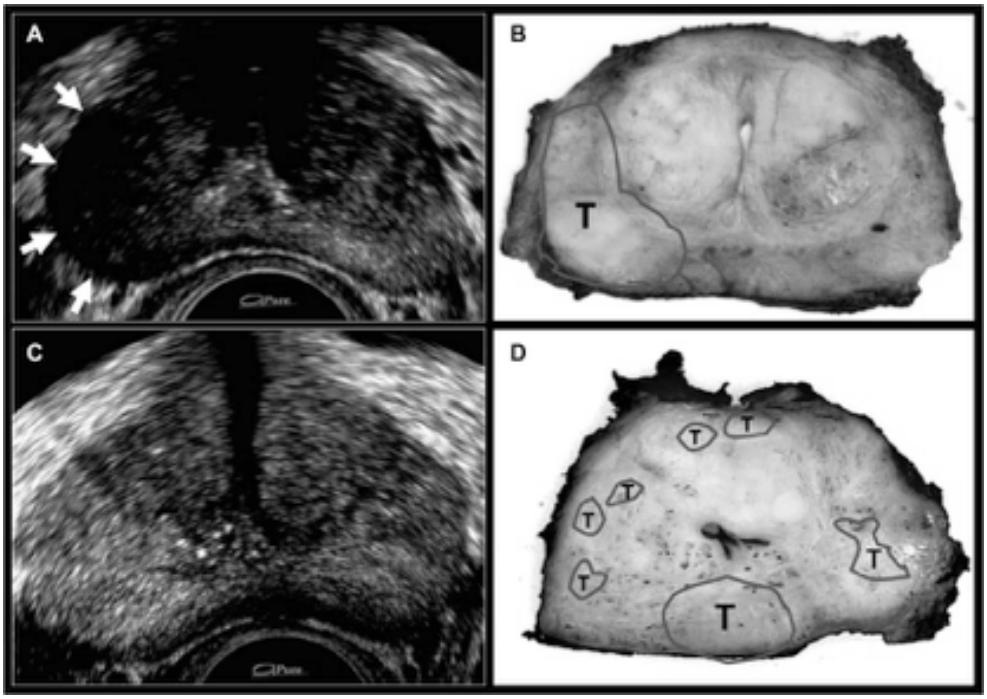

Figure 1. (A) Axial gray-scale transrectal ultrasound image (AplioTM, Toshiba) of the prostate of a 65-year-old man (PSA level 19.02 ng/ml, biopsy Gleason score 6, normal digital rectal examination). A hypoechoic lesion was observed in the right peripheral zone (arrows). (B) Histopathology of the prostatectomy specimen confirmed the presence of a Gleason 3 + 4 adenocarcinoma (T). (C) In another patient (69 years, PSA level 3.59 ng/ml, biopsy Gleason score 7, normal digital rectal examination), the axial gray-scale image did no show any echogenic abnormality while at histopathology (D) a number of cancer foci (T) were reported.

Contrast-enhanced TRUS. An innovation is the application of gas-filled microbubble contrast agents, such as Levovist® (Schering, Berlin, Germany) and SonoVue® (Bracco, Milan, Italy) [48]. These microbubbles remain intravascular, thereby enhancing the visibility of the vascular tree in and around the prostate. This improves the ability to detect PC and to thus target areas more representative of the aggressiveness of PC. In experienced hands, it is reported that compared with systematic biopsy, targeting only lesions with pathological enhancement after contrast administration requires less than half the number of biopsy cores to obtain the same diagnostic yield [49–51]. A recent randomized clinical trial comparing systematic biopsy and contrast-enhancement targeted biopsy confirmed these findings [52]. In addition, contrast-enhanced TRUS biopsies on average detected significantly more aggressive cancers compared with systematic biopsy. Therefore, we can speculate that by using this technique the difference in Gleason score between biopsy and prostatectomy specimens would most likely diminish. If the latter is confirmed by future studies, pre-

therapeutic risk assessment of patients will increase in accuracy. Disadvantages of using contrast agents are the longer duration and higher degree of invasiveness of the examination; however, the risk of hypersensitivity to the substance is rare and most adverse events are minor and self-resolving [53]. Sensitivities and specificities of PC detection using contrast-enhanced TRUS varied between 48–94% and 46–88%, respectively (Table I). A preliminary study suggests that a 14-day prebiopsy course of dutasteride, a dual 5α-reductase inhibitor, causes a relative high reduction in blood flow in healthy prostate tissue compared with cancer tissue and could increase the diagnostic yield of contrast-enhanced TRUS targeted biopsy [54].

Sonoelastography. Transrectal sonoelastography is a new non-invasive technique that analyzes the compression characteristics of prostate tissue. A study by König et al. of 404 men undergoing biopsies based on real-time sonoelastography revealed a detection rate of 37.4% [55]. In a comparative study, Pallwein et al. found a significantly higher per core detection rate for sonoelastography-targeted biopsy compared with systematic biopsy. Sonoelastography-targeted biopsy was 2.9 times more likely to detect cancer [56]. A drawback of the latter study was the heterogeneity of the population since more than half of the patients had already undergone one or more negative biopsy sessions. A study comparing real-time sonoelastography with radical prostatectomy reported a localization sensitivity of 88% [57]. While sonoelastography-based targeted biopsy improves the diagnostic yield it is not yet clear whether it can replace systematic biopsy [58]. Future randomized studies are required to determine the true value of sonoelastography in prostate cancer detection and localization.

Computed Tomography (CT) scanning: Inadequate soft tissue contrast and radiation burden

The literature search resulted in identifying only one recent study on the ability of CT scanning to document histologic PC sites within the prostate gland. This study revealed that contrast-enhanced helical CT scanning was able to detect only 58% of the 102 histologic PC sites documented by TRUS-guided biopsies in 25 patients [59]. In general, CT scanning has inadequate soft tissue contrast resolution to discern the subtle tissue changes due to PC (Figure 2A) and, therefore, should not be used for PC detection and localization. An additional disadvantage of CT is that it involves ionizing radiation.

Endorectal Magnetic Resonance Imaging (MRI) and Magnetic Resonance Spectroscopic Imaging (MRSI): High soft-tissue resolution, radiation-free, but costly and time consuming

T2-weighted imaging. Contrary to CT scanning, MRI has a high soft-tissue contrast resolution. The use of an endorectal coil (ERC) combined with other external coils at 1.5 tesla (T) increases soft-tissue contrast significantly and is now the accepted standard for MRI of the prostate [60]. A drawback is the extra time required for insertion and checking of the position of the disposable ERC, as well as substantial expense.

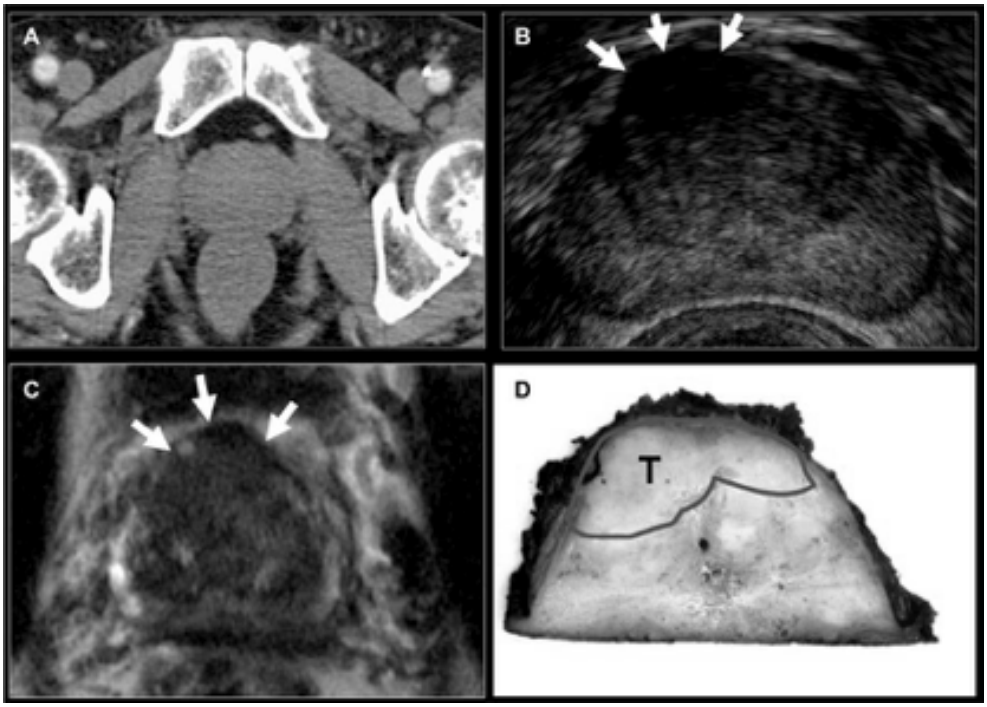

Figure 2. A comparison of the soft-tissue resolution between CT scanning, transrectal ultrasound, and MRI in a 67-year-old man with a PSA level of 38.72 ng/ml, a biopsy Gleason score of 6, and normal digital rectal examination. (A) On the axial CT-scan image the prostate (P) could be discerned. After contrast administration (arrow) no clear enhancement within the prostate was seen. (B) On gray-scale transrectal ultrasound imaging (Viking®, BK Medical) an area of hypoechogenicity (arrows) was visible ventrally. (C) The ventral cancer focus (arrows) was also visible on axial MRI at 3 T with external surface coils. (D) Histopathology confirmed the presence of a ventral cancer focus (Gleason score 7) corresponding to the area of echogenicity on transrectal ultrasound and low signal intensity on MRI.

On MRI, PC typically appears as an area of low signal intensity within the brighter, healthy PZ using a T2-dominated sequence [61–63] (Figure 3A–E). In the central gland, PC is not as clearly discernable because the central gland generally has lower signal intensity than the PZ and is more inhomogeneous due to BPH-induced architectural changes that may mimic PC. A recent study showed that a homogeneous low T2 signal intensity and lenticular shape were significantly associated with presence of central gland PC [64]. It was reported that higher Gleason score cancers had lower signal intensities (relative to muscle) compared with low Gleason score cancers [63]. T2-weighted imaging can be performed in multiple planes or as a three dimension (3D) volume acquisition [65]. Comparing T2-weighted MRI with prostatectomy specimens, MR attained high (52– 83%) sensitivities in PC localization, while specificities were somewhat lower (46–88%) (Table I).

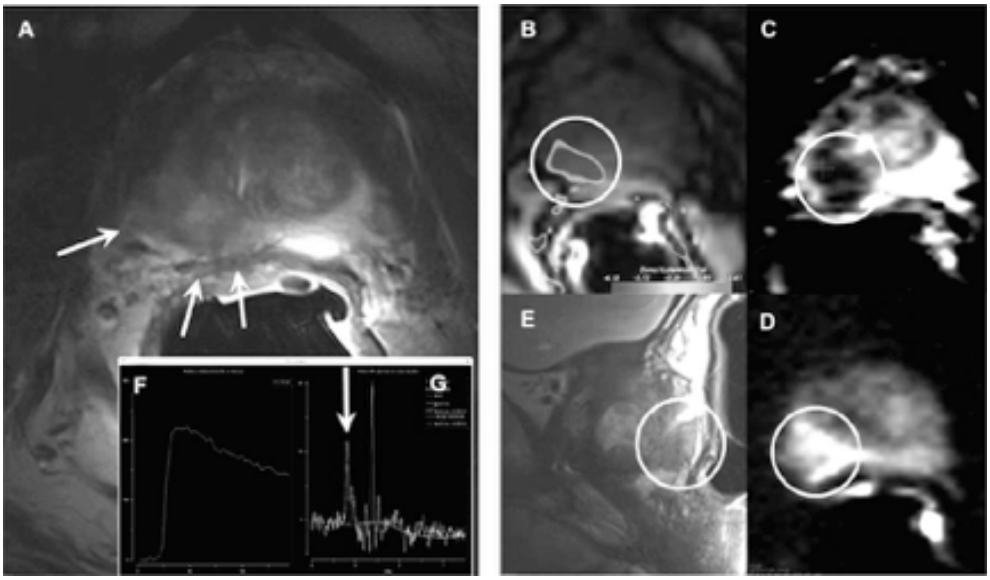

Figure 3. 59-year-old patient with PSA 12, Gleason 8 tumor (circle) right PZ, stage T3a (arrows) at prostatectomy. (A) T2-w axial image, (B) DCE image showing wash-out at the tumor site, (C) ADC-map tumor shows marked restriction, which argues for high Gleason grade, (D) DWI image (b 800) tumor has high signal, (E) sagital T2-weighted image, (F) concentration time curve shows fast wash-in and fast wash-out. G. MR spectrum shows high choline (arrow). This patient scores for all modalities five points (20/20). Scale: 1 no tumor, 5 definitely tumor.

A study that directly compared endorectal MRI with digital rectal and TRUS-guided biopsy localization revealed significant incremental value from MRI [66]. In patients subjected to multiple prior negative TRUS-guided biopsies, anatomical MRI by means of T2-dominated acquisition plays an important role. In this patient population, an 83% sensitivity and 50% positive predictive value for MRI have been established [67].

Postbiopsy hemorrhage causes areas of low signal intensity on T2-weighted imaging, thereby making prostate cancer detection more difficult. However, it was shown recently that the amount of hemorrhage was significantly lower in areas of cancer compared with healthy tissue [68].

MRSI. Additionally, MRSI (Figure 3G) can be added to the protocol to provide metabolic information based on the citrate, choline, and creatine levels, and their ratios within the prostate. This is highly informative since the ratio between choline and citrate alters during the transformation from healthy to malignant prostatic cells [69,70] and an increasing choline + creatine/citrate ratio was correlated with higher Gleason scores [71]. Presently, 3D MRSI of the entire prostate can be performed [72], thereby aiding in the diagnosis of central

gland PC. The addition of 3D MRSI to MRI has increased localization accuracy, particularly by raising specificity up to 91% [73]. However, a limitation of MRSI is its low spatial resolution. Compared to systematic biopsy, PC localization by means of MRI and MRSI was found to be more sensitive (67% and 76% versus 50%) but less specific (69% and 57% versus 82%) than systematic biopsy [74]. With whole-mount section histopathology as standard of reference, 3D MRSI had a significantly larger area under the receiver-operating curve (AUC) of 0.80 in localizing cancer, compared with 0.68 with T2-weighted MRI [75]. Adding the combination of T2-weighted imaging and MRSI to clinical data was shown to have the highest accuracy (AUC 0.85) in predicting the probability of a patient having insignificant prostate cancer [76], significantly higher than that of clinical nomograms. A recent multi-institutional American College of Radiology Imaging Network study raised doubts on the additive value of MRSI over T2-weighted imaging alone [77]. However, potential factors for this result were the selected prostatectomy population, the small average cancer focus size, and the inclusion of centers without any previous MRSI experience.

Diffusion weighted imaging (DWI). DWI is a novel non-invasive technique that measures the fractional anisotropy of water molecules within the prostate which is expressed in apparent diffusion coefficient (ADC) mapping. Thereby, cancer tissue is deemed to result in a more restricted movement of water molecules and thus producing lower ADC values (Figure 3C, D) [78,79]. A recent study in 38 patients, performed at 1.5T with an ERC observed that the mean ADC values of regions of interest placed within prostate cancer tissue was significantly lower than those placed within healthy prostate tissue [80]. In preliminary studies, combining this technique with MRSI [80] or T2-weighted imaging [81] significantly improved the localization accuracy. A recent study in 37 patients revealed a significant increase in sensitivity from 51% for T2-weighted imaging to 71% for combined T2-weighted and DWI reading [82]. In a recent multiparametric analysis, DWI was the best-performing parameter [83]. Preliminary studies at 3T show promising results [84–86]. The b value used appears to affect the PC localization accuracy, as in a preliminary study imaging with a b value of 2000 s/mm^2 was shown to have a significantly higher accuracy compared with 1000 s/mm^2 [87], possibly due to a fall in the signal-to-noise ratio. At biopsy, DWI may aid in differentiating between low-risk and high-risk patients [88].

Dynamic contrast-enhanced MRI [83,89]. To further enhance localization accuracy of MRI, one may use contrast agents. Dynamic contrast-enhanced endorectal MRI, in which the contrast agent concentration is followed in time [90], is able to discriminate between healthy prostatic tissue and PC [91]. Early contrast enhancement and high (relative) peak enhancement are the most accurate predictors of PC of the PZ, while fast washout of contrast agent and high permeability of the blood vessels (Figure 3B, F) are most sensitive for central gland PC [92,93]. A recent study showed that the AUC for localizing PC increased significantly from 0.68 with regular anatomical MRI to 0.91 by applying contrast agent [75].

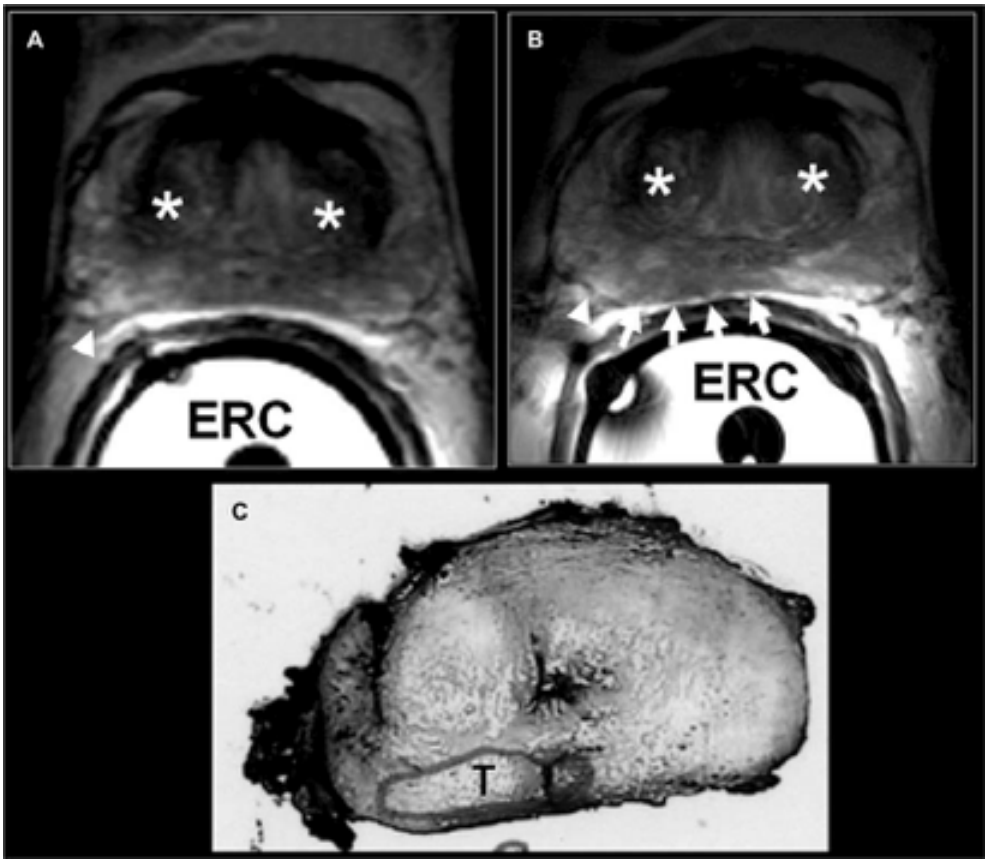

Figure 4. A comparison of the image quality between axial endorectal coil (ERC) MRI at 1.5 T (A) and 3 T (B) in the same patient (age: 58 years, PSA level: 2.7 ng/ml, Gleason biopsy score: 6, normal digital rectal examination). The visibility of the internal architecture of the central gland (*) increased and the capsule (arrowheads) is better delineated at a field strength of 3 T and the tumor (T) as outlined by the histopathology (C) is also better appreciated (arrows).

However, limitations of using contrast agents are the higher costs and possible adverse reactions, of which the most serious, anaphylaxis, is rare [94,95].

Multiparametric imaging. Combining any number of these techniques ('multiparametric imaging') has shown to increase the ability of MRI to detect and localize prostate cancer (Figure 3A–G) [96–98].

High-field imaging. An important future direction is the use of higher magnetic field strengths (e.g. 3T) [99–101] (Figure 4). Compared with body array coil MRI, the higher resolution obtained with ERC MRI at 3T significantly improved PC localization accuracy [102].

Biopsy. Another development is to directly biopsy the prostate by means of MRI [103]. Preliminary results of direct MR-guided transrectal biopsy of suspicious lesions on pre-biopsy MRI in patients with prior negative or inconclusive TRUS-guided biopsy results demonstrated the feasibility of MR prostate biopsy without complications. Nevertheless, disadvantages of the biopsy device are its limited reach, particularly towards the base of the prostate, and procedure duration [104]. In a study of 68 patients with at least two prior negative TRUS biopsy sessions, MR guided biopsy established cancer in 59% [105].

Positron Emission Tomography (PET) Scanning: Metabolic information yet not sufficiently discriminatory from benign disease

FDG. The utility of PET scanning with fluorine-18-labelled deoxyglucose (FDG) in detecting PC is compromised by the relatively low uptake of FDG by prostate cancer cells [106] and significant overlap with marker uptake by BPH. Moreover, reports of FDG uptake correlating with PC aggressiveness have been conflicting, although FDG uptake was substantially higher in metastasized compared to organ-confined primary cancers [107]. A further drawback is that the normal urinary FDG excretion results in high bladder activity which obscures pathological FDG uptake in the prostate. Generally, FDG PET is not recommended for evaluation of the prostate as sensitivities are as low as of 4–64% with a specificity in the order of 50% [108–110].

^{11}C-choline. Another tracer, carbon-11-labelled choline (^{11}C-choline), accumulates in prostatic cells and has the advantage that, unlike FDG, it is not excreted via the urinary tract, and thereby does not influence the visualization of the prostate [111]. Furthermore, the prostate is the only organ in the pelvis to accumulate ^{11}C-choline. The ^{11}C-choline uptake was higher in PC compared with BPH, but the difference was not significant [112]. In a direct comparison between ^{11}C-choline PET and MRSI, a significant linear correlation was observed between the maximum standardized uptake value (SUV) of ^{11}C-choline and the MRSI metabolite ratios. Also, ^{11}C-choline PET was more accurate than MRSI in accurately predicting the laterality (i.e. left- or right-sidedness) of the cancer: 81% (13/16) versus 50% (8/16), respectively [113]. Recently, it was shown that ^{11}C-choline preferentially detected more aggressive prostate cancer foci [114]. Drawbacks are the high costs of ^{11}C-choline and the short half-life of ^{11}C-choline (20 minutes). This latter precludes application of ^{11}C-choline in centers without cyclotrons. Nevertheless, the results of the first two studies combining ^{11}C-choline PET/CT scanning were encouraging, with a sensitivity of 66% and specificity between 81–84% on a sextant basis [115,116]. However, the high rate of false negative findings was a concern. A direct preoperative comparison between ^{11}C-choline PET, FDG PET, and MRI in 43 patients showed that ^{11}C-choline outperformed FDG PET in localizing prostate cancer but that MRI was superior to both [117].

Other radiopharmaceuticals. A preliminary PET/CT study using fluoro-18-choline (^{18}F-choline) demonstrated its feasibility, but reported its inability to distinguish cancer from BPH [118]. In a small population of both primary and recurrent disease, dual-phase ^{18}F-choline showed that areas of malignancy had stably high or increasing uptake while benign areas had decreasing uptake [119]. Thereby, this technique may aid in differentiating malignant from benign prostatic tissue. In a double-tracer study, ^{11}C-acetate PET was more sensitive than FDG, showing consistently increased uptake in PC lesions [120]. A further advantage was that ^{11}C-acetate did not accumulate in the urine. Again, a considerable uptake overlap was described between normal prostatic tissue, BPH and PC [121].

ProstaScint® scanning: No place in regular clinical practice

ProstaScint® (Cytogen, Princeton, NJ) is an Indium-111 labeled monoclonal mouse antibody specific for prostate-specific membrane antigen. A significant association between the PSA level and detection of ProstaScint® activity in the prostate was reported [122]. A recent study revealed sensitivities between 37–87% and specificities between 0–50%, concluding that the scan could not be used to reliably localize prostate cancer foci within the prostate [123]. In a single study of only seven patients in which the results of ProstaScint® fusion with CT scanning were correlated with systematic biopsy a sensitivity and specificity of 79% and 80%, respectively, were found [124]. In 47 of 51 (92%) preoperative patients at high risk of metastatic disease an increased ProstaScint® activity in the prostate was observed [125].
A drawback is that the antibodies clear slowly from the vasculature and muscle. Blood and bone modality has no place in primary prostate cancer detection and localization.

CONCLUSIONS AND DISCUSSION

In summary, new developments in ultrasound imaging (Doppler imaging and particularly the application of contrast agents) have proved capable of increasing the PC detection rate with fewer biopsy cores necessary as well as detecting relatively more aggressive cancer foci. This is a substantial improvement for the patient, who will have to undergo fewer biopsies. In addition, treatment guidance is improved since more representative areas are discovered at biopsy and thus the subsequent diagnostic process can be more accurately performed. TRUS remains the primary imaging tool because of its ease-of-use and its role in guiding prostate biopsy. However, TRUS accuracies varied widely among studies, in part due to the inherent high inter-observer variation, particularly in Doppler imaging.

MRI achieves high accuracy rates, particularly when functional information from dynamic contrast-enhanced MR and MRSI are added. A multiparametric approach was shown to optimize the diagnostic accuracy. This compensates for the longer examination time and the discomfort of the use of an ERC. Nevertheless, on a cost-effectiveness basis, MRI cannot be performed in all patients at risk of PC [126]. In patients with one or more prior negative TRUS-guided biopsy sessions and continuing suspicion of PC, MRI can provide valuable

additional information for PC detection and localization and thereby reduce the future number of biopsies the patient must undergo. Direct MRI guided biopsy is a novel method of performing targeted prostate biopsy.

CT scanning does not play a role in PC detection or localization because of its low soft-tissue resolution and radiation burden. This also applies to PET scanning due to its high costs and invasive nature, as well as the availability of alternative imaging modalities. PET scanning may possibly be used in instances in which TRUS-guided biopsies are negative and absence of evidence of PC on MRI. In addition, combining or fusing PET scanning with, for instance, MRI may be of additional value.

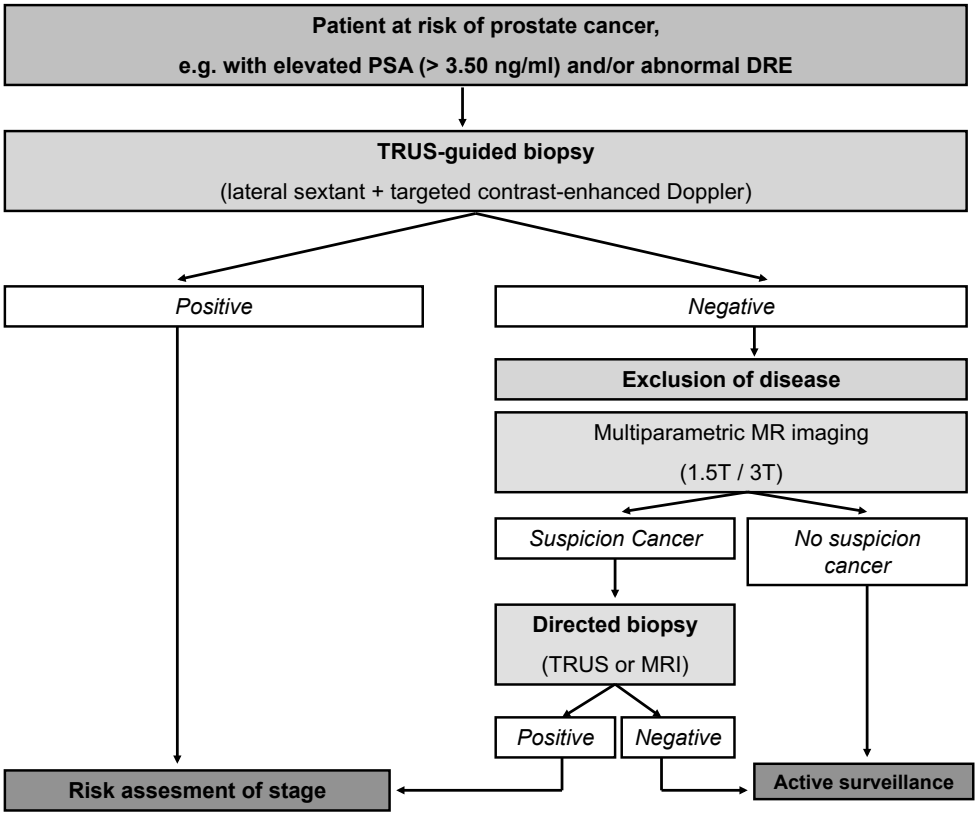

Figure 5. Proposed scheme for optimal use of imaging in patients at risk of prostate having prostate cancer. *Abbreviations:* PSA, prostate-specific antigen; DRE, digital rectal examination; TRUS, transrectal ultrasound; PPA, pelvic phased-array coil.

PROPOSALS FOR OPTIMAL USAGE OF IMAGING

Scheme

Based on the abovementioned, the authors propose the following scheme for patient care in patients at risk for prostate cancer (Figure 5).

Comparison with AUA and EAU guidelines [127–129]

Both associations recognize that the stage migration during the PSA era necessitates more accurate techniques in detecting and localizing prostate cancer. Use of TRUS to guide biopsy is regarded the standard of reference. The EAU's guideline, however, does not mention any contrast-enhanced Doppler imaging based biopsy strategies. This is in contrast to the data presented in our review. Neither CT scanning nor MRI is recommended or mentioned in relation to prostate cancer diagnosis. The latter is in contrast with our proposal in which MRI is used in patients in whom no cancer was found on first TRUS biopsy but with persistently high or rising PSA levels.

ACKNOWLEDGEMENTS

The authors would like to thank Yvonne L. Hoogeveen for her assistance in preparing the manuscript and Pieter H. M. de Mulder for his guiding recommendations while editing the manuscript.

REFERENCES

[1] Jemal AJ, Siegel R, Xu J, Ward E. CA Cancer J Clin 2010; 60(5):277–300.

[2] Carter HB, Piantadosi S, Isaacs JT. Clinical evidence for and implications of the multistep development of prostate cancer. J Urol 1990;143:742–6.

[3] Parkin DM, Bray FI, Devesa SS. Cancer burden in the year 2000. The global picture. Eur J Cancer 2001;37(Suppl 8): S4–66.

[4] Konety BR, Bird VY, Deorah S, Dahmoush L. Comparison of the incidence of latent prostate cancer detected at autopsy before and after the prostate specific antigen era. J Urol 2005;174:1785–8.

[5] Crawford ED. Epidemiology of prostate cancer. Urology 2003;62(Suppl 1):3–12.

[6] Stewart SL, King JB,ThompsonTD, Friedman C,Wingo PA, et al. Cancer mortality surveillance – United States, 1990– 2000. MMWR Surveill Summ 2004;53:1–108.

[7] Catalona WJ, Loeb S, Han M. Viewpoint: Expanding prostate cancer screening. Ann Intern Med 2006;144:441–3.

[8] Hoffman RM. Viewpoint: Limiting prostate cancer screening. Ann Intern Med 2006;144:438–40.

[9] Graif T, Loeb S, Roehl KA, Gashti SN, Griffin C, Yu X, et al. Under diagnosis and over diagnosis of prostate cancer. J Urol 2007;178(1):88–92.

[10] Max W, Rice DP, Sung H, Michel M, Breuer W, Zhang X, et al. The economic burden of prostate cancer, California, 1998. Cancer 2002;94:2906–13.

[11] Mangar SA, Huddart RA, Parker CC, Dearnaley DP, Khoo VS, Horwich A. Technological advances in radiotherapy for the treatment of localised prostate cancer. Eur J Cancer 2005;41:908–21.

[12] Meraney AM, Haese A, Palisaar J, Graefen M, Steuber T, Huland H, et al. Surgical management of prostate cancer: Advances based on a rational approach to the data. Eur J Cancer 2005;41:888–907.

[13] Bucci MK, Bevan A, Roach M, III. Advances in radiation therapy: Conventional to 3D, to IMRT, to 4D, and beyond. CA Cancer J Clin 2005;55:117–34.

[14] Hricak H, Wang L, Wei DC, Coakley FV, Akin O, Reuter VE, et al. The role of preoperative endorectal magnetic resonance imaging in the decision regarding whether to preserve or resect neurovascular bundles during radical retropubic prostatectomy. Cancer 2004;100:2655–63.

[15] Cellini N, Morganti AG, Mattiucci GC, Valentini V, Leone M, Luzi S, et al. Analysis of intraprostatic failures in patients treated with hormonal therapy and radiotherapy: Implications for conformal therapy planning. Int J Radiat Oncol Biol Phys 2002;53:595–9.

[16] Roach M, III. Reducing the toxicity associated with the use of radiotherapy in men with localized prostate cancer. Urol Clin North Am 2004;31:353–66.

[17] Baxter NN, Tepper JE, Durham SB, Rothenberger DA, Virnig BA. Increased risk of rectal cancer after prostate radiation: A population-based study. Gastroenterology 2005;128: 819–24.

[18] McNeal JE. Normal anatomy of the prostate and changes in benign prostatic hypertrophy and carcinoma. Semin Ultrasound CT MR 1988;9:329–34.

[19] Coakley FV, Hricak H. Radiologic anatomy of the prostate gland: A clinical approach. Radiol Clin North Am 2000;38:15–30.

[20] Chen ME, Johnston DA, Tang K, Babaian RJ, Troncoso P. Detailed mapping of prostate carcinoma foci: Biopsy strategy implications. Cancer 2000;89:1800–9.

[21] McNeal JE, Redwine EA, Freiha FS, Stamey TA. Zonal distribution of prostatic adenocarcinoma. Correlation with histologic pattern and direction of spread. Am J Surg Pathol 1988;12:897–906.

[22] Miller GJ, Cygan JM. Morphology of prostate cancer: The effects of multifocality on histological grade,

tumor volume and capsule penetration. J Urol 1994;152(Pt 2):1709–13.

[23] Brossner C, Winterholer A, Roehlich M, Diouhy-Schutz E, Serra V, Sonnleithner M, et al. Distribution of prostate carcinoma foci within the peripheral zone: Analysis of 8,062 prostate biopsy cores. World J Urol 2003;21:163–6.

[24] Horninger W, Reissigl A, Rogatsch H, Volgger H, Studen M, Klocker H, et al. Prostate cancer screening in the Tyrol, Austria: Experience and results. Eur J Cancer 2000;36:1322–35.

[25] Ohori M, Kattan M, Scardino PT, Wheeler TM. Radical prostatectomy for carcinoma of the prostate. Mod Pathol 2004;17:349–59.

[26] Gleason DF. Histologic grade, clinical stage, and patient age in prostate cancer. NCI Monogr 1988;7:15–8.

[27] Gleason DF. Histologic grading of prostate cancer: A perspective. Hum Pathol 1992;23:273–9.

[28] Egevad L, Granfors T, Karlberg L, Bergh A, Stattin P. Prognostic value of the Gleason score in prostate cancer. BJU Int 2002;89:538–42.

[29] Rasiah KK, Stricker PD, Haynes AM, Delprado W, Turner JJ, Golovsky D, et al. Prognostic significance of Gleason pattern in patients with Gleason score 7 prostate carcinoma. Cancer 2003;98:2560–5.

[30] Lee F, Gray JM, McLeary RD, McHugh TA, Solomon MH, Kumasaka GH, et al. Prostatic evaluation by transrectal sonography: Criteria for diagnosis of early carcinoma. Radiology 1986;158:91–5.

[31] Meirelles LR, Billis A, Cotta AC, Nakamura RT, Caserta NMG, Prando A. Prostatic atrophy: Evidence for a possible role of local ischemia in its pathogenesis. Int Urol Nephrol 2002;34:345–50.

[32] Ellis WJ, Brawer MK. The significance of isoechoic prostatic carcinoma. J Urol 1994;152(Pt 2):2304–7.

[33] Frauscher F, Klauser A, Berger AP, Halpern EJ, Feuchtner G, Koppelstaetter F, et al. The value of ultrasound (US) in the diagnosis of prostate cancer. Radiologie. 2003;43: 455–63.

[34] Hodge KK, McNeal JE, Terris MK, Stamey TA. Random systematic versus directed ultrasound guided transrectal core biopsies of the prostate. J Urol 1989;142:71–4.

[35] Presti JC, Jr. Prostate biopsy: How many cores are enough? Urol Oncol 2003;21:135–40.

[36] Eskicorapci SY, Baydar DE, Akbal C, Sofikerim M, Gunay M, Ekici S, et al. An extended 10-core transrectal ultrasonography guided prostate biopsy protocol improves the detection of prostate cancer. Eur Urol 2004;45:444–8.

[37] Pelzer AE, Bektic J, Berger AP, Halpern EJ, Koppelstätter F, Klauser A, et al. Are transition zone biopsies still necessary to improve prostate cancer detection? Results from the Tyrol screening project. Eur Urol 2005;48(6):916–21.

[38] King CR, McNeal JE, Gill H, Presti JC, Jr. Extended prostate biopsy scheme improves reliability of Gleason grading: Implications for radiotherapy patients. Int J Radiat Oncol Biol Phys 2004;59:386–91.

[39] Ching CB, Moussa AS, Li J, Lane BR, Zippe C, Jones JS et al. Does transrectal ultrasound probe configuration really matter? End fire versus side fire probe prostate cancer detection rates. J Urol 2009;181:2077–82.

[40] Gore JL, Shariat SF, Miles BJ, Kadmon D, Jiang N,Wheeler TM, et al. Optimal combinations of systematic sextant and laterally directed biopsies for the detection of prostate cancer. J Urol 2001;165:1554–9.

[41] Scherr DS, Eastham J, Ohori M, Scardino PT. Prostate biopsy techniques and indications: When, where, and how? Semin Urol Oncol 2002;20:18–31.

[42] Djavan B, Remzi M, Schulman CC, Marberger M, Zlotta AR, et al. Repeat prostate biopsy: Who, how and when? A review. Eur Urol 2002;42:93–103.

[43] Wilson NM, Masoud AM, Barsoum HB, Refaat MM, Moustafa MI, Kamal TA, et al. Correlation of power Doppler with microvessel density in assessing prostate needle biopsy. Clin Radiol 2004;59:946–50.

[44] Okihara K, Kojima M, Nakanouchi T, Okada K, Miki T. Transrectal power Doppler imaging in the detection of prostate cancer. BJU Int 2000;85:1053–7.

[45] Eisenberg ML, Cowan JE, Carroll PR, Shinohara K. The adjunctive use of power Doppler imaging in the preoperative assessment of prostate cancer. BJU Int 2010;105(9):1237–41.

[46] Rifkin MD, Sudakoff GS, Alexander AA. Prostate: Techniques, results, and potential applications of color Doppler US scanning. Radiology 1993;186:509–13.

[47] Lavoipierre AM, Snow RM, Frydenberg M, Gunter D, Reisner G, Royce PL, et al. Prostatic cancer: Role of color Doppler imaging in transrectal sonography. AJR Am J Roentgenol 1998;171:205–10.

[48] J akobsen JA, Correas JM. Ultrasound contrast agents and their use in urogenital radiology: Status and prospects. Eur Radiol 2001;11:2082–91.

[49] Frauscher F, Klauser A,Volgger H, Halpern EJ, Pallwein L, Steiner H, et al. Comparison of contrast enhanced color Doppler targeted biopsy with conventional systematic biopsy: Impact on prostate cancer detection. J Urol 2002;167:1648–52.

[50] Pelzer A, Bektic J, Berger AP, Pallwein L, Halpern EJ, Horninger W, et al. Prostate cancer detection in men with prostate specific antigen 4 to 10 ng/ml using a combined approach of contrast enhanced color Doppler targeted and systematic biopsy. J Urol 2005;173:1926–9.

[51] Mitterberger M, Pinggera GM, Horninger W, Bartsch G, Strasser H, Schäfer G, et al. Comparison of contrast enhanced color doppler targeted biopsy to conventional systematic biopsy: Impact on Gleason score. J Urol 2007;178(2): 464–8.

[52] Mitterberger M, Horninger W, Pelzer A, Strasser H, Bartsch G, Moser P, et al. A prospective randomized trial comparing contrast-enhanced targeted versus systematic ultrasound guided biopsies: Impact on prostate cancer detection. Prostate 2007;67:1537–42.

[53] Jakobsen JA, Oyen R, Thomsen HS, Morcos SK. Safety of ultrasound contrast agents. Eur Radiol 2005;15:941–5.

[54] Mitterberger M, Pinggera G, Horninger W, Hannes Strasser, Halpern E, Pallwein L, et al. Dutasteride prior to contrast-enhanced colour Doppler ultrasound prostate biopsy increases prostate cancer detection. Eur Urol 2008;53: 112–7.

[55] Konig K, Scheipers U, Pesavento A, Lorentz A, Ermert H, Senge T. Initial experiences with real-time elastography guided biopsies of the prostate. J Urol 2005;174:115–7.

[56] Pallwein L, Mitterberger M, Struve P, Horninger W, Aigner F, Bartsch B, et al. Comparison of sonoelastography guided biopsy with systematic biopsy: Impact on prostate cancer detection. Eur Radiol 2007;17(9):2278–85.

[57] Frauscher F, Klauser A, Koppelstaetter F, Berger AP, Horninger W, Bartsch G, et al. Real-time elastography for prostate cancer detection: Preliminary experience. Eur Radiol 2004; 14(S2):150.

[58] Nelson ED, Slotoroff CB, Gomella LG, Halpern EJ. Targeted biopsy of the prostate: The impact of color Doppler imaging and elastography on prostate cancer detection and Gleason score. Urology 2007;70:1136–40.

[59] Prando A, Wallace S. Helical CT of prostate cancer: Early clinical experience. AJR Am J Roentgenol 2000;175: 343–6.

[60] Tempany CM, Zhou X, Zerhouni EA, Rifkin MD, Quint LE, Piccoli CW, et al. Staging of prostate cancer: Results of Radiology Diagnostic Oncology Group

project comparison of three MR imaging techniques. Radiology 1994;192:47–54.

[61] Cruz M, Tsuda K, Narumi Y, Kuroiwa Y, Nose T, Kojima Y, et al. Characterization of low-intensity lesions in the peripheral zone of prostate on pre-biopsy endorectal coil MR imaging. Eur Radiol 2002;12:357–65.

[62] Claus FG, Hricak H, Hattery RR. Pretreatment evaluation of prostate cancer: Role of MR imaging and 1H MR spectroscopy. Radiographics 2004;24(S1):S167–80.

[63] Wang L, Mazaheri Y, Zhang J, Ishill NM, Kuroiwa K, Hricak H. Assessment of biologic aggressiveness of prostate cancer: Correlation of MR signal intensity with Gleason grade after radical prostatectomy. Radiology 2008;246:168–76.

[64] Akin O, Sala E, Moskowitz CS, Kuroiwa K, Ishill NM, Pucar D, et al. Transition zone prostate cancers: Features, detection, localization, and staging at endorectal MR imaging. Radiology 2006;239:784–92.

[65] Rosenkrantz AB, Neil J, Kong X, Melamed J, Babb JS,Taneja SS, et al. Prostate cancer: Comparison of 3D T2-weighted with conventional 2D T2-weighted imaging for image quality and tumor detection. AJR Am J Roentgenol 2010;194:446–52.

[66] Mullerad M, Hricak H, Kuroiwa K, Pucar D, Chen H, Kattan MW, et al. Comparison of endorectal magnetic resonance imaging, guided prostate biopsy and digital rectal examination in the preoperative anatomical localization of prostate cancer. J Urol 2005;174:2158–63.

[67] Beyersdorff D, Taupitz M, Winkelmann B, Fischer T, Lenk S, Loening SA, et al. Patients with a history of elevated prostate-specific antigen levels and negative transrectal US-guided quadrant or sextant biopsy results: Value of MR imaging. Radiology 2002;224:701–6.

[68] TamadaT, SoneT, JoY,Yamamoto A,YamashitaT, Egashira N, et al. Prostate cancer: Relationships between postbiopsy hemorrhage and tumor detectability at MR diagnosis. Radiology 2008;248:531–9.

[69] Kurhanewicz J,Vigneron DB, Hricak H, Narayan P, Carroll P, Nelson SJ. Three-dimensional H-1 MR spectroscopic imaging of the in situ human prostate with high [0.24-0.7 cm^3] spatial resolution. Radiology 1996;198:795–805.

[70] Coakley FV, Qayyum A, Kurhanewicz J. Magnetic reso- nance imaging and spectroscopic imaging of prostate cancer. J Urol 2003;170(Pt 2):S69–75.

[71] Zakian KL, Sircar K, Hricak H, Chen H, Shukla-Dave A, Eberhardt S, et al. Correlation of proton MR spectroscopic imaging with Gleason score based on step-section pathologic analysis after radical prostatectomy. Radiology 2005;234:804–14.

[72] Scheenen TW, Klomp DW, Roll SA, Fütterer JJ, Barentsz JO, Heerschap A. Fast acquisition-weighted three-dimensional proton MR spectroscopic imaging of the human prostate. Magn Reson Med 2004;52:80–8.

[73] Scheidler J, Hricak H,Vigneron DB, Kyle K,Yu KK , Sokolov DL, et al. Prostate cancer: Localization with three-dimensional proton MR spectroscopic imaging – clinicopathologic study. Radiology 1999;213:473–80.

[74] Wefer AE, Hricak H,Vigneron DB, Coakley FV, LuY,Wefer J, et al. Sextant localization of prostate cancer: Comparison of sextant biopsy, magnetic resonance imaging and magnetic resonance spectroscopic imaging with step section histology. J Urol 2000;164:400–4.

[75] Fütterer JJ, Heijmink SWTPJ, Scheenen TWJ, Veltman J, Huisman HJ, Vos P, et al. Prostate cancer localization with dynamic contrast-enhanced MR imaging and proton MR spectroscopic imaging. Radiology 2006;241:449–58.

[76] Shukla-Dave A, Hricak H, Kattan MW, Pucar D, Kuroiwa K, Chen H, et al. The

utility of magnetic resonance imaging and spectroscopy for predicting insignificant prostate cancer: An initial analysis. BJU Int 2007;99:786–93.

[77] Weinreb JC, Blume JD, Coakley FV, Wheeler T, Cormack JB, Sotto CK, et al. Prostate cancer: Sextant localization at MR imaging and MR spectroscopic imaging before prostatectomy – results of ACRIN prospective multi-institutional clinicopathologic study. Radiology 2009;251:122–33.

[78] Sato C, Naganawa S, Nakamura T, Kumada H, Miura S, Takizawa O, et al. Differentiation of noncancerous tissue and cancer lesions by apparent diffusion coefficient values in transition and peripheral zones of the prostate. J Magn Reson Imaging 2005;21:258–62.

[79] Zelhof B, Pickles M, Liney G, Peter Gibbs P, Rodrigues G, Kraus S, et al. Correlation of diffusion-weighted magnetic resonance data with cellularity in prostate cancer. BJU Int 2009;103:883–8.

[80] Mazaheri Y, Shukla-Dave A, Hricak H, Fine SW, Zhang, J, Inurrigarro G, et al. Prostate cancer: Identification with combined diffusion-weighted MR imaging and 3D 1H MR spectroscopic imaging – correlation with pathologic findings. Radiology 2008;246:480–8.

[81] Haider MA, Van Der Kwast TH, Tanguay J, Evans AJ, Hashmi A, Lockwood G, et al. Combined T2-weighted and diffusion-weighted MRI for localization of prostate cancer. AJR Am J Roentgenol 2007;189:323–8.

[82] Yoshimitsu K, Kiyoshima K, Irie H, Tajima T, Asayama Y, Hirakawa M, et al. Usefulness of apparent diffusion coefficient map in diagnosing prostate carcinoma: Correlation with stepwise histopathology. J Magn Reson Imaging 2008; 27:132–9.

[83] Langer DL, Van Der Kwast TH, Evans AJ, Trachtenberg J, Wilson BC, Haider A. Prostate cancer detection with multi-parametric MRI: Logistic regression analysis of quantitative T2, diffusion-weighted imaging, and dynamic contrast-enhanced MRI. J Magn Reson Imaging 2009;30:327–34.

[84] Gibbs P, Pickles MD, Turnbull LW. Diffusion imaging of the prostate at 3.0 tesla. Invest Radiol 2006;41:185–8.

[85] Pickles MD, Gibbs P, Sreenivas M,Turnbull LW. Diffusion-weighted imaging of normal and malignant prostate tissue at 3.0T. J Magn Reson Imaging 2006;23:130–4.

[86] Miao H, Fukatsu H, Ishigaki T. Prostate cancer detection with 3-T MRI: Comparison of diffusion-weighted and T2-weighted imaging. Eur J Radiol 2007;61:297–302.

[87] Kim CK, Park BK, Kim B. High-b-Value diffusion-weighted imaging at 3 T to detect prostate cancer: Comparisons between b values of 1,000 and 2,000 s/mm2. AJR Am J Roentgenol 2010;194:W33–7.

[88] Woodfield CA, Tung GA, Grand DJ, Pezzullo JA, Machan JT, Renzulli JF, et al. Diffusion-weighted MRI of peripheral zone prostate cancer: Comparison of tumor apparent diffusion coefficient with Gleason score and percentage of tumoroncorebiopsy. AJR Am J Roentgenol 2010;194:W316– 22.

[89] Langer DL, Van Der Kwast TH, Evans AJ, Plotkin A, Trachtenberg J, Wilson BC, et al. Prostate tissue composition and MR measurements: Investigating the relationships between ADC, T2, K[trans], v[e], and corresponding histologic features. Radiology 2010;255:485–94.

[90] Barentsz JO, Engelbrecht M, Jager GJ, de LaRosette J, van Der Sanden BP, Huisman HJ, et al. Fast dynamic gadolinium-enhanced MR imaging of urinary bladder and prostate cancer. J Magn Reson Imaging 1999;10:295–304.

[91] Padhani AR, Gapinski CJ, Macvicar DA, Parker GJ, Suckling J, Revell PB, et al. Dynamic contrast enhanced MRI of prostate cancer: Correlation with morphology and tumour stage, histological grade and PSA. Clin Radiol 2000;55:99–109.

[92] Engelbrecht MR, Huisman HJ, Laheij RJ, Jager GJ, van Leenders GJLH, Hulsbergen-Van De Kaa CA, et al. Discrimination of prostate cancer from normal peripheral zone and central gland tissue by using dynamic contrast-enhanced MR imaging. Radiology 2003;229:248–54.

[93] Van Dorsten FA, Van Der Graaf M, Engelbrecht MR, van Leenders GJ, Verhofstad A, Rijpkema M, et al. Combined quantitative dynamic contrast-enhanced MR imaging and [1] H MR spectroscopic imaging of human prostate cancer. J Magn Reson Imaging 2004;20:279–87.

[94] Runge VM. Safety of approved MR contrast media for intravenous injection. J Magn Reson Imaging 2000;12: 205–13.

[95] Lin SP, Brown JJ. MR contrast agents: Physical and pharmacologic basics. J Magn Reson Imaging 2007;25: 884–99.

[96] Kitajima K, Kaji Y, Fukabori Y, Yoshida K, Suganuma N, Sugimura K. Prostate cancer detection with 3 T MRI: Comparison of diffusion-weighted imaging and dynamic contrast-enhanced MRI in combination with T2-weighted imaging. J Magn Reson Imaging 2010;31:625–31.

[97] Sciarra A, Panebianco V, Ciccariello M, Salciccia S, Cattarino S, Lisi D, et al.Value of magnetic resonance spectroscopy imaging and dynamic contrast-enhanced imaging for detecting prostate cancer foci in men with prior negative biopsy. Clin Cancer Res 2010;16:1875–83.

[98] Turkbey B, Pinto PA, Mani H, Bernardo M, Pang Y, McKinney YL, et al. Prostate cancer: Value of multiparametric MR imaging at 3 T for detection-–histopathologic correlation. Radiology 2010;255:89–99.

[99] Futterer JJ, Scheenen TW, Huisman HJ, Klomp DW J, van Dorsten, FA, Hulsbergen-van de Kaa, CA, et al. Initial experience of 3 Tesla endorectal coil magnetic resonance imaging and 1H-spectroscopic imaging of the prostate. Invest Radiol 2004;39:671–80.

[100] Beyersdorff D, Taymoorian K, Knosel T, Schnorr D, Felix R, Hamm B, et al. MRI of prostate cancer at 1.5 and 3.0 T: Comparison of image quality in tumor detection and staging. AJR Am J Roentgenol 2005;185:1214–20.

[101] Scheenen TW, Heijmink SW, Roell SA, Hulsbergen-Van de Kaa CA, Knipscheer BC, Alfred Witjes JA, et al. Three-dimensional proton MR spectroscopy of human prostate at 3 T without endorectal coil: Feasibility. Radiology 2007;245:507–16.

[102] Heijmink SWTPJ, Futterer JJ, Hambrock T, Takahashi S, Scheenen TWJ, Huisman HJ, et al. Prostate cancer: Body-array versus endorectal coil MR imaging at 3 T – Comparison of image quality, localization, and staging performance. Radiology 2007;244:184–95.

[103] Yakar D, Hambrock T, Hoeks C, Barentsz JO, Fütterer, JJ. Magnetic resonance-guided biopsy of the prostate: Feasibility, technique, and clinical applications. Top Magn Reson Imaging 2008;19:291–5.

[104] Beyersdorff D, Winkel A, Hamm B, Severin Lenk S, Loening SA, Taupitz M. MR imaging-guided prostate biopsy with a closed MR unit at 1.5 T: Initial results. Radiology 2005;234:576–81.

[105] Hambrock T, Somford DM, Hoeks C, Bouwense SA, Huisman H, Yakar D, et al. Magnetic resonance imaging guided prostate biopsy in men with repeat negative biopsies and increased prostate specific antigen. J Urol 2010;183:520–7.

[106] Shreve PD, Grossman HB, Gross MD,Wahl RL. Metastatic prostate cancer: Initial findings of PET with 2-deoxy-2-[F-18]fluoro-D-glucose. Radiology 1996;199:751–6.

[107] Oyama N, Akino H, Suzuki Y, Kanamaru H, Sadato N, Yonekura Y, et al. The increased accumulation of [18F] fluorodeoxyglucose in untreated prostate cancer. Jpn J Clin Oncol 1999;29:623–9.

[108] Effert PJ, Bares R, Handt S, Wolff JM, Bull U, Jakse G. Metabolic imaging

of untreated prostate cancer by positron emission tomography with 18fluorine-labeled deoxyglucose. J Urol 1996;155:994–8.

[109] Haseman MK, Reed NL, Rosenthal SA. Monoclonal antibody imaging of occult prostate cancer in patients with elevated prostate-specific antigen. Positron emission tomography and biopsy correlation. Clin Nucl Med 1996;21: 704–13.

[110] Liu IJ, Zafar MB, Lai YH, Segall GM, Terris MK. Fluoro-deoxyglucose positron emission tomography studies in diagnosis and staging of clinically organ-confined prostate cancer. Urology 2001;57:108–11.

[111] Hara T, Kosaka N, Kishi H. PET imaging of prostate cancer using carbon-11-choline. J Nucl Med 1998;39:990–5.

[112] Sutinen E, Nurmi M, Roivainen A, Varpula M, Tolvanen T, Lehikoinen P, et al. Kinetics of [[11]C]choline uptake in prostate cancer: A PET study [correction for stydy]. Eur J Nucl Med Mol Imaging 2004;31:317–24.

[113] Yamaguchi T, Lee J, Uemura H, Sasaki T, Takahashi N, Oka T, et al. Prostate cancer: A comparative study of [11] C-choline PET and MR imaging combined with proton MR spectroscopy. Eur J Nucl Med Mol Imaging 2005; 32:742–8.

[114] Piert M, Park H, Khan A, Siddiqui J, Hussain H, Chenevert T, et al. Detection of aggressive primary prostate cancer with 11C-choline PET/CT using multimodality fusion techniques. J Nucl Med 2009;50:1585–93.

[115] Farsad M, Schiavina R, Castellucci P, Nanni C, Barbara Corti B, Martorana G, et al. Detection and localization of prostate cancer: Correlation of [11]C-choline PET/CT with histopathologic step-section analysis. J Nucl Med 2005;46:1642–9.

[116] Martorana G, Schiavina R, Corti B, Farsad M, Salizzoni E, Brunocilla E, et al. 11C-Choline positron emission tomography/computerized tomography for tumor localization of primary prostate cancer in comparison with 12-core biopsy. J Urol 2006;176:954–60.

[117] Watanabe H, Kanematsu M, Kondo H, Kako N, Yamamoto N, Yamada T, et al. Preoperative detection of prostate cancer: A comparison with 11C-choline PET, 18F-fluorodeoxyglucose PET and MR imaging. J Magn Reson Imaging 2010;31:1151–6.

[118] Schmid DT, John H, Zweifel R, Cservenyak T, Westera G, Goerres GW, et al. Fluorocholine PET/CT in patients with prostate cancer: Initial experience. Radiology 2005; 235:623–8.

[119] Sandblom G, Sörensen J, Lundin N, Häggman M, Malmström PU. Positron emission tomography with C11-acetate for tumor detection and localization in patients with prostate-specific antigen relapse after radical prostatectomy. Urology 2006;67:996–1000.

[120] Oyama N, Akino H, Kanamaru H, Suzuki Y, Muramoto S, Yonekura Y, et al. 11C-acetate PET imaging of prostate cancer. J Nucl Med 2002;43:181–6.

[121] Kato T, Tsukamoto E, Kuge Y, Takei T, Shiga T, Shinohara N, et al. Accumulation of [11C]acetate in normal prostate and benign prostatic hyperplasia: Comparison with prostate cancer. Eur J Nucl Med Mol Imaging 2002;29:1492–5.

[122] Sodee DB, Malguria N, Faulhaber P, Resnick MI , Albert J, Bakale G, et al. Multicenter ProstaScint imaging findings in 2154 patients with prostate cancer. The ProstaScint Imaging Centers. Urology 2000;56:988–93.

[123] Mouraviev V, Madden JF, Broadwater G, Mayes JM, Burchette JL Schneider F, et al. Use of 111in-capromab pendetide immunoscintigraphy to image localized prostate cancer foci within the prostate gland. J Urol 2009;182: 938–47.

[124] Ellis RJ, Kim EY, Conant R, Sodee DB, Spirnak JP, Dinchman KH, et al. Radioimmunoguided imaging of prostate cancer foci with histopathological correlation. Int J Radiat Oncol Biol Phys 2001;49:1281–6.

[125] Burgers JK, Hinkle GH, Haseman MK. Monoclonal antibody imaging of recurrent and metastatic prostate cancer. Semin Urol 1995;13:103–12.

[126] Jager GJ, Severens JL,Thornbury JR, de la Rosette JJMCH, Ruijs SHJ, Barentsz JO. Prostate cancer staging: Should MR imaging be used? – A decision analytic approach. Radiology 2000;215:445–51.

[127] Report on the management of clinically localized prostate cancer. Available from: http://www.auanet.org/guidelines/proscan07.cfm. 2007.

[128] Heidenreich A, Aus G, Abbou CC, Bolla M, Joniau S, Matveev V, Schmid HP, et al. Guidelines on prostate cancer 2007.

[129] Thompson I, Thrasher JB, Aus G, Burnett AL, Canby-Hagino ED, Cookson MS, et al. Guideline for the management of clinically localized prostate cancer: 2007 update. J Urol 2007;177:2106–31.

[130] Salomon L, Colombel M, Patard JJ, Lefrère-Belda MA, Bellot J, Chopin D, et al. Value of ultrasound-guided systematic sextant biopsies in prostate tumor mapping. Eur Urol 1999;35:289–93.

[131] Cornud F, Belin X, Piron D, Chrétien Y, Flam T, Casanova JM, et al. Color Doppler-guided prostate biopsies in 591 patients with an elevated serum PSA level: Impact on Gleason score for nonpalpable lesions. Urology 1997;49:709–15.

[132] Halpern EJ, Strup SE. Using gray-scale and color and power Doppler sonography to detect prostatic cancer. AJR Am J Roentgenol 2000;174:623–7.

[133] Kuligowska E, Barish MA, Fenlon HM, Blake M. Predictors of prostate carcinoma: Accuracy of gray-scale and color Doppler US and serum markers. Radiology 2001; 220:757–64.

[134] Sauvain JL, Palascak P, Bourscheid D, Chabi C, Atassi A, Bremon JM, et al. Value of power doppler and 3D vascular sonography as a method for diagnosis and staging of prostate cancer. Eur Urol 2003;44:21–30.

[135] Remzi M, Dobrovits M, Reissigl A, Ravery V, Waldert M, Wiunig C, et al. Can Power Doppler enhanced transrectal ultrasound guided biopsy improve prostate cancer detection on first and repeat prostate biopsy? Eur Urol 2004; 46:451–6.

[136] Unal D, Sedelaar JP, Aarnink RG, van Leenders GJ, Wijkstra H, Debruyne FM, et al. Three-dimensional contrast-enhanced power Doppler ultrasonography and conventional examination methods: The value of diagnostic predictors of prostate cancer. BJU Int 2000;86:58–64.

[137] Halpern EJ, Rosenberg M, Gomella LG. Prostate cancer: Contrast-enhanced us for detection. Radiology 2001; 219:219–25.

[138] Yuen JS, Thng CH, Tan PH, Khin LW, Phee SJ, Xiao D, et al. Endorectal magnetic resonance imaging and spectroscopy for the detection of tumor foci in men with prior negative transrectal ultrasound prostate biopsy. J Urol 2004;171:1482–6.

[139] Graser A, Heuck A, Sommer B, Massmann J , Scheidler J, Maximillian Reiser M, et al. Per-sextant localization and staging of prostate cancer: Correlation of imaging findings with whole-mount step section histopathology. AJR Am J Roentgenol 2007;188:84–90.

[140] Zakian KL, Sircar K, Hricak H, Chen H, Shukla-Dave A, Eberhardt S, et al. Correlation of proton MR spectroscopic imaging with Gleason score based on step-section pathologic analysis after radical prostatectomy. Radiology 2005;234:804–14.

[141] Fütterer JJ, Scheenen TWJ, Heijmink SWTPJ, Huisman HJ, Hulsbergen-van de Kaa CA, Witjes JA, et al. Standardized threshold approach using three-dimensional proton magnetic resonance spectroscopic imaging in prostate cancer localization of the entire prostate. Invest Radiol 2007;42:116–22.

CHAPTER 3

State-of-the-art uroradiologic imaging to determine prostate cancer stage

Stijn W. T. P. J. Heijmink
Jurgen J. Fütterer
Stephen S. Strum
Wim J. G. Oyen
Ferdinand Frauscher
J. Alfred Witjes
Jelle O. Barentsz

Unpublished

In the diagnostic process of prostate cancer (PC), radiologic imaging modalities significantly contribute to the determination of extent of the disease. Establishing the exact local disease extent in either organ-confined or locally advanced, as well as establishing is highly important in determining the optimal patient therapy plan. Within this review, after evaluation of the literature, we will discuss the advantages and disadvantages of these imaging modalities in clarifying the patient's clinical status. Bone scintigraphy remains the most sensitive method to detect metastatic bone disease but should only be used in high-risk patients. Lymph node specific MR contrast agents are promising in nodal staging. However, conventional size and shape criteria are still the standard of reference. In determining the local disease stage, MR imaging is superior to other imaging techniques. Subsequently, a proposal for optimal use of radiologic imaging is presented.

With three out of every ten newly diagnosed male cancers being prostate cancer (PC) and one in ten male cancer deaths being due to PC [1], the disease burden is considerable. After PC has been diagnosed, it is the function of the attending physicians – the urologist, radiation therapist, and medical oncologist – as well as the patient and his family, to arrive at treatment options that will best serve the patient. It is now believed to be common practice that clinicians involved in the treatment of PC patients employ nomograms to determine therapeutic options [2-4]. The most frequently used nomogram, the Partin tables, estimates the chance of organ-confined disease, extracapsular extension, seminal vesicle invasion and lymph node metastasis, based on the results of the traditional triad of digital rectal examination, biopsy Gleason score, and prostate-specific antigen (PSA) value [5]. Subsequent imaging studies requested by the clinician are based theoretically on the outcomes of such nomograms. Likewise, imaging plays an important role in risk stratification. While two patients may turn out to have the same PSA level and biopsy Gleason score (a measure of cancer aggressiveness scaled from 2 to 10 [6;7]), no two patients will have identical transrectal ultrasound (TRUS) or magnetic resonance (MR) imaging findings, an example of which is shown in Figure 1.

Each treatment strategy was shown to be associated with distinct patterns of changes in quality of life related effects [8]. Additionally, there are factors within the context of the patient's clinical setting that affect the ultimate treatment decision, e.g. expected patient longevity, overall health, insurance coverage along with other financial issues, patient perceptions of treatment risks, as well as personal preferences [9-11]. Nonetheless, the first step in the decision-making process is to answer the crucial question: is the PC organ-confined or is there spread of cancer beyond the scope of the scalpel, outside of the radiation port, beyond the realm of the cryosurgical ice ball, or outside the ultrasound field of high intensity focused ultrasound (HIFU)?

This review (1) presents an overview of the currently available imaging modalities to determine metastatic spread to the bones and lymph nodes in patients with PC. (2) Subsequently, the various imaging modalities for the assessment of local spread are assessed with emphasis placed on both the advantages and drawbacks of all methods. (3) From the preceding, a scheme is proposed for optimal evidence-based use of imaging in determining the PC disease stage.

2. LITERATURE SEARCH

Relevant articles were retrieved using combinations of both Medical Subject Headings (MeSH) and free search terms in the MedLine® (WebSPIRS Version 5.12, Build 20060224, Ovid Technologies) and Pubmed (U.S. National Library of Medicine) online search engines.

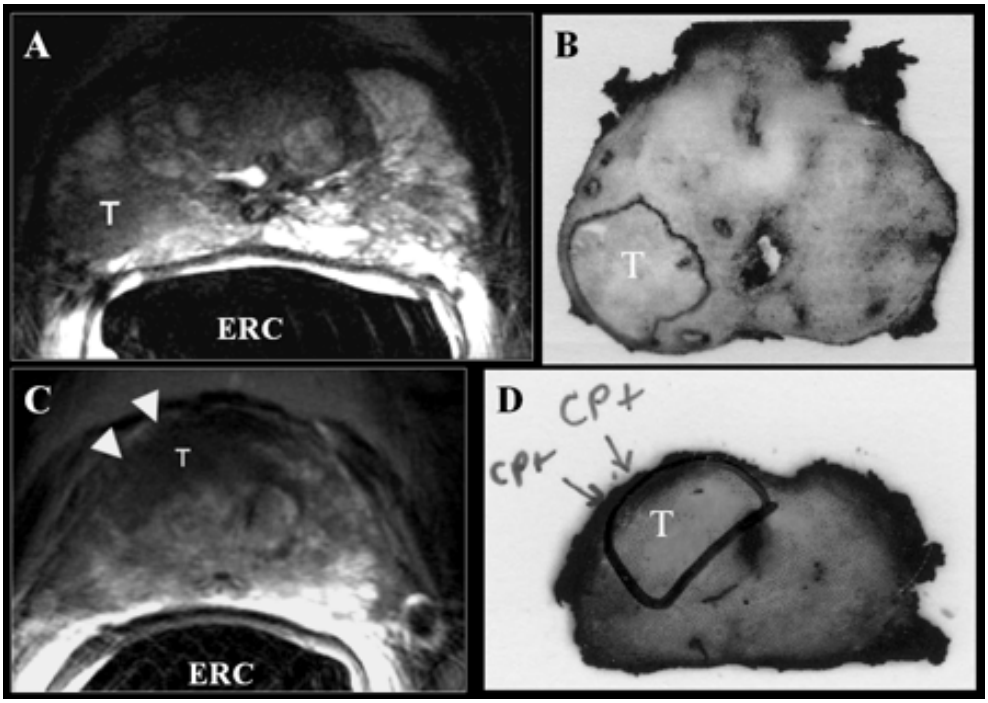

Figure 1. An example of two patients (both 61 years of age) with identical PSA levels (5.8 ng/ml), biopsy Gleason scores (3+3) and normal DRE, but with markedly different MR imaging findings. The MR image (A, axial slice) with an endorectal coil (ERC) of patient 1 showed an area of low signal intensity (T) in the right peripheral zone towards the base of the prostate without signs of extraprostatic extension. Gross pathology (B) and histopathology (not shown) confirmed the diagnosis of a Gleason (4+3) tumor (T) (pathological stage T2b, and negative surgical margins). Preoperative endorectal MR imaging (C, axial slice) of patient 2 showed a low signal intensity lesion (T) in the ventral part in the base of the prostate. This was accompanied by signs of bulging, indicative of extracapsular extension (arrowheads). Gross pathology (D) and histopathology (not shown) revealed a Gleason (3,4) tumor (T) in the ventral part of the prostate with capsular penetration (CP) with a radial extent of 0.5 mm over an area with a diameter of 4 mm (pathological stage T3a).

MeSH terms included: “Prostate”, “Anatomy”, “Prostatic Neoplasms”, “Neoplasm Staging”, “Ultrasonography”, “Tomography, X-Ray Computed”, “Magnetic resonance imaging”, “Magnetic Resonance Spectroscopy”, “Radionuclide Imaging”, and “Positron-Emission Tomography”.

Free search terms included: “prost*”, “cancer”, “detect*”, “localization”, “localisation”, “biops*”, “stag*”, “capsul*”, “extracapsular penetration”, “extracapsular extension”, “seminal vesicle invasion”, “transrectal ultraso*”, “TRUS”, “computed tomography”, “CT”, “magnetic resonance imaging”, “MRI”, “ferumoxtran-10”, “magnetic resonance spectroscopy”,

"spectroscopy", "MRS", "bone scan*", "bone scintigraphy", "positron-emission tomography", "PET", and "ProstaScint".

Reference lists of selected articles were further analyzed for relevant articles.

3. NORMAL PROSTATE ANATOMY IN COMPARISON TO LOCAL, REGIONAL & METASTATIC PROSTATE CANCER

3.1. Normal Prostate Anatomy

With the exception of the apex, the whole prostate is surrounded by a thin (2-3 mm) layer of fibromuscular tissue, designated as the prostatic capsule [12;13]. Since it is inseparable from the prostatic tissue, it is often called a 'pseudocapsule'. Opposite the apex of the prostate, and superior and posterior to the base of the prostate, lie the seminal vesicles (SV) [14] (Figure 2A). The SV are an accessory gland of the prostate that forms seminal coagulum, modifies sperm functions such as motility, and performs phagocytosis of fragments of spermatozoa [15]. Via the ejaculatory ducts, the SV empty into the urethra at the verumontanum. The dorsolaterally situated neurovascular bundles supply the prostate with blood and nerves (Figure 2B).

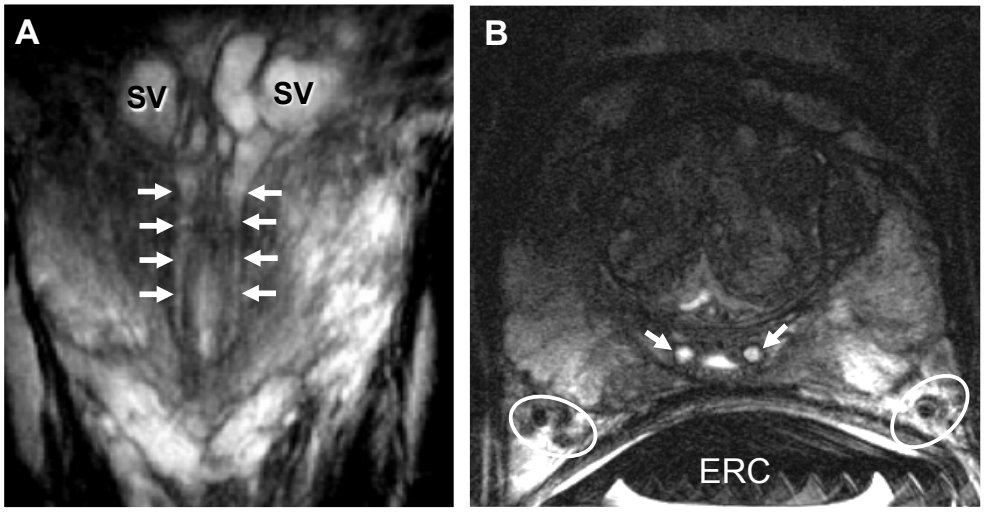

Figure 2: MR images of a 53-year-old patient (PSA level 3.74 ng/ml, normal digital rectal examination) depicting the anatomy of the prostate related to locoregional spread. (A) The seminal vesicles (SV) are cranially located on the base of the prostate and the ejaculatory ducts (arrows) drain into the verumontanum. (B) The neurovascular bundle (NVB) (white circles) is situated parasagittally to the dorsolateral part of the peripheral zone of the prostate. From the NVB, vessels sprout towards the prostate. *Abbreviations*: ERC: endorectal coil.

3.2. PC Anatomy Related to Local, Regional and Metastatic Spread

Predilection sites for local extraprostatic PC spread include the apex, the neurovascular bundles, and the SV. Because the (pseudo)capsule is virtually non-existent at the apex, this region is vulnerable to extraprostatic spread. In peripheral zone PC, the most common location of extracapsular spread is dorsolaterally where the neurovascular bundles penetrate the capsule [16]. The SV can be invaded through direct growth of cancer along the ejaculatory ducts, by cancer extension outside the capsule and into the SV, or by isolated metastasis to the SV without adherence to the primary cancer focus [17].

PC is considered locally advanced if it penetrates the prostatic capsule, extends into the periprostatic fat, or invades the SV (i.e. TNM stage T3 [18]) or invades other surrounding organs, for instance the bladder or rectal wall (stage T4 disease).

PC metastatic degeneration is a lengthy, multistep process [19] and the major locations for systemic disease spread are the regional lymph nodes and the bones [20-22]. There is a wide variety of lymph drainage paths [23]. However, the nodes in the obturator fossa and around the internal iliac vessels appear to be the most frequent route of dissemination, occurring in 68% of autopsy patients that have lymph node metastatic disease, although a direct spread to the para-aortic lymph nodes has also been described (in 43%) [24-26]. The vertebral column, ribs, skull, and proximal ends of the long bones are the most frequent locations of metastatic bone disease due to their rich blood supply [27]. Such metastases are usually observed at high serum PSA levels (>20 ng/ml), even though they may also be present in patients with a high Gleason score (8-10) and relatively low PSA levels, i.e. a low PSA leak [28-31]. Only in late-stage PC are metastases to the lungs and liver seen [24]; other metastatic sites are anecdotal [25;32].

4. IMAGING TO EXCLUDE SYSTEMIC AND REGIONAL DISEASE

4.1. Exclusion of Metastatic Bone Disease

4.1.1. Conventional X-ray: Too insensitive

A 50% change in bone mineral density is needed for metastatic bone lesions to be visible on conventional X-ray images [33] and most PC lesions are sclerotic [24]. Comparing X-ray with bone scintigraphy, in 61% of all positive cases, the X-ray examination revealed fewer or no lesions compared with scintigraphy [34]. This was concurrent with another study which concluded that the X-ray examination detected approximately half of all cases of PC metastatic to bone [33]. Therefore, this modality is not sufficiently sensitive for detection of metastatic bone disease (Figure 3). It can, however, be used as an adjunctive tool to exclude false-positive findings due to conditions such as trauma, degenerative joint disease, or other chronic diseases on bone scintigraphy.

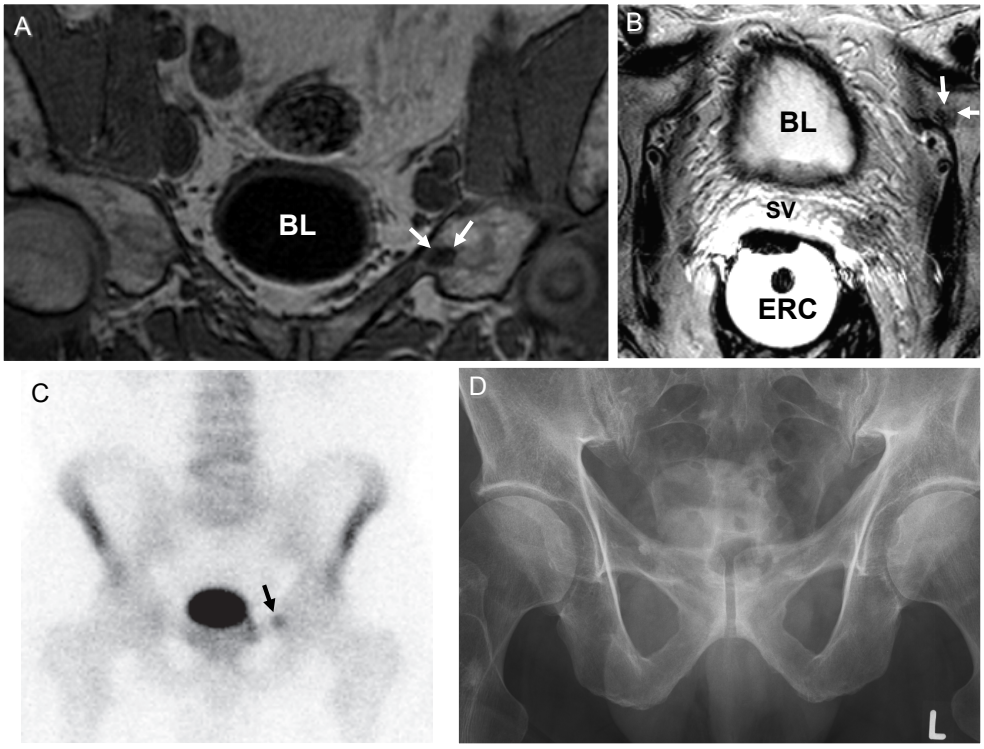

Figure 3: An example of the sensitivity of MR imaging and bone scintigraphy for detecting metastatic bone disease, which went undetected by the conventional X-ray examination. A 69-year-old man with histologically-proven prostate cancer (PSA level 12.1 ng/ml, Gleason score (3+4) in the left side of the prostate, normal digital rectal examination) underwent preoperative endorectal MR imaging. A round lesion (white arrows) with low signal intensity was observed in the left superior ramus of the ischium on (A) the T1-weighted magnetisation prepared rapid gradient-echo series and (B) the T2-weighted axial imaging series. (C) On bone scintigraphy, the hot spot (black arrow) was confirmed. (D) On the conventional X-ray image, however, no apparent lesion could be detected.

4.1.2. Computed tomography (CT) scanning: No studies reported

The literature search did not result in identifying any study performing CT scanning for determining PC metastatic bone disease.

4.1.3. Bone scintigraphy: Most Sensitive, Still the Standard of Reference

The first and foremost diagnostic test to detect or exclude metastatic bone disease is technetium-99m-diphosphonate bone scintigraphy. It is difficult to determine its true diagnostic performance since most often it is used as standard of reference. In a mixed group of cancer types, Charkes et al. validated bone scintigraphy by performing biopsy on all lesions observed on scintigraphy and found a detection rate of 79% [35]. Schaffer et

al. established a 100% sensitivity and 97% specificity with positive and negative predictive values of 97% and 100%, respectively [36].

A meta-analysis of 23 PC studies found detection rates of 2.3%, 5.3% and 16.2%, for patients with PSA levels below 10 ng/ml, between 10 and 19.9 ng/ml, and between 20 to 49.9 ng/ml, respectively. Above this level the detection rates rose accordingly [37]. In a large retrospective study comprising 852 patients, Oesterling et al. found that in patients with PSA levels below 20 ng/ml the false-negative rate was less than 2% [38]. In these patients, the negative predictive value for bone metastases was 87% [39]. This shows that an in-depth debate is necessary to determine the precise indications for bone scintigraphy. Bone scintigraphy lacks specificity as primary skeletal diseases such as degenerative joint disease, traumatic injury to the bones, and, more rarely, Paget's disease, bone infarcts, and primary neoplasms of the bone may cause false positive findings.

4.1.4. MR Imaging: Radiation-free, Fast, Whole-Body MR Imaging has Future Potential

Until recently, MR imaging of the whole body was impossible within clinically acceptable time periods. Today, whole-body MR imaging, which can be performed without having to adjust the patient position, appears to be a very sensitive tool for determining PC bone metastases. A 30-minute axial skeleton MR screening (a so-called 'marrow screening') correctly diagnosed 91% of patients, while the 9% of missed metastatic foci were located in the peripheral skeleton [40]. A study compromising a heterogeneous group of cancers showed that on a patient-by-patient basis, MR imaging scored better than bone scintigraphy in detecting metastatic bone disease [41]. A recent study in which axial skeleton MR imaging was performed in 66 patients revealed a 100% sensitivity and 88% specificity [42]. Advantages of MR imaging are the absence of radiation exposure and the ability to also detect non-skeletal metastases.

4.1.5. Positron Emission Tomography (PET) Scanning: FDG PET Less Sensitive Compared with Bone Scintigraphy But Promising for Therapy Follow-Up

Fluorine-18-labelled deoxyglucose (FDG) – Relatively few studies have performed PET for detecting metastatic PC. Bone metastases in PC are primarily sclerotic lesions, and these purely sclerotic lesions take up FDG less avidly in comparison to purely lytic or mixed metastases [43]. Sensitivity of FDG PET for detecting PC metastatic to bone varied between 18-75% [20;44-46]. In an analysis of androgen independent PC patients, only 24 of 131 (18%) sites that were positive on bone scintigraphy displayed increased FDG uptake [45]. A biological explanation might be that the metabolism of metastatic cells uses a substance different from glucose or that metastatic cells demonstrate a level of metabolism similar to normal bone marrow. In another study, FDG PET showed a high positive predictive value of 98% [44]. A limitation of this study was that most patients with metastatic disease detected by FDG PET had PSA levels over 50 ng/ml and metastatic disease was already established

or highly likely. Therefore, FDG PET may not be sufficiently accurate in patients with lower pre-test risk of metastatic disease. Generally, FDG PET is considered to be inferior to bone scintigraphy for PC [47]. Interestingly, however, Morris et al. showed that PET allowed earlier detection of a number of bone lesions compared to bone scintigraphy. These authors also suggested that FDG PET was able to discriminate between active and dormant lesions observed on bone scintigraphy [48]. An advantage of FDG PET over bone scintigraphy is its ability to detect also non-skeletal metastatic disease. An important role of PET imaging may lie in its ability to detect early treatment response in patients with metastatic disease receiving chemotherapy. This could spare patients weeks to months of on-going therapy with drugs that are not effective in shutting down cancer metabolism as evidenced by PET scan results [20].

Other radiopharmaceuticals – New radiopharmaceuticals are currently under study. A double-tracer study comparing FDG with carbon-11-labeled (^{11}C-) methionine PET in patients with progressive metastatic PC revealed that these radiopharmaceuticals had markedly different sensitivities in detecting bone lesions (48% and 72%, respectively) [20]. Heterogeneity of cancer metabolism, which correlates with metabolic transformation to a more malignant state, may account for these differences.

Uptake of ^{11}C-choline in PC foci is higher than FDG and, because it is not excreted via urine, does not obscure the prostate gland. In this respect, ^{11}C-choline PET was thought to be superior over FDG PET. However, non-specific uptake of ^{11}C-choline in bone marrow may lead to false-positive results [49]. A disadvantage of ^{11}C-methionine is the short half-life of the radionuclide, thereby restricting its use to study sites with access to a cyclotron.

A lesion-by-lesion comparison between a novel radiolabelled structural analogue of 5α-dihydrotestosterone, 16β-^{18}F-fluoro-5α-dihydrotestosterone (^{18}F-FDHT), which binds to androgen receptors, and FDG was performed [50]. In detection of mostly bone metastases in castrate patients with laboratory or clinical evidence of disease progression, the detection rates were 78% (46/59) for ^{18}F-FDHT and 97% (57/59) for FDG. Therapeutically, ^{18}F-FDHT may be applied to analyze the androgen receptor status of the metastases.

A recent study by Even-Sapir et al. directly compared ^{18}F-fluoride PET, ^{18}F-fluoride PET-CT, and bone scintigraphy in a patient population at high risk of bone metastases [51]. On a lesion-basis, the sensitivity of ^{18}F-fluoride PET, with or without combined CT scanning, was 100% in determining metastatic bone disease. While the specificity for ^{18}F-fluoride PET alone was only 79%, it increased to 100% when PET was fused with CT scanning. This technique, therefore, shows great promise in detection of metastatic bone disease.

4.1.6. ProstaScint® Scanning: Better Alternatives Available

One study concluded that the ProstaScint® (Cytogen Corporation, Princeton, NJ, U.S.A.) interpretation score did not significantly correlate with the risk of distant metastasis [52]. Considering the better performance of the alternative imaging modalities, ProstaScint® is not recommended for detecting metastatic bone disease.

4.2. Exclusion of Metastatic Lymph Node Disease (Table 1)

If the chance of lymph node metastasis is relatively high based on nomograms many institutions perform staging pelvic lymph node sampling [53] during radical prostatectomy or as a separate intervention before radical prostatectomy. The threshold levels for surgical intervention vary among institutions. However, imaging can play a role in selecting patients for lymph node sampling.

4.2.1. Ultrasound: No Role

Ultrasound plays no role in this phase of staging. Although it may possibly aid in characterizing superficial lymph nodes [54], deep lying lymph nodes would cause difficulties in visualization. A single study from 1988 on this topic showed 0% sensitivity in detecting positive PC lymph nodes [55].

4.2.2. CT Scanning: Size-Only Criteria with Low Sensitivity, But Well-Suited for Biopsy Procedures

CT interpretation of lymph nodes essentially is based on size and to a lesser extent on shape criteria. A recent systematic review of the accuracy in staging of lymph nodes in PC showed that CT was not sufficiently accurate, particularly in patients with PSA levels below 20 ng/ml and relatively well-differentiated cancer on biopsy. While the upper limit of normal lymph node size generally is 10 mm [56], some studies used thresholds as small as 6 mm [57]. While highly specific (95-100%), sensitivity is too low (0-25%) (Table 1) for it to be useful in regular clinical practice for the evaluation of metastatic lymph node disease [58]. Some authors advocate restricting the use of CT scanning for high risk patients (e.g. with PSA levels above 20 ng/ml) in order for it to be cost-effective [59;60]. In case a suspicious pelvic lymph node is observed, CT scanning is the imaging procedure of choice for performing biopsy and is associated with relatively few complications [57].

4.2.3. MR Imaging: Only Lymphotropic Contrast Agent Perfects Diagnostic Accuracy, However No Direct Biopsy Possibility Yet

Like CT scanning, conventional MR imaging uses size and shape criteria in assessing lymph node status. In a retrospective study of 174 patients, Wolf et al. found a 25% sensitivity of detection of positive lymph nodes with a 97% specificity [60] by MR imaging alone. In a recent landmark study comprising 80 patients from two centers, a sensitivity and specificity of respectively 35% and 90% were achieved on a node-by-node analysis [61]. A recent study

found that combining MR imaging of the lymph nodes with local MR imaging features of prostate cancer, such as extracapsular extension or seminal vesicle invasion, significantly increased the diagnostic accuracy [62].

MR lymphography (MRL) using lymphotropic ultrasmall superparamagnetic iron-oxide-containing (USPIO) nanoparticles that migrate to lymph nodes after intravenous injection and subsequent phagocytosis by macrophages [63], has heralded a new era in lymph node imaging. These contrast agents visualize nodes by disturbing the magnetic field, thereby turning healthy lymph nodes hypointense using an ironsensitive sequence (Figure 4). In metastastic lymph nodes, the metastatic deposits displace contrast-laden macrophages. Thereby, these areas of metastasis do not display disturbance to the magnetic field and therefore remain hyperintense. Using the USPIO agent ferumoxtran-10 (Combidex®/ Sinerem®, Guerbet, France), Harisinghani and Barentsz et al. achieved 97.3% accuracy with high sensitivity (90.5%) and specificity (97.8%) on a node-by-node basis [61]. A meta-analysis of studies using ferumoxtran-10 in various cancer types showed a significantly improved precision in lymph node staging [64].

MRL will provide major benefits to non-invasively evaluate the nodal status of patients with PC, particularly patients at high risk, and allow many to forego lymph node sampling. This will lead to fewer complications [65] and markedly decreased healthcare costs [23;66]. Furthermore, MRL should also enable the biopsy of lymph nodes that are outside the

Figure 4: An example of a positive internal iliac region 5.5 mm lymph node in a 66-year-old patient (PSA: 18 ng/ml, Gleason biopsy score (4+3), and abnormal DRE). (A) CT scan in sagittal reformat of a small lymph node of normal size. (B) Post-ferumoxtran-10 T1-weighted TSE MR image (which is insensitive to iron) shows one gray normal-sized node (circle). (C) On the post-ferumoxtran-10 T2*-weighted MEDIC MR image (which is iron-sensitive) this node is white (circle). Histopathology confirmed that the lymph node was completely involved by metastatic PC.

normal anatomical (obturator) area from which urologists routinely obtain samples [23]. MRL will improve staging and provide patients with more tailored treatment, which should translate into improved survival.
Inflamed lymph nodes could mimic positive findings. Hyperplastic, reactive lymph nodes will turn black after administration of ferumoxtran-10. An additional probable difficulty will be that during surgery the urologist may not find all the lymph nodes identified on MRL; this due to the small size of the nodes and the disturbed visual plane, a common feature during laparoscopic surgery. However, both the Food and Drug Administration (FDA) and the European Medicines Agency (EMEA) have not approved ferumoxtran-10 for clinical use. In future, proton MR spectroscopic imaging may possibly be of help in differentiating benign from malignant lymph nodes [67].

4.2.4. PET Scanning: Metabolic Information with Low Spatial Resolution and Risk of False-Positives

Poor anatomical correlation is a major limiting factor in interpreting images with PET. FDG PET uptake by positive lymph nodes is insufficiently consistent to be useful for decision-making [68]. The use of integrated PET-CT scanners improves image interpretation as CT will provide the anatomical background for abnormalities identified by PET.

An advantage of using ^{11}C-choline-PET over FDG-PET is that the urinary activity of ^{11}C-choline is negligible [49]. ^{11}C-choline-PET is able to detect lymph node metastases as small as 5 mm. Below this size, false-negativity is an important issue. False-positivity may be due to bowel motion, bowel uptake, reactive lymph nodes, or non-specific uptake in lymph nodes [69;70].

Improvement is required and new tracers are constantly being tested. In a preliminary study, ^{18}F-fluorocholine showed higher uptake in both primary and metastatic PC than FDG [71]. In another preliminary study in recurrence patients, ^{11}C-choline-PET revealed promising results with a high PPV of 86%, although the NPV was relatively low (72%) [72]. However, the presence of a cyclotron nearby is needed for these radionuclide tracers.

4.2.5. ProstaScint® Scanning: Costly, with Intermediate Diagnostic Accuracy

The ProstaScint® (Cytogen Corp., Princeton, NJ) scan uses Indium-111-labelled monoclonal antibodies specific for prostate-specific membrane antigen. Sensitivities and positive predictive values varied substantially, ranging between 17-75% and 11-79%, respectively, while specificities and negative predictive values were less variable between 72-94% (Table 1). Many studies, however, used the procedure in patients with already established or (very) high probability of metastatic disease [73;74]. Disadvantages that preclude its use in the routine diagnostic work-up are the high number of false-positives [75], the high costs, and the necessity of acquiring several scans over multiple days.

5. Patients in Whom Systemic Spread of Disease Has Been Excluded: Imaging to Exclude Locally Advanced Disease (Table 2, Figure 5)

After exclusion of systemic disease spread, the next clinical question is whether the disease is locally advanced or organ-confined. When locally advanced, curative surgery or radiation therapy may no longer be a curative option.

5.1. TRUS: Wide Range of Accuracies Found, No Strict Diagnostic Criteria

While no strict criteria for determining locally advanced disease have been formulated, bulging of the prostatic capsule is most often used. Accuracies of gray-scale TRUS in determining the local disease stage varied from 63 to 91%, with sensitivities and specificities ranging between 30-84% and 77-96%, respectively (Table 2). In most studies the accuracy for identification of SV invasion (81-97%) was higher than that of extracapsular extension (57-94%) [76-80].

Particularly, three-dimensional TRUS was found to aid in assessing local disease extension for both extracapsular extension and seminal vesicle invasion [78;81]. Also, increased capsular flow on color Doppler imaging has been applied as a criterion [82]. However, only one study performed staging with Doppler TRUS and showed a rather low (59%) sensitivity for detecting locally advanced disease [83].

5.2. CT Scanning: Radiation Burden and Low Sensitivity

Few recent studies have been published. A pre-radiation therapy staging study of 85 patients showed that CT staging had only a marginal effect on treatment decisions [84]. Platt et al. cautioned against using CT in decision-making for prostatectomy candidates due to suboptimal sensitivity (33%) and specificity (60%) for SV invasion, while for periprostatic fat invasion, sensitivity and specificity were 75% and 60%, respectively [85]. Hricak et al. found a low accuracy of 65% and noted that overstaging was a serious problem [86].

It is important to emphasize that most reports on CT staging studies were performed before the routine use of PSA. Thus with stage migration towards smaller volume and earlier-stage disease [87], the value of CT is further compromised. Two more recent studies revealed low sensitivity (26-29%) with a reasonable specificity (80-89%) [88;89].

5.3. MR and proton MR spectroscopic imaging (MRSI): High-Resolution Anatomical and Metabolic Information with High Sensitivity and Specificity

The application of MR imaging to determine whether PC is locally advanced remains controversial due to varying results across institutions. The most reliable MR signs of extracapsular extension are bulging of the prostate into the periprostatic fat, obliteration of the rectoprostatic angle, and asymmetry of the neurovascular bundles [90]. Seminal vesicle

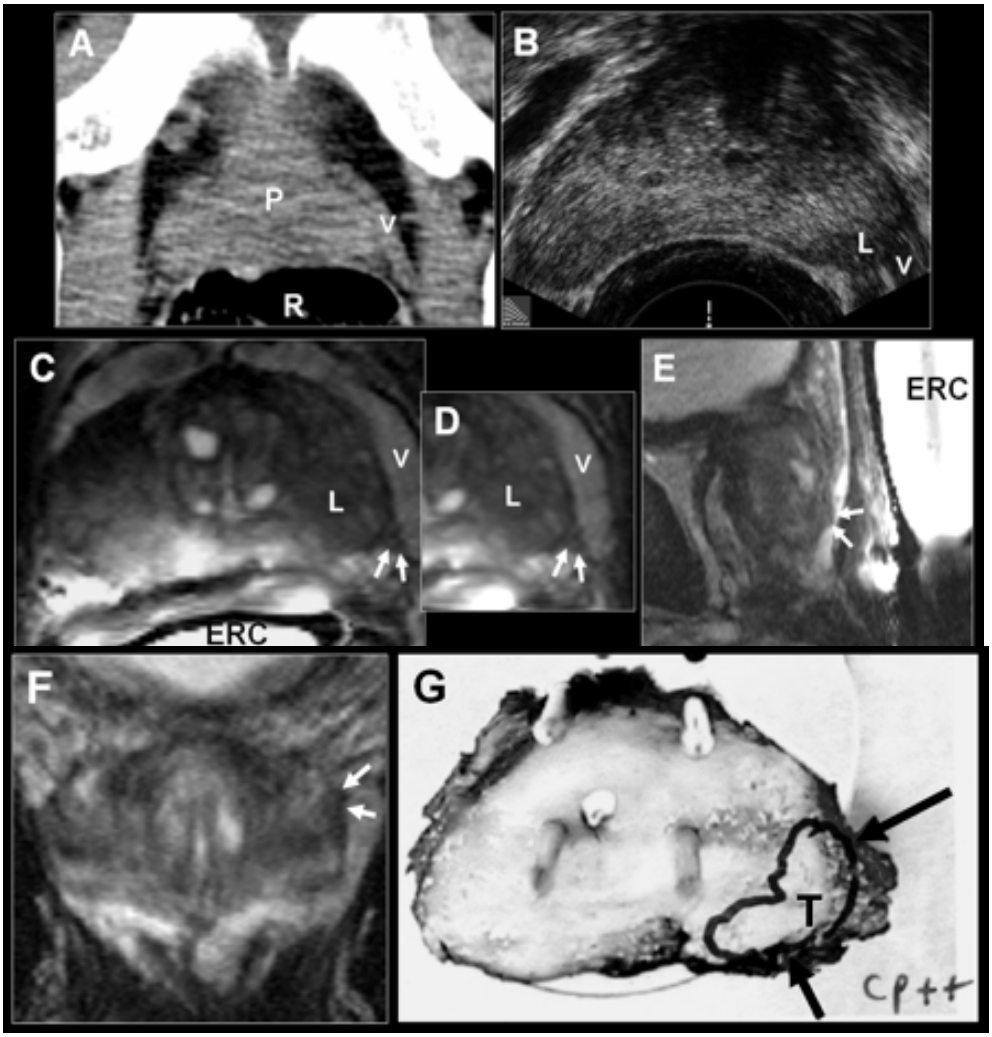

Figure 5: An example of imaging to detect locally advanced disease. A 63-year-old man with biopsy-proven prostate cancer (PSA level 8.2 ng/ml, Gleason biopsy sum score 7 on the left side of the prostate, negative digital rectal examination). (A) No abnormalities were seen on the CT scan. Note that it is difficult to distinguish the prostate (P) contour from the periprostatic venous plexus (v). (B) A TRUS examination showed a lesion (L) with low echogenicity in the left peripheral zone of the prostate near the neurovascular bundle. On both CT and TRUS the prostate cancer was staged as organ-confined disease. Endorectal 1.5T MR imaging in the axial (C), sagittal (E) and coronal (F) plane revealed an area of low signal intensity (L) in the left peripheral zone. This area extended into the periprostatic fat (white arrows, (D) magnified image of the area of capsular penetration) and the cancer was staged as locally advanced. Note that the venous plexus was distinguished easily from the prostatic capsule. (G) Histopathology confirmed the lesion (T) with a Gleason sum score of 7 and extracapsular extension (area between the black arrows) with a radial distance of 2 mm. *Abbreviations*: R: rectum, ERC: endorectal coil.

invasion is usually easily detectable by areas of low signal intensity in the brighter seminal fluid.

Two meta-analyses on local staging by MR imaging at 1.5 tesla (T) found combined maximum sensitivities and specificities of 71-74%, while sensitivity was 62-69% at a specificity of 80% [91;92]. Imaging in more than one plane as well as utilizing an endorectal coil resulted in a significantly better staging performance. A large study conducted by Cornud et al. comprising 336 patients found an overall sensitivity, specificity, positive, and negative predictive value of 40%, 95%, 79%, and 76%, respectively [93]. High-specificity MR reading (allowing only definite locally advanced cases to be excluded from curative therapy) is now the optimal local staging method [94;95].

It was established that adding MR imaging with an endorectal coil to clinical data such as PSA, biopsy Gleason score, or the Kattan nomogram resulted in a significantly increased accuracy of predicting disease stage, extracapsular extension, and seminal vesicle invasion [90;96;97]. Recently, it was shown that the presence and the degree of MR imaging predicted preradiation therapy extracapsular extension was a predictor of posttherapy outcomes [98].

Experience was found to be an important factor [99]. However, the accuracy of a less experienced reader could be increased by applying contrast agent [100]. Likewise, reading MR images with multiplanar cross-referencing significantly improved staging accuracy compared with reading without cross-referencing [101]. Also, addition of three-dimensional MRSI to MR imaging improved staging accuracies, particularly for less experienced readers and increased interobserver agreement [102]. A drawback is the longer duration (by approximately 15 minutes) of the examination.

Imaging at higher magnetic field strengths (e.g. 3T) results in higher image resolution. Although not yet widely available for clinical work, two studies on local staging at 3T reported sensitivities and specificities of experienced readers of 80-88% and 94-100%, respectively [103;104]. In the current PSA era, this higher resolution is mandatory as PC is detected at earlier stages. Likewise, if extracapsular extension is present, it will most often be minimal.

5.4. PET Scanning: No Studies Reported

The literature search did not result in identifying any study on the topic of PET to determine the local disease stage.

5.5. ProstaScint® Scanning: No Studies Reported

The literature search did not result in identifying any study directly using ProstaScint® to determine the local disease stage. One study did report that when integrating ProstaScint®

scores in an artificial neural network, it did not contribute to determining the local disease stage [52].

6. CONCLUSIONS

Exclusion of metastatic bone disease – Bone scintigraphy remains the single most sensitive method of detecting bone metastases. Targeted conventional X-ray can be used as an adjunct to scintigraphy to exclude false-positive findings. The use of bone scintigraphy should be limited to prevent its unnecessary use in patients with negligible risk of metastatic bone disease. Therefore, it should only be used in patients with PSA levels above 20 ng/ml or with biopsy Gleason scores of (4,3) or higher, or in whom the digital rectal examination was positive. In the future, whole-body MR imaging may play a role, especially due to the ability to detect also non-skeletal metastases within the same examination. Although still speculative, FDG-PET may be helpful in facilitating an early assessment of response to treatment. This may result in the patient being spared multiple cycles of chemotherapy with its inherent toxicity and costs.

Exclusion of metastatic lymph node disease – Lymph nodes are the first station of dissemination for PC and optimal sensitivity (91%) and specificity (98%) is achieved by using USPIO-enhanced MR imaging in patients with an intermediate to high risk of metastatic disease. FDG-PET scanning suffers from a lack of spatial resolution that is overcome by the use of integrated PET-CT, but generally low uptake of the radiopharmaceuticals in metastatic PC cells remains an important issue. FDG-PET may again serve as an early predictor of treatment response to a particular chemotherapy agent. CT scanning is too insensitive to be used in detecting positive lymph nodes but is the modality of choice for pelvic lymph node biopsy. With other alternatives available, ProstaScint® scanning should not be part of routine staging protocols.

Exclusion of locally advanced disease – Initial results of TRUS before the introduction of the PSA screening test were excellent. However, the subsequent stage migration towards less advanced cancers after the introduction of the PSA test necessitates staging modalities of higher resolution to assess correctly the extent of PC. MR imaging at 1.5T using an endorectal coil combined with a pelvic phased-array coil is currently the optimal clinical choice for determining the local disease stage. MRSI and contrast agents can be used to increase the staging accuracy for less experienced readers. With endorectal MR imaging at 3T, the sensitivity of detecting even minimal capsular penetration can be further increased. CT scanning is too insensitive to play a role in local disease staging.

A proposed scheme for optimal use of imaging in staging of prostate cancer is shown in Figure 6.

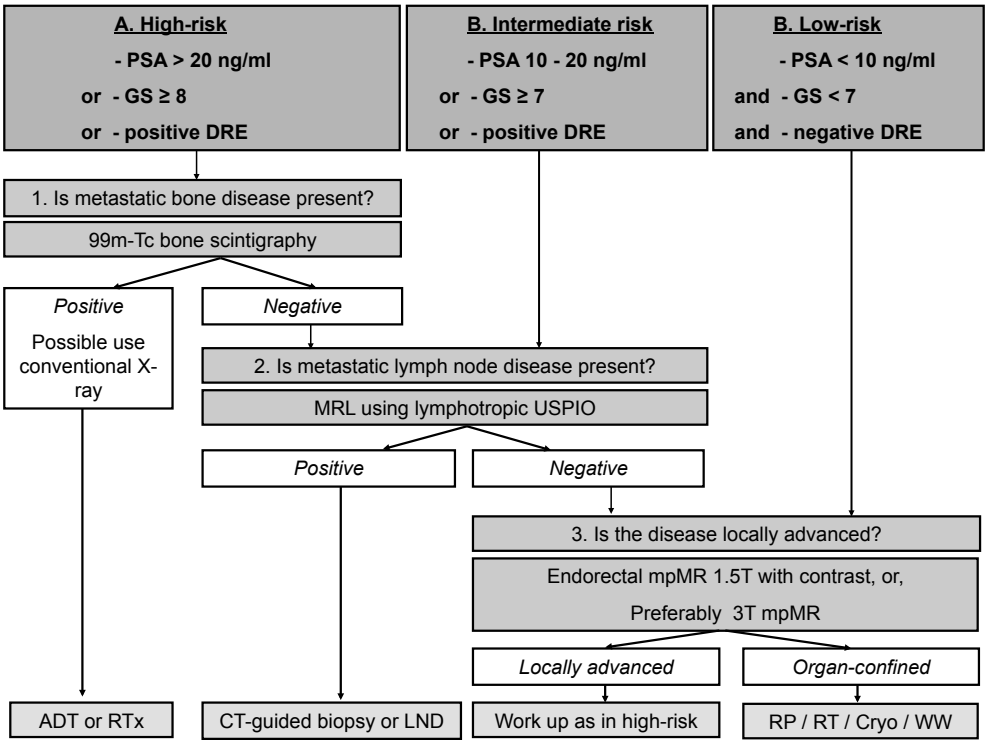

Figure 6: Proposed scheme for optimal use of imaging in patients in whom prostate cancer has been diagnosed. The scheme is based on three basic clinical questions that need to be answered and patient risk stratification: 1. Is metastatic bone disease present? 2. Is metastatic lymph node disease present? 3. Is the disease locally advanced? Each answer to these questions will change the course of therapy and each step can be aided by applying diagnostic imaging. A deviation from the AUA and EAU guidelines is indicated with double asterisks (**). *Abbreviations*: PSA: prostate-specific antigen, GS: Gleason biopsy sum score, DRE: digital rectal examination, Tc: Technetium, MRL: magnetic resonance lymphography, USPIO: ultrasmall paramagnetic iron-oxide containing particles, ADT: androgen deprivation therapy, RT: radiation therapy, CT: computed tomography, LND: lymph node dissection, WW: watchful waiting, RP: radical prostatectomy, Cryo: cryotherapy.

Table 1: Overview of Studies that Examined the Diagnostic Performance of Staging Metastatic Lymph Node Disease in Prostate Cancer by Imaging Modality

Imaging modality/ First author, publication date	Reference	Number of patients	Accuracy (%)	Sensitivity (%)	Specificity (%)	PPV (%)	NPV (%)	Standard of reference
Computed Tomography scanning			31-92	0-25	95-100	27-100	31-95	
Magnusson, 1988	[55]	42	69	7	100	100	68	PLND
Flanigan, 1996	[108]	173	92	25	95	27	95	PLND, CT-biopsy
Rørvik, 1998	[109]	50	86	25	98	67	87	PLND
Manyak, 1999	[110]	129	62	4	100	100	61	PLND
Borley, 2003	[111]	13	31	0	100	N/A	31	PLND
Magnetic Resonance imaging			65-98	27-100	79-100	50-100	67-100	
Jager, 1996	[112]	63	89	60	98	90	89	PLND, targeted biopsy, or autopsy
Borley, 2003	[111]	42	81	27	100	100	80	PLND
Harisinghani, 2003	[61]	80	65	45	79	60	67	PLND, CT-guided biopsy
Wang, 2006	[62]	441	88	27	98	50	96	PLND
USPIO								
Harisinghani, 2003	[61]	80	98	100	96	94	100	PLND, CT-guided biopsy
Positron Emission Tomography								
FDG								
Heicappell, 1999	[113]	17	88	67	100	100	85	PLND
^{11}C-choline								
De Jong, 2002	[69]	25	92	80	95	80	95	PLND
De Jong, 2003	[70]	67	93	80	96	86	94	N/A
^{18}F-Fluoride								
Even-Sapir, 2006	[51]	44	77	100	62	74	100	PET/CT, biopsy, or follow-up
ProstaScint® scanning			68-85	17-75	72-90	11-79	72-94	
Babaian, 1994	[114]	19	76	44	86	50	83	PLND
Hinkle, 1998	[115]	51	81	75	86	79	83	PLND
Manyak, 1999	[110]	152	68	63	72	62	72	PLND
Polascik, 1999	[116]	198	N/A	62	80	67	76	PLND
Rosenthal, 2001	[117]	152	68	63	72	62	72	PLND
Ponsky, 2002	[75]	22	85	17	90	11	94	PLND

Abbreviations: PPV: positive predictive value, NPV: negative predictive value, N/A: not available, PLND: pelvic lymph node dissection, USPIO: ultrasmall superparamagnetic iron-oxide particles, ^{18}F-FDG: 18-fluorine-labelled deoxyglucose, ^{11}C-choline: carbon-11 labelled choline.

Table 2: Overview of Studies that Examined the Diagnostic Performance of Local Disease Staging of Prostate Cancer by Imaging Modality.

Imaging modality/ First author, publication date	References	Number of patients	Accuracy (%)	Sensitivity (%)	Specificity (%)	PPV (%)	NPV (%)	Standard of reference
Transrectal ultrasound †								
Gray-scale			63-91	30-84	77-96	63-93	58-91	
Ekici, 1999	[77]	23	65	50	77	63	67	RP
May, 2001	[79]	54	63	30	96	89	58	RP
3D gray-scale								
Mitterberger, 2007	[81]	180	91	84	96	93	91	RP
Doppler								
Sauvain, 2003	[83]	63	79	59	94	89	76	RP
Computed Tomography scanning			47-67	29-50	73-89	48-86	47-77	
Hricak, 1987	[86]	46	67	38	73	61	68	RP
Platt, 1987	[85]	32	67	50	75	48	77	RP
Salo, 1987	[118]	38	57	39	88	83	47	RP
Tarcan, 1996	[88]	30	47	29	89	86	35	RP
Magnetic Resonance imaging ‡								
At 1.5 tesla			58-93	23-96	48-100	60-100	52-93	
Cornud, 2000	[119]	94	58	23	100	100	52	RP
May, 2001	[79]	54	72-93	93-96	48-93	65-93	93	RP
Cornud, 2002	[93]	336	76	40	95	79	76	RP
Nakashima, 2004	[120]	95	76	62	82	60	83	RP
Fütterer, 2005	[100]	99	79-84	50-60	93-97	78-91	79-83	RP
Graser, 2007	[121]	106	83-92	85-91	78-83	N/A	N/A	RP
At 3 tesla			89-94	73-88	96-100	92-100	88-96	
Fütterer, 2006	[103]	32	94	88	96	88	96	RP
Heijmink, 2007	[104]	46	89-94	73-80	97-100	92-100	88-91	RP

Abbreviations: PPV: positive predictive value, NPV: negative predictive value; RP: radical prostatectomy; N/A: not available.

†: Only English-language studies from the period 1999-2005 were included.

‡: Only English-language studies from the period 2000-2007 that used T2-weighted images obtained with an integrated pelvic phased-array and endorectal coil setup were included. For a full overview of all studies on this topic the reader is referred to two previously performed meta-analyses [91;92].

REFERENCES

[1] Siegel R, Naishadham D, Ward E, et al. Cancer statistics, 2008. CA Cancer J Clin 2012;62:10-29.

[2] Ross PL, Scardino PT, Kattan MW. A catalog of prostate cancer nomograms. J Urol 2001;165:1562-1568.

[3] Ross PL, Gerigk C, Gonen M, et al. Comparisons of nomograms and urologists' predictions in prostate cancer. Semin Urol Oncol 2002;20:82-88.

[4] Reckwitz T, Potter SR, Partin AW. Prediction of locoregional extension and metastatic disease in prostate cancer: a review. World J Urol 2000;18:165-172.

[5] Khan MA, Partin AW. Partin tables: past and present. BJU Int 2003; 92:7-11.

[6] Gleason DF. Histologic grade, clinical stage, and patient age in prostate cancer. NCI Monogr 1988;15-18.

[7] Gleason DF. Histologic grading of prostate cancer: a perspective. Hum Pathol 1992; 23:273-279.

[8] Sanda MG, Dunn RL, Michalski J, et al. Quality of life and satisfaction with outcome among prostate-cancer survivors. N Engl J Med 2008; 358:1250-1261.

[9] Bauvin E, Soulie M, Menegoz F, et al. Medical and non-medical determinants of prostate cancer management: a population-based study. Eur J Cancer 2003;39:2364-2371.

[10] Potosky AL, Davis WW, Hoffman RM, et al. Five-year outcomes after prostatectomy or radiotherapy for prostate cancer: the prostate cancer outcomes study. J Natl Cancer Inst 2004;96:1358-1367.

[11] Bill-Axelson A, Holmberg L, Ruutu M, et al. Radical prostatectomy versus watchful waiting in early prostate cancer. N Engl J Med 2005; 352:1977-1984.

[12] Coakley FV, Hricak H. Radiologic anatomy of the prostate gland: a clinical approach. Radiol Clin North Am 2000;38:15-30.

[13] Kiyoshima K, Yokomizo A, Yoshida T, et al. Anatomical features of periprostatic tissue and its surroundings: a histological analysis of 79 radical retropubic prostatectomy specimens. Jpn J Clin Oncol 2004;34:463-468.

[14] Villeirs GM, Verstraete L, De Neve WJ, De Meerleer GO. Magnetic resonance imaging anatomy of the prostate and periprostatic area: a guide for radiotherapists. Radiother Oncol 2005;76:99-106.

[15] Aumuller G, Riva A. Morphology and functions of the human seminal vesicle. Andrologia 1992;24:183-196.

[16] McNeal JE, Villers AA, Redwine EA, Freiha FS, Stamey TA. Capsular penetration in prostate cancer. Significance for natural history and treatment. Am J Surg Pathol 1990; 14:240-247.

[17] Ohori M, Scardino PT, Lapin SL, Seale-Hawkins C, Link J, Wheeler TM. The mechanisms and prognostic significance of seminal vesicle involvement by prostate cancer. Am J Surg Pathol 1993; 17:1252-1261.

[18] Greene F, Page D, Fleming I, et al. AJCC Cancer Staging Manual. 6th ed. New York: Springer Verlag, 2002.

[19] Singh AS, Figg WD. In vivo models of prostate cancer metastasis to bone. J Urol 2005;174:820-826.

[20] Nunez R, Macapinlac HA, Yeung HW, et al. Combined 18F-FDG and 11C-methionine PET scans in patients with newly progressive metastatic prostate cancer. J Nucl Med 2002;43:46-55.

[21] Thurairaja R, McFarlane J, Traill Z, Persad R. State-of-the-art approaches to detecting early bone metastasis in prostate cancer. BJU Int 2004;94:268-271.

[22] Hess KR, Varadhachary GR, Taylor SH, et al. Metastatic patterns in adenocarcinoma. Cancer 2006;106:1624-1633.

[23] Burkhard FC, Studer UE. The role of lymphadenectomy in prostate cancer. Urol Oncol 2004;22:198-202.

[24] Elkin M, Mueller HP. Metastases from cancer of the prostate; autopsy and roentgenological findings. Cancer 1954;7:1246-1248.

[25] Saitoh H, Yoshida K, Uchijima Y, Kobayashi N, Suwata J, Kamata S. Two different lymph node metastatic patterns of a prostatic cancer. Cancer 1990;65:1843-1846.

[26] Wawroschek F, Vogt H, Wengenmair H, et al. Prostate lymphoscintigraphy and radio-guided surgery for sentinel lymph node identification in prostate cancer. Technique and results of the first 350 cases. Urol Int 2003;70:303-310.

[27] Carlin BI, Andriole GL. The natural history, skeletal complications, and management of bone metastases in patients with prostate carcinoma. Cancer 2000;88:2989-2994.

[28] Aihara M, Lebovitz RM, Wheeler TM, Kinner BM, Ohori M, Scardino PT. Prostate specific antigen and gleason grade: an immunohistochemical study of prostate cancer. J Urol 1994;151:1558-1564.

[29] Wolff JM, Bares R, Jung PK, Buell U, Jakse G. Prostate-specific antigen as a marker of bone metastasis in patients with prostate cancer. Urol Int 1996;56:169-173.

[30] Wolff JM, Zimny M, Borchers H, Wildberger J, Buell U, Jakse G. Is prostate-specific antigen a reliable marker of bone metastasis in patients with newly diagnosed cancer of the prostate? Eur Urol 1998;33:376-381.

[31] Birtle AJ, Freeman A, Masters JR, Payne HA, Harland SJ. Clinical features of patients who present with metastatic prostate carcinoma and serum prostate-specific antigen. (PSA) levels < 10 ng/mL: the "PSA negative" patients. Cancer 2003;98:2362-2367.

[32] Long MA, Husband JE. Features of unusual metastases from prostate cancer. Br J Radiol 1999;72:933-941.

[33] Lentle BC, McGowan DG, Dierich H. Technetium-99M polyphosphate bone scanning in carcinoma of the prostate. Br J Urol 1974;46:543-548.

[34] Osmond JD, III, Pendergrass HP, Potsaid MS. Accuracy of 99mTC-diphosphonate bone scans and roentgenograms in the detection of prostate, breast and lung carcinoma metastases. Am J Roentgenol Radium Ther Nucl Med 1975;125:972-977.

[35] Charkes ND, Young I, Sklaroff DM. The pathologic basis of the strontium bone scan. Studies following administration of strontium chloride Sr 85 and strontium nitrate Sr 85. JAMA 1968;206:2482-2488.

[36] Schaffer DL, Pendergrass HP. Comparison of enzyme, clinical, radiographic, and radionuclide methods of detecting bone metastases from carcinoma of the prostate. Radiology 1976;121:431-434.

[37] Abuzallouf S, Dayes I, Lukka H. Baseline staging of newly diagnosed prostate cancer: a summary of the literature. J Urol 2004;171:2122-2127.

[38] Oesterling JE, Martin SK, Bergstralh EJ, Lowe FC. The use of prostate-specific antigen in staging patients with newly diagnosed prostate cancer. JAMA 1993;269:57-60.

[39] Bruwer G, Heyns CF, Allen FJ. Influence of local tumour stage and grade on reliability of serum prostate-specific antigen in predicting skeletal metastases in patients with adenocarcinoma of the prostate. Eur Urol 1999;35:223-227.

[40] Traill ZC, Talbot D, Golding S, Gleeson FV. Magnetic resonance imaging versus radionuclide scintigraphy in screening for bone metastases. Clin Radiol 1999;54:448-451.

[41] Lauenstein TC, Goehde SC, Herborn CU, et al. Whole-body MR imaging: evaluation of patients for metastases. Radiology 2004;233:139-148.

[42] Lecouvet FE, Geukens D, Stainier A, et al. Magnetic resonance imaging of the axial skeleton for detecting bone metastases in patients with high-risk prostate cancer: diagnostic and cost-effectiveness and comparison with current detection strategies. J Clin Oncol 2007;25:3281-3287.

[43] Cook GJ, Houston S, Rubens R, Maisey MN, Fogelman I. Detection of bone metastases in breast cancer by 18FDG PET: differing metabolic activity in osteoblastic and osteolytic lesions. J Clin Oncol 1998;16:3375-3379.

[44] Shreve PD, Grossman HB, Gross MD, Wahl RL. Metastatic prostate cancer: initial findings of PET with 2-deoxy-2-[F-18]fluoro-D-glucose. Radiology 1996;199:751-756.

[45] Yeh SD, Imbriaco M, Larson SM, et al. Detection of bony metastases of androgen-independent prostate cancer by PET-FDG. Nucl Med Biol 1996;23:693-697.

[46] Oyama N, Akino H, Suzuki Y, et al. The increased accumulation of [18F] fluorodeoxyglucose in untreated prostate cancer. Jpn J Clin Oncol 1999;29:623-629.

[47] Shreve PD, Grossman HB, Gross MD, Wahl RL. Metastatic prostate cancer: initial findings of PET with 2-deoxy-2-[F-18]fluoro-D-glucose. Radiology 1996;199:751-756.

[48] Morris MJ, Akhurst T, Osman I, et al. Fluorinated deoxyglucose positron emission tomography imaging in progressive metastatic prostate cancer. Urology 2002;59:913-918.

[49] Hara T, Kosaka N, Kishi H. PET imaging of prostate cancer using carbon-11-choline. J Nucl Med 1998;39:990-995.

[50] Larson SM, Morris M, Gunther I, et al. Tumor localization of 16beta-18F-fluoro-5alpha-dihydrotestosterone versus 18F-FDG in patients with progressive, metastatic prostate cancer. J Nucl Med 2004;45:366-373.

[51] Even-Sapir E, Metser U, Mishani E, Lievshitz G, Lerman H, Leibovitch I. The detection of bone metastases in patients with high-risk prostate cancer: 99mTc-MDP planar bone scintigraphy, single- and multi-field-of-view SPECT, 18F-Fluoride PET, and 18F-Fluoride PET/CT. J Nucl Med 2006;47:287-297.

[52] Murphy GP, Snow PB, Brandt J, Elgamal A, Brawer MK. Evaluation of prostate cancer patients receiving multiple staging tests, including ProstaScint scintiscans. Prostate 2000;42:145-149.

[53] Heidenreich A, Ohlmann CH, Polyakov S. Anatomical extent of pelvic lymphadenectomy in patients undergoing radical prostatectomy. Eur Urol 2007;52:29-37.

[54] Esen G. Ultrasound of superficial lymph nodes. Eur J Radiol 2006;58:345-359.

[55] Magnusson A, Fritjofsson A, Norlen BJ, Wicklund H. The value of computed tomography and ultrasound in assessment of pelvic lymph node metastases in patients with clinically locally confined carcinoma of the prostate. Scand J Urol Nephrol 1988;22:7-10.

[56] Salo JO, Kivisaari L, Rannikko S, Lehtonen T. The value of CT in detecting pelvic lymph node metastases in cases of bladder and prostate carcinoma. Scand J Urol Nephrol 1986;20:261-265.

[57] Oyen RH, Van Poppel HP, Ameye FE, Van de Voorde WA, Baert AL, Baert LV. Lymph node staging of localized prostatic carcinoma with CT and CT-guided fine-needle aspiration biopsy: prospective study of 285 patients. Radiology 1994;190:315-322.

[58] Tiguert R, Gheiler EL, Tefilli MV, et al. Lymph node size does not correlate with the presence of prostate cancer metastasis. Urology 1999;53:367-371.

[59] Levran Z, Gonzalez JA, Diokno AC, Jafri SZ, Steinert BW. Are pelvic computed tomography, bone scan and pelvic lymphadenectomy necessary in the staging of prostatic cancer? Br J Urol 1995;75:778-781.

[60] Wolf JS, Jr., Cher M, Dall'era M, Presti JC, Jr., Hricak H, Carroll PR. The use and accuracy of cross-sectional imaging and fine needle aspiration cytology for detection of pelvic lymph node metastases before radical prostatectomy. J Urol 1995;153:993-999.

[61] Harisinghani MG, Barentsz J, Hahn PF, et al. Noninvasive detection of clinically occult lymph-node metastases in prostate cancer. N Engl J Med 2003;348:2491-2499.

[62] Wang L, Hricak H, Kattan MW, et al. Combined endorectal and phased-array MRI in the prediction of pelvic lymph node metastasis in prostate cancer. AJR Am J Roentgenol 2006;186:743-748.

[63] Saksena MA, Saokar A, Harisinghani MG. Lymphotropic nanoparticle enhanced MR imaging (LNMRI) technique for lymph node imaging. Eur J Radiol 2006;58(3):367-74.

[64] Will O, Purkayastha S, Chan C, et al. Diagnostic precision of nanoparticle-enhanced MRI for lymph-node metastases: a meta-analysis. Lancet Oncol 2006;7:52-60

[65] Link RE, Morton RA. Indications for pelvic lymphadenectomy in prostate cancer. Urol Clin North Am 2001;28:491-498.

[66] Hovels AM, Heesakkers RA, Adang EM, Jager GJ, Barentsz JO. Cost-analysis of staging methods for lymph nodes in patients with prostate cancer: MRI with a lymph node-specific contrast agent compared to pelvic lymph node dissection or CT. Eur Radiol 2004;14:1707-1712.

[67] Heijmink SWTPJ, Scheenen TWJ, Futterer JJ, et al. Prostate and lymph node proton magnetic resonance (MR) spectroscopic imaging with external array coils at 3 T to detect recurrent prostate cancer after radiation therapy. Invest Radiol 2007;42:420-427.

[68] Sanz G, Robles JE, Gimenez M, et al. Positron emission tomography with 18fluorine-labelled deoxyglucose: utility in localized and advanced prostate cancer. BJU Int 1999;84:1028-1031.

[69] de Jong IJ, Pruim J, Elsinga PH, Vaalburg W, Mensink HJ. Visualization of prostate cancer with 11C-choline positron emission tomography. Eur Urol 2002;42:18-23.

[70] de Jong IJ, Pruim J, Elsinga PH, Vaalburg W, Mensink HJ. Preoperative staging of pelvic lymph nodes in prostate cancer by 11C-choline PET. J Nucl Med 2003;44:331-335.

[71] Price DT, Coleman RE, Liao RP, Robertson CN, Polascik TJ, DeGrado TR. Comparison of [18 F]fluorocholine and [18 F]fluorodeoxyglucose for positron emission tomography of androgen dependent and androgen independent prostate cancer. J Urol 2002;168:273-280.

[72] Scattoni V, Picchio M, Suardi N, et al. Detection of lymph-node metastases with integrated [11C]choline PET/CT in patients with PSA failure after radical retropubic prostatectomy: results confirmed by open pelvic-retroperitoneal lymphadenectomy. Eur Urol 2007;52:423-429.

[73] Sodee DB, Malguria N, Faulhaber P, Resnick MI, Albert J, Bakale G. Multicenter ProstaScint imaging findings in 2154 patients with prostate cancer. The ProstaScint Imaging Centers. Urology 2000;56:988-993.

[74] Lange PH. PROSTASCINT scan for staging prostate cancer. Urology 2001;57:402-406.

[75] Ponsky LE, Cherullo EE, Starkey R, Nelson D, Neumann D, Zippe CD. Evaluation of preoperative ProstaScint scans in the prediction of nodal disease. Prostate Cancer Prostatic Dis 2002;5:132-135.

[76] Presti JC, Jr., Hricak H, Narayan PA, Shinohara K, White S, Carroll PR. Local staging of prostatic carcinoma: comparison of transrectal sonography and endorectal MR imaging. AJR Am J Roentgenol 1996;166:103-108.

[77] Ekici S, Ozen H, Agildere M, et al. A comparison of transrectal ultrasonography and endorectal magnetic resonance imaging in the local staging of prostatic carcinoma. BJU Int 1999;83:796-800.

[78] Garg S, Fortling B, Chadwick D, Robinson MC, Hamdy FC. Staging of prostate

cancer using 3-dimensional transrectal ultrasound images: a pilot study. J Urol 1999;162:1318-1321.

[79] May F, Treumann T, Dettmar P, Hartung R, Breul J. Limited value of endorectal magnetic resonance imaging and transrectal ultrasonography in the staging of clinically localized prostate cancer. BJU Int 2001;87:66-69.

[80] Okihara K, Kamoi K, Lane RB, Evans RB, Troncoso P, Babaian RJ. Role of systematic ultrasound-guided staging biopsies in predicting extraprostatic extension and seminal vesicle invasion in men with prostate cancer. J Clin Ultrasound 2002; 30:123-131.

[81] Mitterberger M, Pinggera GM, Pallwein L, et al. The value of three-dimensional transrectal ultrasonography in staging prostate cancer. BJU Int 2007;100:47-50.

[82] Ismail M, Petersen RO, Alexander AA, Newschaffer C, Gomella LG. Color Doppler imaging in predicting the biologic behavior of prostate cancer: correlation with disease-free survival. Urology 1997;50:906-912.

[83] Sauvain JL, Palascak P, Bourscheid D, et al. Value of power doppler and 3D vascular sonography as a method for diagnosis and staging of prostate cancer. Eur Urol 2003;44:21-30.

[84] Burcombe RJ, Ostler PJ, Ayoub AW, Hoskin PJ. The role of staging CT scans in the treatment of prostate cancer: a retrospective audit. Clin Oncol (R Coll Radiol) 2000;12:32-35.

[85] Platt JF, Bree RL, Schwab RE. The accuracy of CT in the staging of carcinoma of the prostate. AJR Am J Roentgenol 1987;149:315-318.

[86] Hricak H, Dooms GC, Jeffrey RB, et al. Prostatic carcinoma: staging by clinical assessment, CT, and MR imaging. Radiology 1987;162:331-336.

[87] Derweesh IH, Kupelian PA, Zippe C, et al. Continuing trends in pathological stage migration in radical prostatectomy specimens. Urol Oncol 2004;22:300-306.

[88] Tarcan T, Turkeri L, Biren T, Kullu S, Gurmen N, Akdas A. The effectiveness of imaging modalities in clinical staging of localized prostatic carcinoma. Int Urol Nephrol 1996;28:773-779.

[89] Barbieri A, Monica B, Sebastio N, Incarbone GP, Di Stefano C. [Value and limitations of transrectal ultrasonography and computer tomography in preoperative staging of prostate carcinoma]. Acta Biomed Ateneo Parmense 1997;68:23-26.

[90] Wang L, Mullerad M, Chen HN, et al. Prostate cancer: incremental value of endorectal MR imaging findings for prediction of extracapsular extension. Radiology 2004;232:133-139.

[91] Sonnad SS, Langlotz CP, Schwartz JS. Accuracy of MR imaging for staging prostate cancer: a meta-analysis to examine the effect of technologic change. Acad Radiol 2001;8:149-157.

[92] Engelbrecht MR, Jager GJ, Laheij RJ, Verbeek AL, van Lier HJ, Barentsz JO. Local staging of prostate cancer using magnetic resonance imaging: a meta-analysis. Eur Radiol 2002;12:2294-2302.

[93] Cornud F, Flam T, Chauveinc L, et al. Extraprostatic spread of clinically localized prostate cancer: factors predictive of pT3 tumor and of positive endorectal MR imaging examination results. Radiology 2002;224:203-210.

[94] Langlotz CP, Schnall MD, Malkowicz SB, Schwartz JS. Cost-effectiveness of endorectal magnetic resonance imaging for the staging of prostate cancer. Acad Radiol 1996;3 Suppl 1:S24-S27.

[95] Jager GJ, Severens JL, Thornbury JR, de la Rosette JJ, Ruijs SH, Barentsz JO. Prostate cancer staging: should MR imaging be used?--A decision analytic approach. Radiology 2000;215:445-451.

[96] Wang L, Hricak H, Kattan MW, Chen HN, Scardino PT, Kuroiwa K. Prediction of organ-confined prostate cancer: incremental value of MR Imaging and MR spectroscopic imaging to staging

nomograms. Radiology 2006;238:597-603.

[97] Wang L, Hricak H, Kattan MW, et al. Prediction of seminal vesicle invasion in prostate cancer: incremental value of adding endorectal MR imaging to the Kattan nomogram. Radiology 2007;242:182-188.

[98] McKenna DA, Coakley FV, Westphalen AC, et al. Prostate Cancer: Role of Pretreatment MR in Predicting Outcome after External-Beam Radiation Therapy--Initial Experience. Radiology 2008;247(1):141-6.

[99] Mullerad M, Hricak H, Wang L, Chen HN, Kattan MW, Scardino PT. Prostate cancer: detection of extracapsular extension by genitourinary and general body radiologists at MR imaging. Radiology 2004;232:140-146.

[100] Fütterer JJ, Engelbrecht MR, Huisman HJ, et al. Staging Prostate Cancer with Dynamic Contrast-enhanced Endorectal MR Imaging prior to Radical Prostatectomy: Experienced versus Less Experienced Readers. Radiology 2005;237:541-549.

[101] Wang L, Zhang J, Schwartz LH, et al. Incremental value of multiplanar cross-referencing for prostate cancer staging with endorectal MRI. AJR Am J Roentgenol 2007;188:99-104.

[102] Yu KK, Scheidler J, Hricak H, et al. Prostate cancer: prediction of extracapsular extension with endorectal MR imaging and three-dimensional proton MR spectroscopic imaging. Radiology 1999;213:481-488.

[103] Fütterer JJ, Heijmink SW, Scheenen TW, et al. Prostate cancer: local staging at 3-T endorectal MR imaging--early experience. Radiology 2006;238:184-191.

[104] Heijmink SWTPJ, Futterer JJ, Hambrock T, et al. Prostate Cancer: Body-Array versus Endorectal Coil MR Imaging at 3 T--Comparison of Image Quality, Localization, and Staging Performance. Radiology 2007;244:184-195.

[105] Thompson I, Thrasher JB, Aus G, et al. Guideline for the management of clinically localized prostate cancer: 2007 update. J Urol 2007;177:2106-2131.

[106] Heidenreich A, Aus G, Abbou CC, et al. Guidelines on prostate cancer 2007.

[107] AUA report on the management of clinically localized prostate cancer.

[108] Flanigan RC, McKay TC, Olson M, Shankey TV, Pyle J, Waters WB. Limited efficacy of preoperative computed tomographic scanning for the evaluation of lymph node metastasis in patients before radical prostatectomy. Urology 1996;48:428-432.

[109] Rorvik J, Halvorsen OJ, Albrektsen G, Haukaas S. Lymphangiography combined with biopsy and computer tomography to detect lymph node metastases in localized prostate cancer. Scand J Urol Nephrol 1998;32:116-119.

[110] Manyak MJ, Hinkle GH, Olsen JO, et al. Immunoscintigraphy with indium-111-capromab pendetide: evaluation before definitive therapy in patients with prostate cancer. Urology 1999;54:1058-1063.

[111] Borley N, Fabrin K, Sriprasad S, et al. Laparoscopic pelvic lymph node dissection allows significantly more accurate staging in “high-risk” prostate cancer compared to MRI or CT. Scand J Urol Nephrol 2003;37:382-386.

[112] Jager GJ, Barentsz JO, Oosterhof GO, Witjes JA, Ruijs SJ. Pelvic adenopathy in prostatic and urinary bladder carcinoma: MR imaging with a three-dimensional TI-weighted magnetization-prepared-rapid gradient-echo sequence. AJR Am J Roentgenol 1996;167:1503-1507.

[113] Heicappell R, Muller-Mattheis V, Reinhardt M, et al. Staging of pelvic lymph nodes in neoplasms of the bladder and prostate by positron emission tomography with 2-[(18)F]-2-deoxy-D-glucose. Eur Urol 1999;36:582-587.

[114] Babaian RJ, Sayer J, Podoloff DA, Steelhammer LC, Bhadkamkar VA, Gulfo JV. Radioimmunoscintigraphy of pelvic

lymph nodes with 111indium-labeled monoclonal antibody CYT-356. J Urol 1994;152:1952-1955.

[115] Hinkle GH, Burgers JK, Neal CE, et al. Multicenter radioimmunoscintigraphic evaluation of patients with prostate carcinoma using indium-111 capromab pendetide. Cancer 1998; 83:739-747.

[116] Polascik TJ, Manyak MJ, Haseman MK, et al. Comparison of clinical staging algorithms and 111indium-capromab pendetide immunoscintigraphy in the prediction of lymph node involvement in high risk prostate carcinoma patients. Cancer 1999;85:1586-1592.

[117] Rosenthal SA, Haseman MK, Polascik TJ. Utility of capromab pendetide (ProstaScint) imaging in the management of prostate cancer. Tech Urol 2001;7:27-37.

[118] Salo JO, Kivisaari L, Rannikko S, Lehtonen T. Computerized tomography and transrectal ultrasound in the assessment of local extension of prostatic cancer before radical retropubic prostatectomy. J Urol 1987;137:435-438.

[119] Cornud F, Hamida K, Flam T, et al. Endorectal color doppler sonography and endorectal MR imaging features of nonpalpable prostate cancer: correlation with radical prostatectomy findings. AJR Am J Roentgenol 2000;175:1161-1168.

[120] Nakashima J, Tanimoto A, Imai Y, et al. Endorectal MRI for prediction of tumor site, tumor size, and local extension of prostate cancer. Urology 2004;64:101-105.

[121] Graser A, Heuck A, Sommer B, et al. Per-sextant localization and staging of prostate cancer: correlation of imaging findings with whole-mount step section histopathology. AJR Am J Roentgenol 2007;188:84-90.

CHAPTER 4

Prostate Cancer: Local Staging at 3-T Endorectal MR Imaging—Early Experience

Jurgen J. Fütterer
Stijn W. T. P. J. Heijmink
Tom W. J. Scheenen
Gerrit J. Jager
Christina A. Hulsbergen-Van de Kaa
J. Alfred Witjes
Jelle O. Barentsz

Radiology 2006;238(1):184-91.

Purpose: To prospectively investigate the local staging accuracy of 3-T endorectal magnetic resonance (MR) imaging for prostate cancer by using whole-mount-section histopathologic analysis as the standard of reference.

Materials and Methods: This study was approved by the institutional review board, and informed consent was obtained from all patients. In 35 consecutive patients (median age, 62.3 years) with biopsy-proved prostate cancer, 3-T endorectal MR imaging was performed. High-spatial-resolution endorectal T2-weighted fast spin-echo images of the prostate were obtained in three planes. MR images were prospectively evaluated by two experienced radiologists and a third radiologist who was less experienced with regard to local disease extent by using five established extracapsular criteria. Whole-mount-section histopathologic analysis was the standard of reference. Evaluation was performed according to octant and patient. Sensitivity, specificity, positive and negative predictive values, overall accuracy, and interobserver agreement were calculated.

Results: Thirty-two patients who underwent radical prostatectomy were enrolled in this study. Accuracy, sensitivity, and specificity of local staging were 94% (30 of 32), 88% (seven of eight), and 96% (23 of 24), respectively, for both experienced radiologists, and these values were 81% (26 of 32), 50% (four of eight), and 92% (22 of 24), respectively, for the less experienced radiologist. There was substantial agreement between both experienced readers ($\kappa = 0.42–0.79$) and moderate agreement between the less experienced reader and the experienced readers with respect to all extracapsular criteria. In regard to the three cases of minimal capsular invasion, two were detected by both experienced radiologists.

Conclusion: In this study, high accuracy for staging of prostate cancer at 3-T endorectal MR imaging, with moderate to substantial observer agreement, was demonstrated. In addition, minimal capsular invasion could be detected.

Prostate carcinoma is the second most frequent cause of cancer-related death in men [1]. The increase in the number of the aged, as well as the advent and the ever more frequent use of the prostate-specific antigen serum test for detection, has resulted in an increase in prostate cancer incidence [2,3]. Determination of the tumor extension in prostate cancer is important not only to allow optimal choice between the various therapeutic options but also to influence prognosis and treatment [4–6].

Presently, the role of magnetic resonance (MR) imaging of the prostate for detection of extension beyond the capsule is being debated because of limited availability, high costs, and variability in results [7–9]. A large heterogeneity in local staging performance exists [4,9–14]. A frequently described limitation is the inability to demonstrate microscopic capsular penetration [7].

MR imaging at 1.5-T (the standard clinical field strength) with T2-weighted fast spin-echo sequences and combined endorectal and phased-array coils has enabled the acquisition of MR images of the prostate and its surrounding tissues with high spatial resolution. Although a relatively high spatial resolution can be achieved within a clinically acceptable examination time, reported accuracy values for staging vary from 54% to 88% [4,7–15]. Jager et al [16] stated that staging with MR imaging in the preoperative work-up of prostate cancer is cost effective and should be performed with a high specificity (95%). In attaining this specificity, however, a low sensitivity (36%) has to be considered [17].

For several years, whole-body MR imaging at high magnetic field strengths (>1.5 T) has been used for research purposes only. At present, however, high-field-strength MR imaging systems are becoming more widely available in routine clinical settings. Generally, use of a higher field strength increases the signal-to-noise ratio linear to the magnetic field strength [18], thereby affording the possibility of an increase in either the spatial or the temporal resolution of MR imaging. Other effects of clinical MR imaging at high field strengths are the increased susceptibility differences in tissues that cause magnetic field inhomogeneities, as well as possibly shorter T2 along with longer T1 relaxation times.

Preliminary results with endorectal MR imaging at 3 T in patients with prostate cancer contributed to increased spatial resolution of T2-weighted imaging with a voxel volume of 13 μm3 [19]. To the authors' knowledge, the role of endorectal MR imaging at magnetic field strengths of 3 T in the evaluation of local staging in patients with prostate cancer prior to radical prostatectomy has not yet been reported. Thus, the purpose of our study was to prospectively investigate the local staging accuracy of 3-T endorectal MR imaging for prostate cancer by using whole-mount-section histopathologic analysis as the standard of reference.

MATERIALS AND METHODS

Medrad, Pittsburgh, Pa, supplied the prototypes of balloon-mounted disposable endorectal surface coils and interface devices. The authors, however, had control of the data and the information submitted for publication.

Patient Characteristics

From July 2002 until July 2004, 35 consecutive patients with biopsy-proved prostate cancer underwent endorectal coil MR imaging examinations at 3 T. Patients who were scheduled for radical prostatectomy within 6 weeks (range, 2–42 days; median, 8 days) after MR imaging were included in the study. Exclusion criteria were previous hormonal therapy, lymph nodes positive for metastases at frozen section analysis during surgery, contraindications to MR imaging (eg, cardiac pacemakers, intracranial clips), and contraindications to endorectal coil insertion (eg, anorectal surgery, inflammatory bowel disease). The study was approved by the institutional review board, and informed consent was obtained from all patients.

Median patient age was 62.3 years, with a range of 51–72 years. Median prostate-specific antigen serum level was 8.9 ng/mL (range, 1–45 ng/mL), and median Gleason score was 6 (range, scores 4–7), respectively. MR imaging was performed at least 4 weeks after transrectal ultrasonographically guided sextant biopsy.

MR Imaging Acquisition Protocol

All MR images were obtained with a commercially available 3.0-T whole-body scanner (Magnetom TRIO; Siemens Medical Solutions, Erlangen, Germany). A quadrature birdcage body coil was used for transmission, and prototypes of balloon-mounted disposable endorectal surface coils (Medrad) for 3-T MR imaging were used for receiving the MR signals. After digital rectal examination, the endorectal surface coil was inserted and inflated with demineralized water to a volume of approximately 60 cm^3. Peristalsis was suppressed in all patients with an intramuscular injection of 1 mg of glucagon (Glucagen; Novo Nordisk, Bagsvaerd, Denmark) immediately before the start of the examination.

The protocol for acquisition consisted of a localizer and two fast turbo gradient spin-echo measurements for patient and coil positioning and high-spatial-resolution T2-weighted fast spin-echo imaging in three planes. The imaging parameters for the T2-weighted images were as follows: repetition time msec/(effective) echo time msec, 4000/109; flip angle, 180°; field of view, 280 mm; matrix, 512 × 256; number of sections, 15–18; section thickness, 4 mm; section gap, zero. The frequency direction was anteroposterior to decrease coil motion artifacts over the prostate. In addition, transverse high-spatial-resolution T2-weighted fast spin-echo images (matrix, 768–1024 × 512; field of view, 180 mm) were acquired with a voxel volume of 13 μm^3, and this acquisition exploited the increased signal-to-noise ratio of the endorectal coil at 3 T. Possible biopsy-related hematomas were detected with images from

a three-dimensional T1-weighted spoiled gradient-echo pulse sequence performed with the following parameters: 8.6/4; flip angle, 15°; number of sections, 32; section thickness, 1.5 mm; field of view, 130 mm; matrix, 128 × 256; and in-plane resolution, 0.51 × 0.51 mm. Total examination time for the aforementioned protocol and coil insertion was approximately 20–25 minutes.

MR Image Evaluation

Prospectively, all MR images were independently read by three radiologists who were aware that patients had biopsy-proved prostate cancer and were scheduled for radical prostatectomy. They were unaware of the other clinical findings. The three radiologists had different levels of experience in interpretation of findings from prostate endorectal MR examinations. Radiologist A (J.O.B.) had 10 years of experience (total of approximately 700 studies), radiologist B (J.J.F.) had 3 years of experience (total of approximately 250 studies), and radiologist C (S.W.T.P.J.H.), who was considered less experienced than radiologists A and B, had 6 months of experience (total of approximately 30 studies). MR imaging studies were interpreted at a digital workstation (Impax; Agfa, Mortsel, Belgium). MR image evaluation was performed in three planes. All MR images were rated for overall quality as good, intermediate, or poor. Image quality was considered to be good if the images showed high anatomic detail and minimal artifacts and poor if poor anatomic detail or extensive artifacts disallowed the evaluation of the images. All other images were considered to be of intermediate quality.

The readers drew lesion and extraprostatic extension locations in standard schemes of the prostate for comparison with the whole-mount sections. The prostate capsule was divided into octants; that is, the prostate was split in half (from apex to base) and then further divided into four areas: right and left peripheral zone and right and left central gland. The most likely sites of capsular extension were identified in each octant and numbered on the drawings. T1-weighted images were used to rule out false-positive findings caused by postbiopsy hemorrhage; if a low-signal-intensity lesion on a T2-weighted MR image matched a high-signal-intensity lesion on the corresponding T1-weighted MR image, this area was considered to be a hematoma due to biopsy [20].

The presence of extracapsular extension was evaluated on the basis of five specific features described in the literature as highly indicative of extracapsular extension. These features were as follows: neurovascular bundle asymmetry, obliteration of the rectoprostatic angle, irregular bulging of the prostatic contour, tumor signal intensity within the periprostatic fat, and overt extracapsular tumor [8,21–23]. The criterion used for determination of seminal vesicle invasion was abnormal asymmetric low signal intensity within the lumen on T2-weighted images [11,23].

The readers expressed the likelihood of each criterion -extracapsular extension and seminal vesicle invasion- with a five-point scale. A rating with a score of 1 indicated that extraprostatic disease was definitely not present; that with a score of 2, that disease was probably not present; that with a score of 3, that disease was possibly present; that with a score of 4, that disease was probably present; and that with a score of 5, that disease was definitely present. When a score of 4 or 5 was assigned, the criterion was considered to be present. When a score of 1–3 was assigned, the criterion was considered not to be present. Reading was performed at a high-specificity setting [24,25] for extraprostatic disease (ie, only if the reader was certain of stage T3 disease, the disease rated as this stage). This was done to prevent the withholding of potentially curative therapy because of the classification of false-positive stage T3 disease in a patient with actual stage T2 disease.

Histopathologic Analysis

Three urologists, including one author (J.A.W., with 17 years of experience) and two other urologists with 11 years and 4 years of experience, who had knowledge of the MR imaging results performed the prostatectomy procedures. The prostatectomy specimens were fixed overnight in 10% neutral buffered formaldehyde and were coated with India ink. Seminal vesicles were separated from the prostate and examined separately. Transverse whole-mount step sections were created at 4-mm intervals in a plane parallel to the transverse plane used to perform the T2-weighted sequence. All sections were routinely embedded in paraffin. Tissue sections of 5 μm were prepared and stained with hematoxylin-eosin. The presence and extent of cancer were outlined on the glass cover with the tissue section by an experienced genitourinary pathologist (C.A.H.) who had 12 years of experience and who was blinded to the imaging results. Staging of the prostatectomy specimens was performed according to the present TNM classification [26].

Data Analysis

The MR imaging–predicted extraprostatic extension was compared with the findings at histopathologic analysis by one radiologist (J.J.F., with 3 years of experience) after assignment of scores and evaluation of the data were performed. The T2-weighted fast spin-echo MR images were aligned with the whole-mount sections. The morphologic characteristics of the central gland and peripheral zone—apex and base of the prostate, cysts, calcifications, and urethra—were used as landmarks. Aligning of MR images and whole-mount sections is considered difficult [10]. Although no literature is available on this subject, to our knowledge, we were confident that our alignment was within 8-mm accuracy (eg, two sections). If the detected extraprostatic extension in the whole-mount section was within 4 mm from the aligned MR image–detected location and on the correct side, this was considered a match.

Statistical Analysis

A finding was considered true-positive in a case in which the imaging results were correlated with the histopathologic findings, as mentioned previously. The sensitivity, specificity, positive and negative predictive values, and overall accuracy for the prediction of extraprostatic criteria, tumor stage, extracapsular extension, and seminal vesicle invasion were calculated by dichotomizing the readings. When a score of 4 or 5 was assigned, these features were considered to be present. When a score of 1–3 was assigned, the features were considered not to be present. This analysis was performed according to patient and according to octant.

The statistical analysis included the evaluation of the interobserver agreement by using nonweighted κ statistics. The following qualitative terms were used to describe the strength of the various values of κ: 0–0.20, poor agreement; 0.21–0.40, fair agreement; 0.41–0.60, moderate agreement; 0.61–0.80, substantial agreement; and 0.81–1.00, near-perfect agreement (27). Two-tailed tests were used to calculate all P values; a P value of .05 or less was considered to represent a statistically significant difference. All statistical analyses were performed with software (SPSS, version 9.0; SPSS, Chicago, Ill).

RESULTS

Surgical Specimens

In three patients, performance of the standard of reference was not available because the urologist did not remove the prostate as a result of lymph node metastases, and on the basis of this finding, the urologist decided not to resect the prostate. These patients subsequently underwent a combination of radiation and/or hormonal therapy. One of these three patients had clear invasion of the seminal vesicles at MR imaging, and this finding was reported to the urologist. The urologist then performed a biopsy of the seminal vesicle, and results were positive for cancer. These three patients were excluded from further analysis; thus, 32 patients were included in our study. Eight of 32 patients had extracapsular extension; in three of these patients, seminal vesicle invasion was observed. In the remaining patients, disease was confined to the prostate (stage T2a disease in nine patients and stage T2b disease in 15 patients). The image quality was good in 29 patients and intermediate in three patients. In six patients, postbiopsy artifacts were visible on T1-weighted images; however, the artifacts were not in the area of capsular extension or seminal vesicle invasion.

Staging

The staging results, with scores assigned according to octant, are presented in Table 1. Two hundred fifty-six capsular sites were evaluated for extracapsular extension on the MR images. Of these 256 sites, 13 had capsular extension at histopathologic evaluation. Of these 13 sites, one was not identified as a site of possible capsular extension on MR images by all three readers. The penetration depth of this extension was only 0.5 mm. In three sites,

the penetration depth of the capsular extension was less than 2 mm (Figure 1). Two of these sites were identified by the two experienced readers (readers A and B).

Table 1. Staging and Statistical Analysis Results for Three Readers according to Octant

A: Histopathologic Staging Results*

	Reader A		Reader B		Reader C	
MR Imaging	Stage T3	Stage T2	Stage T3	Stage T2	Stage T3	Stage T2
Stage T3	11	3	11	3	6	15
Stage T2	2	240	2	240	5	228

B: Statistical Results

Statistic	Reader A	Reader B	Reader C
Sensitivity†	85 (11/13)	85 (11/13)	55 (6/11)
Specificity†	99 (240/243)	99 (240/243)	94 (228/243)
Accuracy†	98 (251/256)	98 (251/256)	91 (234/256)
Positive predictive value†	79 (11/14)	79 (11/14)	29 (6/21)
Negative predictive value†	99 (240/242)	99 (240/242)	98 (228/233)

Note.—Readers A and B were experienced, and reader C was less experienced.

* Data are numbers of sites with capsular extension.

† Data are percentages. Numbers in parentheses were used to calculate percentages.

The staging results, with scores assigned according to patient, are shown in Table 2. The overall accuracy in prostate cancer staging (T3 disease vs T2 disease) was 94% (30 of 32) according to patient for the experienced readers A and B and 81% (26 of 32) for the less experienced reader C. No statistically significant difference was present among readers A, B, and C.

Table 2. Staging and Statistical Analysis Results for Three Readers according to Patient

A: Histopathologic Staging Results*

	Reader A		Reader B		Reader C	
MR Imaging	Stage T3	Stage T2	Stage T3	Stage T2	Stage T3	Stage T2
Stage T3	7	1	7	1	4	2
Stage T2	1	23	1	23	4	22

B: Statistical Results

Statistic	Reader A	Reader B	Reader C
Sensitivity†	88 (7/8)	88 (7/8)	50 (4/8)
Specificity†	96 (23/24)	96 (23/24)	92 (22/24)
Accuracy†	94 (30/32)	94 (30/32)	81 (26/32)
Positive predictive value†	88 (7/8)	88 (7/8)	67 (4/6)
Negative predictive value†	96 (23/24)	96 (23/24)	85 (22/26)

Note - Readers A and B were experienced, and reader C was less experienced.

* Data are numbers of patients.

† Data are percentages. Numbers in parentheses were used to calculate percentages.

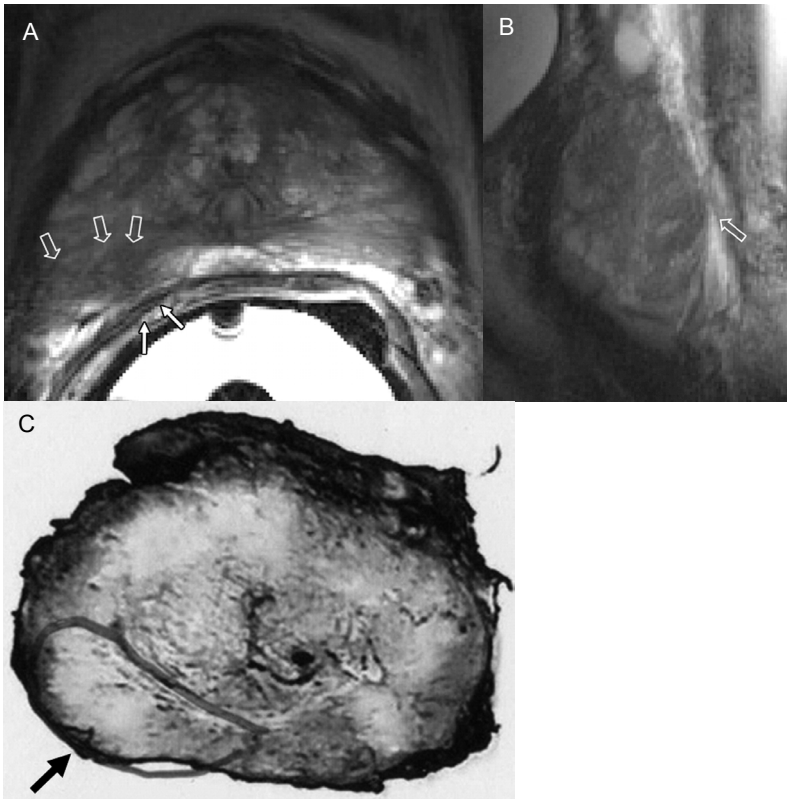

Figure 1. Image in a 62-year-old patient with prostate-specific antigen serum level of 8.2 ng/mL and Gleason score of 6 show histologically confirmed stage T3a prostate carcinoma. (A) Transverse T2-weighted fast spin-echo MR image (4000/109) shows suspicious area of low signal intensity (open arrows) in the right peripheral zone. Experienced radiologists identified this area as irregular border (solid arrows) of the prostate capsule and classified the disease as stage T3a. (B) Sagittal T2-weighted fast spin-echo MR image (4124/109) demonstrates disrupted prostate capsule in the same patient (arrow). (C) Histopathologic section reveals stage T3a disease with minimal capsule penetration (arrow) in the right peripheral zone.

The results of the readers' observation of diagnostic features of extracapsular extension are given in Table 3. The mean sensitivity values for the individual criteria of extracapsular extension ranged from 44% to 88%. All readers obtained a high sensitivity for irregular bulging (Figure 1) of the prostatic contour. High specificity was established for all criteria (Table 3).

In the three patients in whom seminal vesicle invasion was observed, results were confirmed with findings at analysis of the specimen removed at prostatectomy. All readers identified the invasion of seminal vesicles, and this result yielded an accuracy of 100% (Figure 2).

Table 3. Results of Readers' Observation of Diagnostic Features for Extracapsular Extension

Feature	Sensitivity*	Specificity*	Accuracy*	Negative Predictive Value*	Positive Predictive Value*	$\kappa 1^{\dagger}$	$\kappa 2^{\ddagger}$
Neurovascular bundle asymmetry	46	99	85	87	85	0.52	0.45
Obliteration of rectoprostatic angle	44	100	86	100	85	0.52	0.42
Irregular bulging of prostatic contour	88	100	97	100	96	0.71	0.51
Tumor signal intensity within periprostatic fat	63	100	91	100	89	0.79	0.62
Overt extracapsular tumor	69	98	91	93	91	0.62	0.53

* Numbers are mean values in percentages for the two experienced readers.

† Value signifies interobserver agreement between the experienced readers.

‡ Value signifies interobserver agreement between the less experienced and the experienced readers.

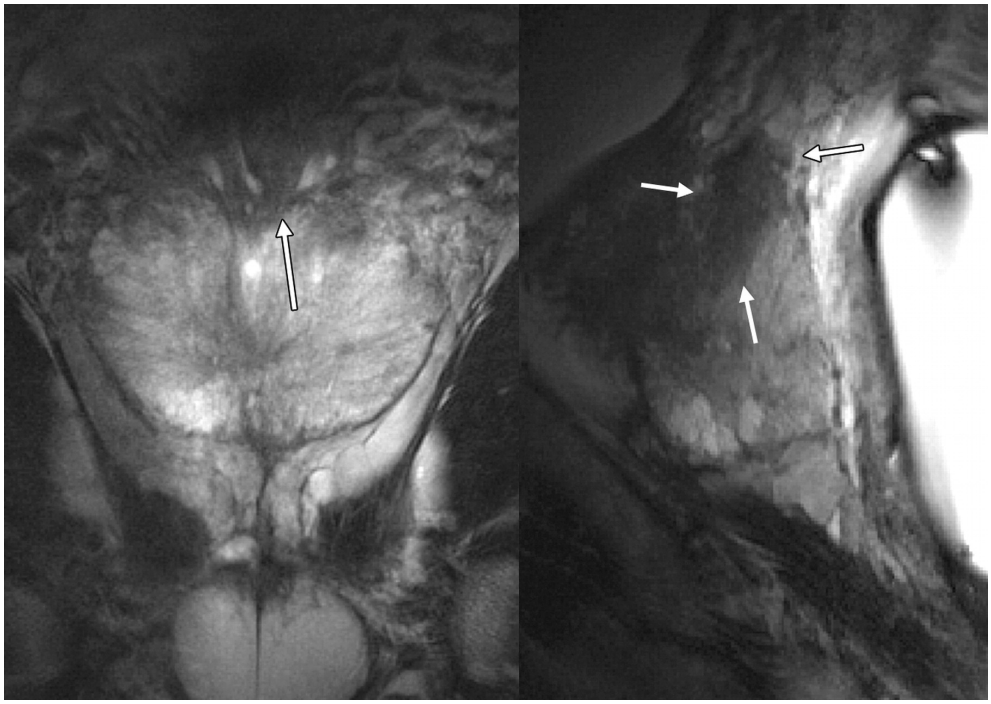

Figure 2. Images in a 66-year-old patient with prostate-specific antigen serum level of 4.5 ng/mL and Gleason score of 6 show seminal vesicle invasion. Coronal and sagittal T2-weighted fast spin-echo MR image (4130/109) obtained through the prostate and seminal vesicles. Area of low signal intensity is present in base of prostate and extends into seminal vesicle (arrows). This finding was confirmed with whole-mount-section histopathologic analysis.

Interobserver Agreement

The results of the interobserver agreement analysis are displayed in Table 3. Assessment of interobserver variability showed moderate to substantial agreement (κ = 0.42–0.79) for ratings in regard to extracapsular extension for all three readers. Agreement was best for ratings in regard to tumor signal intensity within the periprostatic fat and irregular bulging of the prostatic contour, and agreement was the worst for ratings in regard to obliteration of the rectoprostatic angle.

DISCUSSION

The most important findings of our study were the high sensitivity of 88% in the staging of prostate cancer, the retention of a specificity of 96%, and the detection of minimal capsular extension through the prostate capsule by experienced readers. Two of three cases of minimal capsular penetration were recognized by the experienced radiologists (readers A and B). This finding suggests a role for prostate MR imaging at 3-T. Although we did not perform a comparative study between 1.5-T MR imaging and 3-T MR imaging, the results

of this study indicated that with the 3-T technique the accuracy in staging was increased to a level that was higher than that reported for 1.5-T imaging, with a range in accuracy of 54%–88% [8–11,15].

So far, only four studies about in vivo prostate imaging at high field strengths have been published, as far as we know. Kim et al [28] used a relatively large external transceive coil for prostate imaging without exploring staging and localization performance with MR imaging. In our study, we used an endorectal receiver coil for imaging of the prostate, and use of this coil resulted in images with a high in-plane resolution and a voxel volume as small as 0.13 mm^3. This resolution and voxel volume would be very difficult to achieve within a reasonable time without the use of a local coil. Sosna et al [29] reported results of volume assessment of the prostate at 3-T MR imaging with an external phased-array coil. They concluded that in vivo volume determinations were very close to ex vivo imaging volume determinations. They, however, did not investigate performance of MR imaging for staging. Bloch et al [30] showed a proof of principle of MR imaging of the prostate at 3 T with an endorectal coil in a limited study with six volunteers.

In a concurrent study by Fütterer et al [19], patients with prostate cancer were examined by using an endorectal coil at 3-T MR imaging. It was shown that the increased signal-to-noise ratio with an endorectal coil at 3 T has great potential to improve either the spatial or temporal resolution of T2-weighted (dynamic) contrast material–enhanced and spectroscopic MR imaging of the prostate. In the current study, we applied this signal-to-noise ratio to obtain images with high in-plane resolution for clear delineation of the prostate capsule. Because of this increased resolution, we were able to display minimal capsular extension in two of three cases. Findings in reports from the early 1990s suggested that minimal capsular penetration of less than 1 mm does not adversely affect the surgical cure rate [31,32]. No recent data in the literature, however, have confirmed these results.

With the demonstrated ability to detect minimal capsular penetration, the question arises about whether the progression from stage T2 disease to stage T3 disease should be used as the basis on which clinicians should choose between surgical resection of the prostate or a combination of radiation therapy and hormonal therapy for treatment. If minimal capsular penetration is detected, curative surgery will be withheld in a patient in whom the treatment for the disease is potentially curative. Perhaps the reported early detection of stage T3 disease, when it is treated as stage T2 disease, does not affect patient outcome. The effect of the detection of minimal capsular penetration, as well as possible implications in treatment, has to be evaluated in future studies.

In our study, we found a mean sensitivity of 62% (range, 44%–88%) and a high specificity for the criteria of extracapsular extension with moderate to substantial interobserver

agreement. Outwater et al [23] found only poor accuracy for the extracapsular criteria at 1.5-T MR imaging. This difference in accuracy could be caused by the increased in-plane resolution in our study (voxel volume of 0.61 μm^3) versus that of 0.18 μm^3 in the study of Outwater et al. All the radiologists read the images with the focus on high specificity [24,25]. To prevent overstaging, only if the reader was certain of stage T3 disease was the disease rated as such.

The results of the current study showed that there was a difference in accuracy according to experience of the reader; these results also showed a difference particularly in sensitivity (88% vs 50%). This difference was also found in other studies performed at 1.5-T MR imaging [14,33]. The sensitivity and specificity at 1.5-T MR imaging found by Yu et al [33] were 17% and 94% and 54% and 95% for the less experienced and experienced readers, respectively. This difference in sensitivity values was much smaller in the present study, where sensitivity and specificity were 50% and 92% and 88% and 96% for the less experienced and experienced readers, respectively.

Despite the promising results of our study, some limitations need to be considered. The correlation between findings at MR imaging and the findings at corresponding whole-mount-section histopathologic analysis was difficult to determine in most patients. This difficulty is a frequently encountered problem. The angle at which the whole-mount sections were cut in the prostate specimens was never exactly the same compared with the angulation of the MR images obtained in vivo. After the prostate specimens are fixed in formaldehyde, the specimen shrinks and deforms. We tried to overcome these problems by using all whole-mount sections in the assessment of the corresponding level.

Because prostate-specific antigen serum levels and Gleason scores were low, only four patients with seminal vesicle invasion were included in this study. In one patient with seminal vesicle invasion who was excluded from this study because no results of analysis with the standard of reference were obtained, the urologist changed the treatment on the basis of MR imaging findings, and such a change suggests that the technique used in this study may influence a decision about treatment and patient outcome. Such a suggestion, however, requires confirmation in a future study.

The number of patients included in this study may be considered rather low. In their meta-analyses, Engelbrecht et al [12] and Sonnad et al [17] showed that studies with 50 patients or fewer had more favorable results than did studies with a higher number of patients. In an article titled “Clinical Efficacy of MR Needs Rigorous Study” (Diagn Imaging 1990;12:69,71,161), Kent, however, estimated that 30–70 patients would be required for a comparison of the diagnostic accuracy of MR imaging with that of a reference standard. In

a future study, a multicenter approach has to be used to confirm our promising preliminary results.

The role of endorectal MR imaging in local staging of cancer of the prostate is still controversial. A number of articles indicated the poor capability of MR imaging in the staging of cancer of the prostate [7–9]. May et al [9] even suggested that treatment decisions should not be altered as a result of endorectal MR imaging findings. In contrast, Jager et al [16] developed an analytic model for decision making that supported the opinion that MR imaging for staging in the preoperative work-up of prostate cancer is cost effective and should be performed with a high specificity. Langlotz et al [24] and Langlotz [25] emphasized this need for high specificity to ensure that as few patients as possible will be unnecessarily turned down for potentially curative therapy on the basis of false-positive MR imaging results. D'Amico et al [34] suggested using endorectal MR imaging in patients with intermediate risk only; in this group, the probability of extraprostatic disease is high enough to warrant the use of MR imaging. If the prevalence of extracapsular disease is, for example, 30% and MR imaging is performed with a specificity of 97% and a sensitivity of 33%, then only in one of 10 patients will MR imaging results affect the treatment. This could be a reason why urologists do not use MR imaging as a modality for staging. If the results of our study are reproducible, this number could be extrapolated to one of three or four.

With consideration of the thus far published data, results of this study indicate that 3-T endorectal MR imaging of the prostate in staging is of additional value in patients with prostate cancer. MR imaging of the prostate at 3 T should be performed only in patients with intermediate risk of having extraprostatic disease [34], and it should be performed with high-specificity readings by experienced genitourinary radiologists [14]. Nonetheless, it remains difficult for less experienced readers to interpret MR images of the prostate; however, at 3-T MR imaging, it may be anticipated that interpretation will improve.

In conclusion, in this study, high accuracy for staging with moderate to substantial observer agreement at 3-T MR imaging was demonstrated. In addition, minimal capsular invasion could be detected. These outcomes suggest a future role for high-field-strength MR imaging in the staging of prostate cancer.

The authors gratefully acknowledge Vincent Cuijpers, MSc (Department of Pathology), and Yvonne Hoogeveen, PhD (Department of Radiology), for their contributions.

REFERENCES

[1] Jemal A, Tiwari RC, Murray T, et al. Cancer statistics, 2004. CA Cancer J Clin 2004;54(1):8–29.

[2] Yancik R. Epidemiology of cancer in the elderly: current status and projections for the future. Rays 1997;22(S1):3–9.

[3] Sarma AV, Schottenfeld D. Prostate cancer incidence, mortality, and survival trends in the United States: 1981–2001. Semin Urol Oncol 2002;20:3–9.

[4] Yu KK, Hricak H, Alagappan R, Chernoff DM, Bacchetti P, Zaloudek CJ. Detection of extracapsular extension of prostate carcinoma with endorectal and phased-array coil MR imaging: multivariate feature analysis. Radiology 1997;202(3):697–702.

[5] D'Amico AV, Whittington R, Malkowicz SB, et al. A multivariate analysis of clinical and pathological factors that predict for prostate specific antigen failure after radical prostatectomy for prostate cancer. J Urol 1995;154:131–138.

[6] Steinfeld AD. Questions regarding the treatment of localized prostate cancer. Radiology 1992;184(3):593–598.

[7] Presti JC Jr, Hricak H, Narayan PA, et al. Local staging of prostatic carcinoma: comparison of transrectal sonography and endorectal MR imaging. AJR Am J Roentgenol 1996;166:103–108.

[8] Tempany CM, Zhou X, Zerhouni EA, et al. Staging of prostate cancer: results of radiology diagnostic oncology group project comparison of three MR imaging techniques. Radiology 1994;192:47–54.

[9] May F, Treumann T, Dettmar P, Hartung R, Breul J. Limited value of endorectal magnetic resonance imaging and transrectal ultrasonography in the staging of clinically localized prostate cancer. BJU Int 2001;87(1):66–69.

[10] Jager GJ, Ruijter ET, van de Kaa VA, et al. Local staging of prostate cancer with endorectal MR imaging: correlation with histopathology. AJR Am J Roentgenol 1996;166(4):845–852.

[11] Hricak H, White S, Vigneron D, et al. Carcinoma of the prostate gland: MR imaging with pelvic phased-array coils versus integrated endorectal-pelvic phased-array coils. Radiology 1994;193:703–709.

[12] Engelbrecht MR, Jager GJ, Laheij RJ, Verbeek AL, Van Lier HJ, Barentsz JO. Local staging of prostate cancer using magnetic resonance imaging: a meta-analysis. Eur Radiol 2002;12:2294–2302.

[13] Wang L, Mullerad M, Chen HN, et al. Prostate cancer: incremental value of endorectal MR imaging findings for prediction of extracapsular extension. Radiology 2004;232(1):133–139. Abstract/FREE Full Text

[14] Mullerad M, Hricak H, Wang L, Chen HN, Kattan MW, Scardino PT. Prostate cancer: detection of extracapsular extension by genitourinary and general body radiologists at MR imaging. Radiology 2004;232(1):140–146.

[15] Huch Boni RA, Boner JA, Lutolf UM, et al. Contrast-enhanced endorectal coil MRI in local staging of prostate carcinoma. J Comput Assist Tomogr 1995;19(2):232–237.

[16] Jager GJ, Severens JL, Thornbury JR, de La Rosette JJ, Ruijs SH, Barentsz JO. Prostate cancer staging: should MR imaging be used? a decision analytic approach. Radiology 2000;215(4):445–451.

[17] Sonnad SS, Langlotz CP, Schwartz JS. Accuracy of MR imaging for staging prostate cancer: a meta-analysis to examine the effect of technologic change. Acad Radiol 2001;8(2):149–157.

[18] Bottomley PA, Foster TH, Argersinger RE, et al. A review of normal tissue hydrogen NMR relaxation times and relaxation mechanisms from 1–100 MHz: dependence on tissue type, NMR frequency, temperature, species, excision, and age. Med Phys 1984;11(4):425–448.

[19] Fütterer JJ, Scheenen TWJ, Huisman HJ, et al. Initial experience of 3T endorectal coil MR imaging and 1H-spectroscopic imaging of the prostate. Invest Radiol 2004;39(11):671–680.

[20] White S, Hricak H, Forstner R, et al. Prostate cancer: effect of postbiopsy hemorrhage on interpretation of MR images. Radiology 1995;195(2):385–390.

[21] Schiebler ML, Yankaskas BC, Tempany C, et al. MR imaging in adenocarcinoma of the prostate: interobserver variation and efficacy for determining stage C disease. AJR Am J Roentgenol 1992;158(3):559–562.

[22] Schiebler ML. In discussion of: Schiebler ML, Yankaskas BC, Tempany C, et al. MR imaging in adenocarcinoma of the prostate: interobserver variation and efficacy for determining stage C disease. AJR Am J Roentgenol 1992;158(3):563–564.

[23] Outwater EK, Petersen RO, Siegelman ES, Gomella LG, Chernesky CE, Mitchell DG. Prostate carcinoma: assessment of diagnostic criteria for capsular extension on endorectal coil images. Radiology 1994; 193(2): 333–339.

[24] Langlotz C, Schnall M, Pollack H. Staging of prostatic cancer: accuracy of MR imaging. Radiology 1995;194(3):645–646.

[25] Langlotz C. In discussion of: Langlotz C, Schnall M, Pollack H. Staging of prostatic cancer: accuracy of MR imaging. Radiology 1995;194(3):647–648

[26] Greene FL, Page DL, Fleming ID, et al. AJCC cancer staging manual, 6th ed. New York, NY: Springer-Verlag, 2002.

[27] Landis JR, Koch GG. The measurement of observer agreement for categorical data. Biometrics 1977;33:159–174.

[28] Kim HW, Buckley DL, Peterson DM, et al. In vivo prostate magnetic resonance imaging and magnetic resonance spectroscopy at 3 Tesla using a transceive pelvic phased array coil: preliminary results. Invest Radiol 2003;38(7):443–451.

[29] Sosna J, Rofsky NM, Gaston SM, et al. Determinations of prostate volume at 3-Tesla using an external phased array coil: comparison to pathologic specimens. Acad Radiol 2003;10(8):846–853.

[30] Bloch BN, Rofsky NM, Baroni RH, Marquis RP, Pedrosa I, Lenkinski RE. 3 Tesla magnetic resonance imaging of the prostate with combined pelvic phased-array and endorectal coils: initial experience. Acad Radiol 2004;11(8):863–867.

[31] Epstein JI, Carmichael MJ, Pizov G, Walsh PC. Influence of capsular penetration on progression following radical prostatectomy: a study of 196 cases with long-term follow-up. J Urol 1993;150(1):135–141.

[32] Hering F, Rist M, Roth J, Mihatsch M, Rutishauser G. Does microinvasion of the capsule and/or micrometastases in regional lymph nodes influence disease-free survival after radical prostectomy? Br J Urol 1990;66(2):177–181.

[33] Yu KK, Scheidler J, Hricak H, et al. Prostate cancer: prediction of extracapsular extension with endorectal MR imaging and three-dimensional proton MR spectroscopic imaging. Radiology 1999;213:481–488.

[34] D'Amico AV, Schnall M, Whittington R, et al. Endorectal coil magnetic resonance imaging identifies locally advanced prostate cancer in select patients with clinically localized prostate cancer. Urology 1998;51(3):449–454.

CHAPTER 5

Prostate Cancer: Body-Array versus Endorectal Coil MR Imaging at 3 T—Comparison of Image Quality, Localization, and Staging Performance

Stijn W. T. P. J. Heijmink
Jurgen J. Fütterer
Thomas Hambrock
Satoru Takahashi
Tom W. J. Scheenen
Henkjan J. Huisman
Christina A. Hulsbergen-Van de Kaa
Ben C. Knipscheer
Lambertus A. L. M. Kiemeney
J. Alfred Witjes
Jelle O. Barentsz

Radiology 2007;244(1):184-95.

Purpose: To prospectively compare image quality and accuracy of prostate cancer localization and staging with body-array coil (BAC) versus endorectal coil (ERC) T2-weighted magnetic resonance (MR) imaging at 3 T, with histopathologic findings as the reference standard.

Materials and Methods: After institutional review board approval and written informed consent, 46 men underwent 3-T T2-weighted MR imaging with a BAC (voxel size, 0.43 x 0.43 x 4.00 mm) and an ERC (voxel size, 0.26 x 0.26 x 2.50 mm) before radical prostatectomy. Four radiologists independently evaluated data sets obtained with the BAC and ERC separately. Ten image quality characteristics related to prostate cancer localization and staging were assigned scores. Prostate cancer presence was recorded with a five-point probability scale in each of 14 segments that included the whole prostate. Disease stage was classified as organ-confined or locally advanced with a five-point probability scale. Whole-mount-section histopathologic examination was the reference standard. Areas under the receiver operating characteristic curve (AUCs) and diagnostic performance parameters were determined. A difference with a P value of less than .05 was considered significant.

Results: Forty-six patients (mean age, 61 years) were included for analysis. Significantly more motion artifacts were present with ERC imaging ($P < .001$). All other image quality characteristics improved significantly ($P < .001$) with ERC imaging. With ERC imaging, the AUC for localization of prostate cancer was significantly increased from 0.62 to 0.68 ($P < .001$). ERC imaging significantly increased the AUCs for staging, and sensitivity for detection of locally advanced disease by experienced readers was increased from 7% (one of 15) to a range of 73% (11 of 15) to 80% (12 of 15) ($P < .05$), whereas a high specificity of 97% (30 of 31) to 100% (31 of 31) was maintained. Extracapsular extension as small as 0.5 mm at histopathologic examination could be accurately detected only with ERC imaging.

Conclusion: Image quality and localization improved significantly with ERC imaging compared with BAC imaging. For experienced radiologists, the staging performance was significantly better with ERC imaging.

Magnetic resonance (MR) imaging can play a role in the diagnosis of prostate cancer. First, the characteristic pattern of prostate cancer as a low-signal-intensity lesion on T2-weighted MR images makes MR imaging suitable for detection and localization purposes [1,2]. However, at standard clinical field strengths of 1.5 T, an endorectal coil (ERC) is necessary to obtain a sufficiently high signal-to-noise ratio with subsequent spatial resolution to allow reliable cancer delineation [3] in a clinically reasonable time frame. At higher field strengths such as 3-T [4], the signal-to-noise ratio increases [5], and the need for an ERC for detection or localization of prostate cancer at this field strength has yet to be determined. The use of a body-array coil (BAC) alone for signal reception [6] would save time and costs and would cause less discomfort for the patient. A clinical application that requires accurate localization of cancer is intensity-modulated radiation therapy [7,8]. Accurate localization can further aid in preoperative decisions about the status of the neurovascular bundles, in the direction of ultrasound-guided biopsy in patients with negative findings at previous biopsy, or in the guidance of high-intensity focused ultrasound treatment.

Second, MR imaging can help in the determination of the extent of local disease, specifically whether the cancer is organ confined (stage T2) or locally advanced (stage T3). Recently, it was shown that MR imaging at 1.5 T with an ERC outperformed staging nomograms [9]. Nevertheless, its use for prostate cancer staging is still a matter of debate [10]. Previously, it was shown that staging by means of 1.5-T MR imaging had a joint maximum sensitivity and specificity of 71% [11]. Researchers in a preliminary study in 32 patients in whom T2-weighted MR imaging with an ERC at 3 T was performed found a sensitivity for staging of 88% (seven of eight), with a high specificity of 96% (23 of 24), for experienced readers [12]. However, to our knowledge, no studies have been published about prostate cancer staging at 3-T MR imaging with the use of only a BAC for signal reception, nor about comparisons of the use of a BAC with that of an ERC at 3-T MR imaging. Therefore, it is important to determine whether an ERC is still necessary or a BAC could suffice for staging purposes at 3-T MR imaging.

Thus, the purpose of our study was to prospectively compare image quality and accuracy of prostate cancer localization and staging with a BAC versus those with an ERC at T2-weighted MR imaging at 3 T, with histopathologic findings as the reference standard.

MATERIALS AND METHODS

Medrad (Pittsburgh, Pa) unconditionally supplied the prototypes of the balloon-mounted disposable 3-T surface ERCs and the interface device. The authors had complete control of the data and information submitted for publication.

Patient Characteristics

The study was approved by the institutional review board. Before inclusion, all patients gave their written informed consent. From June 2004 to January 2006, consecutive patients who met our study criteria and had biopsy-proved and clinically localized prostate cancer were scheduled to undergo MR imaging at 3T with both a BAC and an ERC prior to radical prostatectomy. Exclusion criteria were contraindications for MR imaging (eg, pacemaker, metal cerebral clips) or ERC insertion (eg, prior anorectal surgery, inflammatory bowel disease), as well as severe claustrophobia and high anal sphincter tension that prevented ERC introduction. For all included patients, the time between the last biopsy procedure and MR imaging, as well as the time between MR imaging and surgery, was determined.

MR Imaging Acquisition

All images were obtained by using a 3-T whole-body imager (Magnetom Trio; Siemens Medical Solutions, Erlangen, Germany). In the first part of the examination, a commercially available eight-element standard BAC was placed around the pelvic area with the patient in the supine position. After localizing images were obtained, T2-weighted fast spin-echo image series in the transverse, sagittal, and coronal planes were obtained, with the transverse image series aligned perpendicularly to the anterior rectal wall. Radiofrequency power deposition from the spin-echo train was reduced by using hyperechoes [13]. The optimized sequence parameters were as follows: repetition time msec/echo time (TE) msec, 3700/124; field of view, 220 x 100 mm; section thickness, 4 mm; matrix, 512 x 512; voxel size, 0.43 x 0.43 x 4.00 mm; number of signals acquired, two; and acquisition time, 4 minutes 57 seconds. A three-dimensional T1-weighted gradient-echo image series was obtained to exclude hemorrhage after biopsy.

In the second part of the examination, after removal of the BAC and performance of a digital rectal examination, a prototype ERC (Medrad) was inserted, with the patient in the left lateral decubitus position. The balloon was then inflated with either 40-60 mL of demineralized water or perfluoro polyether (Fomblin; Solvay Solexis, Milan, Italy). The patient was placed in the supine position, and bowel movement was suppressed with an intramuscular injection of 1 mg glucagon (Glucagen; Novo Nordisk, Bagsvaerd, Denmark). An ERC localization image series was obtained and, if necessary, the ERC position was readjusted. Subsequently, T2-weighted fast spin-echo images were obtained with the use of hyperechoes in the transverse, sagittal, and coronal planes, with the transverse image series aligned perpendicularly to the anterior rectal wall. Sequence parameters were as follows: 5000/153; field of view, 200 x 100 mm; section thickness, 2.5 mm; matrix, 768 x 384; voxel size, 0.26 x 0.26 x 2.50 mm; number of signals acquired, one; and acquisition time, 2 minutes 58 seconds. Last, a three-dimensional T1-weighted gradient-echo image series was obtained. No adverse events were reported, and all patients tolerated the examination well.

MR Imaging Interpretation

Prospectively, four radiologists, two experienced and two less experienced, independently read all imaging data sets from which patient identification was removed. The two experienced readers, radiologists A (J.J.F.) and B (S.W.T.P.J.H.), had 4 and 2 years of experience, respectively, in ERC prostate MR imaging interpretation, which corresponded to the previous reading of 400 and 150 ERC MR studies, respectively. The two less experienced readers, radiologists C (S.T.) and D (T.H.), both had 3 months of experience in preoperative ERC prostate MR image interpretation; this experience corresponded to the reading of approximately 20 MR studies each. Radiologist C, however, had 8 years of experience (which corresponded to the reading of 100 MR studies) with preoperative prostate cancer MR imaging with the use of a pelvic phased-array coil at 1.5 T. Contrary to the experience level of radiologist C, radiologist D participated in a short training course about the reading of ERC prostate MR images obtained at 3 T prior to assignment of scores. This course comprised the reading of MR images obtained in approximately 15 patients with prostate cancer, with direct histopathologic feedback. These patients were not included in the current study.

To prevent information bias of either MR study influencing the other, imaging sets obtained with the BAC and the ERC in the same patient were never read in the same session, and the order was randomized. The authors were in control of the number of sessions and time between sessions. The readers knew the patients had histopathologically confirmed prostate cancer at biopsy but were blinded to all other clinical data. Readers classified the image quality of each set as excellent, sufficient, or insufficient on the basis of the presence of any artifacts that affected image interpretation, as well as the signal-to-noise ratio. If artifacts or a low signal-to-noise ratio hampered interpretation of the images, sets were classified as insufficient. If no artifacts were present and the signal-to-noise ratio was high, sets were classified as excellent. All other imaging sets were classified as sufficient. If either imaging set was classified as insufficient by two or more readers, the patient was excluded from analysis.

First, the readers were asked to assign a score to 10 image quality characteristics derived from both the literature [5,14] and the authors' (J.J.F., J.O.B.) prior experience. Characteristics related to localization included the following: the discrimination between the peripheral zone and the central gland, visibility of the peripheral zone itself, visibility of the central gland itself, visibility of the lesion, and visualization of the internal architecture of the central gland. Staging-related characteristics included the following: the delineation of the prostatic capsule, visualization of the neurovascular bundle, and visualization of the rectoprostatic angle. A general characteristic was the impression of the overall image quality. These nine characteristics were assigned scores on a five-point scale as follows: score 1, poor; score 2, moderate; score 3, satisfactory; score 4, good; and score 5, excellent. The final characteristic, the presence of motion artifacts that affected image interpretation, was assigned a score on

the basis of the following five-point scale: score 1, no artifacts were present; score 2, hardly any motion artifacts were present; score 3, image quality was satisfactory; score 4, image quality was moderately affected, and score 5, image quality was severely affected by motion artifacts. All assignment of scores was performed subjectively without specific criteria for each of the five points on the scale.

Second, for the purpose of cancer localization, the prostate was divided into apex, mid gland, and base regions. Both apex and base were subdivided into quadrants, and the mid gland was divided into sextants; thus, the whole prostate was mapped into 14 segments. All readers determined the presence of cancer in each segment with a five-point probability scale as follows: score 1, definitely absent; score 2, probably absent; score 3, possibly present; score 4, probably present; and score 5, definitely present. The criterion for assignment of a classification to a segment as cancerous in the peripheral zone was the appearance of an area of low signal intensity on T2-weighted fast spin-echo images [2,15]. In the central gland, the criterion was the appearance of an area of homogeneously low signal intensity with ill-defined margins on T2-weighted fast spin-echo images [16,17]. Areas of low signal intensity on T2-weighted fast spin-echo images and areas of high signal intensity on T1-weighted gradient- echo images were considered indicative of hemorrhage after biopsy (18) and were classified as not containing cancer.

Third, the readers assigned a score for the disease stage with a five-point probability scale as follows: score 1, definitely stage T2; score 2, probably stage T2; score 3, possibly stage T3; score 4, probably stage T3; and score 5, definitely stage T3. Criteria derived from the literature for extraprostatic extension included bulging or irregularity of the prostatic capsule, obliteration of the rectoprostatic angle or neurovascular bundle, an area of low signal intensity within the periprostatic fat, and marked seminal vesicle asymmetry or an area of low signal intensity in the seminal vesicles on T2-weighted fast spin-echo images [12,14,19,20]. All radiologists were instructed to perform high-specificity staging [21,22] to prevent false-positive judgments. Readers assigned the localization of the perceived extraprostatic extension to one or more of the 14 segments.

Surgery with Histopathologic Examination as Reference Standard

All radical retropubic prostatectomies were performed by one of two oncologic urologists with 18 (J.A.W.) and 5 (B.C.K.) years of experience who were cognizant of the MR imaging results.

After excision, prostatectomy specimens were fixed overnight in 10% neutral buffered formaldehyde and coated with India ink. Four-millimeter-interval whole-mount sections were cut at a plane comparable to that of the transverse MR imaging plane. All sections were routinely embedded in paraffin. Tissue sections of 5 μm were prepared and stained with hematoxylin-eosin. The exact localization, volume, Gleason score, extent of each

cancer focus, and radial distance [23] of each extracapsular penetration were determined by a genitourinary histopathologist (C.A.H.) with 13 years of experience who was blinded to the MR imaging results. All specimens were assigned to a stage according to the 2002 TNM classification [24].

Data Analysis

Cancer locations and extraprostatic extension predicted on MR images were compared with histopathologic findings by radiologists A and B after they had completed assignment of the scores and evaluation of the data. Landmarks used for the alignment of T2-weighted fast spin-echo MR images with whole-mount sections were the morphologic features of the peripheral zone, central gland, apex, and base of the prostate, as well as cysts, calcifications, the verumontanum, and the urethra [25]. Only cancer foci of 0.5 cm^3 or larger were considered suitable for matching with findings on MR images. Therefore, all foci smaller than 0.5 cm^3 were excluded from analysis. Each of the 14 segments was classified as containing either cancer or healthy tissue. The authors were confident to be within an 8-mm accuracy (eg, two sections) [26].

Statistical Analysis

The 10 scores for image quality characteristics for MR images obtained with the BAC and the ERC were compared by applying the Wilcoxon rank sum test for paired samples to the mean scores of the four radiologists for each patient.

Receiver operating characteristic (ROC) curves were obtained. The localization performance was summarized by using the area under the ROC curve (AUC) [27]. The AUCs were statistically compared by using nonparametric boot-strap resampling, with the patient as the unit of analysis [28,29]. A bootstrap draw either contained a patient, including all regions of interest and the readers who were observing the patient, or did not. The number of bootstrap replicates was set to 999. The *P* values for multiple comparisons were adjusted by using Bonferroni correction. The plotted ROC curve was the mean over all bootstrap curves for a specific factor. In addition, separate analyses were performed for peripheral zone and central gland cancer localization. The AUCs of the overall staging performance were calculated. The sensitivity, specificity, positive predictive value, negative predictive value, and overall accuracy for cancer localization, overall staging, detection of extracapsular penetration, and detection of seminal vesicle invasion were calculated by using dichotomization of the readings. For high-sensitivity localization and thus prevention of false-negative findings, scores of 3 or higher were considered to indicate cancer, whereas scores of 1 and 2 were deemed to indicate healthy tissue. For high-specificity staging and thereby prevention of false-positive findings [21,22], scores of 4 and 5 were considered stage T3 disease, whereas scores of 1–3 were considered stage T2 disease. To compare the

diagnostic performance parameters between MR imaging with the BAC and MR imaging with the ERC, the McNemar test for matched pairs was performed.

All *P* values reported were from two-sided tests. A *P* value of .05 or less was considered to indicate a statistically significant difference. Statistical analyses were performed by using R, version 2.1.0 (30), and software (Rockit, version 0.9.1B, Charles E. Metz, PhD, Department of Radiology, University of Chicago, Chicago, Ill; Prism, version 4.00, Graph-Pad Software, San Diego, Calif; SPSS, version 12.0.1, SPSS, Chicago, Ill).

RESULTS

Patients and Histopathologic Findings

Six patients were excluded from the study (Figure 1). In three patients, the ERC MR image sets were assigned scores for having insufficient quality caused by coupling artifacts of the ERC with the body transmit coil or caused by the presence of excessive motion artifacts, which precluded accurate image interpretation. In two patients, the ERC could not be inserted due to high anal sphincter tension. One patient had gross extracapsular extension on MR images and was subsequently treated with radiation therapy instead of surgery. Forty-six patients were included in the study (Table 1). For inflation of the balloon of the ERC, water and perfluoro polyether were used in 10 and 36 patients, respectively. The mean time between the last biopsy procedure and MR imaging was 112 days (range, 21–226 days), and the mean time between MR imaging and surgery was 14 days (range, 1– 89 days).

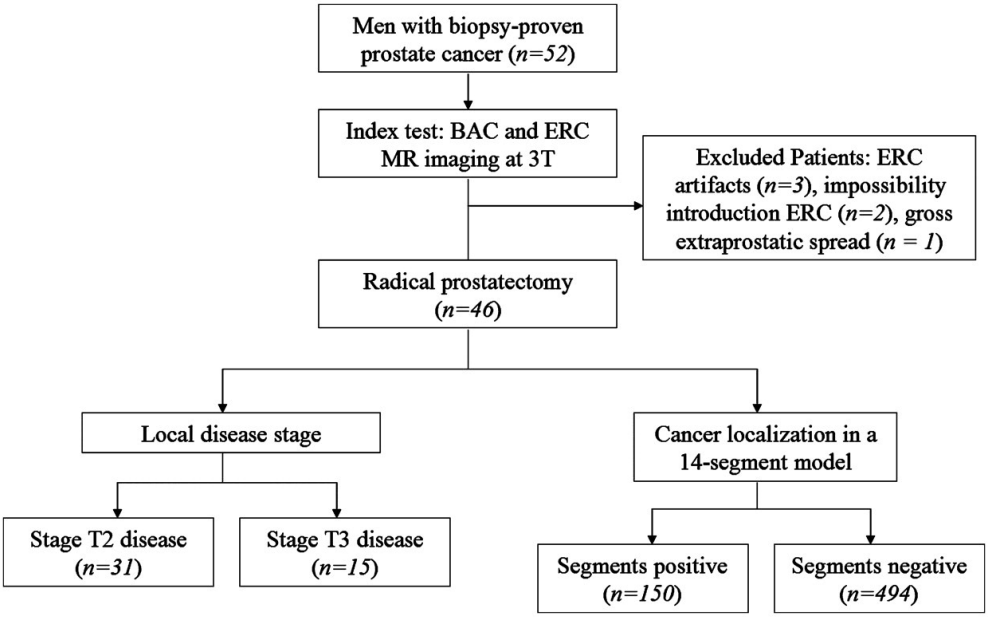

Figure 1: Flow diagram of the study

Table 1. Characteristics of 46 Male Patients Included in the Study

Clinical Data	Value
Preoperative characteristics	
Mean age (y)*	61 (51–70)
Mean preoperative prostate-specific antigen level (ng/mL)*	7.8 (3.5–24.6)
Median final Gleason score at biopsy*	6 (5–9)
Postoperative histopathologic characteristics	
Total no. of separate prostate cancer foci	124
No. of foci $\geq$0.5 cm^3	58
No. of foci $<$0.5 cm^3	66
Origin of cancer foci (%)†	
Peripheral zone	72 (89/124)
Central gland	28 (35/124)
Histopathologic stage	
pT2	31
pT2a	8
pT2b	4
pT2c	19
pT3	15
pT3a	13
pT3b	5‡
Median final Gleason score at prostatectomy*	7 (5–9)
Mean radial distance of extracapsular penetration (mm)	1.4
Radial distance of extracapsular penetration in 13 patients (mm)‡	0.5, 6 patients; 1.5, 2 patients; 2.0, 2 patients; 2.5, 2 patients; 3.0, 1 patient

A total of 124 separate cancer foci were reported at histopathologic examination. Seventy-two percent (89 of 124) of cancer foci were located in the peripheral zone and 28% (35 of 124) were located in the central gland. Fifteen (33%) of 46 patients had locally advanced (stage pT3) disease. Of them, 13 had extracapsular penetration (stage pT3a), and five had seminal vesicle invasion (stage pT3b). Thirty-one patients had organ-confined (stage pT2) disease. The mean radial extracapsular penetration at histopathologic examination in the 13 patients with stage pT3a disease was 1.4 mm (range, 0.5–3.0 mm).

Image Quality Comparison

All image quality characteristics, except motion artifacts, were improved significantly ($P < .001$) with ERC MR imaging compared with BAC MR imaging (Table 2). Significantly more motion artifacts were present during ERC imaging compared with BAC imaging ($P < .001$) (Figure 2). No differences in image quality characteristics were found between images obtained with the ERC filled with water and those obtained with the ERC filled with perfluoro polyether.

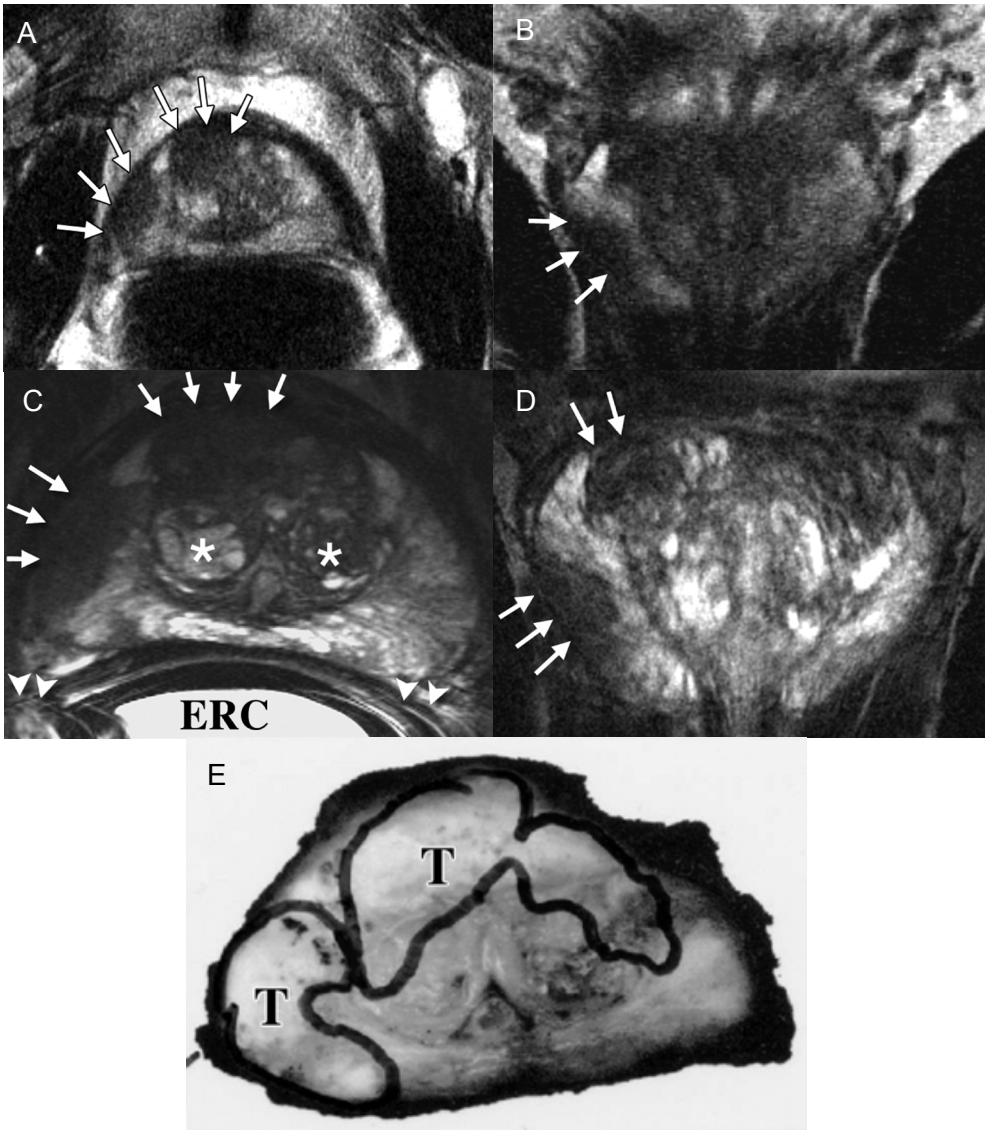

Figure 2. Comparison of image quality of T2-weighted fast spin-echo MR images at 3 T with BAC (3700/124) and ERC (5000/153) in a 58-year-old man (prostate-specific antigen level, 13.9 ng/mL; final Gleason score, 3 + 4; stage, pT3b). (A) Transverse and (B) coronal BAC MR images and (C) transverse and (D) coronal ERC MR images. On all images, the cancer (arrows) was localized correctly. Note the improved visibility of the internal architecture of the central gland (*) and the increased presence of motion artifacts (arrowheads) with ERC imaging on C. A right-left phase-encoding direction was chosen to prevent the motion artifacts from propagating over the prostate. (E) Corresponding axial whole-mount-section histopathologic slice of the mid gland shows the tumor (T) outlined.

Table 2. Comparison of Image Quality between BAC and ERC MR Imaging at 3 T in 46 Patients according to Four Readers

Image Quality Characteristic	BAC MR Imaging*	ERC MR Imaging*
Localization elements		
Discrimination between peripheral zone and central gland	3.27	4.28
Visibility of peripheral zone	3.44	4.32
Visibility of central gland	3.04	4.15
Visibility of lesion	3.09	3.78
Visualization of internal architecture of central gland	2.72	3.94
Staging elements		
Delineation of prostatic capsule	3.27	4.24
Visualization of neurovascular bundle	3.16	3.89
Visualization of rectoprostatic angle	3.47	4.32
General elements		
Impression of overall image quality	3.18	4.03
Presence of motion artifacts†	1.51	2.76

Note.—The two most experienced readers, radiologists A (J.J.F.) and B (S.W.T.P.J.H.), had 4 and 2 years of experience, respectively. Radiologists C (S.T.) and D (T.H.) both had 3 months of prior experience in prostate cancer MR imaging by using an ERC. Radiologist C had 8 years of experience in MR imaging at 1.5 T with a pelvic phased-array coil. For all image quality characteristics, $P < .001$ for comparison between BAC and ERC MR imaging.

* Values are the means of the scores assigned by four independent readers for image quality: score 1, poor; score 2, moderate; score 3, satisfactory; score 4, good; and score 5, excellent.

† Scores were assigned on the basis of a five-point scale: score 1, no artifacts were present; score 2, hardly any motion artifacts were present; score 3, image quality was satisfactory; score 4, image quality was moderately affected; and score 5, image quality was severely affected by motion artifacts

Prostate Cancer Localization Performance

Sixty-six cancer foci smaller than 0.5 cm^3 were excluded from analysis. Of the total of 644 segments (ie, 46 patients with 14 segments each), 150 were classified as containing prostate cancer foci of 0.5 cm^3 or larger on the basis of histopathologic findings. One hundred two were located in the peripheral zone, whereas 48 were located in the central gland. When the data for all readers were pooled, the AUC for localization increased significantly from 0.62 with BAC MR imaging to 0.68 with ERC MR imaging ($P < .001$) (Figure 3, Table 3). The AUC for localization of peripheral zone cancer foci increased significantly from 0.58 with BAC MR imaging to 0.68 with ERC MR imaging ($P < .001$) (Table 3). Likewise, the AUC for localization of central gland cancer foci increased significantly from 0.60 with BAC MR imaging to 0.66 with ERC MR imaging ($P < .001$) (Table 3). Improved localization performance was noted for ventral prostate cancer foci (Figure 4). For all readers, the sensitivity of localization of prostate cancer increased significantly with ERC MR imaging, whereas specificity remained stable (Table 4). No significant differences were found between BAC MR imaging and ERC MR imaging for localization performance in peripheral zone and central gland cancer foci for any reader or for all readers combined (Table 3).

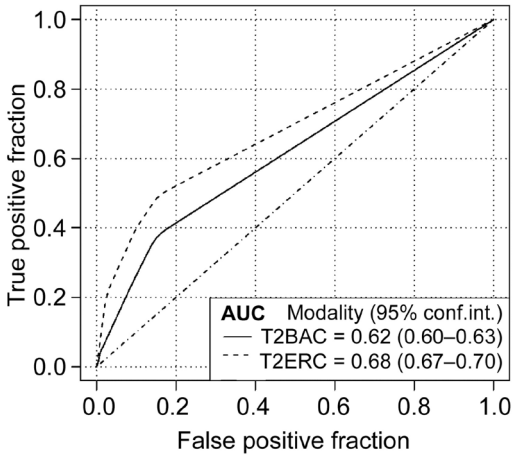

Figure 3. ROC curves and AUCs of prostate cancer localization for all four radiologists combined. At 3 T, the AUC improved significantly from 0.62 with BAC MR imaging to 0.68 with ERC MR imaging (P < .001). The AUCs for the individual readers are presented in Table 3. T2BAC = T2-weighted BAC MR imaging, T2ERC = T2-weighted ERC MR imaging.

Table 3. AUCs for Prostate Cancer Localization with BAC and ERC MR Imaging for Four Readers

Coil and Reader	All Cancer Foci	Peripheral Zone Cancer Foci	Central Gland Cancer Foci
BAC MR imaging			
All	0.62	0.58	0.60
Radiologist A	0.61	0.54	0.65
Radiologist B	0.59	0.57	0.58
Radiologist C	0.61	0.59	0.62
Radiologist D	0.55	0.57	0.50
ERC MR imaging			
All	0.68*	0.68*	0.66*
Radiologist A	0.67*	0.69*	0.64
Radiologist B	0.67*	0.69*	0.66
Radiologist C	0.63	0.63	0.62
Radiologist D	0.59*	0.58	0.59

Note.—See Table 2 for the level of experience of the radiologists.

* Value indicates a statistically significant increase (P < .05) with ERC MR imaging, compared with BAC MR imaging.

Table 4. Diagnostic Performance Parameters for Prostate Cancer Localization with BAC and ERC MR Imaging at 3 T in 46 included Patients for 644 Prostate Segments

Coil and Reader	Accuracy	Sensitivity	Specificity	PPV	NPV
BAC MR imaging					
Radiologist A	76 (487/644)	45 (67/150)	85 (420/494)	48 (67/141)	83 (420/503)
Radiologist B	76 (488/644)	41 (61/150)	86 (427/494)	48 (61/128)	83 (427/516)
Radiologist C	78 (502/644)	27 (41/150)	93 (461/494)	55 (41/74)	81 (461/570)
Radiologist D	67 (433/644)	33 (49/150)	78 (384/494)	31 (49/159)	79 (384/485)
ERC MR imaging					
Radiologist A	80 (512/644)*	58 (87/150)*	86 (425/494)	56 (87/156)	87 (425/488)
Radiologist B	76 (489/644)	53 (80/150)*	83 (409/494)	48 (80/165)	85 (409/479)
Radiologist C	79 (509/644)	39 (58/150)*	91 (451/494)	57 (58/101)	83 (451/543)
Radiologist D	71 (460/644)*	45 (68/150)*	79 (392/494)	40 (68/170)	83 (392/474)

Note.—All values are percentages. Numbers in parentheses were used to calculate the percentages. See Table 2 for the level of experience of the radiologists. NPV = negative predictive value, PPV = positive predictive value.

* Value indicates a statistically significant increase (P < .05) with ERC MR imaging, compared with BAC MR imaging.

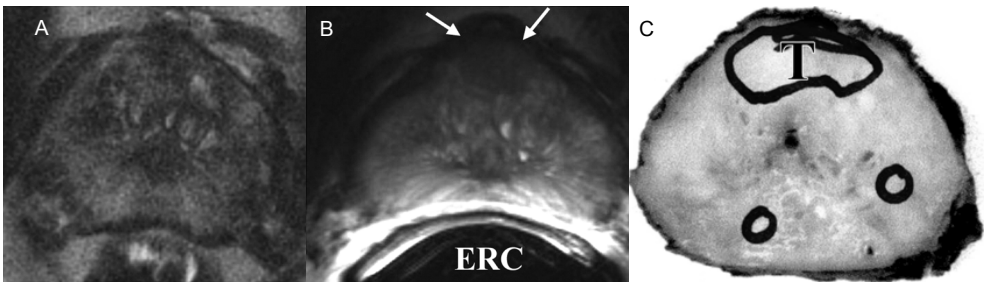

Figure 4. Example of a 1.8-cm^3 prostate cancer focus located in the central gland that was localized correctly only with ERC MR imaging in a 64-year-old man (prostate-specific antigen level, 6.9 ng/mL; final Gleason score, 3+3; stage, pT2c). (A) All four radiologists missed the cancer focus with BAC MR imaging. (B) With ERC MR imaging, three of the four radiologists localized the focus (arrows) correctly. (C) Histopathologic examination revealed the ventral cancer focus (T) outlined in blue, as well as two small peripheral zone tumor foci (volumes, <0.5 cm^3) outlined in blue.

Prostate Cancer Staging Performance

For radiologists A, B, and D, the AUCs (Figure 5) for staging increased significantly from 0.76, 0.61, and 0.55, respectively, with BAC MR imaging to 0.97, 0.97, and 0.79, respectively, with ERC MR imaging (P < .05). For radiologist C, the AUCs for BAC MR imaging and ERC MR imaging were 0.74 and 0.69, respectively (P < .05).

For all readers, the sensitivity for detection of locally advanced disease increased with ERC MR imaging (Table 5). For the most experienced radiologists, readers A and B, sensitivity increased significantly from 7% to 73%–80% (P < .05). For radiologist C, it increased from 7%

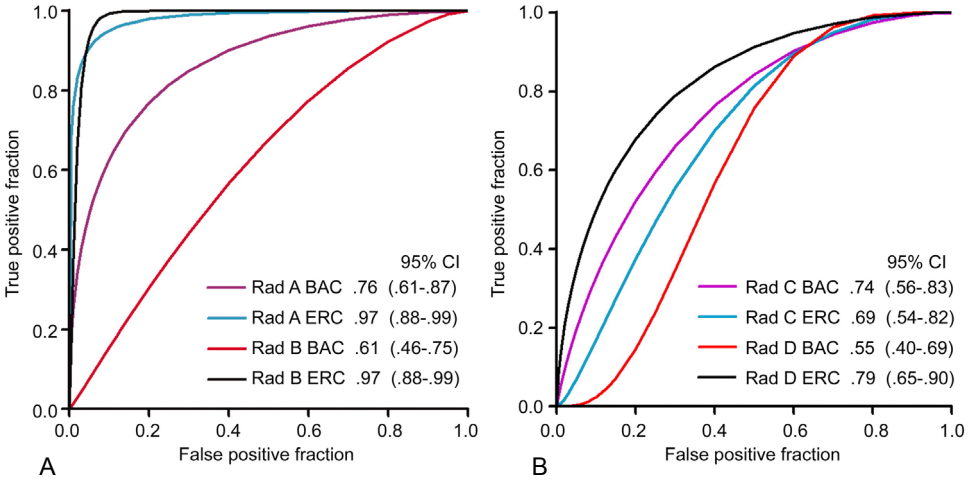

Figure 5. (a) ROC curves and AUCs of prostate cancer staging for the experienced radiologists A (J.J.F.) and B (S.W.T.P.J.H.) with 4 and 2 years of experience, respectively, in prostate MR imaging. The AUCs for both radiologists improved significantly (P < .05) with the ERC. (b) ROC curves and AUCs of prostate cancer staging for radiologists C (S.T.) and D (T.H.) with 3 months of experience. Radiologist C had 8 years of experience in MR imaging at 1.5 T with a pelvic phased-array coil. The AUC for radiologist D, who participated in a short training course about reading endorectal prostate MR images obtained at 3 T prior to assignment of scores, increased significantly (P < .05).

to 13%, and for radiologist D, it increased from 13% to 33% (P < .05). All readers achieved a high specificity of 94%–100% with ERC MR imaging.

Table 5. Diagnostic Performance of Prostate Cancer Staging for Stage pT3 versus Stage pT2 Disease with BAC and ERC MR Imaging at 3 T in 46 Patients Included in the Study

Coil and Reader	Accuracy	Sensitivity	Specificity	PPV	NPV
BAC MR imaging					
Radiologist A	70 (32/46)	7 (1/15)	100 (31/31)	100 (1/1)	69 (31/45)
Radiologist B	65 (30/46)	7 (1/15)	94 (29/31)	33 (1/3)	67 (29/43)
Radiologist C	70 (32/46)	7 (1/15)	100 (31/31)	100 (1/1)	69 (31/45)
Radiologist D	59 (27/46)	13 (2/15)	81 (25/31)	25 (2/8)	66 (25/38)
ERC MR imaging					
Radiologist A	93 (43/46)*	80 (12/15)*	100 (31/31)	100 (12/12)	91 (31/34)
Radiologist B	89 (41/46)*	73 (11/15)*	97 (30/31)	92 (11/12)	88 (30/34)
Radiologist C	67 (31/46)	13 (2/15)	94 (29/31)	50 (2/4)	69 (29/42)
Radiologist D	74 (34/46)	33 (5/15)	94 (29/31)	71 (5/7)	74 (29/39)

Note.—All values are percentages. Numbers in parentheses were used to calculate the percentages. See Table 2 for the level of experience of the radiologists. NPV = negative predictive value, PPV = positive predictive value.

* Value indicates a statistically significant increase (P < .05) with ERC MR imaging, compared with BAC MR imaging.

The sensitivity for detection of extracapsular penetration (stage pT3a disease) also improved for all readers with the use of an ERC (Figure 6). For the two most experienced radiologists, this increase was significant ($P < .05$). The sensitivity values for radiologists A, B, C, and D with BAC MR imaging were 8% (one of 13), 0% (0 of 13), 8% (one of 13), and 8% (one of 13), respectively, whereas specificity was 100% (33 of 33), 97% (32 of 33), 100% (33 of 33), and 91% (30 of 33), respectively. The respective accuracy values were 74% (34 of 46), 70% (32 of 46), 74% (34 of 46), and 67% (31 of 46). For ERC MR imaging, the sensitivity values for radiologists A, B, C, and D were 77% (10 of 13), 69% (nine of 13), 8% (one of 13), and 31% (four of 13), respectively, with specificity values of 94% (31 of 33), 97% (32 of 33), 94% (31

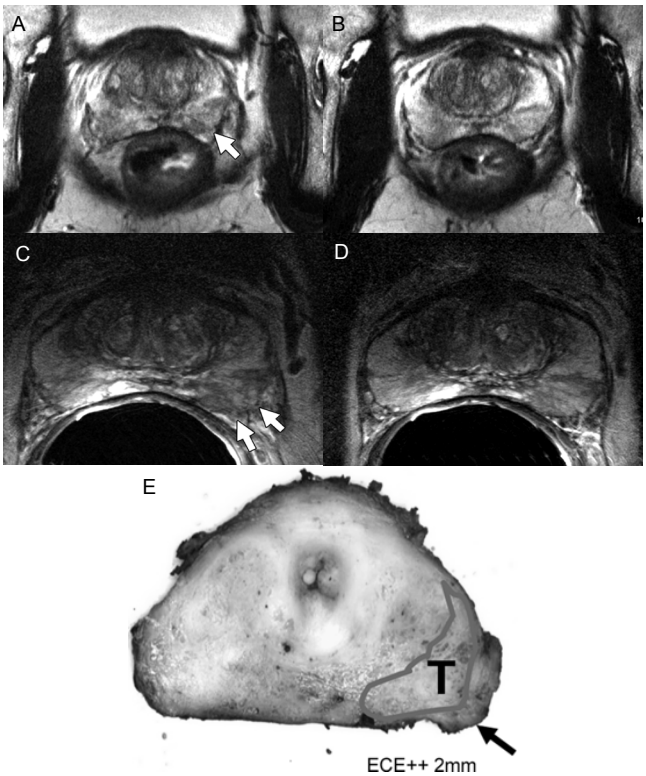

Figure 6. Example of a tumor with 2-mm radial distance of extracapsular extension (prostate-specific antigen level, 8.6 ng/mL; final Gleason score, 3 + 4; stage, pT3a) that was detected only with ERC MR imaging in a 61-year-old man. (A, B) Two consecutive transverse BAC T2-weighted fast spin-echo MR images (3700/124) show an area of low signal intensity in the left peripheral zone (arrow in a) that displayed no signs of locally advanced disease. (C, D) Corresponding consecutive transverse ERC T2-weighted fast spin-echo MR images (5000/153) show the area of low signal intensity with irregular bulging and obliteration of the rectoprostatic angle (arrows in C). (E) After wide excision at the left lateral side and resection of the neurovascular bundle on the left side, histopathologic examination confirmed the presence of tumor (T), outlined in blue, and the 2-mm radial extracapsular extension (ECE++ 2mm) (arrow) with surgical margins negative for tumor.

of 33), and 97% (32 of 33), respectively. The respective accuracy values were 89% (41 of 46), 89% (41 of 46), 70% (32 of 46), and 78% (36 of 46).

Of all six patients with extracapsular penetration with a radial distance (as determined by using histopathologic findings) of 0.5 mm or less, radiologists A, B, C, and D identified five, four, one, and two, respectively, with ERC MR imaging. Only one patient with extracapsular penetration of 0.5 mm or less was identified with BAC MR imaging by reader C, whereas the other readers did not identify any patient.

The sensitivity and specificity for detection of seminal vesicle invasion (stage pT3b disease) for radiologist A with BAC MR imaging were 0% (zero of five) and 100% (41 of 41), respectively, whereas for radiologist B these values were 20% (one of five) and 90% (37 of 41), respectively. The ERC MR imaging results were the same for radiologists A and B: Sensitivity and specificity values were 40% (two of five) and 100% (41 of 41), respectively. For BAC imaging, radiologists C and D had a sensitivity of 0% (zero of five) and 20% (one of five), respectively, with a specificity of 100% (41 of 41) and 88% (36 of 41), respectively. For ERC MR imaging, radiologists C and D had sensitivity values of 20% (one of five) and 0% (zero of five), respectively, with a specificity of 100% (41 of 41).

DISCUSSION

Results of our study show that, compared with BAC MR imaging at 3 T, ERC MR imaging at 3 T significantly improved image quality and, combined with higher spatial resolution, significantly increased the localization and staging performance for the experienced radiologists and the less experienced radiologist who participated in a short training course about reading images of the prostate obtained with ERC MR imaging at 3 T prior to assignment of scores.

The significant improvement in image quality is supported by an initial study in healthy volunteers in which the researchers concluded that several details of the prostate seen with endorectal MR imaging at 3 T could not be seen with endorectal MR imaging at 1.5 T or 3 T without the ERC [31].

Localization performance results of our study are similar to those obtained at 1.5 T for MR imaging with an ERC by investigators who found AUCs for localization by using T2-weighted imaging that varied between 0.67 and 0.83 when the results were compared with findings at radical prostatectomy [32]. This point illustrates that localization on T2-weighted MR images alone remains difficult without addition of functional MR imaging techniques. Dynamic contrast material–enhanced MR imaging and proton MR spectroscopic imaging have been reported to increase the localization performance of MR imaging at 1.5T [33–35]. Addition of these techniques at 3 T [5] may enhance the capability for localization of

prostate cancer, also in areas of hemorrhage after biopsy, and for staging of the disease [26]. In our study, we classified areas of low signal intensity on T2-weighted fast spin-echo images with corresponding areas of high signal intensity on T1-weighted gradient-echo images as negative because biopsy artifacts precluded interpretation. Thus, cancer foci could have been missed since hemorrhage after biopsy does not exclude the presence of cancer.

The significant increase in capsular delineation, visualization of the neurovascular bundle and rectoprostatic angle, and visibility of the lesion with endorectal MR imaging, caused by higher spatial resolution, improved staging performance. This finding explains the increase in sensitivity for detection of locally advanced disease for all readers. The significant increase in AUC for staging by the reader who participated in a short course with direct histopathologic feedback may indicate the need for such a course for radiologists with little experience with endorectal imaging at 3 T. Our results are congruous with earlier results by Mullerad et al [36] who re- ported a substantially improved staging performance for radiologists who specialized in urogenital radiology compared with general body radiologists. In our study, the radiologists who had 2 or more years of experience in prostate MR imaging obtained the highest AUCs and sensitivity values for staging. The differences in results between the experienced and less experienced readers were particularly large with the use of the ERC, thereby providing evidence for the particular expertise necessary to interpret endorectal MR images obtained at 3 T. This finding also is supported by the fact that reader C, who had experience with pelvic phased-array coil MR imaging at 1.5 T, performed better with the BAC than with the ERC at 3 T. It thus appears that in order to obtain accurate high-specificity staging with ERC MR imaging at 3 T, experience is an important factor.

It is difficult to compare our results with those of studies from the 1980s or early 1990s, because, currently, patients are identified earlier, and also, therefore, the number of patients with extraprostatic disease spread is lower and the spread is likely to be smaller as well. In our patient population, the average extraprostatic spread was 1.4 mm (range, 0.5–3.0 mm), and six of 13 patients had an extension of 0.5 mm or less. With BAC MR imaging, this small extension is extremely difficult to depict and determine with certainty. This difficulty in depiction, coupled with high-specificity reading, could explain the low sensitivity values for BAC imaging in the staging of patients. Comparison with previous studies is difficult because in none has the exact amount of the extraprostatic extent been described. Nevertheless, the spatial resolution of BAC imaging is too low for detection of the small extraprostatic extent that one can depict with ERC MR imaging.

Our staging results are in accordance with those obtained from an initial study of staging with 3-T ERC MR imaging, which show consistent high diagnostic performance with ERC imaging [12]. These results exceed those obtained at 1.5 T. Particularly when the

ERC is used at 3 T, minimal capsular penetration can be detected more accurately. In a large (*n* = 336) published study about ERC MR imaging at 1.5 T, only extensive locally advanced disease could be detected accurately: A sensitivity of only 40% (45 of 113) with a specificity of 95% (211 of 223) was obtained by two radiologists reading in consensus [37]. Nakashima et al (38) found a sensitivity of 62% (18 of 29) in the detection of locally advanced disease. With ERC 1.5-T MR imaging, two independent readers with 5 and 2 years of experience achieved sensitivity values of 54% (13 of 24) and 17% (four of 24), respectively, for the detection of extracapsular penetration [19].

Although specificity values for determination of seminal vesicle invasion were high (88%–100%) for all readers with both BAC MR imaging and ERC MR imaging, the sensitivity values were low (0%– 40%). Other researchers in studies with imaging at 1.5 T also found rather low sensitivity values (38). With the same cutoff point as used in our study, Sala et al (20) also found high (97%–99%) specificity with lower (50%– 63%) sensitivity with ERC 1.5-T MR imaging in 354 patients with a prevalence of seminal vesicle invasion of 14% (51 of 354). The small number of patients with seminal vesicle invasion limited the interpretation of the results of our study, and the diagnostic performance for detection of seminal vesicle invasion at 3 T needs to be investigated in larger patient populations. By its low prevalence (five patients in our study), it appears that readers are less likely to detect seminal vesicle invasion. Continuous training with imaging sets obtained in patients who had seminal vesicle invasion may increase the performance.

A general limitation of ERC MR imaging is that it is technically more challenging and may not be performed in all patients. In our study, in five of the six excluded patients, the reason for the exclusion was related to the ERC.

A limitation of our study is the relatively low prevalence (15 of 46, 33%) of patients with locally advanced disease. Also, extracapsular penetration was small (mean penetration distance, 1.4 mm). Nevertheless, these factors reflect the current patient population in general urologic clinics because of the widespread use of the prostate-specific antigen level for screening [39].

Furthermore, by applying bowel movement suppression only before ERC MR imaging, we may have artificially increased ERC image quality. However, the introduction and presence of the ERC in the rectum itself causes bowel discomfort and reactionary bowel movement, as can be deduced from the higher motion artifact scores with ERC imaging.

Thus, bowel suppression actually may have enhanced objective comparison between BAC MR imaging and ERC MR imaging.

In our study, the choice of the TE for both BAC MR imaging and ERC MR imaging was restricted by a combination of the specific absorption rate, matrix size, and echo train length. To fully use the high signal-to-noise ratio of the ERC, a large matrix size was applied. As shortening of the radiofrequency pulses was precluded by the specific absorption rate limit, the larger matrix size increased the inter-TE and thereby also the TE of the image series. Thus, our TEs were longer than the established mean T2 value of the entire prostate at 3 T [40]. However, using TEs beyond the T2 of the prostate is common practice at 1.5 T (eg, TE of 96–132 msec vs T2 of 88 msec) (16,26), as the difference in signal intensity between healthy prostate tissue and cancerous prostate tissue is important. At longer TEs, this difference is more profound, provided the tissue with shortest T2 still has adequate signal-to-noise ratio. With novel radiofrequency pulse techniques, however, it is advised that TEs of approximately 100 msec are used when the signal is acquired.

Readers could not be blinded to whether they were reviewing BAC MR images or ERC MR images, since the presence or absence of the ERC and the prostate shape already would have indicated the type of image. This could possibly have led readers to systematically provide lower scores for BAC images. To minimize bias, BAC and ERC image sets were evaluated separately and randomly. Furthermore, readers were instructed to perform a certain type of reading (high-sensitivity localization and high-specificity staging). This specification of the type of reading could have influenced our results, particularly the sensitivity in staging. Possibly, this factor influenced BAC MR imaging more than it did ERC MR imaging. Nevertheless, in preoperative prostate cancer staging, it is common practice to perform high-specificity reading.

The limitation of a possible discrepancy and potential difficulty in comparing both BAC MR imaging and ERC MR imaging findings with histopathologic examination findings because of the changed alignment of the prostate after insertion of the ERC was minimized by using anatomic landmarks of the prostate [25] to correlate results of T2- weighted fast spin-echo imaging with histopathologic findings.
Endorectal MR imaging can play a role in accurate delineation of cancer foci in the planning of intensity-modulated radiation therapy and enable radiation boosting to areas within the prostate. Moreover, it can facilitate nerve-sparing decisions with determination of the proximity of the cancer to the neurovascular bundle [41]. Likewise, since the clinical implications of small extracapsular penetration are being debated as to whether this penetration has an effect on patient survival, prior knowledge of its localization may aid urologists in obtaining negative surgical margins.

In conclusion, MR image quality of the prostate improved significantly with the use of an ERC. For prostate cancer localization, performance with ERC MR imaging was significantly better than was that with BAC MR imaging. Also, when we used the ERC, the staging performance

improved significantly in the two experienced readers and the less experienced reader who participated in a short course about endorectal prostate MR reading at 3 T prior to assignment of scores. Therefore, also at 3 T, the ERC is necessary for accurate localization and staging of prostate cancer.

Acknowledgments: The authors thank Yvonne L. Hoogeveen, PhD (Radboud University Nijmegen Medical Center, Nijmegen, the Netherlands), for her assistance in preparing the manuscript, as well as George J. Misic (Medrad, Pittsburgh, Pa) and Dennis W. J. Klomp, BSc (Radboud University Nijmegen Medical Center, Nijmegen, the Netherlands), for their expertise and work on the prototype 3-T endorectal coil.

REFERENCES

[1] Carrol CL, Sommer FG, McNeal JE, Stamey TA. The abnormal prostate: MR imaging at 1.5 T with histopathologic correlation. Radiology 1987;163:521–525.

[2] Claus FG, Hricak H, Hattery RR. Pretreatment evaluation of prostate cancer: role of MR imaging and 1H MR spectroscopy. RadioGraphics 2004;24:S167–S180.

[3] Hricak H, White S, Vigneron D, et al. Carcinoma of the prostate gland: MR imaging with pelvic phased-array coils versus integrated endorectal–pelvic phased-array coils. Radiology 1994;193:703-709.

[4] Rouviere O, Hartman RP, Lyonnet D. Prostate MR imaging at high-field strength: evolution or revolution? Eur Radiol 2006;16:276–284.

[5] Fütterer JJ, Scheenen TW, Huisman HJ, et al. Initial experience of 3 Tesla endorectal coil magnetic resonance imaging and 1H-spectroscopic imaging of the prostate. Invest Radiol 2004;39:671–680.

[6] Sosna J, Pedrosa I, Dewolf WC, Mahallati H, Lenkinski RE, Rofsky NM. MR imaging of the prostate at 3 Tesla: comparison of an external phased-array coil to imaging with an endorectal coil at 1.5 Tesla. Acad Radiol 2004;11:857–862.

[7] Zelefsky MJ, Fuks Z, Leibel SA. Intensity-modulated radiation therapy for prostate cancer. Semin Radiat Oncol 2002;12:229–237.

[8] Hong TS, Ritter MA, Tome WA, Harari PM. Intensity-modulated radiation therapy: emerging cancer treatment technology. Br J Cancer 2005;92:1819–1824.

[9] Wang L, Hricak H, Kattan MW, Chen HN, Scardino PT, Kuroiwa K. Prediction of organ-confined prostate cancer: incremental value of MR Imaging and MR spectroscopic imaging to staging nomograms. Radiology 2006;238:597–603.

[10] Jager GJ, Severens JL, Thornbury JR, de la Rosette JJ, Ruijs SH, Barentsz JO. Prostate cancer staging: should MR imaging be used? a decision analytic approach. Radiology 2000;215:445–451.

[11] Engelbrecht MR, Jager GJ, Laheij RJ, Verbeek AL, van Lier HJ, Barentsz JO. Local staging of prostate cancer using magnetic resonance imaging: a meta-analysis. Eur Radiol 2002;12:2294–2302.

[12] Fütterer JJ, Heijmink SW, Scheenen TW, et al. Prostate cancer: local staging at 3-T endorectal MR imaging— early experience. Radiology 2006;238:184–191.

[13] Hennig J, Scheffler K. Hyperechoes. Magn Reson Med 2001;46:6–12.

[14] Beyersdorff D, Taymoorian K, Knosel T, et al. MRI of Prostate cancer at 1.5 and 3.0 T: comparison of image quality in tumor detection and staging. AJR Am J Roentgenol 2005;185:1214 –1220.

[15] Cruz M, Tsuda K, Narumi Y, et al. Characterization of low-intensity lesions in the peripheral zone of prostate on pre-biopsy endorectal coil MR imaging. Eur Radiol 2002;12:357–365.

[16] Akin O, Sala E, Moskowitz CS, et al. Transition zone prostate cancers: features, detection, localization, and staging at endorectal MR imaging. Radiology 2006;239:784–792.

[17] Li H, Sugimura K, Kaji Y, et al. Conventional MRI capabilities in the diagnosis of prostate cancer in the transition zone. AJR Am J Roentgenol 2006;186:729–742.

[18] White S, Hricak H, Forstner R, et al. Prostate cancer: effect of postbiopsy hemorrhage on interpretation of MR images. Radiology 1995;195:385–390.

[19] Yu KK, Scheidler J, Hricak H, et al. Prostate cancer: prediction of extracapsular extension with endorectal MR imaging and three-dimensional proton MR spectroscopic imaging. Radiology 1999;213:481–488.

[20] Sala E, Akin O, Moskowitz CS, et al. Endorectal MR imaging in the evaluation of seminal vesicle invasion: diagnostic

accuracy and multivariate feature analysis. Radiology 2006;238:929–937.

[21] Jager GJ, Ruijter ET, van de Kaa CA, et al. Local staging of prostate cancer with endorectal MR imaging: correlation with histopathology. AJR Am J Roentgenol 1996;166:845– 852.

[22] Langlotz CP, Schnall MD, Malkowicz SB, Schwartz JS. Cost-effectiveness of endorectal magnetic resonance imaging for the staging of prostate cancer. Acad Radiol 1996;3(S1):S24-27.

[23] Davis BJ, Pisansky TM, Wilson TM, et al. The radial distance of extraprostatic extension of prostate carcinoma: implications for prostate brachytherapy. Cancer 1999;85:2630–2637.

[24] Greene F, Page D, Fleming I, et al. AJCC Cancer staging manual. 6th ed. New York, NY: Springer Verlag, 2002.

[25] Zakian KL, Sircar K, Hricak H, et al. Correlation of proton MR spectroscopic imaging with Gleason score based on step-section pathologic analysis after radical prostatectomy. Radiology 2005;234:804–814.

[26] Fütterer JJ, Engelbrecht MR, Huisman HJ, et al. Staging prostate cancer with dynamic contrast-enhanced endorectal MR imaging prior to radical prostatectomy: experienced versus less experienced readers. Radiology 2005;237:541–549.

[27] Fütterer JJ, Heijmink SW, Scheenen TW, et al. Prostate cancer localization with dynamic contrast-enhanced MR imaging and proton MR spectroscopic imaging. Radiology 2006;241:449–458.

[28] Obuchowski NA, Lieber ML, Powell KA. Data analysis for detection and localization of multiple abnormalities with application to mammography. Acad Radiol 2000;7:516-525.

[29] Rutter CM. Bootstrap estimation of diagnostic accuracy with patient-clustered data. Acad Radiol 2000;7:413–419.

[30] Ihaka R, Gentleman R. R: a language for data analysis and graphics. J Comput Graph Stat 1996;5:299–314.

[31] Bloch BN, Rofsky NM, Baroni RH, Marquis RP, Pedrosa I, Lenkinski RE. 3 Tesla magnetic resonance imaging of the prostate with combined pelvic phased-array and endorectal coils: initial experience. Acad Radiol 2004;11:863–867.

[32] Mullerad M, Hricak H, Kuroiwa K, et al. Comparison of endorectal magnetic resonance imaging, guided prostate biopsy and digital rectal examination in the preoperative anatomical localization of prostate cancer. J Urol 2005;174:2158–2163.

[33] Kurhanewicz J, Swanson MG, Nelson SJ, Vigneron DB. Combined magnetic resonance imaging and spectroscopic imaging approach to molecular imaging of prostate cancer. J Magn Reson Imaging 2002;16:451–463.

[34] Engelbrecht MR, Huisman HJ, Laheij RJ, et al. Discrimination of prostate cancer from normal peripheral zone and central gland tissue by using dynamic contrast-enhanced MR imaging. Radiology 2003;229:248–254.

[35] van Dorsten FA, van der Graaf M, Engelbrecht MR, et al. Combined quantitative dynamic contrast-enhanced MR imaging and (1)H MR spectroscopic imaging of human prostate cancer. J Magn Reson Imaging 2004;20:279–287.

[36] Mullerad M, Hricak H, Wang L, Chen HN, Kattan MW, Scardino PT. Prostate cancer: detection of extracapsular extension by genitourinary and general body radiologists at MR imaging. Radiology 2004;232:140–146.

[37] Cornud F, Flam T, Chauveinc L, et al. Extraprostatic spread of clinically localized prostate cancer: factors predictive of pT3 tumor and of positive endorectal MR imaging examination results. Radiology 2002;224:203–210.

[38] Nakashima J, Tanimoto A, Imai Y, et al. Endorectal MRI for prediction of tumor

site, tumor size, and local extension of prostate cancer. Urology 2004;64:101–105.

[39] Okihara K, Nakanishi H, Nakamura T, Mizutani Y, Kawauchi A, Miki T. Clinical characteristics of prostate cancer in Japanese men in the eras before and after serum prostate-specific antigen testing. Int J Urol 2005;12:662–667.

[40] de Bazelaire CM, Duhamel GD, Rofsky NM, Alsop DC. MR imaging relaxation times of abdominal and pelvic tissues measured in vivo at 3.0 T: preliminary results. Radiology 2004;230:652–659.

[41] Hricak H, Wang L, Wei DC, et al. The role of preoperative endorectal magnetic resonance imaging in the decision regarding whether to preserve or resect neurovascular bundles during radical retropubic prostatectomy. Cancer 2004;100:2655–2663.

CHAPTER 6

Changes in Prostate Shape and Volume and Their Implications for Radiotherapy after Introduction of Endorectal Balloon as Determined by MRI at 3T

Stijn W. T. P. J. Heijmink
Tom W. J. Scheenen
Emile N. J. T. van Lin
Andries G. Visser
Lambertus A. L. M. Kiemeney
J. Alfred Witjes
Jelle O. Barentsz

Int J Radiat Oncol Biol Phys 2009;73(5):1446-53.

Purpose: To determine the changes in prostate shape and volume after the introduction of an endorectal coil (ERC) by means of magnetic resonance imaging (MRI) at 3T.

Methods and materials: A total of 44 consecutive patients with biopsy-proven prostate cancer underwent separate MRI examinations at 3T with a body array coil and subsequently with an ERC inflated with 50 mL of fluid. Prospectively, two experienced readers independently evaluated all data sets in random order. The maximal antero-posterior, right-to-left, and craniocaudal prostate diameters, as well as the total prostate and peripheral zone and central gland volumes were measured before and after ERC introduction. The changes in prostate shape and volume were analyzed using Wilcoxon's test for paired samples.

Results: The introduction of the ERC significantly changed the prostate shape in all three directions, with mean changes in the anteroposterior, right-to-left, and craniocaudal diameters of 15.7% (5.5 mm), 7.7% (3.5 mm), and 6.3% (2.2 mm), respectively. The mean total prostate, peripheral zone, and central gland volume decreased significantly after ERC introduction by 17.9% (8.3 cm^3), 21.6% (4.8 cm^3), and 14.2% (3.4 cm^3), respectively.

Conclusion: ERC introduction as observed by 3T MRI changed the prostate shape and volume significantly. The mean anteroposterior diameter was reduced by nearly one-sixth of its original diameter, and the mean total prostate volume was decreased by approximately 18%. This could cause difficulties and should be considered when using ERC-based MRI for MRI-computed tomography fusion and radiotherapy planning.

INTRODUCTION

Advanced imaging techniques that provide both anatomic and functional information are being gradually introduced into clinical practice. In radiation oncology, prostate magnetic resonance imaging (MRI) techniques can be fused with planning computed tomography (CT) scans and have been shown to enable improved target delineation [1, 2].

Functional MRI techniques, such as dynamic contrast-enhanced MRI [3, 4] and proton MRI spectroscopic imaging [5–9], can lead to more accurate localization and staging of prostate cancer [4, 10, 11] and are established methods for the early evaluation of the radiotherapy (RT) effect [12, 13]. These advanced MRI techniques can also detect so-called intraprostatic dominant lesions and have opened the way for advanced "dose-painting" RT delivery in both brachytherapy [14–17] and external beam RT [18, 19]. The integration of the anatomic prostate on MRI with the CT-MRI marker-based fusion method described by Huisman et al. [20] has been implemented into our daily clinical practice. The use of the endorectal coil (ERC) increases the resolution and improves the localization and staging compared with application of external coils alone [21, 22]. Compared with 1.5T, imaging at high-field strengths such as 3T improves the resolution. Performing imaging without an ERC would have a number of advantages, including less patient discomfort, lower costs, and better correlation with RT planning, if the latter has been performed without an endorectal balloon (ERB). However, the use of an ERB in localized prostate RT has been proved advantageous [19, 23–26] and well tolerated [27, 28]. For RT planning and during RT sessions, ERBs that are similar to the ERC in construction and shape can be used. Nevertheless, the introduction of an ERC causes changes in both the shape and possibly the volume of the prostate [29, 30]. The purpose of this study was to determine the exact changes in prostate shape by comparing the prostate diameters and volumes before and after the introduction of an ERC using MRI at a field strength of 3T and to discuss the possible implications for RT.

METHODS AND MATERIALS

Patient characteristics

The institutional review board approved this prospective study. Before inclusion, all patients provided written informed consent. Between September 2004 and December 2005, 44 consecutive patients with biopsy-proven prostate cancer who had not received any form of hormonal therapy, surgery, or RT were scheduled to undergo MRI. The exclusion criteria were contraindications to MRI (e.g., the presence of a pacemaker or metal cerebral clips), severe claustrophobia, or contraindications to ERC insertion (e.g., previous anorectal surgery, inflammatory bowel disease, high anal sphincter tension). For all included patients, the interval between the last biopsy procedure and MRI was determined.

MRI acquisition

All images were obtained using a 3T whole-body scanner (Magnetom TRIO, Siemens Medical Solutions, Erlangen, Germany). Before the examination, patients were asked to void to empty the bladder as much as possible. First, T2-weighted images in three planes with an external body array coil were obtained [22]. Second, after removal of the body array coil and a digital rectal examination, an ERC (Medrad, Pittsburgh, PA; Figure 1) was inserted, and, subsequently, the balloon was inflated with 50 mL of fluid. The fluids used were either demineralized water or perfluoropolyether (Fomblin, Solvay Solexis, Milan, Italy). Bowel motion was suppressed by an intramuscular injection of 1 mg of glucagon (Glucagen, Novo Nordisk A/S, Denmark). T2-weighted images in three planes were obtained [22].

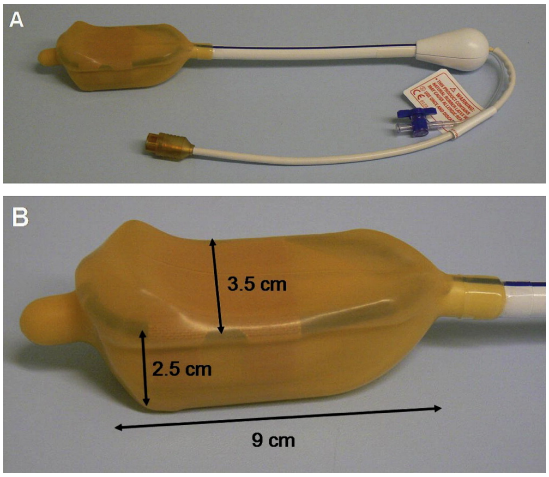

Figure 1. (A) Overview of commercially available 3T endorectal coil (Medrad, Pittsburgh, PA). (B) Detailed view of diameters of endorectal coil balloon tip before filling.

MRI measurements

To prevent an information bias, the readers never scored the imaging sets of the same patient in the same session and the order of reading was randomized.

Image quality determination. Two of us, a radiologist (S.W.T.P.J.H.) with 3 years of experience in endorectal prostate MRI interpretation corresponding to previously having read 250 endorectal MRI studies, and an MRI spectroscopist (T.W.J.S.) with 4.5 years of experience in reviewing prostate MRI examinations (approximately 300 previous studies), independently reviewed all imaging sets. Both readers scored the image quality of each set according to the presence of motion artifacts affecting image interpretation, particularly the visualization of the prostate contours. If either imaging set was scored as insufficient by one of the readers, the patient was excluded from additional analysis.

Prostate size. Both readers assessed the prostate size in three directions on a digital workstation (Agfaweb Impax, Agfa, Mortsel, Belgium). The largest medial anteroposterior and right-to-left diameters were measured in the axial plane, and the largest craniocaudal diameter was assessed in the coronal plane.

Prostate volume. The prostate volume was calculated by manually determining the prostate outline on every axial T2-weighted MRI slice. One reader (S.W.T.P.J.H.) drew a freehand contour around the prostate on each imaging slice on a commercially available workstation (Syngo VX49B, Leonardo VD10B, Siemens AG, Berlin, Germany). For each slice, the number of pixels within the contour was automatically established, and, with the known in-plane resolution and slice thickness, the prostate volume was calculated. Subsequently, a separate contour was drawn around the peripheral zone alone to obtain its volume. By subtracting the peripheral zone volume from the total volume, the volume of the central gland (i.e., transition zone, central zone, and periurethral area) was obtained. Finally, the relative volume changes (expressed as percentages of the volume before ERC introduction) were calculated.

Statistical analysis

The diameters as determined by both observers were compared by calculating the mean differences between the readers in absolute terms and as a percentage of the readers' mean. Likewise, of the total number of 264 observations (44 patients x 2 imaging settings x 3 diameters), the absolute differences were analyzed to determine the interobserver variation. Subsequently, 95% confidence intervals of the means were calculated.

The changes in prostate diameter and prostate volumes were compared using Wilcoxon's signed rank test for paired samples. To investigate whether the original size of the prostate influenced the changes in diameters and volumes, changes in large prostates (clinically deemed enlarged; i.e., 40 cm^3 before ERC introduction) and small prostates (< 40 cm^3) were evaluated separately by applying the t test for unpaired samples. The diameter and volume changes were visualized on Bland-Altman plots.

All p values reported were from two-sided tests, with $p \leq 0.05$ considered statistically significant. Statistical analyses were performed using MedCalc, version 8.1.0.0 (MedCalc Software, Mariakerke, Belgium).

RESULTS

Patient characteristics

Both readers scored the image quality of all individual patients as sufficient; therefore, the data from all 44 analyzed patients were included in the study. The mean age, mean prostate-specific antigen level, and median Gleason biopsy score was 61 years (range, 51–70), 7.77

ng/mL (median, 6.07; range, 3.48–24.63), and 6 (range, 5-9), respectively. The average interval between biopsy and MRI was 112 days (range, 21–226).

Observer variations

In 133 (50%) of 264 observations, the difference between the two readers was ≤ 1 mm, and in 186 (70%), the difference was ≤ 2 mm. The mean of the differences between the diameter scores of the readers before ERC introduction was 1.87 mm (mean difference as a percentage of the mean score, 4.9%, 95% confidence interval, 3.9–5.9%). After ERC introduction, the mean of the differences was 2.34 mm (mean difference as a percentage of the mean score, 6.1%, 95% confidence interval, 5.0–7.2%).

Changes in prostate diameters

All three prostate diameters changed and the change was statistically significant ($p < 0.05$) after ERC introduction (Table 1 and Figures 2 and 3). On average, the anteroposterior prostate diameter decreased by 5.4 mm, corresponding to a reduction of 15.7% from the original diameter. The mean right-to-left and craniocaudal diameter increased by 3.5 mm (8%) and 2.2 mm (7%), respectively. No differences were observed between the water and perfluoro polyether filling of the ERC.

Table 1. Comparison of prostate diameters before and after endorectal coil introduction

Mean prostate diameter* (mm)	ERC insertion		Mean difference (95% CI)	Mean difference as percentage before ERC insertion (95% CI)	P
	Before	After			
AP	35.03	29.66	-5.38 (-3.88--6.87)	-15.7 (-11.1--20.3)	<0.05
RL	48.67	52.16	+3.49 (1.34-4.73)	+7.69 (4.39-11.0)	<0.05
CC	39.90	42.14	+2.24 (0.38-4.10)	+6.28 (1.16-11.4)	<0.05

Abbreviations: ERC = endorectal coil; CI = confidence interval; AP = anteroposterior; RL = right-to-left; CC = craniocaudal.

* All data presented as mean of two independent readers.

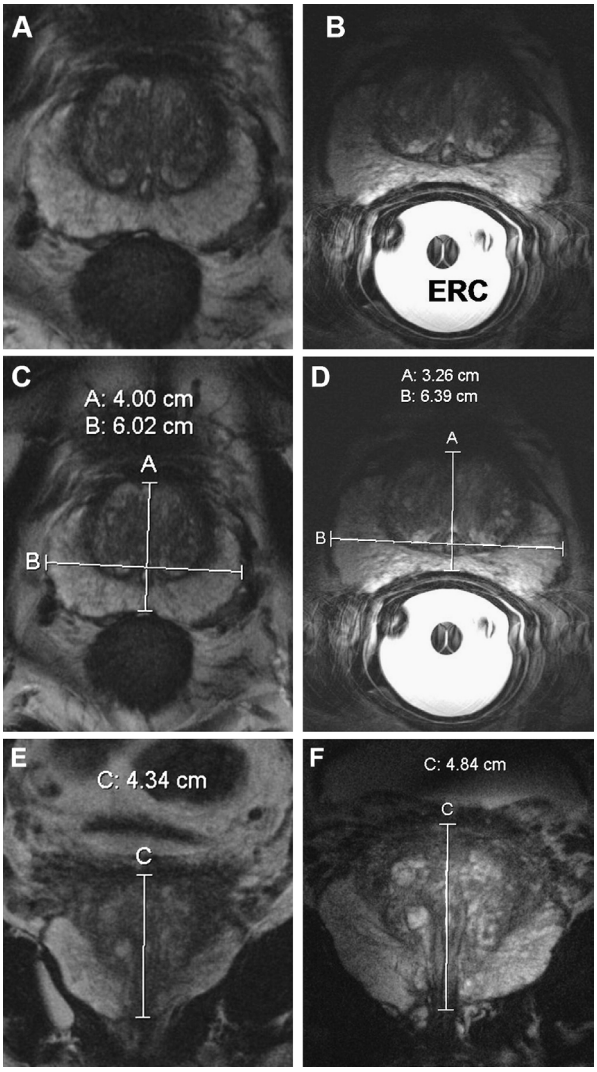

Figure 2. Example of MR images obtained with (A,C,E) external surface coils and (B,D,F) endorectal coil (ERC) filled with demineralized water. (C,D) Maximal prostate diameter change after introduction and inflation of ERC in anteroposterior direction decreased by 18.5% and right-to-left diameter increased by 6.1%. (E,F) Maximal craniocaudal diameter increased by 11.5%.

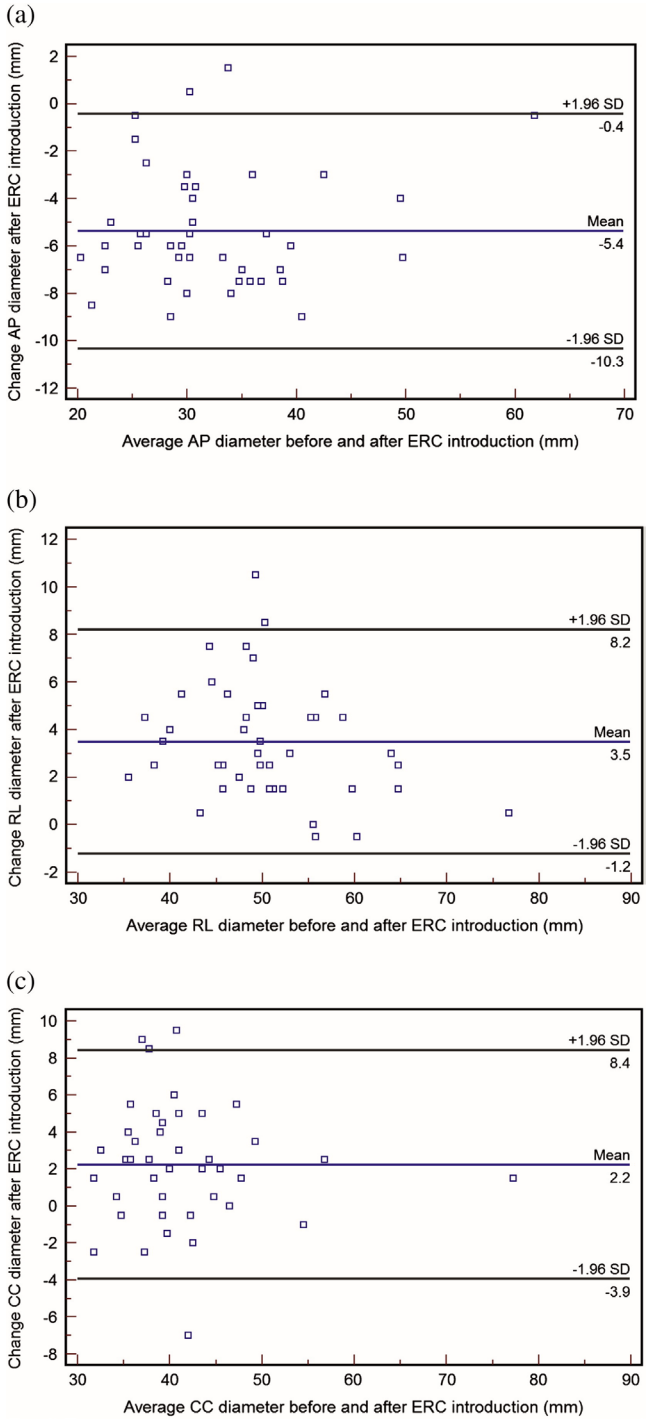

Figure 3. Bland-Altman plots of absolute change in (a) anteroposterior (AP), (b) right-to-left (RL), and (c) craniocaudal (CC) diameters of the prostate after endorectal coil (ERC) introduction.

Changes in prostate volume with introduction of ERC

The mean total prostate volume decreased significantly ($p < 0.05$) from 50.4 cm^3 before ERC introduction to 42.2 cm^3 after (Table 2 and Figures 4 and 5). The change in volume ranged from 0.3 to 23.9 cm^3. For the peripheral zone alone, the mean volume decreased significantly ($p < 0.05$) from 21.9 cm^3 to 17.0 cm^3, with a range of volume change of 0.3–11.2 cm^3. Also, the mean central gland volume decreased significantly ($p < 0.05$) from 28.6 cm^3 to 25.2 cm^3 (volume change range, 0–13.3). The mean relative change in the volume of the peripheral zone (21.6%) was significantly ($p < 0.05$) greater than that of the total prostate volume (17.9%) and central gland volume (14.2%).

Table 2. Comparison of prostate volumes before and after endorectal coil introduction

Mean prostate Volume (cm^3)	ERC insertion		Mean difference (95% CI)	Mean difference as percentage before ERC insertion (95% CI)	P
	Before	After			
Total prostate gland	50.44	42.18	-8.26 (-6.53--9.98)	-17.9 (-14.7--21.1)	<0.05
Peripheral zone	21.85	17.03	-4.83 (-3.94--5.72)	-21.6 (-18.3--24.8)	<0.05
Central gland	28.58	25.15	-3.43 (-2.37--4.50)	-14.2 (-10.2--18.2)	<0.05

Abbreviations as in Table 1.

* Defined as total prostate gland volume minus peripheral zone volume and thus including transition zone, central zone, and periurethral area.

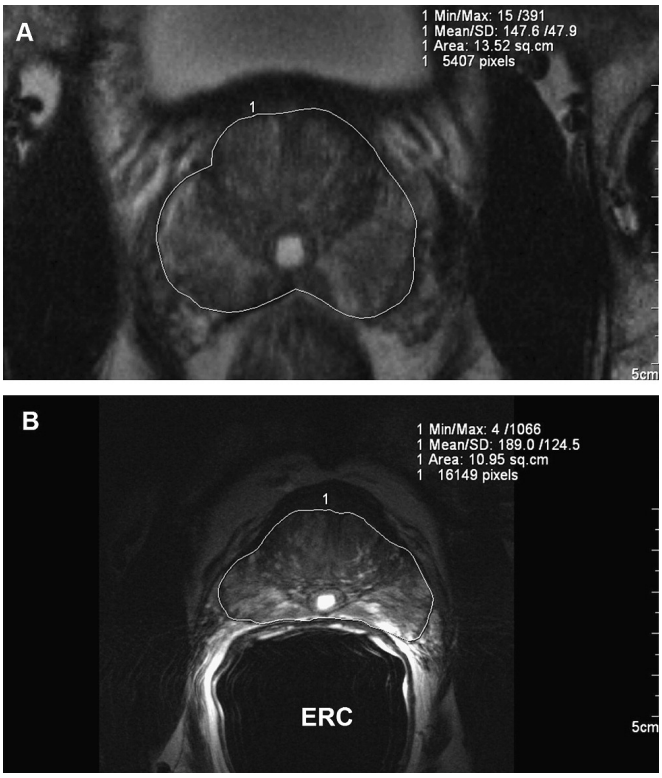

Figure 4. Determination of prostatic volume using example determination in one slice with (A) body-array coil and (B) endorectal coil (ERC) filled with perfluoropolyether (Fomblin, Solvay Solexis, Milan, Italy). After drawing region of interest around prostate, number of pixels calculated automatically. With known slice thickness and in-plane resolution, volume per slice could be determined: 4.0 cm^3 (5407 × 0.43 × 0.43 × 4 mm^3) for slice with body-array coil and 3.3 cm^3 (16149 × 0.26 × 0.26 × 3 mm^3) for slice with endorectal coil.

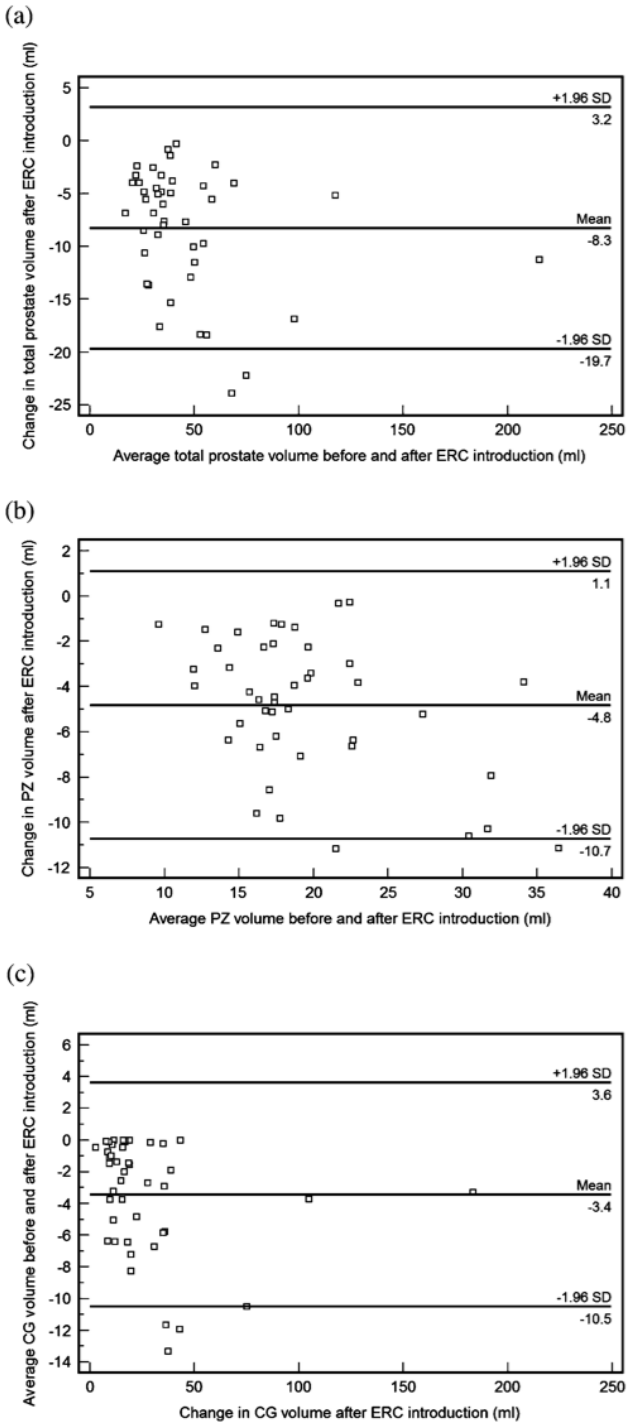

Figure 5. Bland-Altman plots of absolute change in volume of (a) entire prostate, (b) peripheral zone, and (c) central gland after introduction of endorectal coil (ERC). All mean volumes changed significantly ($p < 0.05$). PZ = peripheral zone; CG = central gland.

The relative prostate volume change for larger (>40 cm^3) and smaller (<40 cm^3) prostates did not differ significantly ($p > 0.05$) at 17.0% and 18.8%, respectively.

No differences were observed between the water and perfluoro polyether ERC filling.

DISCUSSION

Our results have demonstrated that the ERC causes significant changes in the prostate diameters and a significant volume decrease. The main advantage of using an ERC is the greater imaging resolution. However, our study has shown that the changes between situations without and with the ERC or ERB are substantial, and we believe that RT planning and procedures should be performed in the same setting in which the MRI has been performed.

Our results show that the introduction of an ERC at 3T significantly changes all three prostate diameters, most markedly in the anteroposterior direction, compressing the prostate by nearly 16% of its original diameter. A significant decrease in volume was observed for both the peripheral zone and the central gland and, thereby, for the entire prostate. Because biologic materials are generally considered to be incompressible [31], we hypothesized that this decrease in prostate volume originated from expulsion of fluid. Seminal fluid and fluids within the ducts could be extruded by application of pressure, similar to what happens during ejaculation. Also, blood vessels could be compressed by the substantial pressure of the balloon, resulting in a decrease in blood volume.

Our results regarding the prostate diameter changes are in line with those of a previous study of 10 prostate cancer patients by Kim et al. [30] that demonstrated that an expandable 1.5T ERC caused more prostate deformation than did a rigid coil. They found a mean anteroposterior diameter compression of 4.1 mm (our study, 5.4 mm) and a mean right-to-left diameter expansion of 3.8 mm (our study, 3.5 mm). The change in the craniocaudal diameter was not analyzed in-depth; however, it was reported to be <3 mm in all patients (our study, mean change of 2.2 mm). The investigators, however, did not describe the volume to which the ERC was inflated, making direct comparisons with our results more difficult. Also, the prostate volumes were not analyzed in that study. In contrast, our study was performed at 3T. Therefore, our imaging spatial resolution was greater than theirs at 1.5T imaging, thereby increasing the accuracy in determining the diameters in our study.

Because the setup, shape, and expansive characteristics of the 3T ERC do not differ substantially from that of the 1.5T ERC, it can be assumed that the presented results obtained at 3T can be generalized to those of 1.5T ERC-based MRI. In our study, patients with a wide range of prostate-specific antigen levels and biopsy Gleason scores were included.

Therefore, we are confident that our results can be generalized to the whole population of prostate cancer patients with biopsy-proven prostate cancer who are undergoing RT.

Our observations could have several implications for RT planning. First, registration (or fusion) of MRI studies, obtained with an ERC, and CT images, performed without an ERB similar to the ERC in construction and shape, could cause substantial difficulties and result in less accurate delineation of the pelvic structures. To overcome these problems, algorithms have been developed [14, 16] or MRI-defined volumes have been manually entered into the planning system and the gland distortion only addressed visually [15, 17]. A recently presented MRI-CT fusion study for high-dose intraprostatic dominant lesion–intensity-modulated RT, in which an ERB identical to the MRI ERC was used for CT scanning [19], resulted in almost equal deformation of the prostate gland on the MRI and CT studies, and thereby obtaining an accurate intraprostatic dominant lesion projection onto the CT images. The iterative closest point method, in which the gold marker surface models are automatically registered, yielded an MRI-CT fusion precision of 1.1 mm in a data set of 21 patients, using five operators [20]. However, it is unclear whether the extensive prostate deformations due to the introduction of the ERC that were found in our study might be sufficiently compensated for by any algorithm.

Second, the clinical use and tolerability of an ERB during treatment has been extensively described [19, 23–28]. The use of the ERB adds only few (range, 3–5) minutes to the whole RT procedure. Although an ERB does not reduce the day-to-day interfraction prostate displacements completely [32, 33], it is advisable to use the ERB in combination with a prostate position verification and correction protocol.

Third, by using an ERC and ERB, the target volume for RT will be decreased. Thus, the overall volume that is subjected to the radiation dose will be decreased, particularly in larger prostates. A reduction in the target volume might also reduce the volumes of neighboring organs exposed to high dose levels and consequently reduce the toxicity.

Fourth, most prostate cancer foci arise in the peripheral zone of the prostate [34], which showed the largest relative decrease in volume. Hypothetically, the increased pressure on the rectal wall and prostatic tissue could cause compression of the vasculature, possibly leading to a degree of acute hypoxia within the tissue, in turn affecting the RT [35]. Theoretically, this might affect either the radiosensitivity of the rectal wall mucosa (which would be advantageous) or the prostate tumor cells (which would be disadvantageous). Data on both issues do yet not exist; however, no clinical evidence to date has shown the balloon resulted in a decrease in the clinical outcome [36].

Fifth, RT planning using fusion between CT and MRI at 1.5T with an ERC has previously been established [19, 37]. By using an ERC at a field strength of 3T, prostate delineation might even be more accurate because of the greater spatial resolution achieved at this field strength.

Our study had a number of limitations. First, by having both imaging sets read by two readers, we might have introduced an information bias. This was minimized by reading the imaging sets of the same patient in our substantial (n = 44) patient group in separate sessions. Second, by applying bowel motion suppression only before ERC-based MRI, we might have introduced a bias toward better image quality obtained with the ERC-based MRI. In a previous study [22], however, it was shown that even with bowel suppression, more motion artifacts were present using ERC-based MRI vs. the body array coil. Third, by using the greater signal-to-noise ratio of the ERC, the in-plane spatial resolution of ERC-based MRI was greater. This increased the accuracy in delineating the prostate structures and might have caused more accurate volume determination with ERC-based MRI. It is unclear whether this would have resulted in systematically lower or greater determined volumes.

CONCLUSION

Our results have shown that the introduction of a 3T ERC, similar to an ERB, caused significant changes in all prostate diameters and a significant mean absolute and relative reduction in prostate volume of the total prostate gland, peripheral zone, and central gland, which could cause problems using ERC-based MRI scans for MRI-CT image fusion. The use of algorithms or applying an ERB, similar in volume to the ERC, for CT scanning and treatment might overcome these problems.

REFERENCES

[1] Roach M III, Faillace-Akazawa P, Malfatti C, et al. Prostate volumes defined by magnetic resonance imaging and computerized tomographic scans for three-dimensional conformal radiotherapy. Int J Radiat Oncol Biol Phys 1996;35:1011–1018.

[2] Rasch C, Barillot I, Remeijer P, et al. Definition of the prostate in CT and MRI: A multi-observer study. Int J Radiat Oncol Biol Phys 1999;43:57–66.

[3] Engelbrecht MR, Huisman HJ, Laheij RJ, et al. Discrimination of prostate cancer from normal peripheral zone and central gland tissue by using dynamic contrast-enhanced MR imaging. Radiology 2003;229:248–254.

[4] Fütterer JJ, Heijmink SWTPJ, Scheenen TWJ, et al. Prostate cancer localization with dynamic contrast-enhanced MR imaging and proton MR spectroscopic imaging. Radiology 2006;241:449–458.

[5] Heerschap A, Jager GJ, van der Graaf M, et al. In vivo proton MR spectroscopy reveals altered metabolite content in malignant prostate tissue. Anticancer Res 1997;17:1455–1460.

[6] Fütterer JJ, Scheenen TW, Huisman HJ, et al. Initial experience of 3 Tesla endorectal coil magnetic resonance imaging and 1H-spectroscopic imaging of the prostate. Invest Radiol 2004;39:671–680.

[7] Noworolski SM, Henry RG, Vigneron DB, et al. Dynamic contrast-enhanced MRI in normal and abnormal prostate tissues as defined by biopsy, MRI, and 3D MRSI. Magn Reson Med 2005;53:249–255.

[8] Fütterer JJ, Scheenen TWJ, Heijmink SWTPJ, et al. Standardized threshold approach using three-dimensional proton magnetic resonance spectroscopic imaging in prostate cancer localization of the entire prostate. Invest Radiol 2007;42:116–122.

[9] Testa C, Schiavina R, Lodi R, et al. Prostate cancer: Sextant localization with MR imaging, MR spectroscopy, and 11C-choline PET/CT. Radiology 2007;244:797–806.

[10] Coakley FV, Kurhanewicz J, Lu Y, et al. Prostate cancer tumor volume: Measurement with endorectal MR and MR spectroscopic imaging. Radiology 2002;223:91–97.

[11] Fütterer JJ, Engelbrecht MR, Huisman HJ, et al. Staging prostate cancer with dynamic contrast-enhanced endorectal MR imaging prior to radical prostatectomy: Experienced versus less experienced readers. Radiology 2005;237:541–549.

[12] Pickett B, Kurhanewicz J, Coakley F, et al. Use of MRI and spectroscopy in evaluation of external beam radiotherapy for prostate cancer. Int J Radiat Oncol Biol Phys 2004;60:1047–1055.

[13] Pickett B, Ten Haken RK, Kurhanewicz J, et al. Time to metabolic atrophy after permanent prostate seed implantation based on magnetic resonance spectroscopic imaging. Int J Radiat Oncol Biol Phys 2004;59:665–673.

[14] Zaider M, Zelefsky MJ, Lee EK, et al. Treatment planning for prostate implants using magnetic-resonance spectroscopy imaging. Int J Radiat Oncol Biol Phys 2000;47:1085–1096.

[15] DiBiase SJ, Hosseinzadeh K, Gullapalli RP, et al. Magnetic resonance spectroscopic imaging-guided brachytherapy for localized prostate cancer. Int J Radiat Oncol Biol Phys 2002;52:429–438.

[16] Mizowaki T, Cohen GN, Fung AY, et al. Towards integrating functional imaging in the treatment of prostate cancer with radiation: The registration of the MR spectroscopy imaging to ultrasound/CT images and its implementation in treatment planning. Int J Radiat Oncol Biol Phys 2002;54:1558–1564.

[17] Pouliot J, Kim Y, Lessard E, et al. Inverse planning for HDR prostate brachytherapy used to boost dominant intraprostatic lesions defined by magnetic resonance

spectroscopy imaging. Int J Radiat Oncol Biol Phys 2004;59:1196–1207.

[18] Pickett B, Vigneault E, Kurhanewicz J, et al. Static field intensity modulation to treat a dominant intra-prostatic lesion to 90 Gy compared to seven field 3-dimensional radiotherapy. Int J Radiat Oncol Biol Phys 1999;44:921–929.

[19] van Lin EN, Futterer JJ, Heijmink SW, et al. IMRT boost dose planning on dominant intraprostatic lesions: Gold marker-based three-dimensional fusion of CT with dynamic contrast-enhanced and 1H-spectroscopic MRI. Int J Radiat Oncol Biol Phys 2006;65:291–303.

[20] Huisman HJ, Futterer JJ, van Lin EN, et al. Prostate cancer: precision of integrating functional MR imaging with radiation therapy treatment by using fiducial gold markers. Radiology 2005;236:311–317.

[21] Hricak H, White S, Vigneron D, et al. Carcinoma of the prostate gland: MR imaging with pelvic phased-array coils versus integrated endorectal–pelvic phased-array coils. Radiology 1994; 193:703–709.

[22] Heijmink SWTPJ, Futterer JJ, Hambrock T, et al. Prostate cancer: Body-array versus endorectal coil MR imaging at 3 T—Comparison of image quality, localization, and staging performance. Radiology 2007;244:184–195.

[23] D'Amico AV, Manola J, Loffredo M, et al. A practical method to achieve prostate gland immobilization and target verification for daily treatment. Int J Radiat Oncol Biol Phys 2001;51: 1431–1436.

[24] Teh BS, McGary JE, Dong L, et al. The use of rectal balloon during the delivery of intensity modulated radiotherapy (IMRT) for prostate cancer: More than just a prostate gland immobilization device? Cancer J 2002;8:476–483.

[25] Woel R, Beard C, Chen MH, et al. Acute gastrointestinal, genitourinary, and dermatological toxicity during dose-escalated 3D-conformal radiation therapy (3DCRT) using an intrarectal balloon for prostate gland localization and immobilization. Int J Radiat Oncol Biol Phys 2005;62:392–396.

[26] D'Amico AV, Manola J, McMahon E, et al. A prospective evaluation of rectal bleeding after dose-escalated three-dimensional conformal radiation therapy using an intrarectal balloon for prostate gland localization and immobilization. Urology 2006;67:780–784.

[27] Bastasch MD, Teh BS, Mai WY, et al. Tolerance of endorectal balloon in 396 patients treated with intensity-modulated radiation therapy (IMRT) for prostate cancer. Am J Clin Oncol 2006;29:8–11.

[28] Ronson BB, Yonemoto LT, Rossi CJ, et al. Patient tolerance of rectal balloons in conformal radiation treatment of prostate cancer. Int J Radiat Oncol Biol Phys 2006;64:1367–1370.

[29] Husband JE, Padhani AR, MacVicar AD, et al. Magnetic resonance imaging of prostate cancer: Comparison of image quality using endorectal and pelvic phased array coils. Clin Radiol 1998;53:673–681.

[30] Kim Y, Hsu IC, Pouliot J, et al. Expandable and rigid endorectal coils for prostate MRI: Impact on prostate distortion and rigid image registration. Med Phys 2005;32:3569–3578.

[31] Fung Y. Biomechanics: motion, flow, stress and growth. New York: Springer; 1990.

[32] van Lin EN, van der Vight LP, Witjes JA, et al. The effect of an endorectal balloon and offline correction on the interfraction systematic and random prostate position variations: A comparative study. Int J Radiat Oncol Biol Phys 2005;61:278–288.

[33] Wang CW, Chong FC, Lai MK, et al. Set-up errors due to endorectal balloon positioning in intensity modulated radiation therapy for prostate cancer. Radiother Oncol 2007;84:177–184.

[34] Chen ME, Johnston DA, Tang K, et al. Detailed mapping of prostate carcinoma

foci: Biopsy strategy implications. Cancer 2000;89:1800–1809.

[35] Marignol L, Coffey M, Lawler M, et al. Hypoxia in prostate cancer: A powerful shield against tumour destruction? Cancer Treat Rev 2008;34:1367–1370.

[36] Teh BS, Mai W, McGary J, et al. Long-term outcome of a moderate-hypofractionated intensity modulated radiation therapy (IMRT) (77 Gy at 2.2 Gy per fraction) approach utilizing immobilization rectal balloon for localized prostate cancer. Int J Radiat Oncol Biol Phys 2008;69:S335.

[37] Lian J, Xing L, Hunjan S, et al. Mapping of the prostate in endorectal coil-based MRI/MRSI and CT: A deformable registration and validation study. Med Phys 2004;31:3087–3094.

CHAPTER 7

Prostate and Lymph Node Proton Magnetic Resonance (MR) Spectroscopic Imaging with External Array Coils at 3 T to Detect Recurrent Prostate Cancer After Radiation Therapy

Stijn W. T. P. J. Heijmink
Tom W. J. Scheenen
Jurgen J. Fütterer
Dennis W. J. Klomp
Roel A. M. Heesakkers
Christina A. Hulsbergen-van de Kaa
Emile N. J. Th. van Lin
Arend Heerschap
Jelle O. Barentsz

Invest Radiol 2007;42(6):420-7.

In a patient suspected of having recurrent prostate cancer after radiation therapy, we demonstrate the feasibility of noninvasive proton magnetic resonance spectroscopic (1H-MRS) imaging of the prostate and a lymph node at 3 T using a matrix of external surface coils. Written informed consent was obtained from the patient. With 1H-MRS imaging, high choline with low citrate signal was observed in the prostate, and in the lymph node a signal of choline-containing compounds was identified. The tissue level of the compounds in the enlarged lymph node was estimated to be 8.1 mmol/kg water. Subsequent histopathological analysis of systematic transrectal ultrasound-guided prostate biopsy and computed tomography-guided biopsy of the lymph node confirmed the presence of prostate cancer in both.

Presently, 1 in 3 new cases of cancer in the male population [1] of the United States is prostate cancer. As part of the primary diagnostic process the urologist and radiation oncologist as well as the medical oncologist calculate the risk of extraprostatic disease spread and positive lymph nodes based on the serum prostate-specific antigen (PSA) level, the digital rectal examination findings, and the Gleason score at biopsy [2].

After treatment with curative intent, a rise in the PSA level may be indicative of recurrence. Although differentiation between a local or systemic recurrence is difficult, the PSA doubling time may help to discriminate between these [3]. However, also imaging can play a role in establishing recurrent disease in both the prostate and lymph nodes. By establishing (early) local recurrence, potentially curative salvage therapies such as radical prostatectomy or cryotherapy may be performed. Recently, the first prostate cancer studies of magnetic resonance (MR) imaging with and without an endorectal coil and proton MR spectroscopic imaging (1H-MRS) with an endorectal coil at 3 T in preoperative patients have been published [4-8]. No studies have yet been published that performed 1H-MRS with external surface coils only.

The transformation of healthy cells toward malignancy was reported to change the membrane choline phospholipid metabolism [9]. In prostate cancer, using an endorectal coil for signal reception, it was shown that an increase in the choline signal along with a concurrent decrease in the citrate signal, was indicative of malignancy [10–13]. Thereby, choline compounds are important tumor biomarkers. The purpose of this case report is to demonstrate the feasibility of noninvasive 1H-MRS using a matrix of external surface coils to detect recurrent cancer in the prostate and to detect metastatic prostate cancer by quantifying the total choline-containing compounds (tCho) in an enlarged lymph node.

MATERIALS AND METHODS

Case

A 77-year-old man with a PSA level of 30 ng/mL and an adenocarcinoma with a Gleason score of 3 + 5 = 8 on prostate biopsy, underwent an initial staging MR imaging examination at 1.5 T (MAGNETOM Sonata, Siemens Medical Solutions, Erlangen, Germany) with a pelvic phased-array coil because of the patient's intolerability of the endorectal coil. T2-weighted imaging [repetition time (TR)/echo time (TE): 4400/132 milliseconds] was performed in 3 planes and revealed cancer encompassing the whole peripheral zone of the prostate from apex to base with signs of extraprostatic spread (Figure 1A) and seminal vesicle invasion. On the T1- weighted series (TR/TE: 1570/3.9 milliseconds) that covered the region between the prostate and aortic bifurcation, no pathologically enlarged lymph nodes were reported. Bone scintigraphy did not reveal any bone metastases. Successive limited pelvic lymph node dissection, harvesting 10 nodes, showed no metastatic nodal disease. Therefore, the cancer was staged as T3bN0M0. After neoadjuvant hormonal therapy, ie, maximum androgen

blockade, the radiation therapy consisted of irradiation of the entire prostate plus seminal vesicles with a dose of 70 Gy, in 35 daily fractions of 2 Gy using a 4-field "box" conformal technique, from November 21, 2002 to January 9, 2003. Before the radiation treatment, the PSA level was below 0.10 ng/mL and remained at that level until July 2003. Subsequently, it gradually started to rise to 6.34 ng/mL in October 2005. In November 2005, a repeat 1.5 T MR imaging examination (MAGNETOM Avanto; Siemens Medical Solutions, Erlangen, Germany) using a pelvic phased-array coil for local recurrence showed a homogeneously low signal intensity in the entire prostate. On the T1-weighted 3-dimensional gradient-echo sequence (TR/TE: 8.6/4.2 milliseconds; acquisition time: 7 minutes 52 seconds) covering the region from the prostate up toward the aortic bifurcation taken before the contrast administration, a single enlarged lymph node with a maximal diameter of 2.5 cm was seen ventral of the internal iliac artery (Figure 2). Based on its size, the lymph node was reported as suspicious for metastatic disease. Retrospectively, this node was not enlarged on the T1-weighted images of the MR imaging examination performed before radiation therapy. Additionally obtained bone scintigraphy was negative.

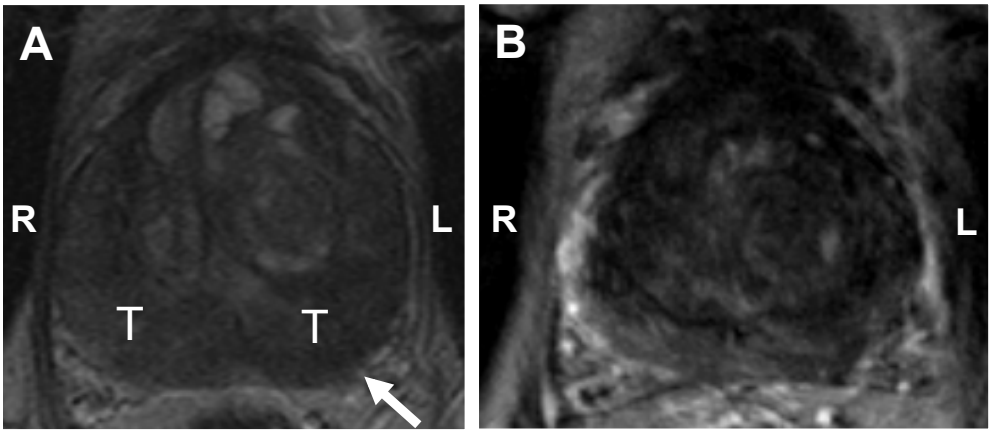

Figure 1. (A) Axial T2-weighted spin-echo MR image at 1.5 T before therapy from the midgland of the prostate of a 77-year- old man with a PSA level of 30 ng/mL and biopsy-proven Gleason 3 + 5 = 8 prostate cancer using a pelvic phased-array coil (TR/TE: 4400/132 milliseconds). A large area of low signal intensity indicative of tumor (T) covering the whole peripheral zone of the prostate from apex to base was observed. Signs of capsular bulging (arrow) and seminal vesicle invasion (not shown) are present. (B) Two and a half years after radiation therapy, the axial T2-weighted fast spin-echo image (TR/TE: 3100/135 milliseconds) at 3 T with combined body and spine matrix coils reveals a homogeneously low signal in the entire prostate, indicative of postradiation therapy effects. L, left; R, right; T, tumor.

Proton MR Spectroscopic Imaging Combining Multiple External Surface Coils at 3 T

After written informed consent, the patient agreed to undergo 1H-MRS of both the prostate and the enlarged lymph node at 3 T (MAGNETOM Trio with total imaging matrix; Siemens

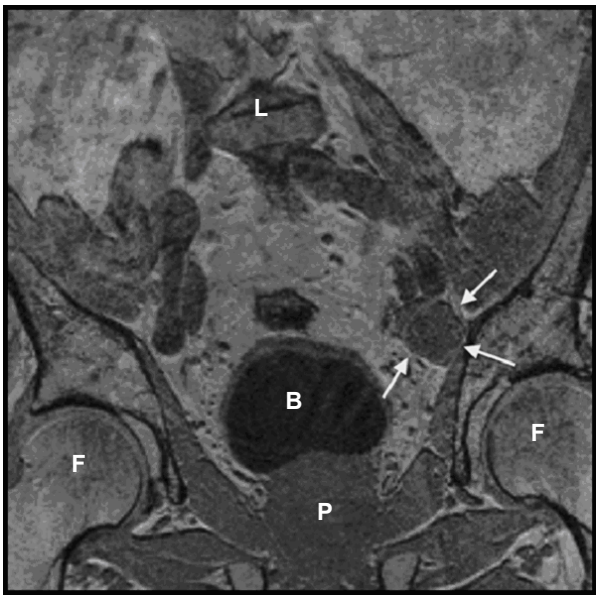

Figure 2. Coronal reconstruction image of the T1-weighted 3-dimensional gradient-echo sequence at 1.5 T (TR/TE: 8.6/ 4.2 milliseconds) showing the single enlarged lymph node (arrows) located ventral of the internal iliac artery. The maximal diameter of the lymph node was 2.5 cm. L, lumbar spine; B, bladder; P, prostate; F, femoral head.

Medical Solutions, Erlangen, Germany) using a matrix of external surface coils for signal reception followed by biopsy of the prostate and lymph node.

Proton MR Spectroscopic Imaging of the Prostate

Immediately before the start of the examination, bowel peristalsis was suppressed by a 1-mg intramuscular injection of glucagon (Glucagen; Novo Nordisk A/S, Denmark). First, T2-weighted fast-spin echo imaging in 3 planes was performed (TR/TE: 3230/108 milliseconds; hyperechoes [14]; field of view (FOV): 256 x 256 mm; matrix size: 512 x 512; 15 slices; slice thickness: 4 mm; no gap; 2 averages; acquisition time: 3 minutes 43 seconds, Figure 1B). Subsequently, 3-dimensional 1H-MRS imaging covering the entire prostate (Figure 3A) was performed combining the signal of multiple external surface coils [15]. The pulse sequence used was similar to the one used for prostate 1H-MRS imaging at 1.5 T [16] with some adaptations to assure an optimal spectral shape of the citrate signal at 3 T [17]. Scan parameters: TR/TE: 750/145 milliseconds; acquisition bandwidth: 1250 Hz; 512 spectral data points; FOV: 84 x 70 x 70; matrix size: 12 x 10 x 10; number of weighted averages: 6; 7 saturation slabs were applied. The voxel resolution (before apodization) was 7 x 7 x 7 mm^3 within a total acquisition time of 8 minutes 15 seconds. A radiologist (S.W.T.P.J.H.) and an MR spectroscopist (T.W.J.S.) analyzed the spectral data. Throughout most of the prostate (Figure 3B, C), choline displayed a higher signal than citrate, indicative of locally recurrent disease [18].

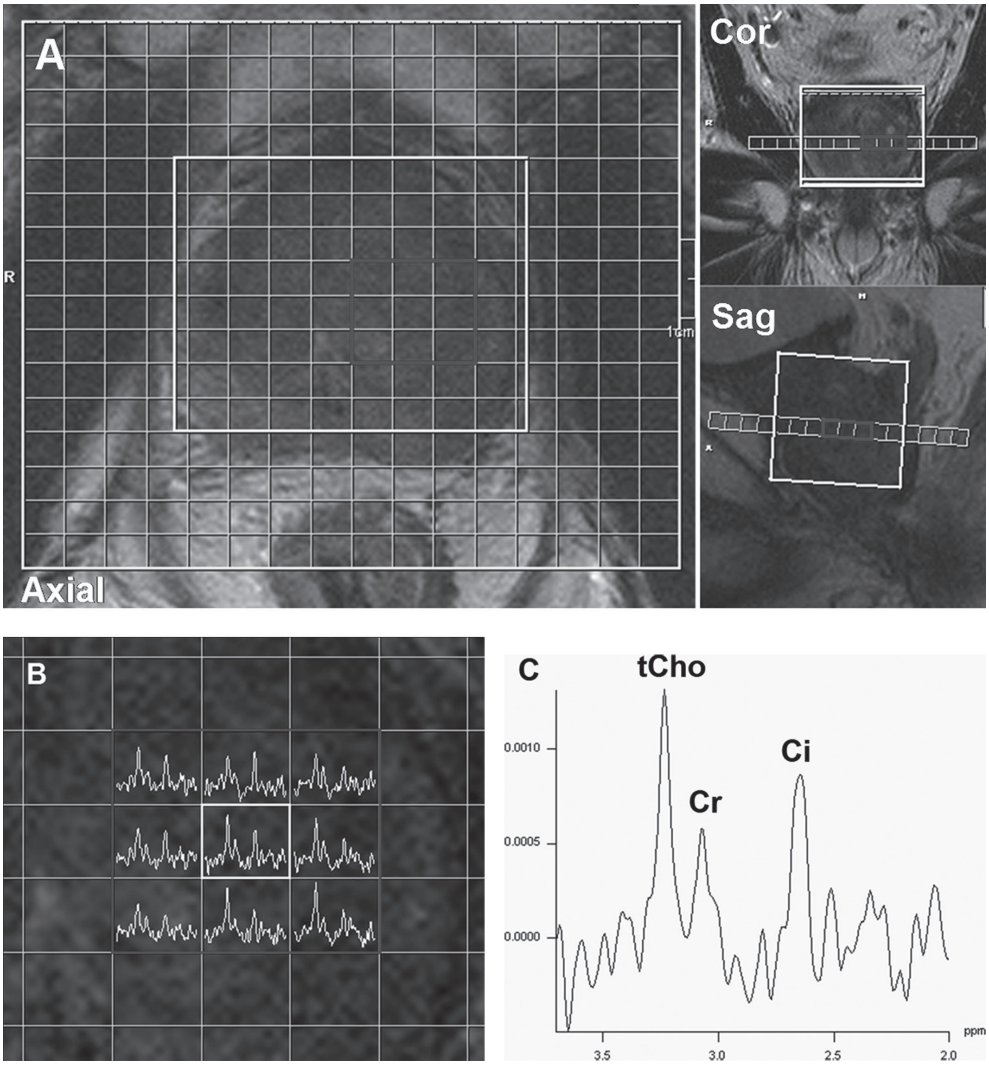

Figure 3. (A) Example of the voxels within an axial partition from the 3-dimensional 1H-MRS imaging acquisition (TR/TE: 750/145 milliseconds) overlaid on T2-weighted imaging, showing the field of view (outer white box) and the volume of interest (inner white box). Within the volume of interest, a number of voxels is selected (dark box) for visualization of individual spectra.
(B) Spectral map of selected voxels (ppm range 2.0–3.7). All selected voxels revealed high tCho signals with lower citrate signals. One voxel was chosen for enlarged display (light box).
(C) tCho, creatine (Cr) and citrate (Ci) signals were observed, with tCho displaying a higher signal than citrate.

Proton MR Spectroscopic Imaging of the Lymph Node

To localize the enlarged lymph node, an axial T2-weighted multislice fast-spin echo imaging series (TR/TE: 3100/135 milliseconds; voxel size: 1 x 1 x 4 mm^3; acquisition time: 3 minutes

34 seconds, Figure 4A) and a T1-weighted 3-dimensional gradient-echo sequence (TR/TE: 6.47/2.54 milliseconds; FOV: 250 x 250 x 225 mm^3; matrix: 320 x 320 x 288; parallel imaging acceleration factor: 2; acquisition time: 5 minutes 58 seconds) covering the region from the prostate up toward the aortic bifurcation were obtained. Subsequently, an 1H-MR spectrum was obtained from a single voxel of 15 x 17 x 13 mm^3 positioned inside the node using an echo time averaged point resolved spectroscopy sequence (PRESS (19,20) TR 1500 milliseconds, 256 averages; acquisition time 6 minutes 24 seconds). Water and lipid signals were suppressed 2-fold. A combination of 2 dual-frequency selective refocusing pulses and crusher gradients around the second 180-degree PRESS pulse suppressed both water and lipid resonances [21]. In addition, the TE of the PRESS sequence was stepped up from 136 to 272 milliseconds in 64 steps (each averaged 4 times) to cancel residual coupled lipid signals (echo time averaging [22]). Supervised automatic shimming and automatic adjustments of frequency and transmit power took approximately 5 minutes. With an integrated 1-minute normalization scan the contribution of the different coil elements to the signal intensity of the voxel was calculated. In Figure 4B the location of the voxel inside the lymph node is visualized as well as the corresponding 1H-MR spectrum from 1.0 to 5.5 ppm. In the absence of lipid resonances in the 0.5–2.5 ppm range we attribute the visible resonance at about 3.20 ppm to the methyl protons of choline, phosphocholine, and glycerophosphocholine. In vivo, these multiple resonances cannot be spectrally resolved at 3 T. Thus, they appear as a single peak, termed total choline-containing compounds (tCho). To estimate the amount of tCho in this node we also acquired an unsuppressed, fully relaxed spectrum of the same voxel (TR/TE: 5000/30 milliseconds; 4 averages), in which the tCho signal was also clearly visible. Neglecting T1 saturation of the water and tCho spins at this long TR, using the T2 of choline proton spins to be 220 milliseconds [17] and assuming T2 of water spins to be 94 milliseconds in cancer tissue [23], we estimate a tCho content of 8.1 mmol/kg water, dividing the integral of a Gaussian line fit to the tCho resonance (9 protons) by the integral of a Lorentzian line fit to the water resonance (2 protons), and taking into account the molecular weight of water.

To validate that the choline signal was confined to the lymph node, a 3-dimensional 1H-MRS imaging measurement (TR/TE: 1500/100 milliseconds; FOV: 100 x 100 x 100 mm3; matrix size: 10 x 10 x 10; acquisition time: 7 minutes 31 seconds) with dual frequency selective water and lipid suppression was performed with the volume-of-interest covering the enlarged lymph node and adjacent lipid tissue (Figure 4C, D). Due to filtering of the signal before Fourier transformation in the spatial dimensions, the true size and shape of a voxel is a sphere with a diameter of approximately18 mm. The shown size of a voxel in Figure 4C, D is only 6 x 6 mm^2, therefore locations just outside the lymph node still show a small tCho resonance (the underlined peaks), originating from the node itself. Residual lipid signals are visible outside the node and are associated with surrounding adipose tissue.

Histopathological Confirmation (Standard of Reference)

Systematic 8-core (3 peripheral zone and central gland cores bilaterally) transrectal ultrasound-guided biopsy was performed. No complications were reported. Histopathology confirmed the presence of locally recurrent Gleason 3 + 4 prostate cancer in all 8 prostate biopsy cores (Figure 5A).

The patient underwent computed tomography (CT)-guided histologic biopsy of the enlarged lymph node (SOMATOM Sensation 16 slice; Siemens, Erlangen, Germany). The patient was placed in the supine position and the enlarged lymph node visualized on MR imaging was correlated with CT imaging. During repetitive CT scanning the biopsy needle was positioned against this node and histologic biopsy was performed with a 20-gauge needle using a coaxial system (Bard, Covington, GA). No complications were reported. Histopathology revealed the presence of adenocarcinoma with cribriform growth pattern that stained with a PSA antibody, conclusive for prostate cancer, in all lymph node biopsy cores (Figure 5B).
Because the elevated PSA level remained stable and due to the absence of any abnormality on bone scintigraphy and the absence of any clinical symptoms, the then-81-year-old patient, the patient's family, and physicians decided to delay hormonal therapy and to keep the patient under further active clinical and PSA surveillance.

DISCUSSION

In this technical note and case report we demonstrated that noninvasive 1H-MRS imaging combining the signals of multiple external surface coils at 3 T is feasible in the prostate to detect local recurrence and in a lymph node to detect prostate cancer by quantifying tCho.

^{1}H-MRS of the Prostate

It has been established that tCho is a marker for the phospholipid turnover in the cell membrane [24]. Previous 1H-MRS studies of the prostate have demonstrated that the ratio of tCho + creatine as compared with citrate is an indicator of prostate cancer within the prostate gland [12,13]. Also, there was a trend towards increasing tCho + creatine/citrate ratios in more aggressive prostate cancer foci [25]. Our results, showing generally high tCho peaks with relatively lower citrate signals, are concurrent with previous studies performed at 1.5 T with an endorectal coil in prostate cancer treated with hormonal therapy [26] in which responsive prostate tissue experienced "metabolic atrophy" while any residual cancer exhibited a high tCho peak [18,26,27]. Thus, the feature of choline as an indicator of the presence of recurrent prostate cancer has been well established and it would be logical that metastatic disease could display a tCho peak on 1H-MRS.

We did not perform 1H-MRS of the prostate during the period after radiation therapy in which the PSA level was within the clinical range of normal. Although potentially we cannot exclude that the high tCho peak may have also been present prior to recurrence, it is

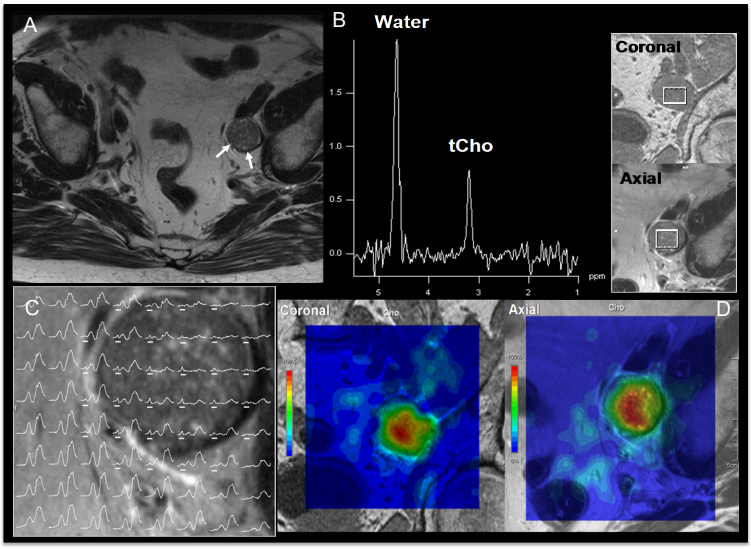

Figure 4. (A) Axial T2-weighted fast spin-echo image (TR/TE: 3100/135 milliseconds) at 3 T with combined body and spine matrix coils for localization of the enlarged lymph node (arrows). (B) The phase-corrected 1H-MR spectrum (without baseline correction) obtained from the TE-averaged and combined water and lipid-suppressed single voxel MR spectroscopy measurement. A peak at 4.7 ppm for residual water spins and a peak at about 3.2 ppm assigned to the methyl groups of choline-containing compounds (tCho) were observed. Note the absence of lipid signals from 1 to 2.5 ppm. The coronal reference image from the T1-weighted 3-dimensional gradient-echo sequence (TR/TE: 6.47/ 2.54 milliseconds) and the axial T2-weighted fast spin-echo image are shown to indicate the voxel placement. (C) An axial spectral map of all voxels inside the volume-of-interest from the 1H-MR spectroscopic imaging measurement (TR/TE: 1500/ 100 milliseconds) in which the tCho resonances are underlined. Outside the lymph node, large lipid signals are present; the tCho signal is only present inside. (D) Interpolated coronal and axial tCho color-coded maps constructed using the integral of a Gaussian fit to the tCho signal.

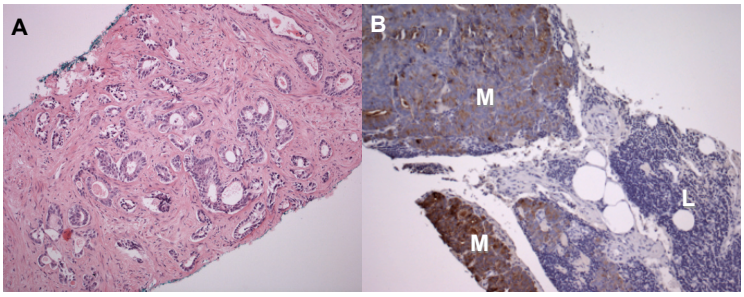

Figure 5. (A) Microscopy (hematoxylin-eosin stain, original magnification X 100) of the prostate needle biopsy revealed recurrent Gleason 3 + 4 prostate cancer. (B) Microscopy (antibody against PSA stain, original magnification X100) of the needle biopsy shows normal lymphatic tissue (L) along with metastasis (M) of an acinar adenocarcinoma with cribriform growth pattern and prominent nucleoli, characteristic for prostate carcinoma.

generally assumed that metabolic and biochemical response are related and that metabolic atrophy is present when the PSA level is at nadir level [28].

Proton MRS imaging of the prostate has previously been performed with the use of an endorectal coil at both 1.5 T [12,13,29] and 3 T [5]. In our case report we demonstrated that it is feasible to perform 1H-MRS of the prostate without an endorectal coil at 3 T. Particularly in patients that have undergone radiation therapy, introduction of the endorectal coil can cause discomfort due to radiation treatment effects on the rectum and adjacent structures. Other advantages of not having to use an endorectal coil are the lower costs and time gained by not having to introduce the coil and check its position.

To obtain a sufficiently high spectral signal to noise ratio within clinically reasonable scanning times, the voxel size was larger than at both 1.5 and 3 T with an endorectal coil. Using our voxel size, small cancer foci may be missed. However, it is unclear if detecting small cancer foci has clinical consequences. In recurrence detection the aim is to detect clinically relevant recurrence in the prostate. Our technique may also be used in other clinical settings, such as in a screening population or radiation therapy planning. In a screening population, the preferential detection of larger, more aggressive cancer foci over smaller, less aggressive ones would be required since most relatively low-grade, small-volume cancer foci will not determine the patient's morbidity and mortality [30,31]. In intensity-modulated radiation therapy planning, by identifying and correctly localizing the areas of the most aggressive prostate cancer foci (the dominant intraprostatic lesions), a radiation therapy dose boost up to 90 Gy can be administered to this region [32]. Since it is hypothesized that most recurrences occur at the localization of the primary cancer [33] this may aid in preventing recurrent disease.

In patients with breast cancer, 1H-MRS has been shown to aid in diagnosis and treatment follow-up [34-36]. Previously, a quantitative approach using single voxel 1H-MRS at 4 T was used in breast cancer patients. It was concluded that the amount of tCho per kilogram of water was a predictor of malignancy [34]. In a recent preliminary study, the addition of 1H-MRS to MR imaging of breast lesions was shown to be of possible help to improve the radiologist's ability to distinguish benign from malignant breast lesions [35].

^{1}H-MRS of the Lymph Node

In an earlier publication, Yeung et al established the feasibility and high diagnostic performance of detecting choline in axillary lymph nodes in 39 breast cancer patients at 1.5 T using either a surface or breast coil with fine-needle aspiration as standard of reference [37]. The authors found high sensitivity 82% (14 of 17 nodes) with perfect specificity (100%, 14 of 14). They reported that the false negative results were due to small (2–4 mm) metastases with an inherently low signal-to-noise ratio and, therefore, undetectable tCho

signal. Furthermore, the authors determined only whether a tCho peak could be assigned, but did not quantify the amount of choline.

The amount of tCho present in the positive lymph node in our case report is similar to the largest values reported in malignant breast lesions (up to 8.5 mmol/kg water) [34,38,39]. Quantification of the tCho concentration has also been performed in other tumors. For gliomas, it was established that the average tCho concentration was 2.86 mmol/L and this increased to 3.21 mmol/L if only grade III gliomas were included in the analysis [40]. In another study, tCho concentrations between 1.5 and 2.7 mmol/mL were found for various types of brain tumors [41]. In 4 patients with hepatocellular carcinoma, tCho concentrations between 3.4 and 14.0 mmol/L have been found [42]. In lymph nodes and in breast tumors, the 1H-MRS voxel is likely to include adipose tissue.

Proton MRS imaging using multiple external surface receiver coils is a noninvasive technique. Another novel technique, MR lymphography using ultrasmall paramagnetic iron-oxide containing particles such as ferumoxtran-10 [43,44], if approved for clinical use, may be an alternative to investigate the state of lymph nodes. A clear advantage of MR lymphography is that it is able to detect much smaller metastatic lymph nodes than 1H-MRS. However, the former technique is not yet available and is more invasive than 1H-MRS. In future, we need to assess the minimal volume necessary for 1H-MRS to detect sufficiently high tCho signals within a lymph node. Performing 1H-MRS at field strengths of 4 T or higher [45] may enable us to reduce the volume necessary to perform single voxel measurements and use 1H-MRS in smaller lymph nodes. In addition, diffusion weighted whole-body MR imaging with fat suppression has potential for detection of metastatic lymph nodes. The feasibility to visualize pathologic lymph nodes has been shown in 11 patients with, among others, malignant lymphoma and breast cancer [46].

We need to consider several limitations. First, our techniques will have to be applied to more patients and in patients who have not undergone prior therapy to determine heir applicability in the general prostate cancer population. Likewise, prospectively, the technique will also have to be compared directly with endorectal 1H-MRS of the prostate at 1.5 T or 3 T to assess its clinical applicability. Second, as for the lymph node, we do not have any reference value as to whether tCho is also present in healthy lymph nodes or nodes reactive to inflammation. In general, these nodes are considerably smaller than the one we have performed 1H-MRS on, resulting in too little tCho to detect with this instrumental set-up. Future studies should perform 1H-MRS on enlarged, healthy lymph nodes to determine the amount of tCho, if at all, present in these nodes. Analogous to 1H-MRS in breast lesions, the calculated concentration of tCho may provide a possibility to differentiate benign from malignant lymph nodes.

Our technique shows promise in aiding radiation oncologists to determine the presence of recurrence in both the prostate and lymph nodes. It may also be applied in patients before undergoing radiation therapy to determine the exact localization of prostate cancer within the prostate gland, for instance for performing dose boosting in dominant lesions with intensity-modulated radiation therapy [32]. Up to now 1H-MRS at a field strength of 1.5 T was only possible using an endorectal coil to achieve clinically relevant spatial information on cancer localization. Nevertheless, also at 1.5 T the technique combining multiple external-surface coils may be applied. To achieve a sufficiently high signal-to-noise ratio, the voxel volume will have to be considerably larger compared with that in our study at 3 T or that with an endorectal coil at 1.5 T.

In conclusion, we demonstrated that in a patient suspected of having recurrent prostate cancer it was feasible to noninvasively detect local recurrence of prostate cancer within the prostate and to detect and quantify the total choline-containing compounds in a lymph node metastasis located deep inside the body, with proton MR spectroscopic imaging at 3 T by combining the signals of multiple external matrix coils. This technique may aid in the diagnosis of local recurrence and regional metastatic lymph node disease. Future studies in a larger patient population will have to be performed to determine the clinical applicability.

REFERENCES

[1] Jemal A, Murray T, Ward E, et al. Cancer statistics, 2005. CA Cancer J Clin 2005;55:10–30.

[2] Ross PL, Scardino PT, Kattan MW. A catalog of prostate cancer nomograms. J Urol 2001;165:1562–1568.

[3] Jhaveri FM, Klein EA. How to explore the patient with a rising PSA after radical prostatectomy: defining local versus systemic failure. Semin Urol Oncol 1999;17:130–134.

[4] Bloch BN, Rofsky NM, Baroni RH, et al. 3 Tesla magnetic resonance imaging of the prostate with combined pelvic phased-array and endorectal coils; initial experience. Acad Radiol 2004;11:863–867.

[5] Fütterer JJ, Scheenen TW, Huisman HJ, et al. Initial experience of 3 Tesla endorectal coil magnetic resonance imaging and 1H-spectroscopic imaging of the prostate. Invest Radiol 2004;39:671–680.

[6] Sosna J, Pedrosa I, Dewolf WC, et al. MR imaging of the prostate at 3 Tesla: comparison of an external phased-array coil to imaging with an endorectal coil at 1.5 Tesla. Acad Radiol 2004;11:857–862.

[7] Cunningham CH, Vigneron DB, Marjanska M, et al. Sequence design for magnetic resonance spectroscopic imaging of prostate cancer at 3 T. Magn Reson Med 2005;53:1033–1039.

[8] Kim CK, Park BK, Kim B. Localization of prostate cancer using 3 T MRI: comparison of T2-weighted and dynamic contrast-enhanced imaging. J Comput Assist Tomogr 2006;30:7–11.

[9] Aboagye EO,Bhujwalla ZM. Malignant transformation alters membrane choline phospholipid metabolism of human mammary epithelial cells. Cancer Res 1999;59:80–84.

[10] Cornel EB, Smits GA, Oosterhof GO, et al. Characterization of human prostate cancer, benign prostatic hyperplasia and normal prostate by in vitro 1H and 31P magnetic resonance spectroscopy. J Urol 1993;150:2019–2024.

[11] Kurhanewicz J, Vigneron DB, Nelson SJ, et al. Citrate as an in vivo marker to discriminate prostate cancer from benign prostatic hyperplasia and normal prostate peripheral zone: detection via localized proton spectroscopy. Urology 1995;45:459–466.

[12] Kurhanewicz J, Vigneron DB, Hricak H, et al. Three-dimensional H-1 MR spectroscopic imaging of the in situ human prostate with high (0.24–0.7 cm3) spatial resolution. Radiology 1996;198:795–805.

[13] Heerschap A, Jager GJ, Van Der GM, et al. In vivo proton MR spectroscopy reveals altered metabolite content in malignant prostate tissue. Anticancer Res 1997;17:1455–1460.

[14] Hennig J, Scheffler K. Hyperechoes. Magn Reson Med 2001;46:6–12.

[15] Brown MA. Time-domain combination of MR spectroscopy data acquired using phased-array coils. Magn Reson Med 2004;52:1207–1213.

[16] Scheenen TW, Klomp DW, Roll SA, et al. Fast acquisition-weighted three-dimensional proton MR spectroscopic imaging of the human prostate. Magn Reson Med 2004;52:80–88.

[17] Scheenen TW, Gambarota G, Weiland E, et al. Optimal timing for in vivo 1H-MR spectroscopic imaging of the human prostate at 3 T. Magn Reson Med 2005;53:1268–1274.

[18] Coakley FV, Teh HS, Qayyum A, et al. Endorectal MR imaging and MR spectroscopic imaging for locally recurrent prostate cancer after external beam radiation therapy: preliminary experience. Radiology 2004;233:441–448.

[19] Bottomley PA. Spatial localization in NMR spectroscopy in vivo. Ann N Y Acad Sci 1987;508:333–348.

[20] Ordidge RJ, Mansfield P, Lohman JA, et al. Volume selection using gradients

and selective pulses. Ann N Y Acad Sci 1987;508:376–385.

[21] Mescher M, Tannus A, Johnson M, et al. Solvent suppression using selective echo dephasing. J Magn Reson A 1996;123:226–229.

[22] Bolan PJ, DelaBarre L, Baker EH, et al. Eliminating spurious lipid sidebands in 1H MRS of breast lesions. Magn Reson Med 2002;48:215–222.

[23] Chen AP, Oh J, Han ET, et al. Multi-parametric MR imaging of prostate cancer at 3 T. Proc Intl Soc Mag Reson Med 2006;1802.

[24] Miller BL. A review of chemical issues in 1H NMR spectroscopy: N-acetyl-L-aspartate, creatine and choline. NMR Biomed 1991;4:47–52.

[25] Zakian KL, Sircar K, Hricak H, et al. Correlation of proton MR spectroscopic imaging with Gleason score based on step-section pathologic analysis after radical prostatectomy. Radiology 2005;234:804–814.

[26] Mueller-Lisse UG, Swanson MG, Vigneron DB, et al. Time-dependent effects of hormone-deprivation therapy on prostate metabolism as detected by combined magnetic resonance imaging and 3D magnetic resonance spectroscopic imaging. Magn Reson Med 2001;46:49–57.

[27] Pickett B, Ten Haken RK, Kurhanewicz J, et al. Time to metabolic atrophy after permanent prostate seed implantation based on magnetic resonance spectroscopic imaging. Int J Radiat Oncol Biol Phys 2004; 59:665–673.

[28] Pickett B, Kurhanewicz J, Pouliot J, et al. Three-dimensional conformal external beam radiotherapy compared with permanent prostate implantation in low-risk prostate cancer based on endorectal magnetic resonance spectroscopy imaging and prostate-specific antigen level. Int J Radiat Oncol Biol Phys 2006;65:65–72.

[29] Heerschap A, Jager GJ, Van Der Graaf M, et al. Proton MR spectroscopy of the normal human prostate with an endorectal coil and a double spin-echo pulse sequence. Magn Reson Med 1997;37:204–213.

[30] Partin AW, Mangold LA, Lamm DM, et al. Contemporary update of prostate cancer staging nomograms (partin tables) for the new millennium. Urology 2001;58:843–848.

[31] Chun FK, Karakiewicz PI, Briganti A, et al. Prostate cancer nomograms: an update. Eur Urol 2006;50:914–926.

[32] van Lin EN, Futterer JJ, Heijmink SW, et al. IMRT boost dose planning on dominant intraprostatic lesions: gold marker-based three-dimensional fusion of CT with dynamic contrast-enhanced and 1H-spectroscopic MRI. Int J Radiat Oncol Biol Phys 2006;65:291–303.

[33] Cellini N, Morganti AG, Mattiucci GC, et al. Analysis of intraprostatic failures in patients treated with hormonal therapy and radiotherapy: implications for conformal therapy planning. Int J Radiat Oncol Biol Phys 2002;53:595–599.

[34] Bolan PJ, Meisamy S, Baker EH, et al. In vivo quantification of choline compounds in the breast with 1H MR spectroscopy. Magn Reson Med 2003;50:1134–1143.

[35] Meisamy S, Bolan PJ, Baker EH, et al. Adding in vivo quantitative 1H MR spectroscopy to improve diagnostic accuracy of breast MR imaging: preliminary results of observer performance study at 4.0 T. Radiology 2005;236:465–475.

[36] Meisamy S, Bolan PJ, Baker EH, et al. Neoadjuvant chemotherapy of locally advanced breast cancer: predicting response with in vivo (1)H MR spectroscopy: a pilot study at 4 T. Radiology 2004;233:424–431.

[37] Yeung DKW, Yang W-S, Tse GMK. Breast cancer: in vivo proton MR spectroscopy in the characterization of histopathologic subtypes and preliminary observations in axillary node metastases. Radiology 2002; 225:190–197.

[38] Roebuck JR, Cecil KM, Schnall MD, et al. Human breast lesions: characterization with proton MR spectroscopy. Radiology 1998;209:269–275.

[39] Bakken IJ, Gribbestad IS, Singstad TE, et al. External standard method for the in vivo quantification of choline-containing compounds in breast tumors by proton MR spectroscopy at 1.5 Tesla. Magn Reson Med 2001;46:189–192.

[40] Stadlbauer A, Gruber S, Nimsky C, et al. Preoperative grading of gliomas by using metabolite quantification with high-spatial-resolution proton MR spectroscopic imaging. Radiology 2006;238:958–969.

[41] Howe FA, Barton SJ, Cudlip SA, et al. Metabolic profiles of human brain tumors using quantitative in vivo 1H magnetic resonance spectroscopy. Magn Reson Med 2003;49:223–232.

[42] Li CW, Kuo YC, Chen CY, et al. Quantification of choline compounds in human hepatic tumors by proton MR spectroscopy at 3 T. Magn Reson Med 2005;53:770–776.

[43] Harisinghani MG, Barentsz J, Hahn PF, et al. Noninvasive detection of clinically occult lymphnode metastases in prostate cancer. N Engl J Med 2003;348:2491–2499.

[44] Will O, Purkayastha S, Chan C, et al. Diagnostic precision of nanoparticle-enhanced MRI for lymphnode metastases: a meta-analysis. Lancet Oncol 2006;7:52–60.

[45] Ugurbil K, Adriany G, Andersen P, et al. Ultrahigh field magnetic resonance imaging and spectroscopy. Magn Reson Imaging 2003;21:1263–1281.

[46] Takahara T, Imai Y, Yamashita T, et al. Diffusion weighted whole body imaging with background body signal suppression (DWIBS): technical improvement using free breathing, STIR and high resolution 3D display. Radiat Med 2004;22:275–282.

CHAPTER 8

Three-dimensional Proton MR Spectroscopy of Human Prostate at 3 T without Endorectal Coil: Feasibility

Tom W. J. Scheenen
Stijn W. T. P. J. Heijmink
Stefan A. Roell
Christina A. Hulsbergen-Van de Kaa
Ben C. Knipscheer
J. Alfred Witjes
Jelle O. Barentsz
Arend Heerschap

Radiology 2007;245(2):507-16.

Purpose - To evaluate sensitivity and specificity of proton magnetic resonance (MR) spectroscopy of the prostate with external surface coil elements at 3 T for differentiation of cancer from healthy tissue within an acceptable measurement time, by using histopathologic findings as the reference standard.

Materials and Methods - The study was approved by the institutional review board; informed consent was obtained. Forty-five men (age range, 51–70 years) underwent 3-T MR imaging with external radiofrequency surface coils for signal reception. MR spectroscopy was performed with acquisition-weighted three-dimensional water- and lipid-suppressed point-resolved spectroscopy pulse sequence. Voxels were classified into healthy peripheral zone, central gland, and periurethral zone and cancer tissue. Cancer voxels were classified according to cancer size and certainty in matching histopathologic findings with MR images. After visual inspection of automated fitting of classified voxels, the choline plus creatine–to-citrate (Cho + Cr/Cit) ratio was calculated for all tissues. Area under the receiver operating characteristic curves (Az) values were used to assess accuracy of discrimination of cancer from healthy tissues. $P < .05$ indicated a significant difference.

Results - After exclusion of four patients with no voxels that passed visual inspection of the automated fit, a median of 82% of the classified voxels per patient was used in the analysis. Mean Cho + Cr/Cit ratios for healthy tissues were 0.22 +/- 0.12 (standard deviation) for peripheral zone, 0.34 +/- 0.14 for central gland, and 0.36 +/- 0.20 for periurethral area; all were significantly different from that of cancer ($P < .001$). Az for discrimination of probable and definite cancer tissue from healthy tissue for the peripheral zone (0.84) was significantly higher than that for the central gland (0.69) ($P < .05$).

Conclusion - Three-dimensional proton MR spectroscopy of the prostate, with a combination of only external radiofrequency surface coils at 3 T, can be used to discriminate cancer from healthy tissue.

Proton magnetic resonance (MR) spectroscopy of the human prostate has proved to be a valuable addition to conventional MR imaging in the localization of prostate cancer [1]. Signals of citrate, creatine, and choline can be detected throughout the prostate, with increased levels of choline and decreased levels of citrate being indicative of cancer tissue [2,3]. A major issue in MR spectroscopy of the prostate is the use of an endorectal coil, either rigid or inflatable. Apart from the discomfort to the patient caused by this coil, its insertion and the necessary evaluation of its position take up valuable MR imaging time. Although the local sensitivity reached with the use of an endorectal coil can never be reached by using only conventional external array coils, it is worthwhile to explore the possibilities of not using the endorectal coil: hydrogen 1 (1H) MR spectroscopic examinations without an endorectal coil would be easier, faster, less expensive, and truly noninvasive. It would make this technique eligible for more wide-spread use in a clinical environment.

MR spectroscopy of the prostate without an endorectal coil has previously been performed at a magnetic field strength of 1.5 T with a single spine-array coil element [4]. The possibility of coherently adding the signals from multiple coil elements into one spectrum for every voxel of a spectroscopic imaging grid [5] has enabled the use of a combination of multiple coils at 1H MR spectroscopy of the prostate. The drawback of using surface coils is their larger size and further distance from the prostate, which leads to a decrease in signal-to-noise ratio. By using 3 T, part of this loss in signal-to-noise ratio is recovered. The optimal timing for 1H MR spectroscopic imaging by using point-resolved spatially localized spectroscopy (PRESS) [6] of the prostate at 3 T has been presented recently, which makes the technique suitable for use in patients [7]. Because the chemical shift (in hertz) of different resonances increases linearly with magnetic field strength, one would expect better separation of the creatine and choline methyl-proton resonances than that in spectra obtained at a field strength of 1.5 T. However, resonances of strongly coupled proton spins from polyamines (spermine, spermidine, among others) or ethanolamine and phosphoethanolamine could be present between 3.0 and 3.3 ppm [8], which prevents the spectrum from reaching the spectral baseline between the creatine and choline signals. Thus, the purpose of our study was to evaluate the sensitivity and specificity of 1H MR spectroscopy of the prostate performed with a combination of external surface coil elements at 3 T for differentiation of cancer from healthy tissue throughout the prostate within a clinically acceptable measurement time, by using histopathologic findings as the reference standard.

MATERIALS AND METHODS

One author (S.A.R.) is employed by Siemens Medical Solutions (Erlangen, Germany). All other authors had control of inclusion of any data and information that might present a conflict of interest.

Patients

The study was approved by our institutional review board, and written informed consent was obtained from all patients. From September 2004 to December 2005, 45 consecutive men with biopsy-proved prostate cancer who underwent radical prostatectomy within 6 weeks after MR imaging and 1H MR spectroscopic imaging at 3 T were eligible for inclusion in our study. A patient exclusion criterion was previous hormonal therapy. Patient age ranged from 51 to 70 years (mean age, 60 years). Mean prostate-specific antigen level was 9.6 ng/mL (range, 3.6-79.2 ng/mL), and the mean Gleason score, based on findings in prostatectomy specimens, was 6.6 (range, 5–9). The median time between transrectal ultrasonographically guided eight-core sextant biopsy and MR examination was 107 days (range, 21–246 days), and that between MR examination and surgery was 7 days (range, 1– 89 days).

MR spectroscopic imaging data were routinely obtained from the entire prostate of all patients. The total examination time of 25–30 minutes consisted of the following parts: 12–15 minutes for all anatomic T2-weighted imaging (transverse, sagittal, and coronal), 4 minutes for shimming, and 9 minutes for spectroscopic imaging measurements.

MR Imaging Acquisition

MR imaging was performed with a 3-T whole body unit (Magnetom Trio; Siemens Medical Solutions), with an eight-element body-array coil (31 patients) and the total imaging matrix concept (Siemens) (14 patients) for signal reception. In the latter case, the user selected the appropriate one or two three-element coil arrays from the supine coil matrix (eight arrays of three coil elements on the patient table) and one or two three-element coil arrays from the body matrix coil placed on top of the patient. Peristalsis was suppressed with an intramuscular injection of 1 mg glucagon (Glucagen; Novo Nordisk, Bagsvaerd, Denmark) immediately before the start of the examination.

With the patient inside the imager, a quick series of three orthogonal gradient-echo images (field of view, 400 x 400 mm; matrix size, 128 x 256; echo time, 5 msec; section thickness, 10 mm) was obtained for localization, after which the prostate anatomy and surrounding tissues were depicted with T2-weighted fast spin-echo MR imaging in three planes. Radiofrequency power deposition was reduced by using hyperechoes: Instead of a train of 180° pulses, the spin echoes were obtained with a train of low-power pulses with modulated flip angles to produce a full spin echo at the effective echo time [9]. The parameters for the T2-weighted images were as follows: repetition time msec/effective echo time msec, 3500-5000/124; field of view, 220 mm; matrix size, 512 x 512; 13-17 sections; section thickness, 4 mm; intersection gap, 0.4 mm; number of signals acquired, two; and acquisition time per plane, 4-5 minutes.

MR Spectroscopic Imaging

After automatic and, if necessary, additional manual shimming (optimization of the main magnetic field homogeneity) of the prostate volume, a 1H MR spectroscopic imaging PRESS pulse sequence was performed to acquire proton MR spectra from every voxel of a three-dimensional (3D) excited subvolume containing the prostate. Because the two protons of the citrate resonance at 2.60 ppm are a strongly coupled spin system, the spectral shape of this resonance depends on magnetic field strength and pulse sequence timing [10]. For an optimal shape of the citrate resonance at a magnetic field strength of 3 T, we used an echo time of 145 msec, at which the signal of citrate appears with large positive in-phase

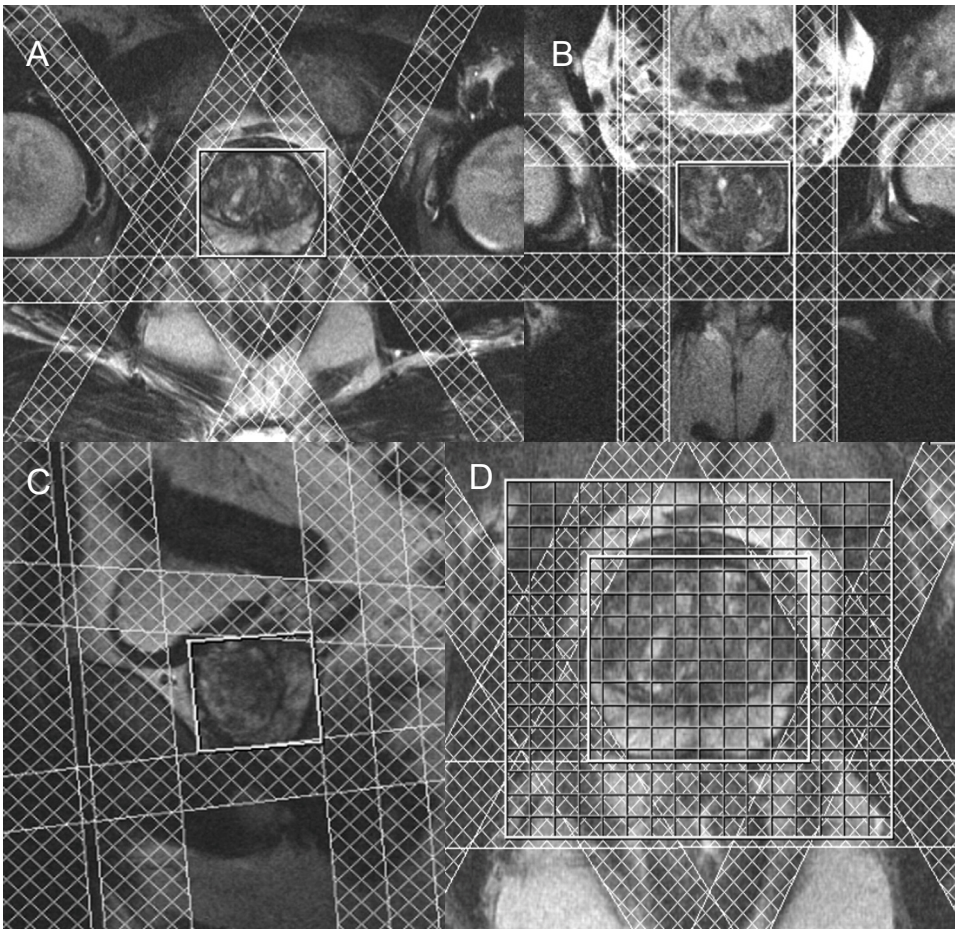

Figure 1. T2-weighted MR imaging (3500/124) and 1H MR spectroscopic data in 61-year-old patient with prostate cancer. (A–C) T2-weighted MR images in transverse, coronal, and sagittal orientation, respectively, show placement of PRESS box (box around prostate) and outer volume saturation slabs (crosshatched bands). (D) Enlarged transverse image with one partition of 3D interpolated 1H MR spectroscopic matrix of 16 × 16 × 16 voxels (outer box). Outer volume saturation slabs extend into PRESS-selected volume of interest (inner box).

inner lines [7]. This echo time is long enough for possible residual lipid signals to decay but is still short enough to depict the metabolites of interest. Water and lipids were suppressed with outer volume saturation slabs (Figure 1) and two 12.6-msec dual-frequency selective Mescher-Garwood pulses with crusher gradients [11,12].

A combination of an elliptic weighted averaged k-space acquisition scheme, zero filling to the nearest power of two, and 3D filtering of the signal in k-space was used [13] to reduce intervoxel signal contamination. Imaging parameters were as follows: 750/145; acquisition bandwidth, 1250 Hz; and 512 spectral data points. Field of view, matrix size, and number of signals acquired were adjusted in every prostate to achieve a nominal voxel resolution (before apodization) of 7 x 7 x 7 mm within a total acquisition time of approximately 9 minutes. After apodization, a voxel could best be approximated as a sphere with a diameter of 12.5 mm and a volume of 1.0 cm^3 [13].

Before Fourier transformation, the signals from the individual coil elements of the body-array coils were zero-order phased on the basis of the first point of the free induction decay and were added with the amplitude of that point as a weight factor [5].

To investigate the appearance of the strongly coupled resonances of polyamines between 3.0 and 3.3 ppm, a two-dimensional MR spectroscopic PRESS measurement of a phantom with a buffered solution of citrate, creatine, choline, and spermine at physiologic concentrations (90.0, 12.0, 9.5, and 18.0 mmol/L, respectively) was performed with the same pulse sequence timing as that used for in vivo spectroscopic imaging (echo time, 145 msec; time from 90° to first 180° pulse, 25.0 msec [7]; field of view of 96 x 96 mm, matrix of 12 x 12, section thickness of 10 mm, nominal voxel resolution before apodization of 8 x 8 x 10 mm, and acquisition time of 1 minute 52 seconds).

Histopathologic Analysis

Prostatectomy specimens were fixed overnight (in 10% neutral buffered form- aldehyde) and coated with India ink. The prostate was sliced at 4-mm intervals in a plane parallel to the transverse T2-weighted sequence. All slices were routinely embedded in paraffin. Tissue slices of 5 μm thickness were prepared and stained with hematoxylin-eosin. The presence and extent of cancer were outlined on the glass cover and marked on photographs of the corresponding slice by a genitourinary pathologist (C.A.H., 13 years of experience) who was blinded to imaging results. All prostatectomy specimens were assigned a stage according to the 2002 TNM classification [14].

Spectroscopic Imaging Voxel Classification

On the basis of histopathologic findings and T2-weighted images in three directions with the overlaid spectroscopic imaging voxel matrix, a radiologist (S.W.T.P.J.H., 3 years of experience)

in consensus with an MR spectroscopist (T.W.J.S., 4 years of experience) assigned 1–4 voxels of the 1H MR spectroscopic imaging matrix to each of the following tissues: healthy peripheral zone, healthy central gland (consisting of combined transition zone and central zone), healthy periurethral zone, and prostate cancer. Both reviewers were blinded to 1H MR spectroscopic imaging spectra. The inclusion of the periurethral zone as tissue separate from the central gland enabled us to study this region as a possible confounder in identifying cancer. The ejaculatory ducts, connecting the seminal vesicles through the central zone of the prostate to the urethra, can have high intensity signals from the ejaculatory ducts around 3.2 ppm. The voxels were assigned to different tissues on the basis of anatomic landmarks in the prostate visible on T2-weighted images (enabling distinction between central gland, peripheral zone, and urethra), rather than on the basis of hyper- or hypointensity of the tissue itself. Matching between histopathologic slices and T2-weighted images was estimated to be within an accuracy of one image section thickness (4 mm) in the craniocaudal direction [15].

For each assigned prostate cancer voxel, the size of the corresponding cancer focus as determined by using histopathologic findings was classified by the radiologist (S.W.T.P.J.H.) and spectroscopist (T.W.J.S.) in consensus as larger than 2 1H MR spectroscopic imaging voxels, between one and two 1H MR spectroscopic imaging voxels, or smaller than 1 1H MR spectroscopic imaging voxel. To acknowledge the difficulties in aligning MR images and histopathologic slices [16], we assigned a certainty score to each selected cancer voxel, noted as a score of 1, possibly inside the cancer; a score of 2, probably inside the cancer; and a score of 3, definitely inside the cancer.

Data Processing and Analysis

For evaluation and quantification of all individual spectra, a software package (PRISMA; University of Bremen, Bremen, Germany, and Siemens Medical Solutions) was used. This software package uses a basis set of metabolic time signals of choline, creatine, and citrate, which are simulated by using literature values of chemical shifts and coupling constants. Especially for the complicated shape of citrate, this is an advantage, because the whole spectral shape is used in the fit [7]. The reported amplitude of the citrate resonance is amplitude fitted to the model time signal, which can differ from the integral of the citrate resonance in the spectrum because its shape comprises both positive and negative signal intensities. After a frequency shift and residual water removal, the complex fit to the spectroscopic data in the time domain was performed, which included baseline artifact handling by truncation and remodeling of the first five data points. For every fitted metabolite, a Cramer-Rao lower bound was calculated, and a visual inspection of the original spectrum together with the curve fit and residual plot was performed by the spectroscopist (T.W.J.S.). Voxels with a correct automatic choice of the resonances (ie, PRISMA-produced signal fits at the correct parts-per-million positions), without lipid signal contamination

and severe baseline distortions and with minimal intensity in the residual plots, passed the visual inspection. From these voxels, the choline-plus-creatine-to-citrate (Cho + Cr/Cit) ratio was calculated by dividing the sum of the fitted amplitudes in the free induction decay of choline and creatine by the fitted amplitude of the citrate signal.

Because the pathologist (C.A.H.) indicated the Gleason score for every outlined cancer focus in the histopathologic slices, we were able to investigate a possible relation between the Gleason score and the Cho + Cr/Cit ratio for every classified cancer voxel.

Statistical Analysis

The area under the receiver operating characteristic (ROC) curve (Az) for discrimination between cancer and healthy tissue was calculated by using the classified voxels as independent values. ROC curves were calculated with cancer voxels that had a matching certainty score of 2 or 3 (probably or definitely inside cancer). Separate analyses were performed for peripheral zone, central gland, and periurethral cancer localization. Sensitivity and specificity at different threshold values for the different tissues were calculated.

P values for comparisons of different tissues were calculated with the Bonferroni multiple comparison test after a one-way analysis of variance; a P value of .05 or less was considered to indicate a significant difference. P values for differences in ROC curves were calculated with two-sided paired t tests. The Spearman rank correlation test was used to calculate r values. Statistical analyses were performed by using software (MedCalc, version 8.1.0.0, MedCalc Software, Mariakerke, Belgium; Prism, version 4.00, GraphPad Software, San Diego, Calif; SPSS, version 12.0.1, SPSS, Chicago, Ill).

RESULTS

Phantom Measurement and in Vivo 1H MR Spectroscopic Imaging

In a representative 1H MR spectroscopic imaging data set accompanied by histopathologic findings of the corresponding resected prostate, signals of citrate, choline, and creatine were depicted throughout the entire prostate (Figure 2). In many spectra in all patients, the choline and creatine resonances could not be clearly separated: Polyamine signals were still present at the used pulse-sequence timing, as is illustrated with the spectrum of a voxel inside the phantom with a solution of relevant prostate metabolites (Figure 3). Although the line width of the signals in this spectrum is quite small (4 Hz), the signals from the strongly coupled protons of spermine overlap with both creatine and choline signals. Therefore, in all voxels of the in vivo measurements with larger line widths and possibly other polyamines present, the complete region from approximately 3.0 to 3.2 ppm, reflected in a fit of two resonances to this region, was summed and used as the numerator of the marker ratio for prostate cancer.

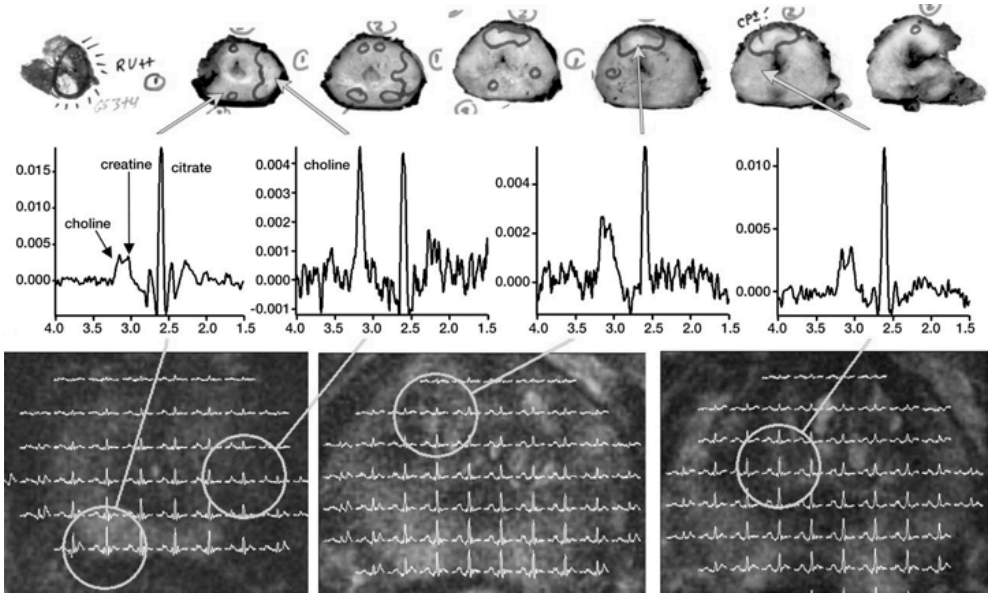

Figure 2. Histopathologic findings and corresponding 3D 1H MR spectroscopic data (750/145) of prostate in 64-year-old patient with prostate cancer (prostate-specific antigen level, 6.86 ng/mL; final Gleason score, 3 + 4; stage, pT2c). Top: Photographs of histopathologic findings from apex to midgland in transverse slices. Arrows = areas of specimen that correspond to location of spectra and images below. Middle: Spectra from in vivo prostate. Left to right: healthy peripheral zone, cancer in peripheral zone, cancer in central gland, and healthy central gland. Scale is adjusted for each spectrum. Bottom: Transverse T2-weighted MR images of three of 16 sections of 3D 1H MR spectroscopic data from apex to midgland overlaid with corresponding spectral maps (range, 2.0–3.5 ppm). True size and location of voxels of which spectra are shown in middle row are indicated with circles. CP±? = possible capsular penetration, RV++ = positive resection margins.

Voxel Classification and Metabolite Ratios

In total, 375 voxels were selected on the basis of histopathologic findings and assigned to one of the four tissues in all 45 patients: 87 voxels to cancer, 118 voxels to healthy peripheral zone, 115 voxels to healthy central gland, and 55 to healthy periurethral tissue. All selected voxels were processed with the automatic signal fit of the PRISMA software package (Figure 4). In four patients (26 voxels) (Figure 5), none of the classified voxels contained useful spectra. With the exclusion of these four patients, the average percentage per patient of voxels that passed the visual inspection of the automated fit procedure was 74% (median, 82%).

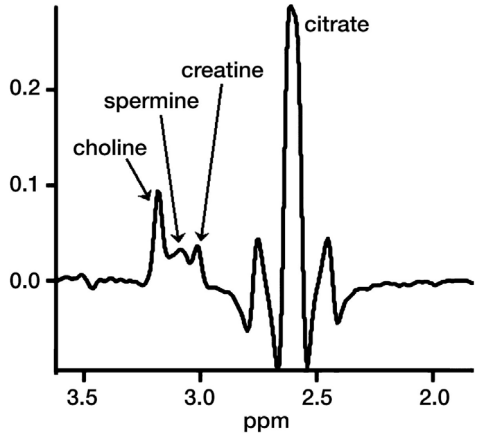

Figure 3. MR spectrum of voxel in phantom with buffered solution of citrate, creatine, choline, and spermine at physiologic concentrations (90.0, 12.0, 9.5, and 18.0 mmol/L, respectively). Spermine, one of the polyamines, has relatively broad relevant signal intensities in 3.0–3.2-ppm range at the used pulse timing. If line widths increase and other polyamines are also present, which is often the case in vivo, it is difficult to reliably quantify resonances of choline, creatine, and polyamines separately.

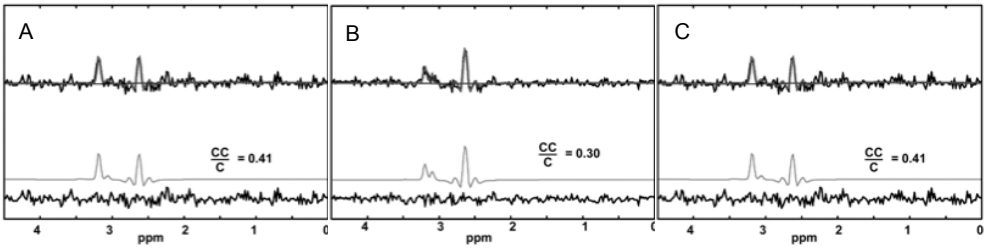

Figure 4. Spectral fits and calculations of Cho + Cr/Cit (CC/C) ratio by using PRISMA software with data of three locations in prostate of 64-year-old patient with prostate cancer. Spectra originate from (a) healthy peripheral zone, (b) transition zone cancer with Gleason score of 2 + 4, and (c) peripheral zone cancer with Gleason score of 3 + 4. From top to bottom for each fit in (a–c) measured spectrum (black line) overlaid with fit (upper gray line) and baseline, metabolite fit (lower gray line), and residual between data and fit.

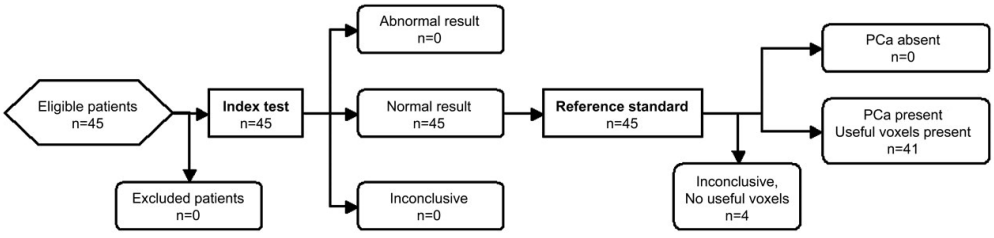

Figure 5. Flowchart of study profile. PCa = prostate cancer.

From 257 included spectra, both mean and median Cho + Cr/Cit ratios of the voxels from healthy tissues significantly differed from those of cancer tissue (Figure 6) (P < .001). The mean Cho + Cr/Cit ratio in the peripheral zone was significantly different from that in central gland and periurethral tissue (P < .05), whereas there was no statistical difference between ratios in the central gland and periurethral tissue (P = .90).

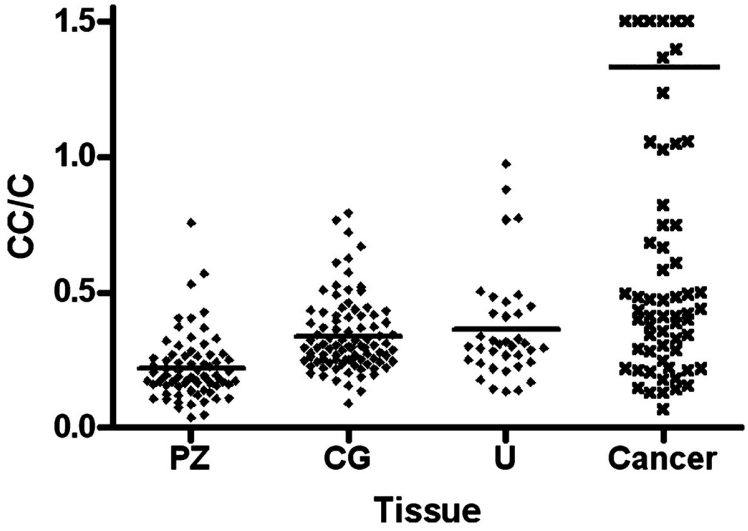

Figure 6. Graph of Cho + Cr/Cit (CC/C) ratio of tissues in prostate. Mean values, indicated with a horizontal line, for Cho + Cr/Cit ratio are 0.22 ± 0.12 (standard deviation) for peripheral zone (PZ), 0.34 ± 0.14 for central gland (CG), 0.36 ± 0.20 for periurethral area (U), and 1.3 ± 3.7 for cancer tissue. For display purposes, 6 voxels with Cho + Cr/Cit ratio greater than 1.5 are shown as 1.5.

However, some voxels in the periurethral area had the highest Cho + Cr/Cit ratios among healthy tissues. Focusing on voxels from cancer tissue only and using the additional classifications concerning cancer size and matching certainty, we found an increase in mean and median Cho + Cr/Cit ratios with both increasing cancer size and matching certainty (Figure 7).

ROC curves were calculated for tissues by using only cancer voxels that were probably or definitely inside cancer (matching certainty scores of 2 and 3), thereby excluding the category possibly inside cancer. In seven patients, only cancer voxels with a matching certainty score of 1 were classified, so ROC curves were constructed with cancer voxels from 34 patients and voxels in healthy tissues from 41 of 45 patients. Because the Cho + Cr/Cit distribution between the central gland and the periurethral area did not differ significantly, we combined the Cho + Cr/Cit distributions from the central gland and the periurethral area into a single ROC curve (Figure 8). The Az for the tissues were 0.84 (95% confidence interval: 0.76, 0.90) for the peripheral zone and 0.69 (95% confidence interval: 0.62, 0.76) for the

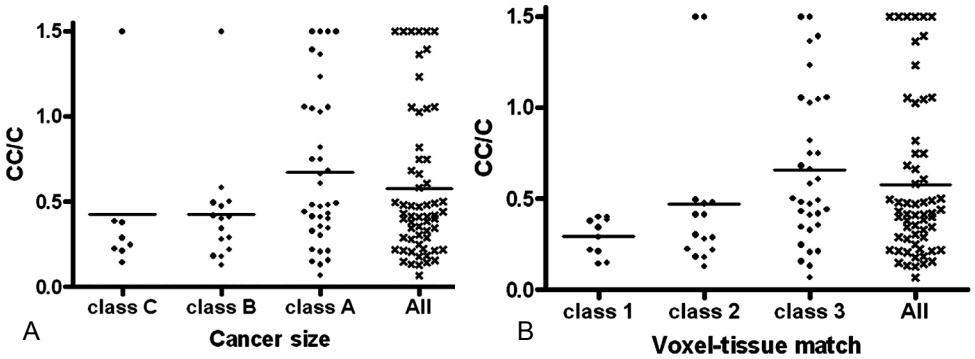

Figure 7. Graphs of valid cancer voxels classified by size and matching certainty score. (A) Cho + Cr/Cit (CC/C) ratio is plotted against size: class A = larger than 2 1H MR spectroscopic voxels (approximately 2 cm^3), class B = between 1 and 2 1H MR spectroscopic voxels (between 1 and 2 cm^3), and class C = smaller than 1 1H MR spectroscopic voxel (approximately 1 cm^3). (B) Relationship with matching certainty score is shown: class 1 = possibly inside cancer, class 2 = probably inside cancer, and class 3 = definitely inside cancer. For display purposes, Cho + Cr/Cit ratios greater than 1.5 are shown as 1.5.

combined central gland and periurethral area (P = .002). In the Table, the sensitivity and specificity at two threshold values for the Cho + Cr/Cit ratio for peripheral zone and central zone tissues are summarized.

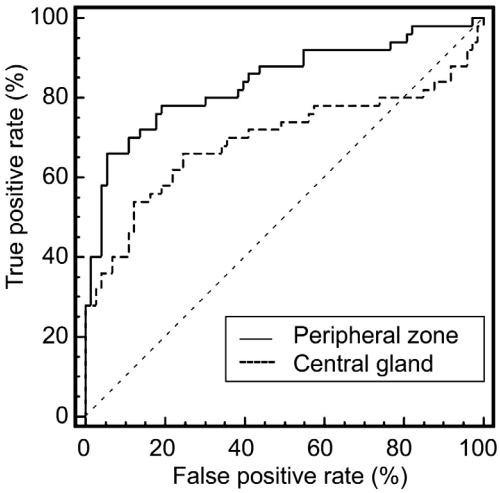

Figure 8. ROC curves summarize accuracy of discrimination of cancer from healthy peripheral zone and central gland tissue at 1H MR spectroscopy with only external surface coils at 3 T.

Although we used only the Cho + Cr/Cit ratio of those voxels that were classified as definitely inside cancer (class 3 only) to relate to cancer aggressiveness (Figure 9), we did not find a correlation between the Cho + Cr/Cit ratio and Gleason score (r = 0.17).

Table. Sensitivity and Specificity of 1H MR Spectroscopy for Discrimination of Cancer from Healthy Peripheral Zone and Central Gland Tissue at Cho + Cr/Cit Thresholds

Tissue and Threshold	Sensitivity (%)	Specificity (%)
Peripheral zone		
0.41	66 (33/50)	95 (69/73)
0.27	78 (39/50)	81 (59/73)
Central gland		
0.41	66 (33/50)	73 (94/128)
0.33	72 (36/50)	62 (79/128)

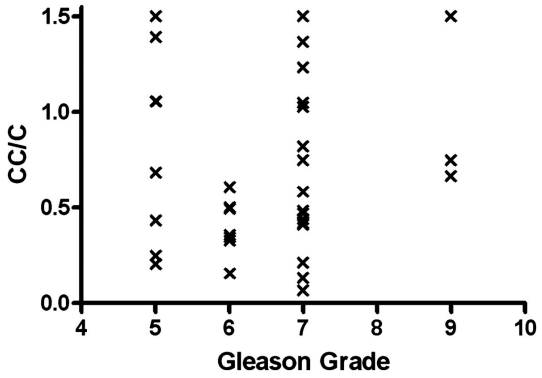

Figure 9. Graph shows that correlation between Cho + Cr/Cit (CC/C) ratio of cancer voxels assigned with high matching certainty and total Gleason score of corresponding cancer focus at histopathologic examination was not found (r = 0.17).

DISCUSSION

Our study results demonstrate that 1H MR spectroscopic imaging of the prostate with the use of external surface coils at 3 T is feasible. The examinations -including MR imaging- were noninvasive and relatively short (<30 minutes). The number of classified voxels that passed visual inspection of the quality of the fit and that were chosen at random in tissues throughout the prostate of every patient can be used as an estimate of what percentage of the voxels of the data set were useful. With the exclusion of four patients because of inadequate shimming values and/or low signal-to-noise ratio, the median amount of 82% of useful voxels per patient reflects the robustness of the pulse sequence, the combination of signals from multiple coil elements, and the automatic fit routine. From these useful voxels, the Cho + Cr/Cit ratio could be calculated, which resulted in a Cho + Cr/Cit threshold value of 0.41. At 0.41, the sensitivity and specificity, respectively, of discrimination of cancer from

healthy tissue were 66% and 95% for the peripheral zone and 66% and 73% for the central gland.

Although we used a different repetition time, echo time, and magnetic field strength, the mean and standard deviation of the Cho + Cr/Cit ratio of voxels in the healthy peripheral zone (0.22 +/- 0.12) were almost identical to values reported previously with similar combined water and lipid suppression at 1.5 T with an endorectal coil (0.22 +/- 0.13) [17]. Apparently, differences in pulse sequence timing equalize with differences in metabolite relaxation times. On one hand, choline and creatine signals are lower than citrate signal because of a slight increase in saturation of these signals at 3 T (T1 of choline in the prostate at 3 T has been reported to be 1.6 seconds +/- 0.5 compared with 0.47 second +/- 0.14 for citrate) [7]. On the other hand, this is compensated by the smaller loss of signal at an echo time of 145 msec because T2 relaxation for choline (T2 of 0.24 second +/- 0.09) [7] is higher than that of citrate (T2 of 0.17 second +/- 0.05) (7) at 3 T.

With complete coverage of the whole prostate at 3D 1H MR spectroscopic imaging, we could differentiate Cho + Cr/Cit values of the peripheral zone from values of the central gland. Another study [18] at 1.5 T on differentiation between central gland and peripheral zone at two-dimensional 1H MR spectroscopic imaging, with use of an endorectal coil and somewhat different MR parameters, revealed slightly deviating mean Cho + Cr/Cit values of healthy tissues (0.38 +/- 0.15 for peripheral zone and 0.43 +/- 0.16 for central gland) but a similar overlap of Cho + Cr/Cit values in cancer with those in healthy tissue. Mean Cho + Cr/Cit values for voxels in cancer tissue are difficult to compare between studies because the distribution in Cho + Cr/Cit values is far from Gaussian: A single or small number of very high Cho + Cr/Cit values dominate the mean value.

Because the mean Cho + Cr/Cit ratio of the central gland is higher than that of the peripheral zone, the overlap with voxels from cancer tissue is larger and the power of using the ratio to discriminate healthy tissue from cancer tissue is smaller, as is reflected in the lower Az of the ROC curve for the central gland than that for the peripheral zone. For a separate analysis of cancer in the central gland and the peripheral zone, the amount of matched voxels of cancer tissue in the central gland was too small. Therefore, voxels of cancer tissue were not subdivided according to their location in the prostate in the analysis.

The shape of the citrate signal at 3 T at the applied pulse timing calls for a postprocessing method that calculates more than the integral of signals in the spectrum only. The integral of the citrate signal varies with its line width and can approach zero when positive and negative lobes of the phased signal cancel each other. This problem was overcome by fitting a complex signal amplitude to a model function in the time domain. As mentioned earlier, the increase in spectral resolution obtained at 3 T compared with that at 1.5 T did

not necessarily increase the accuracy of fitting choline and creatine resonances separately, because polyamine resonances between these two metabolites often still appeared to be present. Adding the integrals of these metabolites, thereby quantifying the complete group of resonances from 3.0 to 3.2 ppm and dividing them by the integral of citrate (represented by the fitted amplitude of the time domain signal), which is a general approach with spectra at 1.5 T, provided a more robust measure for quantifying tissues. A general problem with this approach remains partial cancellation of the sum of resonances by a decrease in polyamine signals together with an increase in choline signals in cancer tissue.

Difficulties in matching histopathologic slices with T2-weigthed MR images were acknowledged with the additional classification we made for the cancer voxels: Both smaller foci and foci that were matched with lower confidence had smaller Cho + Cr/Cit ratios. Furthermore, as a result of apodization to reduce voxel bleed [13], the true size of a voxel (approximately 1 cm^3) was larger compared with what is called a clinically relevant cancer focus volume (> 0.5 cm^3) [19,20] and also was larger than voxel sizes reported at 1.5 T (0.24 – 0.7 cm^3 [1] and 0.6 – 0.8 cm^3 [18], both without apodization). This introduces partial volume effects. In smaller cancers, voxels could contain both cancer and healthy tissue with a corresponding lower Cho + Cr/Cit ratio, which is also reflected in the decrease in median Cho + Cr/Cit ratio with decreasing cancer size. Because the highest Cho + Cr/ Cit values of healthy tissues were present around the urethra, we cannot rule out the urethra and ejaculatory ducts as possible confounders for cancer. However, the size of the voxels and the corresponding partial volume effects when defining a voxel around the urethra could be a reason why we did not find significant differences between the Cho + Cr/Cit ratio of the periurethral area and that of the healthy central gland. Throughout the central gland, including the urethra, the Cho + Cr/Cit ratio is generally larger than that of the healthy peripheral zone. Benign diseases of the central gland that increase the signals from 3.0 to 3.2 ppm or anatomic differences, such as less ductal tissue in which citrate is accumulated, could be reasons for this.

Although such findings were revealed in prostate cancer studies at 1.5 T [15], we were not able to detect a trend between the Cho + Cr/Cit ratio of a voxel in cancer tissue and the corresponding Gleason score at histopathologic analysis. A possible explanation could be that our patients were eligible for prostatectomy and therefore did not have the highest Gleason scores (predominantly 5-7). Consequently, we could not cover the complete range of Gleason scores proportionally with our patient population.

Our study had limitations. Without an endorectal coil, the signal-to-noise ratio inside the prostate was limited, which forced us to use a voxel size of 1.0 cm^3, with its corresponding partial volume effects. If an endorectal coil had been used, the signal-to-noise ratio in the peripheral zone of the prostate would have been four to 10 times higher, depending on the

actual distance from the voxel to the coil conductors. With increasing distance to the coil conductors (in central gland tissues), the benefit of an endorectal coil is less [21].

Not all voxels of all prostates were evaluated in our study. Although the classified voxels were chosen at random locations within the tissues of the prostate, they are a subset of the total number of voxels. But, because the classification was performed on the basis of histopathologic and MR imaging findings, with reviewers blinded to MR spectroscopic results and with the incorporation of both large and smaller cancer foci, we do not expect a bias in quantification with this subset. Furthermore, the MR spectroscopic findings were studied without an extensive comparison with sensitivity and specificity for distinguishing benign from malignant tissue with T2-weighted MR imaging alone at 3 T. Therefore, we are unable to estimate the incremental value of MR spectroscopic imaging over T2-weighted MR imaging -which has been found for 1.5 T [22]- for a field strength of 3T.

Another limitation of our study was its relatively small number of patients. We did not assign a prospective score, or radiologic certainty score, to tissue for the presence of cancer, as has been proposed by Jung et al [23]. We also did not take into account possibly elevated choline or decreased polyamine levels as separate parameters, which can have additional value. We investigated the quantitative value of the Cho + Cr/Cit ratio itself, without the experience of radiologic input but also without the possible bias of radiologic input, as a basis for either radiologic assignment or pure quantitative assessment of future prospective work.

In summary, on the basis of only the numbers of the Cho + Cr/Cit ratio, which originated from 1.0-cm^3 voxels and was measured in less than 10 minutes, 3D proton MR spectroscopy at 3 T with only external array coils had a high specificity for the discrimination of cancer from healthy tissues; therefore, this technique shows potential for the metabolic identification of prostate cancer. Further and larger studies are needed, however, for confirmation.

REFERENCES

[1] Kurhanewicz J, Vigneron DB, Hricak H, Narayan P, Carroll P, Nelson SJ. Three-dimensional H-1 MR spectroscopic imaging of the in situ human prostate with high (0.24-0.7 cm^3) spatial resolution. Radiology 1996; 198:795–805.

[2] Heerschap A, Jager GJ, van der Graaf M, et al. In vivo proton MR spectroscopy reveals altered metabolite content in malignant prostate tissue. Anticancer Res 1997;17:1455–1460.

[3] Kurhanewicz J, Vigneron DB, Nelson SJ, et al. Citrate as an in vivo marker to discriminate prostate cancer from benign prostatic hyperplasia and normal prostate peripheral zone: detection via localized proton spectroscopy. Urology 1995;45:459–466.

[4] Lichy MP, Pintaske J, Kottke R, et al. 3D proton MR spectroscopic imaging of prostate cancer using a standard spine coil at 1.5 T in clinical routine: a feasibility study. Eur Radiol 2005;15:653–660.

[5] Brown MA. Time-domain combination of MR spectroscopy data acquired using phased-array coils. Magn Reson Med 2004;52:1207–1213.

[6] Bottomley PA. Spatial localization in NMR spectroscopy in vivo. Ann N Y Acad Sci 1987;508:333–348.

[7] Scheenen TW, Gambarota G, Weiland E, et al. Optimal timing for in vivo (1) H-MR spectroscopic imaging of the human prostate at 3T. Magn Reson Med 2005;53:1268–1274.

[8] van der Graaf M, Schipper RG, Oosterhof GO, Schalken JA, Verhofstad AA, Heerschap A. Proton MR spectroscopy of prostatic tissue focused on the detection of spermine, a possible biomarker of malignant behavior in prostate cancer. Magma 2000;10:153–159.

[9] Hennig J, Scheffler K. Hyperechoes. Magn Reson Med 2001;46:6–12.

[10] Wilman AH, Allen PS. The response of the strongly coupled AB system of citrate to typical 1H MRS localization sequences. J Magn Reson B 1995;107:25–33.

[11] Mescher M, Tannus A, Johnson MO, Garwood M. Solvent suppression using selective echo dephasing. J Magn Reson A 1996;123:226–229.

[12] Star-Lack J, Nelson SJ, Kurhanewicz J, Huang LR, Vigneron DB. Improved water and lipid suppression for 3D PRESS CSI using RF band selective inversion with gradient dephasing (BASING). Magn Reson Med 1997;38:311–321.

[13] Scheenen TW, Klomp DW, Roll SA, Futterer JJ, Barentsz JO, Heerschap A. Fast acquisition-weighted three-dimensional proton MR spectroscopic imaging of the human prostate. Magn Reson Med 2004;52:80–88.

[14] Greene FL, Page DL, Fleming ID, et al. AJCC cancer staging manual. 6th ed. New York, NY: Springer-Verlag, 2002.

[15] Zakian KL, Sircar K, Hricak H, et al. Correlation of proton MR spectroscopic imaging with Gleason score based on step-section pathologic analysis after radical prostatectomy. Radiology 2005;234:804–814.

[16] Jager GJ, Ruijter ET, van de Kaa CA, et al. Local staging of prostate cancer with endorectal MR imaging: correlation with histopathology. AJR Am J Roentgenol 1996;166:845–852.

[17] Males RG, Vigneron DB, Star-Lack O, et al. Clinical application of BASING and spectral/ spatial water and lipid suppression pulses for prostate cancer staging and localization by in vivo 3D 1H magnetic resonance spectroscopic imaging. Magn Reson Med 2000;43: 17–22.

[18] van Dorsten FA, van der Graaf M, Engelbrecht MR, et al. Combined quantitative dynamic contrast-enhanced MR imaging and (1)H MR spectroscopic imaging of human prostate cancer. J Magn Reson Imaging 2004;20:279–287.

[19] Augustin H, Hammerer PG, Graefen M, et al. Insignificant prostate cancer in radical prostatectomy specimen: time

trends and preoperative prediction. Eur Urol 2003;43:455– 460.

[20] Stamey TA, Freiha FS, McNeal JE, Redwine EA, Whittemore AS, Schmid HP. Localized prostate cancer: relationship of tumor volume to clinical significance for treatment of prostate cancer. Cancer 1993;71:933–938.

[21] Futterer JJ, Scheenen TW, Huisman HJ, et al. Initial experience of 3 Tesla endorectal coil magnetic resonance imaging and 1H-spectroscopic imaging of the prostate. Invest Radiol 2004;39:671–680.

[22] Futterer JJ, Heijmink SW, Scheenen TW, et al. Prostate cancer localization with dynamic contrast-enhanced MR imaging and proton MR spectroscopic imaging. Radiology 2006;241:449–458.

[23] Jung JA, Coakley FV, Vigneron DB, et al. Prostate depiction at endorectal MR spectroscopic imaging: investigation of a standardized evaluation system. Radiology 2004;233:701–708.

[24] Scheenen T, van Hecke P, Bachert P, et al. First results of IMAPS: an international multi-centre assessment of prostate MR spectroscopy [abstr]. In: Radiological Society of North America scientific assembly and annual meeting program. Oak Brook, Ill: Radiological Society of North America, 2005;419.

CHAPTER 9

Initial Results of 3-Dimensional 1H-Magnetic Resonance Spectroscopic Imaging in the Localization of Prostate Cancer at 3 Tesla: Should We Use an Endorectal Coil?

Derya Yakar
Stijn W. T. P. J. Heijmink
Christina A. Hulsbergen-van de Kaa
Henkjan Huisman
Jelle O. Barentsz
Jurgen J. Fütterer
Tom W. J. Scheenen

Invest Radiol 2011;46(5):301-6.

Purpose: The purpose of this study was to compare the diagnostic performance of 3 Tesla, 3-dimensional (3D) magnetic resonance spectroscopic imaging (MRSI) in the localization of prostate cancer (PCa) with and without the use of an endorectal coil (ERC).

Materials and Methods: Our prospective study was approved by the institutional review board, and written informed consent was obtained from all patients. Between October 2004 and January 2006, 18 patients with histologically proven PCa on biopsy and scheduled for radical prostatectomy were included and underwent 3D-MRSI with and without an ERC. The prostate was divided into 14 regions of interest (ROIs). Four readers independently rated (on a 5-point scale) their confidence that cancer was present in each of these ROIs. These findings were correlated with whole-mount prostatectomy specimens. Areas under the receiver-operating characteristic curve were determined. A difference with a $P < 0.05$ was considered significant.

Results: A total of 504 ROIs were rated for the presence and absence of PCa. Localization of PCa with MRSI with the use of an ERC had a significantly higher areas under the receiver-operating characteristic curve (0.68) than MRSI without the use of an ERC (0.63) ($P = 0.015$).

Conclusion: The use of an ERC in 3D MRSI in localizing PCa at 3 Tesla slightly but significantly increased the localization performance compared with not using an ERC.

Prostate cancer (PCa) is the most commonly diagnosed noncutaneous form of cancer in men and is the second largest cause of cancer-related mortality in this population [1]. Like many cancers, PCa is treated most effectively if localized and staged correctly. Thus, reliable knowledge of the location and spatial extent of the disease within and beyond the gland is crucial.

The most frequently used diagnostic tools in daily clinical practice (eg, digital rectal examination, prostate-specific antigen [PSA] level, and transrectal ultrasound [TRUS]-guided biopsy) are often inaccurate or inadequate. Digital rectal examination misses a substantial proportion of cancers, PSA alone cannot accurately stage an individual patient, and TRUS suffers from major sampling errors [2-6].

Magnetic resonance (MR) imaging is a noninvasive examination, which can provide anatomic, functional, and metabolic information. MR spectroscopic imaging (MRSI), that generates metabolic spectra, has been investigated before for cancer localization. Some promising results have been reported with sensitivities and specificities of 63% to 80% and 75% to 84%, respectively [7,8]. In addition, MRSI and MR imaging are still evolving techniques where recent insights about new metabolic markers such as polyamines [9,10], and new approaches with dynamic contrast-enhanced and diffusion-weighted MR imaging could further improve its localization ability [11-14].

The use of an endorectal coil (ERC) as an essential part of the optimal prostate MR imaging protocol is still a matter of debate. The obvious advantage of using the ERC is the increase in signal-to-noise ratio compared with non-ERC MR imaging. Even though several authors have demonstrated the advantages of the use of such an ERC for localizing and staging PCa on T2-weighted MR imaging [15,16], the direct comparison between ERC and non-ERC MR examinations has not been investigated for PCa localization with three-dimensional (3D) MRSI.

We hypothesized that the use of an ERC will increase the diagnostic performance of MRSI in localizing PCa. Therefore, the purpose of this study was to compare the diagnostic performance of 3 Tesla (3T), 3D MRSI in the localization of PCa with and without the use of an ERC.

MATERIALS AND METHODS

Patients

Our prospective study was approved by the institutional review board, and written informed consent was obtained from all patients. During the time period in which 3D MRSI at 3T was firstly initiated and performed at our institution (between October 2004 and January 2006), 18 consecutive patients with histologically proven PCa on biopsy and scheduled for radical

prostatectomy were included and underwent 3D-MRSI (at least 3 weeks after biopsy) with and without an ERC. Patient characteristics were as follows: median age 66 years (range, 56–75 years), median PSA 4.9 ng/mL (range, 3.6–24.6 ng/mL), median time between TRUS guided biopsy and MR examination 64 days (range, 21–104 days), median time between MR examination and radical prostatectomy 7 days (range, 1–89 days), and median Gleason score, based on prostatectomy specimens, 6.5 (range, 5–9). Exclusion criteria were previous hormonal therapy and contraindications to MR imaging (eg, cardiac pacemakers, intracranial clips, prior anorectal surgery).

MR Imaging Protocol

MR imaging of the prostate was performed using a 3T whole-body MR system (Siemens Trio Tim, Erlangen, Germany) with the spine array and body array coil elements, with a total examination time of between 45 and 50 minutes. Bowel peristalsis was suppressed with an intramuscular injection of 1 mg of glucagon (Glucagen, Novo Nordisk, Bagsvaerd, Denmark). At first, patients were imaged without the use of an ERC according to the following MR imaging protocol sequences: T2-weighted fast spin echo sequence in 3 orthogonal planes, with the field of view of the axial plane obtained perpendicular to the rectal wall, (repetition time/ echo time [TR/TE], 3700/124 milliseconds; field of view, 220 x 220 mm; matrix size, 512 x 512; slice thickness, 4 mm; number of averages, 2; total acquisition time per plane, 4 –5 minutes), followed by 3D 1H-MRSI of the entire prostate with a point-resolved spectroscopy pulse sequence15 (TR/TE, 750/145 milliseconds; acquisition bandwidth, 1250 Hz; voxel resolution, 7 x 7 x 7 mm; total acquisition time, approximately 9 minutes).

Subsequently, in the same patient an ERC was inserted rectally and filled with 40 mL perfluorocarbon liquid (Fomblin, Solvay-Solexis, Milan, Italy). After a quick series of images obtained to depict ERC position and ERC adjustment if necessary, a T2-weighted fast spin echo sequence in 3 planes (TR/TE, 5000/153; field of view, 200 x 100 mm; matrix size, 768 x 384; slice thickness, 2.5 mm; number of averages, 1; total acquisition time per plane, 2–3 minutes) was obtained, with the field of view of the axial plane obtained perpendicular to the rectal wall, followed by 3D ^{1}H-MRSI (TR/TE, 750/145 milliseconds; acquisition bandwidth, 1250 Hz; voxel resolution, 6 x 6 x 6 mm; total acquisition time, approximately 9 minutes).

Data Postprocessing

Semi-automatic postprocessing of all voxels within the prostate was performed with a software work-in-process package (Metabolite report, Siemens, Erlangen, Germany). A basic set of simulated complex model signals of choline, creatine, and citrate was fitted to the time domain signals of the voxels after a frequency shift, residual water removal, and remodeling of the first 5 data points to handle baseline artifacts. The amplitudes of the individually fitted signals were used to calculate the choline+creatine-to-citrate ratio (CC/C) and the choline-to-creatine ratio (C/C). A similar approach has been used before (17).

Scoring and Evaluation of Data

All MRSI datasets were evaluated overlaid on the T2- weighted datasets. The prostate was divided into 14 regions of interest (ROIs) (Figure 1).

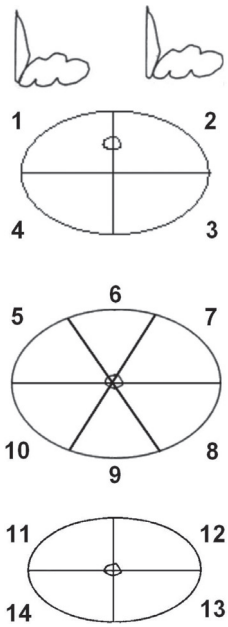

Figure 1. A schematic overview of the 14 regions of interest in which the prostate was divided.

The T2-weighted images were only used for transfer of the 14 ROIs to the MRSI data and subsequently correlating this with pathology. Four readers (reader I, Radiologist; II, Radiologist; III, Radiologist; and IV, Spectroscopist with 0, 4, 6, and 8 years of experience in MRSI data evaluation, respectively) independently rated cancer presence in each of these ROIs on a 5-point scale, using a standardized scoring system.18 This scale was based on the CC/C and C/C ratios for the peripheral zone and the central gland determined before by Scheenen et al [19] (Table 1).

Table 1. Five-point scale

Score and score definition	PZ CC/C ratio	CG CC/C ratio	C/C ratio adjustment
1. Definitely benign tissue	≤ 0.34	≤ 0.48	If C/C ratio ≥ 2, then:
2. Probably benign tissue	> 0.35 - 0.46	> 0.49 - 0.62	adjust 3 and 2 into 4
3. Possibly malignant tissue	> 0.47 - 0.58	> 0.63 - 0.76	
4. Probably malignant tissue	> 0.59 - 0.70	> 0.77 - 0.90	If C/C ratio < 2, then:
5. Definitely malignant tissue	≥ 0.71	≥ 0.91	adjust 5 into 4 and 4 into 3

Adapted from Radiology 2007;245:507–516 [19]

PZ indicates peripheral zone; CG, central gland; CC/C, choline-creatine-to-citrate; C/C, choline-to-creatine.

All datasets were anonymized, and readers were blinded to all clinical parameters. They were only aware of the fact that all patients were histopathologically diagnosed with PCa. First, all MRSI examinations without the ERC were rated. For each ROI, all spectra were read and interpreted and the final score for that ROI was based on the highest CC/C present within the ROI, and adjusted based on the C/C ratio for the corresponding voxel (Table 1). Second, after a period of 4 weeks, during a different reading session, MRSI with the ERC was rated likewise. Readers were allowed to rate ROIs as nonrateable if ratios were not reliably fitted because of low signal-to-noise ratios of the metabolite spectra (more than 50% of the voxels within a certain ROI).

Histopathological Analysis

Prostatectomy specimens were fixed overnight in 10% neutral buffered formaldehyde and coated with India ink. These prostatectomy specimens were sliced at 4-mm intervals at a plane parallel to the axial T2-weighted images (perpendicular to the rectal wall). All slices were routinely embedded in paraffin. Tissue sections of 5 µm thickness were prepared from the slices and stained with hematoxylin and eosin. A single genitourinary histopathologist (C.A.H. van de K.) with 18 years of experience who was blinded to the MR imaging results determined the exact localization, extent, Gleason score, and volume of each cancer focus.

Data Analysis

After evaluating and scoring all MRSI data, one spectroscopist (T.W.J.S.) and two of the radiologists (J.J.F. and D.Y.) in consensus transferred the histopathologic evaluation (standard of reference) of the prostatectomy specimens to the 14-segment prostate ROI scheme. This transfer was realized by matching the pathologic slice to the level of the T2-weighted images by its location between the apex and the base of the prostate. Subsequently, landmarks such as benign prostatic hyperplasia nodules and the urethra were used to match cancer foci to their corresponding ROIs. The T2-weighted images were only used for correlating pathology to the cancer region relative to the 14-segment ROI-scheme. An ROI was considered true-positive if cancer was present and if this cancer focus was 0.5 cm^3 or larger in volume [20]. All smaller cancer foci were excluded from further analysis. Each of the 14 ROIs for every prostate were classified as containing either cancer or healthy tissue.

Statistical Analysis

For statistical analysis (SPSS version 16.0), the sensitivity, specificity, negative predictive value (NPV), and positive predictive value were calculated by dichotomizing (cut-off point of 3 and above was considered malignant) the readings. Areas under the receiver-operating characteristic curve (AUC) and comparison between these AUCs were determined by using an ROI-ROC analysis [21], with a bootstrap estimation of diagnostic accuracy [22] and a Bonferroni correction. These statistical methods have been used before in studies that collected data according to the ROI paradigm [8,15].

All P values reported were derived at one-sided tests. P values of 0.05 or less were considered significant.

RESULTS

In all, 18 patients were included. A total of 504 ROIs (18 patients with 14 ROIs each, 252 ROIs with and 252 ROIs without ERC) were rated for the presence and absence of PCa (Figure 2). From the histopathologic standard of reference, 81 of 252 (32%) ROIs were assigned as containing PCa. Of these 81 ROIs, 31 containing PCa, were excluded due to low cancer volume (<0.5 cm^3). Of the remaining 50 ROIs classified as containing PCa, 72% (36/50) comprised peripheral zone cancers, whereas 28% (14/50) comprised central gland cancers. These remaining cancer foci had a median volume of 1.1 cm^3 (range, 0.5–12.9 cm^3) (Figure 3).

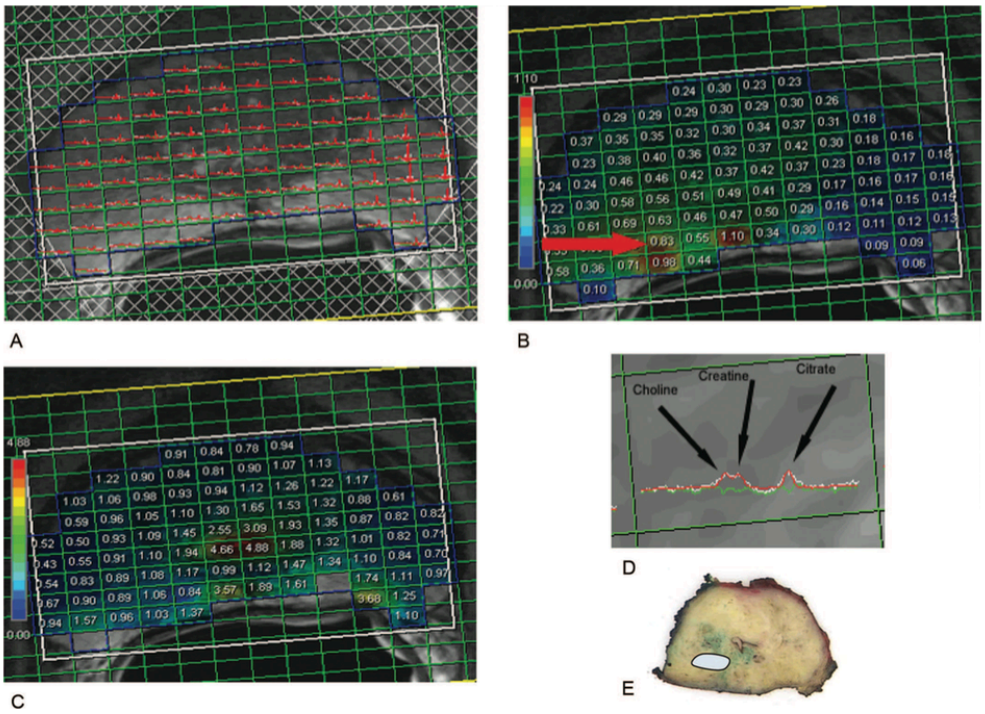

Figure 2. Presentation of how readers were able to evaluate and score the data in 1 view. MR images of a 73-year-old man with a PSA of 5.0 ng/mL. From left to right: Overlaid on transverse T2-weighted multiple-spin-echo image (TR/TE 3700/124) spectral fits (A), choline+creatine-to-citrate ratio (CC/C) (B), and choline-to-creatine ratio (C/C) (C). Magnified view of metabolite spectrum of the voxel at the red arrow (D), which had the highest CC/C ratio of region of interest (ROI) number 10. Measured spectrum (white line), overlaid with fit (red line), and residual between data and fit (green line). This voxel had a CC/C ratio of 0.83 in the peripheral zone of the prostate. The C/C ratio was 1.06 so, according to Table 1 this

voxel, representing segment 10, was classified as probably malignant tissue. Histopathology revealed prostate cancer in this segment with a Gleason score of 3+3 (E).

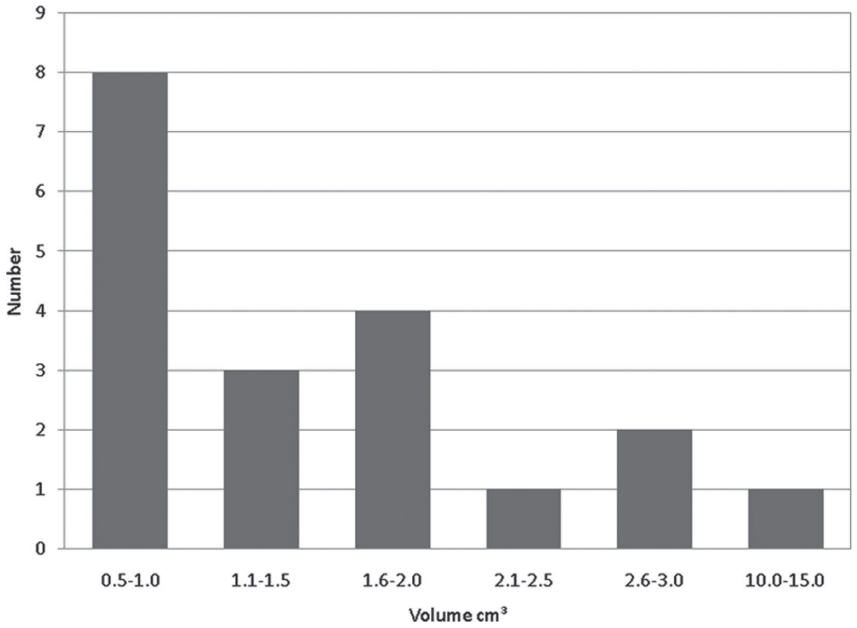

Figure 3. Cancer foci volume distribution on histopathology. Median tumor volume, 1.1 cm^3; range, 0.5 to 12.9 cm^3.

Overall, there were significantly more ROIs nonrateable on MRSI with ERC, 14% (146/1008), than without ERC, 12% (121/1008), (P = 0.007) for all readers together (Table 2). Descriptive statistics of PCa localization with and without an ERC per reader was summarized in Table 3. For the more experienced readers (ie, readers II, III, and IV) MRSI with an ERC had a high specificity (82%–92%), but a low sensitivity (20%–57%). For the novice reader (reader I), MRSI with the use of an ERC had a high sensitivity (80%) and a low specificity (34%). For all readers, the NPVs were high (82%– 89%), whereas the positive predictive values were low (20%–45%) for both imaging with and without ERC.

Table 2. Number of nonrateable ROIs

	MRSI–	MRSI+
Reader I	3% (6/252)	0%
Reader II	18% (50/252)	22% (62/252)
Reader III	8% (20/252)	14% (36/252)
Reader IV	18% (45/252)	19% (48/252)

P = 0.007

MRSI– indicates MR spectroscopic imaging without an endorectal coil; MRSI+ indicates MRSI with an endorectal coil; ROIs: regions of interest.

Table 3. Diagnostic Performance in Localizing Prostate Cancer With MRSI With and Without an ERC

	MRSI–				MRSI+			
	Sensitivity	Specificity	NPV	PPV	Sensitivity	Specificity	NPV	PPV
Reader I	65% (26/40)	43% (76/178)	84% (76/90)	20% (26/128)	80% (33/41)	34% (62/183)	89% (62/70)	21% (33/154)
Reader II	30% (13/43)	88% (164/186)	85% (164/194)	37% (13/35)	20% (9/44)	92% (159/173)	82% (159/194)	39% (9/23)
Reader III	33% (14/43)	70% (133/189)	82% (133/162)	20% (14/70)	32% (13/41)	87% (153/175)	85% (153/181)	37% (13/35)
Reader IV	42% (18/43)	74% (122/164)	83% (122/147)	30% (18/60)	57% (24/46)	82% (129/158)	85% (129/151)	45% (24/53)

The AUCs increased with the experience of the reader (Table 4). The most experienced reader (reader IV) had the highest AUC (0.72) for localization of PCa with MRSI with an ERC. Overall AUCs were calculated for reader II, III, and IV together. Localization of PCa with MRSI with the use of an ERC had a significantly higher AUC (0.68) than MRSI without the use of an ERC (0.63) (P = 0.015) (Figure 4).

Table 4. AUC's for Localizing Prostate Cancer With MRSI With and Without an ERC

	MRSI– AUC	MRSI+ AUC	P
Reader I	0.55	0.61	0.047*
Reader II	0.62	0.65	0.151
Reader III	0.59	0.68	0.014*
Reader IV	0.67	0.72	0.056
Overall (II, III and IV)	0.63	0.68	0.015*

* Considered significant

MRSI– indicates MR spectroscopic imaging without an endorectal coil; MRSI+ indicates MRSI with an endorectal coil; AUC: area under the curve; ROIs: regions of interest.

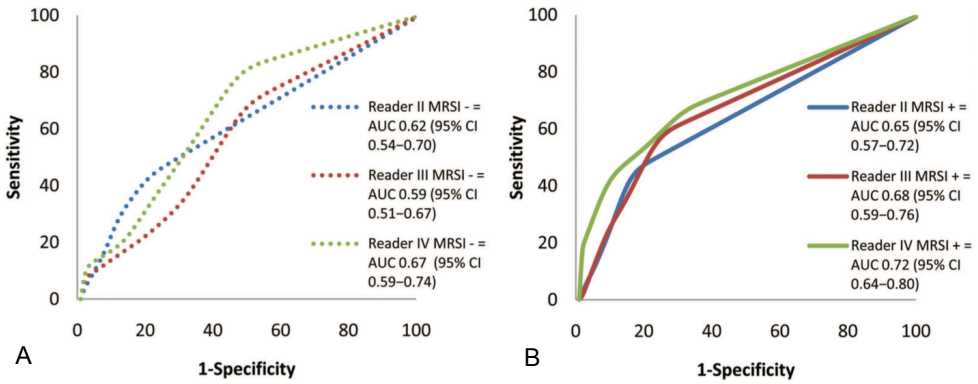

Figure 4. ROI-receiver operating characteristic curves for the experienced readers for localizing prostate cancer with MR spectroscopic imaging without an endorectal coil (MRSI-) (A), and with an endorectal coil (MRSI+) (B).

DISCUSSION

In the localization of PCa with MRSI at 3T, the use of an ERC provided a significantly (P = 0.015) higher AUC (0.68) for experienced readers compared with not using an ERC (AUC, 0.63) (Figure 4). Despite the fact that this difference was statistically significant, such a small increase in the AUC should make one think whether using the ERC is worth the effort, cost, and patient discomfort.

When calculating the general AUCs for all readers together, we excluded the results from reader I. This was done because of the vastly different level of experience of this reader (no experience) for evaluating MRSI data compared with the other three readers (at least 4 years of experience), as evidenced by the contrasting descriptive statistics compared with the other readers. All other readers had high specificities and low sensitivities, whereas reader I had a high sensitivity and a low specificity.

In general, the AUCs for localization with or without the use of an ERC were low compared with earlier published studies in localizing PCa with MR imaging [7,8]. Only one previously published multicenter study on the localization of PCa with MRSI at 1.5T presented even lower AUCs compared with our study [23]. Some of their main arguments for such low AUCs, such as low image quality and limited experience in obtaining data are somewhat shared by us. The results of our study were based partly on MRSI data that were obtained in 2004 when we had just commenced acquiring MRSI on a 3T system. A large number of nonrateable ROIs (Table 2) clearly illustrated this limited experience in 3T data acquisition. With matured technology (improved shimming), better coils and more experienced technicians, current data quality in clinical practice is expected to be improved, possibly resulting in an increased signal to-noise-ratio of the spectra and less nonrateable regions in the prostate. Furthermore, in our study, the experience level of the reader was also shown to be of influence by the fact that the highest AUC (0.72) was achieved by the most experienced reader (reader IV). Altogether this emphasizes the importance of experience in both acquiring and reading spectroscopic data. Future studies should therefore focus on training radiologists to read spectroscopic data (with possible pitfalls such as false positives because of high choline signals from seminal vesicles, and unreliable fits because of low signal-to-noise ratios) as well as technicians in obtaining high image quality data.

Nonetheless, it is important to note that the main purpose of our study was to compare the performance of MRSI in the localization of PCa with and without an ERC. The low overall AUCs did not interfere with our conclusion that the use of the ERC only marginally, but significantly, improves localization performance.

More ROIs were judged nonrateable on MRSI with the use of an ERC than in the set of images without the use of an ERC. In one other study [15], the authors established that

there was a higher presence of motion artifacts in the ERC group (compared with the non-ERC group), which could explain the higher amount of non-rateable ROIs in the ERC group (compared with the non-ERC group) in our study. It is very difficult to assess motion during the MRSI measurements. As the MRSI part of the protocol is performed after T2w MRI in 3 directions (larger time gap from pre-examination glucagon injection), and takes longer than one T2w series alone, motion during MRSI cannot be ruled out and may indeed be a source of error. Even the absence of these artifacts on T2w MRI cannot rule out motion during MRSI. Also, this difference in nonrateable ROIs in favor of the ERC group could be accounted for by decreased signal-to-noise ratio at distances further away from the coil, in the ventral part of the prostate.

Limitations of this study were initially, the low number of patients included, although this was partially compensated for by the 14 ROIs per prostate that were used and the multiple number of readers that were involved. Second, poor SNR and therefore the high number of nonrateable ROIs in these patients, because of this being the first patient cohort. Third, in this study, we did not use T1-weighted images to assess the amount of hemorrhage after biopsy in the prostate gland. Instead, to diminish this hemorrhage effect as much as possible, the time between biopsy and MR examination was kept to a minimum of 3 weeks [25]. Worth noting, any still existing hemorrhage effect would have affected the endorectal group as well as the nonendorectal group equally. Fourth, the readers rating these data were able to see which set of images concerned the MRSI data with the use of an ERC as well as without the use of an ERC. Ideally, data in comparative studies should be presented in a blinded manner. Blinding the use of an ERC is problematic, because it is very difficult to hide the increased SNR, especially at the dorsal aspect of the prostate, and the deformed prostate/rectum from a good radiologist or spectroscopist.

In conclusion, the use of an ERC in 3D MRSI in localizing PCa at 3T slightly but significantly increased the localization performance compared with not using an ERC.

REFERENCES

[1] Jemal A, Siegel R, Ward E, et al. Cancer statistics, 2009. CA Cancer J Clin 2009;59:225–249.

[2] Cooner WH, Mosley BR, Rutherford CL Jr, et al. Prostate cancer detection in a clinical urological practice by ultrasonography, digital rectal examination and prostate specific antigen. J Urol 1990;143:1146–1152.

[3] Catalona WJ, Richie JP, Ahmann FR, et al. Comparison of digital rectal examination and serum prostate specific antigen in the early detection of prostate cancer: results of a multicenter clinical trial of 6630 men. J Urol 1994;151:1283–1290.

[4] Halpern EJ, Strup SE. Using gray-scale and color and power Doppler sonography to detect prostatic cancer. Am J Roentgenol 2000;174:623–627.

[5] Rabbani F, Stroumbakis N, Kava BR, et al. Incidence and clinical significance of false-negative sextant biopsies of the prostate [in German]. Urologe A 1998;37:660.

[6] Partin AW, Carter HB, Chan DW, et al. Prostate specific antigen in the staging of localized prostate cancer: influence of tumor differentiation, tumor volume and benign hyperplasia. J Urol 1990;143:747–752.

[7] Scheidler J, Hricak H, Vigneron DB, et al. Prostate cancer: localization with three-dimensional proton MR spectroscopic imaging – clinicopathologic study. Radiology 1999;213:473–480.

[8] Futterer JJ, Heijmink SW, Scheenen TW, et al. Prostate cancer localization with dynamic contrast-enhanced MR imaging and proton MR spectroscopic imaging. Radiology 2006;241:449–458.

[9] Cheng LL, Wu C, Smith MR, et al. Non-destructive quantitation of spermine in human prostate tissue samples using HRMAS 1H NMR spectroscopy at 9.4 T. FEBS Lett 2001;494:112–116.

[10] van der Graaf M, Schipper RG, Oosterhof GO, et al. Proton MR spectroscopy of prostatic tissue focused on the detection of spermine, a possible biomarker of malignant behavior in prostate cancer. MAGMA 2000;10:153–159.

[11] Kim CK, Park BK, Kim B. Localization of prostate cancer using 3T MRI: comparison of T2-weighted and dynamic contrast-enhanced imaging. J Comput Assist Tomogr 2006;30:7–11.

[12] Kajihara H, Hayashida Y, Murakami R, et al. Usefulness of diffusion-weighted imaging in the localization of prostate cancer. Int J Radiat Oncol Biol Phys 2009;74:399–403.

[13] Gibbs P, Liney GP, Pickles MD, et al. Correlation of ADC and T2 measurements with cell density in prostate cancer at 3.0 Tesla. Invest Radiol 2009;44:572–576.

[14] Yakar D, Hambrock T, Huisman H, et al. Feasibility of 3T dynamic contrast-enhanced magnetic resonance-guided biopsy in localizing local recurrence of prostate cancer after external beam radiation therapy. Invest Radiol 2010;45:121–125.

[15] Heijmink SW, Futterer JJ, Hambrock T, et al. Prostate cancer: body-array versus endorectal coil MR imaging at 3 T–comparison of image quality, localization, and staging performance. Radiology 2007;244:184–195.

[16] Hricak H, White S, Vigneron D, et al. Carcinoma of the prostate gland: MR imaging with pelvic phased-array coils versus integrated endorectal–pelvic phased-array coils. Radiology 1994;193:703–709.

[17] Scheenen TW, Gambarota G, Weiland E, et al. Optimal timing for in vivo 1H-MR spectroscopic imaging of the human prostate at 3T. Magn Reson Med 2005;53:1268–1274.

[18] Jung JA, Coakley FV, Vigneron DB, et al. Prostate depiction at endorectal MR spectroscopic imaging: investigation of a standardized evaluation system. Radiology 2004;233:701–708.

[19] Scheenen TW, Heijmink SW, Roell SA, et al. Three-dimensional proton MR

spectroscopy of human prostate at 3 T without endorectal coil: feasibility. Radiology 2007;245:507–516.

[20] Epstein JI, Walsh PC, Carmichael M, et al. Pathologic and clinical findings to predict tumor extent of nonpalpable (stage T1c) prostate cancer. JAMA 1994;271:368–374.

[21] Obuchowski NA, Lieber ML, Powell KA. Data analysis for detection and localization of multiple abnormalities with application to mammography. Acad Radiol 2000;7:516–525.

[22] Rutter CM. Bootstrap estimation of diagnostic accuracy with patient-clustered data. Acad Radiol 2000;7:413–419.

[23] Weinreb JC, Blume JD, Coakley FV, et al. Prostate cancer: sextant localization at MR imaging and MR spectroscopic imaging before prostatectomy– results of ACRIN prospective multi-institutional clinicopathologic study. Radiology 2009;251:122–133.

[24] White S, Hricak H, Forstner R, et al. Prostate cancer: effect of postbiopsy hemorrhage on interpretation of MR images. Radiology 1995;195:385–390.

[25] Ikonen S, Kivisaari L, Vehmas T, et al. Optimal timing of post-biopsy MR imaging of the prostate. Acta Radiol 2001;42:70–73.

CHAPTER 10

Richtlijn prostaatcarcinoom 2007

INLEIDING

Prostaatcarcinoom is, naast longcarcinoom, de meest voorkomende kanker bij mannen. Het prostaatcarcinoom heeft in Nederland een incidentie van ongeveer 95 op de 100.000 mannen per jaar (Kankerregistratiegegevens 20031). Dit betekent dat in Nederland jaarlijks meer dan 7900 nieuwe patiënten met prostaatcarcinoom worden gediagnosticeerd. Opvallend is de toename van het incidentiecijfer van prostaatcarcinoom in het begin van de jaren negentig. De toename tussen 1989 en 1994 bedroeg ongeveer 40%. Daarna volgde een stabilisatie van het incidentiecijfer op een hoog niveau, maar in 2003 is het incidentiecijfer opnieuw met 6% gestegen. De meest voorkomende vorm is het adenocarcinoom, uitgaande van de klierbuisjes. Vooral de diagnose van een gelokaliseerd prostaatcarcinoom wordt steeds vaker gesteld. Dit gaat samen met een daling van de gemiddelde leeftijd waarop de ziekte wordt vastgesteld. Een en ander wordt in verband gebracht met het op steeds ruimere schaal toepassen van onderzoek naar de prostaatspecifieke merkstof 'prostaat specifiek antigeen' (PSA), waarmee vroege stadia van prostaatcarcinoom kunnen worden opgespoord. Er is dus waarschijnlijk nauwelijks sprake geweest van een reële stijging van de incidentie. De sterfte ten gevolge van prostaatcarcinoom daalde vanaf de tweede helft van de jaren '90. De laatste jaren is vooruitgang geboekt bij de detectie en de behandeling van prostaatcarcinoom, dat kan verklaren dat de sterfte aan prostaatcarcinoom een dalende trend vertoont.

Vanaf het veertigste jaar neemt de incidentie per leeftijdscategorie geleidelijk toe. Op hoge leeftijd komt het prostaatcarcinoom zeer frequent voor. Op basis van vergrijzing en groei van de bevolking is de verwachting dat het aantal mannen bij wie prostaatcarcinoom wordt geconstateerd in de periode 2000-2020 zal toenemen met circa 64% (Van Oers 20022).

Een rationele behandeling van prostaatcarcinoom wordt in zekere zin bemoeilijkt door het veelal ontbreken van goed uitgevoerd onderzoek. De meeste informatie over de behandeling wordt ontleend aan analyses van de behandelingsresultaten van een enkel instituut. Er is nogal wat verschil van mening over de waarde van de diverse behandelingsmogelijkheden. In verband met de hoge incidentie van prostaatcarcinoom en ook vanwege de vele behandelingsmogelijkheden, bestaat de noodzaak om tot een gezamenlijke nationale richtlijn te komen.

Voor de diagnostiek en behandeling van prostaatcarcinoom bestond in Nederland nog geen nationale richtlijn. Derhalve heeft de Nederlandse Vereniging voor Urologie het initiatief genomen een multidisciplinaire, evidence-based richtlijn te ontwikkelen over zowel de diagnostiek als de behandeling van het prostaatcarcinoom. Het Kwaliteitsinstituut voor de Gezondheidszorg CBO verleende hieraan methodologische expertise en logistieke steun. De Vereniging van Integrale Kankercentra coördineerde het proces en voerde het secretariaat.

DOELSTELLING

Deze richtlijn geeft aanbevelingen ter ondersteuning van de dagelijkse praktijkvoering, gericht op optimaal medisch handelen en gebaseerd op de resultaten van wetenschappelijk onderzoek en aansluitende meningsvorming. Er wordt aangegeven wat in het algemeen de beste zorg is voor patiënten met prostaatcarcinoom.

Deze richtlijn geeft aanbevelingen over de diagnostiek, de behandeling, de follow-up en begeleiding van patiënten met prostaatcarcinoom. Er worden geen uitspraken en aanbevelingen gedaan over screening vanwege het ontbreken van voldoende wetenschappelijk bewijsmateriaal. De richtlijn beoogt vooral een leidraad te zijn voor de dagelijkse praktijk en is van toepassing op alle patiënten met prostaatcarcinoom, ongeacht het stadium. De richtlijn kan ook worden gebruikt bij het geven van voorlichting aan patiënten. Daarnaast biedt de richtlijn aanknopingspunten voor bijvoorbeeld lokale (instituuts of regio-) protocollen en/of transmurale zorgafspraken, ter bevordering van de implementatie.

SAMENSTELLING WERKGROEP

Voor het ontwikkelen van de richtlijn werd een multidisciplinaire werkgroep samengesteld, bestaande uit vertegenwoordigers van alle relevante specialismen die met de diagnostiek en behandeling van prostaatcarcinoom te maken hebben. Er werd rekening gehouden met de geografische spreiding van de werkgroepleden en een evenredige vertegenwoordiging van de verschillende verenigingen, 'scholen' en academische achtergrond. De werkgroepleden waren gemandateerd door hun vereniging en hebben een belangenverklaring ingevuld en ondertekend. De samenstelling van de werkgroep als geheel is goedgekeurd door alle deelnemende wetenschappelijke verenigingen. Bij het opstellen van aanbevelingen werd ook een afgevaardigde van de patiëntorganisatie (Stichting Contactgroep Prostaatkanker) betrokken. De werkgroepleden zijn gezamenlijk verantwoordelijk voor de tekst van deze richtlijn.

Kernredactie en voorzitters subwerkgroepen

- Dr. Th.M. de Reijke, uroloog, Academisch Medisch Centrum, Amsterdam, vice-voorzitter tot september 2004; voorzitter vanaf september 2004
- Prof. Dr. J.J. Battermann, radiotherapeut, Universitair Medisch Centrum Utrecht, vice-voorzitter vanaf september 2004
- Prof.dr. S. Horenblas, uroloog, Antoni van Leeuwenhoek ziekenhuis, Amsterdam, voorzitter tot september 2004
- Dr. I.J. de Jong, uroloog, Universitair Medisch Centrum Groningen
- Dr. R.J.A. van Moorselaar, uroloog, VU Medisch Centrum Amsterdam
- Dr. G.O.N. Oosterhof, uroloog, Academisch Ziekenhuis Maastricht
- W. IJzerman, uroloog, Gelre Ziekenhuis, Apeldoorn

- Dr. P.F.W.M. Rosier, arts, Kwaliteitsinstituut voor de Gezondheidszorg CBO, Utrecht, adviseur tot januari 2005
- Dr. J.S. Burgers, programmaleider, Kwaliteitsinstituut voor de Gezondheidszorg CBO, Utrecht, adviseur vanaf januari 2005
- Mw. Dr. P.J.J. Wauben-Penris, hoofd patiëntenzorg, Integraal Kankercentrum Limburg, Maastricht, procesbegeleider namens de VIKC
- Mw. H.W.G. Hamelers-Paulus, secretaresse, Integraal Kankercentrum Limburg, Maastricht namens de VIKC

Overige werkgroepleden

- Dr. G. van Andel, uroloog, Onze Lieve Vrouwe Gasthuis Amsterdam
- Mw. J. Arnts, oncologieverpleegkundige radiotherapie, Universitair Medisch Centrum St. Radboud Nijmegen
- Prof.dr. J.O. Barentsz, radioloog, Universitair Medisch Centrum St. Radboud Nijmegen
- Dr. A.C.M. van de Bergh, radiotherapeut, Universitair Medisch Centrum Groningen
- Dr. R.F.M. Bevers, uroloog, Leids Universitair Medisch Centrum Leiden
- Prof.dr. M.A. Blankenstein, hoofd klinische chemie, VU Medisch Centrum Amsterdam
- Mw. Dr. F.C.J.M. van Gils, radiotherapeut, Maastro Clinic, Heerlen
- Dr. A.J.M. Hendrikx, uroloog, Catharina ziekenhuis Eindhoven
- Drs. S.W.T.P.J. Heijmink, radioloog i.o, Universitair Medisch Centrum St. Radboud, Nijmegen
- Mw. Dr. C.A. Hulsbergen-van de Kaa, patholoog, Universitair Medisch Centrum St. Radboud, Nijmegen
- Mw. Drs. H.K. de Jager-Nowak, radiotherapeut, Haga ziekenhuis, Den Haag
- Dr. P.C.M. Koper, radiotherapeut, Daniel den Hoed Kliniek, Rotterdam (tot juni 2005)
- Prof.dr. Th. van der Kwast, patholoog, University Toronto, Canada (tot oktober 2004)
- Dr. R.C.M. Pelger, uroloog, Leids Universitair Medisch Centrum, Leiden
- J.A. van Spil, nurse practitioner, Universitair Medisch Centrum Groningen
- Drs. Th. Twerda, contactpersoon Stichting Contactgroep Prostaatkanker Utrecht (vanaf september 2005)
- Dr. A.P. Visser, psycholoog, namens NVPO, Helen Dowling Instituut, Utrecht
- Mw. Drs. E.M. de Wit, radiotherapeut, Ziekenhuis Medisch Spectrum, Enschede
- Dr. R. de Wit, medisch oncoloog, Daniel den Hoed kliniek, Rotterdam

BEELDVORMEND ONDERZOEK

Echografie

Bij welke patiënten is het zinvol om transrectale grijswaarde echografie te verrichten voor het stellen van de diagnose prostaatcarcinoom en voor het stageren van de aandoening?

Het aspect van prostaatcarcinoom op het grijswaardebeeld van de transrectale echografie is sterk wisselend. Sinds de invoering van PSA-meting en systematische biopten is het aantal carcinomen dat in een hypo-echogene laesie alleen wordt aangetoond afgenomen. Onur et al. 2004 [23] beschrijven in een prospectieve studie ruim 3900 patiënten. Ondanks de hogere prevalentie van prostaatcarcinoom in prostaten waarin een hypo-echogene laesie werd gezien, bleek deze laesie niet frequenter maligne en werd per biopt een identiek percentage tumoren aangetoond in hypo- en iso-echogene gebieden (respectievelijk 9,3% en 10,4%). Heijmink et al. 2006 [22] vonden in een systematische review met een gemiddelde prostaatcarcinoomprevalentie van 25-33% waarbij hypo-echogene foci werden gebiopteerd, een positief voorspellende waarde tussen 18 en 53%.

Wat is de aanvullende diagnostische waarde van color Doppler, power Doppler en contrastversterkte transrectale ultrasonografie (TRUS) voor het stellen van de diagnose prostaatcarcinoom en voor het stageren van de aandoening?

Doppler beeldvorming, met of zonder contrastversterkende middelen, kan mogelijk helpen prostaatcarcinoomfoci te identificeren aangezien Doppler de doorbloeding van het weefsel zichtbaar maakt. Prostaatcarcinoom kenmerkt zich door een toegenomen aantal nieuwe bloedvaten of een toegenomen capaciteit van reeds bestaande bloedvaten (Wilson, 2004 [32]). 'Color Doppler' geeft informatie over zowel de richting als de snelheid van de doorbloeding. 'Power Doppler' registreert alleen de sterkte van het signaal dat wordt afgegeven door de perfusie, waardoor deze modus kleinere bloedvaten kan weergeven.

Cornud et al. 2000 [24] vonden met color Doppler beeldvorming een grote overlap tussen hypo-echogeniciteit en Doppleraankleuring.

Kravchick et al. 2003 [27] stelden dat hoogsensitiviteitsinstellingen een beter resultaat halen dan hoogspecifieke Dopplerinstellingen en dat Doppler een aanvulling kan zijn op de sextantbiopsie. Kravchick et al. 2004 [28] onderzochten vervolgens 120 opeenvolgende patiënten met color Doppler gerichte biopt en vergeleken dit met sextantbiopsie. Alle focale laesies op grijswaardebeeldvorming en alle gebieden met verhoogd color Dopplersignaal werden gebiopteerd. Bij 71 patiënten werd een hypervasculaire focus gevonden en bij 43 patiënten werd prostaatcarcinoom gediagnosticeerd.

Sextantbiopsieën detecteerden kanker bij 23 patiënten, color Doppler bij 30 patiënten. Van de 37 hypo-echogene laesies in 32 patiënten waren 14 biopten positief. Met color Doppler werden 13 patiënten meer gedetecteerd dan met sextantbiopsie. Er werd geen kanker gedetecteerd in hypo-echogene laesies die geen abnormale flow bij color Doppler hadden.

Remzi et al. 2004 [30] verrichtten power Doppler-geleide biopten bij 101 patiënten tijdens de eerste ronde biopten en bij 35 patiënten tijdens een herhalingsbiopt indien eerdere biopten negatief waren. De auteurs concludeerden dat power Doppler weinig additionele waarde had vergeleken met systematische biopten.

Een nieuwe ontwikkeling bij prostaatbiopten is het gebruik van echocontrastmiddel om met name kleinere tumorvaten beter zichtbaar te maken. Frauscher et al. 2002 [25] vonden in een studie bij 230 patiënten, bij wie het detectiepercentage van maximaal 5 contrastechogeleide TRUS-biopten in aankleurende gebieden werd vergeleken met 10 systematische biopten, een significant hoger percentage biopten dat prostaatcarcinoom bevatte voor contrastgeleide biopten dan voor systematische biopten (10,4% respectievelijk 5,3%).

Pelzer et al. 2005 [29] vergeleken 10 systematische biopten met een contrastversterkt color Doppler geleide biopt van maximaal twee biopten per aankleurende laesie bij 380 patiënten met een PSA >4,0 ng/mL. Hoewel het aantal patiënten gedetecteerd met prostaatcarcinoom gelijk was, was het percentage per naaldbiopt voor contrastgeleide biopten significant hoger. Minder agressieve tumoren (Gleasonscore <6) werden niet gedetecteerd door contrastgeleide biopten.

Halpern et al. 2005 [26] vergeleken diverse typen contrastversterkte geleide TRUS-biopten met serie biopten bij 301 mannen met een PSA >4 ng/mL of een verdacht rectaal toucher. Het aantal positieve biopten was significant hoger bij gebruik van contrastversterkte echografie dan bij serie biopten: 15,5% respectievelijk 10,4%. Op patiëntniveau was er echter geen significant verschil. Met name in de apex werden met contrastversterkte biopten veel tumoren gemist.

Voor lokale stagering met behulp van color Doppler beeldvorming en contrastversterkte beeldvorming zijn nog geen studies gepubliceerd. Power Doppler beeldvorming kan mogelijk hulp bieden bij het bepalen van het lokale stadium door de bloedvaten die door het kapsel naar de tumoren lopen zichtbaar te maken (Sauvain et al. 2003 [31]).

Computer tomografie (CT)

Bij welke patiënten dient een CT-scan te worden gemaakt voor het stellen van de diagnose prostaatcarcinoom en voor de stagering van de aandoening?
Diagnose. Prando en Wallace (2000 [35]) toonden bij 25 patiënten met prostaatcarcinoom aan dat van alle met TRUS-geleide biopten bevestigde foci van prostaatcarcinoom, contrastmiddelversterkte CT slechts 58% van de tumoren in de perifere zone aantoonde.

Prostaatcarcinoomfoci in de transitie zone konden niet van benigne prostaathyperplasie onderscheiden worden.

De meest recente studie over CT-gebaseerde lokale stagering dateert uit 1996. Tarcan et al. 1996 [37] voerden een pre-operatieve CT-scan zonder contrastmiddel uit bij 30 patiënten met middels TRUS-geleide biopten vastgesteld prostaatcarcinoom. Eén radioloog beoordeelde alle CT-scans. De sensitiviteit voor detectie van lokaal uitgebreid prostaatcarcinoom was laag (29%). Het grootste probleem van CT bij lokale stagering in deze studie was de onderstagering: 50% van de patiënten werd ondergestageerd.

Lymfeklierstagering. Tiguert et al.1999 [38] beschreven in een retrospectieve studie dat bij prostaatcarcinoom de grootte van een lymfeklier niet correleerde met de aanwezigheid van een metastase. De onderzoekspopulatie bestond uit 980 patiënten die een radicale prostatectomie met lymfeklierdissectie hadden ondergaan waarvan bij 63 patiënten lymfekliermetastasen waren vastgesteld. Lymfeklierdissectie was de referentie-standaard. Bij 48 patiënten was histopathologisch materiaal beschikbaar voor onderzoek. Bij geen enkele patiënt met lymfekliermetastasen werd met behulp van CT-onderzoek een vergrote (>15 mm) lymfeklier gevonden. Histopathologisch onderzoek wees uit dat driekwart (74%) van de lymfeklieren die metastasen bevatten kleiner was dan 10 mm, een kwart (26%) was zelfs kleiner dan 5 mm. Bovendien bleek 12% van de patiënten zonder lymfekliermetastasen klieren groter dan 15 mm te hebben. In slechts 13 van de 48 patiënten was de grootste lymfeklier ook daadwerkelijk de lokalisatie van de metastase.

Door de “stage shift” ten gevolge van het gebruik van de PSA-test als screeningsinstrument wordt prostaatcarcinoom steeds eerder ontdekt (Derweesh 2004 [33]). Ook lymfekliermetastasen zullen daardoor in een eerder stadium worden aangetroffen. In het algemeen bevinden zich lymfekliermetastasen van prostaatcarcinoom niet in vergrote lymfeklieren. Derhalve zijn de CT-scan en de grootte criteria die worden gehanteerd onvoldoende sensitief om deze vroege metastasering aan te tonen. Dit is ondanks het feit dat nieuwe generaties CT-scanners steeds meer gedetailleerde informatie kunnen weergeven. [34, 36]

Magnetische resonantie beeldvorming (MRI)

Bij welke patiënten moet een magnetische resonantie imaging (MRI) worden gemaakt voor het stellen van de diagnose prostaatcarcinoom en voor het stageren van de aandoening?
Diagnose. Diagnosestelling met een MRI is mogelijk door de karakteristieke laesie met lage signaalintensiteit op T2-gewogen MRI-beelden (Cruz 2002 [41]). In een retrospectieve studie van 106 opeenvolgende patiënten die radicale prostatectomie ondergingen vonden Mullerad et al. 2005 [51] dat het gebruik van endorectale MRI bij een veldsterkte van 1,5 tesla de lokalisatie van prostaatcarcinoom significant verbeterde vergeleken met rectaal

toucher en bioptresultaten. MRI was met name superieur aan de bioptresultaten in de basis van de prostaat terwijl de resultaten voor de apex gelijk waren.

Directe MRI-biopten is (nog) geen gangbare methode om biopten te nemen vanwege de matige sensitiviteit van het onderzoek en de omslachtige procedure met endorectale coil en vervolgens zonder endorectale coil (Beyersdorff 2005 [39]), dan wel met een open MRI en gluteale weg van biopteren (Zangos 2005 [57]).

Lokale stagering.

Een kosteneffectiviteits analyse door Jager et al. 2000 [50] gaf aan dat MRI bij een veldsterkte van 1,5 tesla kosteneffectief is bij patiënten met een a-priori kans van meer dan 39% op uitgroei buiten de prostaat, dat wil zeggen de intermediaire tot hoogrisicogroep. De beste strategie voor het interpreteren van een MRI-scan was 'high specificity reading': het behouden van een hoge specificiteit, desnoods ten koste van de sensitiviteit, om geen patiënten ten onrechte een curatieve behandeling te onthouden.

Cornud et al. 2002 [40] voerden voorafgaand aan radicale prostatectomie een MRI met endorectale spoel bij een veldsterkte van 1,5 tesla uit bij 336 patiënten met klinisch orgaanbeperkt prostaatcarcinoom. De MRI-scans werden geïnterpreteerd door twee radiologen in consensus aan de hand van tevoren opgestelde criteria. Op basis van de histopathologie werden tevens de resultaten bepaald van alleen de groep patiënten met uitgebreide lokale doorgroei buiten de prostaat. In de gehele patiëntengroep werden een sensitiviteit en specificiteit gevonden van respectievelijk 40% (45/113) en 95% (211/223). Voor alleen de detectie van uitgebreide lokale doorgroei waren de uitkomsten 62% (43/69) en 95% (253/267). MRI wist dus slechts twee patiënten die wel uitgroei maar geen uitgebreide uitgroei hadden juist te diagnosticeren. Een beperking van de studie is het ontbreken van de definitie van uitgebreide lokale doorgroei.

Nakashima et al. 2004 [52] onderzochten de waarde van MRI met een endorectale spoel bij een veldsterkte van 1,5 tesla voor de bepaling van het lokale stadium bij 95 patiënten met middels TRUS-biopt vastgesteld prostaatcarcinoom. Radicale prostatectomie was de referentiestandaard. Twee radiologen met 20 jaar ervaring bepaalden het stadium aan de hand van vooraf opgestelde criteria. Zij behaalden een gezamenlijke sensitiviteit en specificiteit van respectievelijk 62% en 82% en een positief en negatief voorspellende waarde van respectievelijk 60% en 83%. De detectie van zaadblaasjesinvasie had een lage sensitiviteit en positief voorspellende waarde (33% respectievelijk 67%). Kapseldoorbraak was eenvoudiger vast te stellen, met zowel een sensitiviteit als positief voorspellende waarde van 57%.

Hricak et al. 2004 [48] beschreven het gebruik van pre-operatieve endorectale MRI bij een veldsterkte van 1,5 tesla bij 135 opeenvolgende patiënten die middels TRUS-biopt vastgesteld prostaatcarcinoom hadden met speciale aandacht voor tumoruitbreiding richting de neurovasculaire bundel. Op basis van de uitkomsten van de MRI werd het beleid bepaald voor wat betreft het doorsnijden of behouden van de neurovasculaire bundels. Bovendien werd het beleid bepaald zonder kennis van de MRI-uitkomsten. Uit histologisch onderzoek van de radicale prostatectomie preparaten bleek bij 44 van de 270 neurovasculaire bundels resectie noodzakelijk. De MRI-bevindingen veranderde de chirurgische planning in 106 van de 270 gevallen (39%). De oppervlakte onder de ROC-curve voor chirurgische planning steeg significant van 0,741 zonder MRI naar 0,832 met MRI-uitkomsten.

Door Fütterer et al. 2005 [43] werd aangetoond dat het gebruik van een contrastmiddel bij endorectale MRI bij een veldsterkte van 1,5 tesla de diagnostische waarde voor bepaling van het lokale stadium kan verbeteren voor relatief onervaren radiologen. Voor een ervaren radioloog had contrasttoediening echter geen effect op de accuratesse. De sensitiviteit van de onervaren radiologen nam toe van 50% met alleen anatomische plaatjes tot 74% als daarbij de contrastmiddel opnames werden geanalyseerd. De specificiteit bleef hierbij hoog (94%).

In een retrospectieve studie van 106 opeenvolgende patiënten vonden Mullerad et al. 2005 [51] dat het gebruik van endorectale MRI bij een veldsterkte van 1,5 tesla de bepaling van de status van de zaadblaasjes significant verbeterde. De oppervlakte onder de ROC-curve nam toe van 0,64 met rectaal toucher tot 0,90 met MRI.

Fütterer et al. 2006 [44] beschreven de eerste resultaten van MRI met een endorectale spoel bij een veldsterkte van 3 tesla in een groep van 32 opeenvolgende patiënten met klinisch orgaanbeperkt prostaatcarcinoom waarbij een radicale prostatectomie werd verricht. Ervaren radiologen behaalden een sensitiviteit van 88% en een specificiteit van 96%. Ervaring bleek een belangrijke rol te spelen voor het verkrijgen van een hoge sensitiviteit voor het detecteren van lokaal uitgebreide tumor. Zelfs minimale kapselpenetratie (<2 mm radiale afstand) kon met deze techniek gedetecteerd worden.

In een grote studie met 612 geïncludeerde patiënten en middels TRUS-biopt vastgesteld prostaatcarcinoom toonden Wang et al. 2006 [55] de significante meerwaarde aan van MRI met een endorectale spoel bij een veldsterkte van 1,5 tesla voor het bepalen van het lokale stadium vergeleken met het gebruik van nomogrammen die het PSA-niveau, de Gleasonscore en het rectaal toucher hanteren. Radicale prostatectomie was de referentiestandaard. MRI had een toegevoegde waarde voor de laag risico, intermediair risico en hoog risico patiënten. Heijmink et al. 2006 [47] vergeleken de stagering met en zonder endorectale spoel bij een veldsterkte van 3 tesla en concludeerden dat alleen met endorectale spoel accuraat

kon worden gestageerd. Ervaren radiologen konden kapselpenetratie van 0.5 mm alleen met endorectale spoel detecteren. Dit kan van nut zijn bij het verkrijgen van negatieve resectiemarges bij radicale prostatectomie.

Sala et al. 2006 [53] beschreven in een groep van 354 patiënten met middels TRUS-biopt vastgesteld prostaatcarcinoom de diagnostische waarde van MRI met een endorectale spoel voor het bepalen van zaadblaasjesinvasie. Radicale prostatectomie was de referentiestandaard. Oppervlakten onder de ROC-curve waren 0,81 en 0,93 voor twee radiologen. Het meest voorspellend voor zaadblaasjesinvasie waren tumor in de basis van de prostaat met kapseldoorbraak en een gebied met lage signaalintensiteit in een zaadblaasje dat de normale architectuur verloren heeft. Endorectale MRI heeft derhalve een grote accuratesse in het bepalen van zaadblaasjesinvasie. Dit kan van belang zijn bij het selecteren van patiënten voor een radicale prostatectomie.

Lymfeklierstagering

Bij een conventionele MRI wordt, gelijk aan de CT-scan, gebruik gemaakt van vorm- en groottecriteria (Jager 1996 [49]). Een kosteneffectiviteitsstudie van Wolf et al. 1995 [56] bij 174 patiënten toonde aan dat conventionele MRI kosteneffectief is bij patiënten die meer dan 45% a-priori kans hebben op lymfekliermetastasen bij een sensitiviteit van 25%.

De meest recente studie met conventionele MRI op 1,5 tesla werd uitgevoerd door Harisinghani et al. 2003 [45] bij 80 patiënten uit twee klinieken. De criteria voor een positieve lymfeklier waren een diameter van de korte as van >10 mm als de klier langgerekt was of >8 mm in geval van een ronde klier. De resultaten werden op zowel patiënt- als lymfeklierniveau bepaald. Als referentiestandaard werd lymfeklierdissectie of CT-geleid biopt gebruikt. Op patiëntniveau werd een sensitiviteit van 45,4% met een specificiteit van 78,8% behaald. Op lymfeklierniveau waren deze respectievelijk 35,4% en 90,4%. Naarmate de lymfeklieren kleiner waren daalde de sensitiviteit. Bij lymfeklieren tussen 5 en 10 mm was deze 28,5%, terwijl bij klieren kleiner dan 5 mm de sensitiviteit 0% was.

Een nieuwe methode voor lymfeklierdiagnostiek is het gebruik van een lymfeklierspecifiek contrastmiddel, de ultrasmall superparamagnetic iron-oxide containing particles (USPIO's), waaronder ferumoxtran-10. In dezelfde studie van Harisinghani et al. werd een directe vergelijking gemaakt tussen conventionele MRI en een MRI met ferumoxtran-10 bij een veldsterkte van 1,5 tesla. Zowel op patiënt- als op lymfeklierniveau verbeterde de sensitiviteit significant: van 45,4% naar 100% op patiëntniveau en van 35,4% naar 90,5% op lymfeklierniveau. Bij lymfeklieren met een diameter tussen 5-10 mm verbeterde de sensitiviteit significant van 28,5% met de conventionele techniek naar 96,4% met ferumoxtran-10. Bij lymfeklieren kleiner dan 5 mm verbeterde de sensitiviteit van 0% naar 41,4%, hoewel dit geen significante verbetering was. Met deze methode kunnen lymfeklieren

tot een grootte van 5 mm met grote nauwkeurigheid gediagnosticeerd worden. Gebruik van deze techniek bij een veldsterkte van 3 tesla kan de beeldvorming nog verder verbeteren (Heesakkers, 2006 [46]). Een huidige beperking voor het gebruik van ferumoxtran-10 is dat het op dit moment nog niet geregistreerd is. Thans is het middel beperkt beschikbaar in enkele centra. [40, 42, 54]

Skeletscan

Bij welke patiënten is het zinvol om een skeletscan te verrichten voor het stellen van de diagnose prostaatcarcinoom en voor het stageren van de aandoening?
Het skelet is de belangrijkste lokalisatie van afstandsmetastasen bij patiënten met prostaatcarcinoom. Botmetastasen bij prostaatcarcinoom hebben meestal een osteoblastisch karakter. Skeletscintigrafie uitgevoerd met 99m Technetium gelabeld difosfonaat is een sensitieve techniek om osteoblastische metastasen af te beelden. Deze techniek wordt sinds decennia als standaard toegepast bij het stageren van patiënten met prostaatcarcinoom.

De incidentie van botmetastasen varieert sterk, van minder dan 1% bij screeningspopulaties, tussen 5-15% bij klinisch gedetecteerde populaties tot meer dan 85% bij patiënten met hormoon refractair prostaatcarcinoom.

In een systematische review beschijven Abuzallouf et al. 2004 [58] de gepoolde resultaten van 23 klinische studies naar de voorspellende waarde van skeletscintigrafie bij patiënten met de primaire diagnose prostaatcarcinoom. In totaal betreft dit een populatie van 8644 patiënten waarvan bij 1453 patiënten botmetastasen werden aangetoond.

Verdeeld naar PSA werd bij respectievelijk 2,3%, 5,3% en 16,2% van de patiënten met PSA van <10, 10,1 tot 19,9 en 20 tot 49,9 ng/mL botmetastasen aangetoond. Verdeeld naar klinisch tumorstadium werden bij 6,4% van de mannen met gelokaliseerd prostaatcarcinoom en bij 49,5% met lokaal gevorderd prostaatcarcinoom botmetastasen aangetoond. Verdeeld naar Gleasonscore werd bij respectievelijk 5,6% en 29,9% van de patiënten met Gleasonscore kleiner of gelijk aan 7 en 8-10 botmetastasen aangetoond.

CONCLUSIES

Echografie

Prostaatcarcinoom heeft geen typische kenmerken bij grijswaarde echografie.
Niveau 1: A2 Onur 2004 [23]; Heijmink 2006 [22]

De positief voorspellende waarde van biopten uit hypo-echogene laesies is laag.
Niveau 1: A2 Onur 2004 [23]; Heijmink 2006 [22]

Grijswaarde echografie heeft geen toegevoegde waarde voor het detecteren van niet-palpabele tumoren.
Niveau 1: A2 Onur 2004 [23]; Heijmink 2006 [22]

Het gebruik van niet-contrastversterkte Doppler beeldvorming geeft slechts een geringe verbetering van de detectie en het positief bioptpercentage.
Niveau 3: A2 Kravchick 2003 [28]; C : Remzi 2004 [30]

Het gebruik van contrastversterkte echografie leidt tot een significant hoger percentage positieve biopten vergeleken met systematische biopten en detecteert relatief meer agressieve prostaatcarcinoomfoci.
Niveau 3: A2 Frauscher 2002 [25], Halpern 2005 [26], Pelzer 2005 [29]

Er is onvoldoende onderzoek gedaan naar de toegevoegde waarde van Doppler beeldvorming bij de lokale stagering van prostaatcarcinoom om hieruit conclusies te trekken.
Niveau 4

Computertomografie

Het weke delen contrast bij een CT-scan, zelfs met gebruik van contrastmiddel, is te laag voor goede differentiatie tussen carcinoomweefsel en gezond weefsel in de prostaat.
Niveau 3: C Prando 2000 [35]

Voor lokale stagering van prostaatcarcinoom zijn de sensitiviteit (29-50%) en de negatief voorspellende waarde (35-77%) van een CT-scan te laag voor standaard klinisch gebruik.
Niveau 3: C Tarcan 1996 [37]

Een CT-scan heeft onvoldoende diagnostische waarde voor detectie van lymfekliermetastasen.
Niveau 3: C Tiguert 1999 [38]

Magnetische resonantie beeldvorming (MRI)

De lokalisatie van prostaatcarcinoom verbetert significant door gebruik van MRI met endorectale spoel bij een veldsterkte van 1,5 tesla vergeleken met rectaal toucher of biopten.
Niveau 3: Mullerad 2005 [51]

De nauwkeurigheid van de chirurgische planning voor het al dan niet reseceren van de neurovasculaire bundel verbetert significant door het pre-operatief gebruik van endorectale MRI bij een veldsterkte van 1,5 tesla.
Niveau 3: C Hricak 2004 [48]

Vanaf een a-priori kans op lokale doorgroei van 39% is stagering met behulp van MRI bij een veldsterkte van 1,5 tesla kosteneffectief.
Niveau 3: C: Jager 2000 [50]

Voor lokale stagering bij een veldsterkte van 1,5 tesla wordt een goede specificiteit bereikt, met beperkte sensitiviteit. Voor onervaren radiologen kan de sensitiviteit verhoogd worden door het gebruik van contrastmiddelopnames. Bij een veldsterkte van 3 tesla verbetert de sensitiviteit bij een gelijkblijvende specificiteit.
Niveau 3: C Fütterer 2006 [44], Heijmink 2006 [47]

De MRI-interpretatie van lymfeklieren op basis van grootte-criteria heeft onvoldoende diagnostische waarde voor detectie van lymfekliermetastasen van prostaatcarcinoom. De sensitiviteit van conventionele MRI voor detectie van positieve lymfeklieren is te laag (27-60%) voor standaard klinisch gebruik in de laag- en intermediaire risicogroepen.
Niveau 2: A2 Harisinghani 2003 [45]

Gebruik van het lymfeklierspecifieke contrastmiddel ferumoxtran-10 voor detectie van lymfeklieren groter dan 8-10 mm verbetert de sensitiviteit significant (van 30 naar 90%) ten opzichte van conventionele MRI.
Niveau 2: A2 Harisinghani 2003 [45]

Skeletscan
Patiënten met een initieel PSA van 20 ng/mL of hoger, lokaal gevorderde tumoren of Gleasonscore 8 en hoger hebben een sterk verhoogde kans op botmetastasen.
Niveau 2: A2 Abuzallouf 2004 [58]

OVERWEGINGEN

Echografie

Aangezien de meeste patiënten zich tegenwoordig presenteren zonder dat er afwijkingen gevoeld worden bij het rectaal toucher, zullen de biopten transrectaal, echogeleid dienen te worden genomen, aangezien op deze wijze de perifere zone het best kan worden geïdentificeerd. Indien er een uitgebreide tumorgroei aanwezig is, kan ook een biopt genomen worden zonder de echografie. Echografie is echter in iedere urologische praktijk aanwezig en er is dan ook geen reden om ook in dit geval geen echogeleide biopten te nemen. Voor het nemen van biopten dienen antibiotica gegeven te worden, welke een goede weefselpenetratie hebben in de prostaat. De patiënt dient geïnformeerd te worden over de mogelijke complicaties van het nemen van prostaatbiopten, zoals bloeding via de anus, hematurie, hemospermie en koorts.

Doppler en contrastversterkte echografie zijn niet algemeen beschikbaar in Nederland.

Computertomografie

Mogelijk is er een toekomstige rol weggelegd voor CT-scan bij gecombineerde PET-CT-scans (Farsad 2005 [34], Schmid 2005 [36]). In de algemene (screenings)populatie zal deze techniek echter te arbeids- en kostenintensief zijn.

Een beperking van de toepassing van CT-scan is de inherente stralingsbelasting voor de patiënt door het gebruik van ioniserende straling. Voor lokale stagering van prostaatcarcinoom zijn TRUS en MRI beschikbaar die geen gebruik maken van ioniserende straling. Voor lymfeklierstagering geldt dat MRI met of zonder specifiek lymfekliercontrastmiddel een alternatief is. Derhalve gaat de voorkeur uit naar deze modaliteit.

De CT-scan kan wel worden gebruikt voor het biopteren van een voor metastase verdachte lymfeklier. Lymfeklieren tot een diameter van 5 mm kunnen in handen van een ervaren radioloog nauwkeurig worden gebiopteerd.

Magnetische resonantie beeldvorming (MRI)

Een functionele MRI-techniek, MR spectroscopie (Kurhanewicz 2002, Coakley 2003) geeft additionele informatie over het metabolisme in de prostaat en heeft toegevoegde waarde bij de diagnosestelling (Van Dorsten 2004, Jung 2004) en lokale stagering (Yu 1999) van prostaatcarcinoom. Deze techniek kan worden toegevoegd aan het reguliere MRI-onderzoek. Echter, gezien het feit dat hiervoor speciale softwarepakketten nodig zijn en de techniek in slechts enkele centra in Nederland op een kwalitatief voldoende hoogstaand niveau kan worden uitgevoerd, is er op dit moment onvoldoende reden om aan te bevelen deze techniek op grote schaal toe te passen.

MRI kan worden toegepast bij de planning van radiotherapie. Door het gebruik van goudmarkers kunnen de CT-scan en MRI gefuseerd worden en kan hierop de radiotherapie worden gepland (Dehnad 2003 [42]). Hierdoor kunnen functionele MRI-technieken het bestralingsprotocol beïnvloeden (Van Lin 2006 [54]). Derhalve kan MRI een belangrijke factor zijn voor het toepassen van intensitiy-modulated radiation therapy (IMRT).

Skeletscan

Naast de skeletscintigrafie worden nieuwe beeldvormende technieken als whole-body MRI en positron emissie tomografie (PET-scan) bij de beoordeling van botmetastasen beschreven. Er ontbreken echter studies met voldoende aantallen patiënten in de literatuur om de plaats van deze technieken te bepalen.

REFERENTIES

[22] Heijmink SW, van Moerkerk H, Kiemeney LA, et al. A comparison of the diagnostic performance of systematic versus ultrasound-guided biopsies of prostate cancer. Eur Radiol 2006;16:927-38.

[23] Onur R, Littrup PJ, Pontes JE, Bianco FJ, Jr. Contemporary impact of transrectal ultrasound lesions for prostate cancer detection. J Urol 2004;172:512-4.

[24] Cornud F, Hamida K, Flam T, et al. Endorectal color doppler sonography and endorectal MR imaging features of nonpalpable prostate cancer: correlation with radical prostatectomy findings. Am J Roentgenol 2000;175:1161-8.

[25] Frauscher F, Klauser A, Volgger H, et al. Comparison of contrast enhanced color Doppler targeted biopsy with conventional systematic biopsy: impact on prostate cancer detection. J Urol 2002;167:1648-52.

[26] Halpern EJ, Ramey JR, Strup SE, et al. Detection of prostate carcinoma with contrast-enhanced sonography using intermittent harmonic imaging. Cancer 2005;104:2373-83.

[27] Kravchick S, Cytron S, Peled R, et al. Using gray-scale and two different techniques of color Doppler sonography to detect prostate cancer. Urology 2003;61:977-81.

[28] Kravchick S, Cytron S, Peled R, et al. Optimal combinations for detection of prostate cancer: systematic sextant and laterally directed biopsies versus systematic sextant and color Doppler-targeted biopsies. Urology 2004;63:301-5.

[29] Pelzer A, Bektic J, Berger AP, et al. Prostate cancer detection in men with prostate specific antigen 4 to 10 ng/ml using a combined approach of contrast enhanced color Doppler targeted and systematic biopsy. J Urol 2005;173:1926-9.

[30] Remzi M, Dobrovits M, Reissigl A, et al. Can Power Doppler enhanced transrectal ultrasound guided biopsy improve prostate cancer detection on first and repeat prostate biopsy? Eur Urol 2004;46:451-6.

[31] Sauvain JL, Palascak P, Bourscheid D, et al. Value of power doppler and 3D vascular sonography as a method for diagnosis and staging of prostate cancer. Eur Urol 2003;44:21-30.

[32] Wilson NM, Masoud AM, Barsoum HB, et al. Correlation of power Doppler with microvessel density in assessing prostate needle biopsy. Clin Radiol 2004;59:946-50.

[33] Derweesh IH, Kupelian PA, Zippe C, et al. Continuing trends in pathological stage migration in radical prostatectomy specimens. Urol Oncol 2004;22:300-6.

[34] Farsad M, Schiavina R, Castellucci P, et al. Detection and localization of prostate cancer: correlation of (11)C-choline PET/CT with histopathologic step-section analysis. J Nucl Med 2005;46:1642-9.

[35] Prando A, Wallace S. Helical CT of prostate cancer: early clinical experience. AJR Am J Roentgenol 2000;175:343-6.

[36] Schmid DT, John H, Zweifel R, et al. Fluorocholine PET/CT in patients with prostate cancer: initial experience. Radiology 2005;235:623-8.

[37] Tarcan T, Turkeri L, Biren T, et al. The effectiveness of imaging modalities in clinical staging of localized prostatic carcinoma. Int Urol Nephrol 1996;28:773-9.

[38] Tiguert R, Gheiler EL, Tefilli MV, et al. Lymph node size does not correlate with the presence of prostate cancer metastasis. Urology 1999;53:367-71.

[39] Beyersdorff D, Winkel A, Hamm B, et al. MR imaging-guided prostate biopsy with a closed MR unit at 1.5 T: initial results. Radiology 2005;234:576-81.

[40] Cornud F, Flam T, Chauveinc L, et al. Extraprostatic spread of clinically localized prostate cancer: factors predictive of pT3 tumor and of positive endorectal MR imaging examination results. Radiology 2002;224:203-10.

[41] Cruz M, Tsuda K, Narumi Y, et al. Characterization of low-intensity lesions in the peripheral zone of prostate on pre-biopsy endorectal coil MR imaging. Eur Radiol 2002;12:357-65.

[42] Dehnad H, Nederveen AJ, van der Heide UA, et al. Clinical feasibility study for the use of implanted gold seeds in the prostate as reliable positioning markers during megavoltage irradiation. Radiother Oncol 2003;67-295-302.

[43] Fütterer JJ, Engelbrecht MR, Huisman HJ, et al. Staging Prostate Cancer with Dynamic Contrast-enhanced Endorectal MR Imaging prior to Radical Prostatectomy: Experienced versus Less Experienced Readers. Radiology 2005;237:541-9.

[44] Fütterer JJ, Heijmink SW, Scheenen TW, et al. Prostate cancer: local staging at 3-T endorectal MR imaging--early experience. Radiology 2006;238:184-91.

[45] Harisinghani MG, Barentsz J, Hahn PF, et al. Noninvasive detection of clinically occult lymph-node metastases in prostate cancer. N Engl J Med 2003;348:2491-9.

[46] Heesakkers RA, Futterer JJ, Hovels AM, et al. Prostate cancer evaluated with ferumoxtran-10-enhanced T2*-weighted MR Imaging at 1.5 and 3.0 T: early experience. Radiology 2006;239:481-7.

[47] Heijmink SWTPJ, Fütterer JJ, Hambrock T, et al. Body array versus endorectal coil MR imaging of prostate cancer at 3 tesla: comparison of image quality, localization, and staging performance with whole-mount section histopathology. Radiology 2007;244(1):184-95.

[48] Hricak H, Wang L, Wei DC, et al. The role of preoperative endorectal magnetic resonance imaging in the decision regarding whether to preserve or resect neurovascular bundles during radical retropubic prostatectomy. Cancer 2004;100:2655-63.

[49] Jager GJ, Barentsz JO, Oosterhof GO, et al. Pelvic adenopathy in prostatic and urinary bladder carcinoma: MR imaging with a three-dimensional TI-weighted magnetization-prepared-rapid gradient-echo sequence. AJR Am J Roentgenol 1996;167:1503-7.

[50] Jager GJ, Severens JL, Thornbury JR, et al. Prostate cancer staging: should MR imaging be used? A decision analytic approach. Radiology 2000;215:445-51.

[51] Mullerad M, Hricak H, Kuroiwa K, et al. Comparison of endorectal magnetic resonance imaging, guided prostate biopsy and digital rectal examination in the preoperative anatomical localization of prostate cancer. J Urol 2005;174:2158-63.

[52] Nakashima J, Tanimoto A, Imai Y, et al. Endorectal MRI for prediction of tumor site, tumor size, and local extension of prostate cancer. Urology 2004;64:101-5.

[53] Sala E, Akin O, Moskowitz CS, et al. Endorectal MR Imaging in the evaluation of seminal vesicle invasion: diagnostic accuracy and multivariate feature analysis. Radiology. 2006;238:929-37.

[54] Van Lin EN, Futterer JJ, Heijmink SW, et al. IMRT boost dose planning on dominant intraprostatic lesions: gold marker-based three-dimensional fusion of CT with dynamic contrast-enhanced and 1H-spectroscopic MRI. Int J Radiat Oncol Biol Phys 2006;65:291-303

[55] Wang L, Hricak H, Kattan MW, et al. Prediction of Organ-confined Prostate Cancer: Incremental Value of MR Imaging and MR Spectroscopic Imaging to Staging Nomograms. Radiology 2006;238:597-603.

[56] Wolf JS, Jr., Cher M, Dall\'era M, et al. The use and accuracy of cross-sectional imaging and fine needle aspiration cytology for detection of pelvic lymph node metastases before radical prostatectomy. J Urol 1995;153:993-9.

[57] Zangos S, Eichler K, Engelmann K, et al. MR-guided transgluteal biopts with an open low-field system in patients with clinically suspected prostate cancer: technique and preliminary results. Eur Radiol 2005;15:174-82.

[58] Abuzallouf S, Dayes I, Lukkra H. Baseline staging of newly diagnosed prostate cancer: a summary of the literature. J Urol 2004;171:2122-7.

Richtlijn Prostaatcarcinoom: diagnostiek en behandeling © 2007

Vereniging van Integrale Kankercentra
Postbus 19001
3501 DA Utrecht
Tel. (030) 234 37 80
Fax. (030) 234 36 32
E-mail: vikc@vikc.nl
www.ikcnet.nl

Kwaliteitsinstituut voor de Gezondheidszorg CBO
Postbus 20064
3502 LB Utrecht
Tel: (030) 284 39 00
Fax: (030) 294 36 44
E-mail: mwr@cbo.nl
www.cbo.nl

CHAPTER 11

Summary and Conclusions

In **Chapter 2**, a systematic review of the recent literature of the various imaging modalities available for detecting and localizing prostate cancer was performed. In order to optimize patient prostate cancer care, imaging can play an important role in prostate cancer diagnosis. Transrectal ultrasound (TRUS), particularly with the usage of intravenous contrast agents, provides an excellent way of directing the biopsy needle towards a suspicious area within the prostate in the general (screening) population. CT scanning should not play a role in local prostate cancer diagnosis. MRI using functional imaging techniques such as diffusion weighted MR imaging (DWI), spectroscopic imaging (^{1}H-MRSI), and dynamic contrast-enhanced imaging is a powerful tool with high sensitivity and specificity for detection and localization of prostate cancer due to its high soft-tissue contrast resolution, particularly in patients with prior negative TRUS-guided biopsies. Water molecule diffusion restriction as shown by DWI may guide biopsy procedures and differentiate between low-grade and high-grade prostate cancer. A promising new development is the performance of biopsy within the MR scanner. PET scanning using FDG has a relatively low accuracy in localizing prostate cancer while usage of 11C-choline may increase this accuracy. Subsequently, a proposal for optimal use of radiologic imaging was presented. Comparison of this scheme with the European and American urological guidelines on prostate cancer revealed that MR imaging is not mentioned regarding prostate cancer localization.

In **Chapter 3**, a systematic review of the recent literature of the imaging modalities available for staging prostate cancer was performed. Bone scintigraphy remained the most sensitive method for detecting bone metastases. However, MR imaging is a promising technique for the evaluation of the axial skeleton, with the advantage of possibly detecting metastatic disease in other organs. In lymph node staging on CT or MRI, the standard of reference is still the size and shape criteria, although lymph node specific contrast agents in a preclinical setting have provided higher accuracies. Even though TRUS is a widely available tool used for the assessment of the local disease stage, MR imaging with an endorectal coil was shown to have superior accuracy in staging prostate cancer. CT scanning should not be used for local staging.

In **Chapter 4**, a prospective study included a total of 32 men with biopsy-proved prostate cancer who underwent endorectal coil (ERC) T2-weighted high-spatial-resolution MR imaging at 3T and subsequent radical prostatectomy. All images were evaluated by three radiologists (two experienced and a third less experienced radiologist) with regard to local disease extent, i.e. extracapsular extension and seminal vesicle invasion. Criteria indicative for locally advanced cancer stage were: neurovascular bundle asymmetry, obliteration of the rectoprostatic angle, irregular bulging of the prostatic contour, tumor signal intensity within the periprostatic fat, overt extracapsular tumor, and abnormal asymmetric low signal intensity within the seminal vesicles. Whole-mount-section histopathologic analysis was the standard of reference. Accuracy, sensitivity, and specificity of local staging were

94%, 88%, and 96%, respectively, for both experienced radiologists, and 81%, 50%, and 92%, respectively, for the less experienced radiologist. There was substantial agreement between both experienced readers (0.42–0.79) and moderate agreement between the less experienced reader and the experienced readers with respect to all extracapsular criteria. In regard to the three cases of minimal capsular invasion, two were detected by both experienced radiologists. Thereby, this study showed that 3T MR imaging using an endorectal coil to accurately stage prostate cancer was feasible.

Chapter 5 contained a prospective study of another cohort of 46 men with biopsy-proved prostate cancer that underwent 3T T2-weighted MR imaging with both a body-array coil (BAC) (voxel size: 0.43 x 0.43 x 4.0 mm) and an ERC (voxel size: 0.26 x 0.26 x 2.5 mm) prior to radical prostatectomy. Four radiologists with different levels of experience independently evaluated all data sets separately. Ten image quality characteristics related to prostate cancer localization and staging (discrimination between peripheral zone and central gland, visibility of the peripheral zone and central gland itself, visibility of the perceived lesion, and visualization of the internal architecture of the central gland, delineation of the prostatic capsule, visualization of the neurovascular bundle, visualization of the rectoprostatic angle, and overall image quality) were assigned scores on a five-point scale. Furthermore, prostate cancer presence was recorded with a five-point probability scale in each of 14 segments covering the entire prostate. Lastly, local disease stage was classified as organ- confined or locally advanced on a five-point probability scale. Whole-mount-section histopathologic examination was the reference standard. Significantly more motion artifacts were present with ERC imaging. All other image quality characteristics improved significantly with ERC imaging. With ERC imaging, the AUC for localization of prostate cancer was significantly increased from 0.62 to 0.68. ERC imaging also significantly increased the AUCs for staging as well as sensitivity for detection of locally advanced disease by experienced readers from 7% to 73-80%, whereas a high specificity of 97-100% was maintained. Extracapsular extension as small as 0.5 mm at histopathologic examination could be accurately detected only with ERC imaging. Thus, this study showed that ERC imaging outperformed BAC imaging in image quality, prostate cancer localization as well as staging, suggesting that an ERC should be used.

Chapter 6 encompassed a study of 44 consecutive men with biopsy-proven prostate cancer who underwent T2-weighted MR imaging examinations in three orthogonal directions at 3T, first with a BAC and second with an inflated ERC. Prospectively, two experienced readers independently evaluated all data sets in random order. The maximal anteroposterior, right-to-left, and craniocaudal prostate diameters with BAC and ERC imaging were determined. Likewise, by drawing a contour around the whole prostate and the peripheral zone on each image slice, the total prostate, peripheral zone and central gland volumes were measured before and after ERC introduction. Due to the ERC, the prostate shape changed

significantly in all three directions, with mean changes in the anteroposterior, right-to-left, and craniocaudal diameters of 15.7% (5.5 mm), 7.7% (3.5 mm), and 6.3% (2.2 mm), respectively. The mean total prostate, peripheral zone, and central gland volume decreased significantly after ERC introduction by 17.9% (8.3 cm^3), 21.6% (4.8 cm^3), and 14.2% (3.4 cm^3), respectively. The mean anteroposterior diameter was thus reduced by nearly one-sixth of its original diameter, and the mean total prostate volume was decreased by approximately 18%. This study revealed that the ERC introduced significant prostate changes that should be considered when using ERC-based MRI for MRI-computed tomography fusion and endorectal balloon radiotherapy planning.

In **Chapter 7**, a novel ^{1}H-MRSI technique at 3T using only external coils was described and applied in both the prostate and an enlarged lymph node. A 77-year-old man, who initially underwent prostate radiation therapy for stage T3bN0M0 prostate cancer, underwent repeated MR imaging more than two years after the procedure due to rising PSA levels. Three-dimensional ^{1}H-MRSI using a combination of external surface coils (TR/TE: 750/145 ms; acquisition bandwidth: 1250 Hz; 512 spectral data points; FOV: 84 x 70 x 70; matrix size: 12 x 10 x 10; number of weighted averages: 6; 7 saturation slabs; voxel size: 7 x 7 x 7 mm^3) revealed high choline levels throughout the prostate indicative of recurrent disease. Furthermore, one single enlarged pelvic lymph node was observed. A single voxel echo time averaged point resolved spectroscopy sequence positioning the voxel within the node was performed (TR 1500 ms, TE 136 to 272, 256 averages, voxel size: 15 x 17 x 13 mm^3) showing a choline peak in the spectrum. To validate the location of the choline within the lymph node, a 3-dimensional ^{1}H-MRS imaging measurement (TR/TE: 1500/100 ms; FOV: 100 x 100 x 100 mm^3; matrix size: 10 x 10 x 10) with dual frequency selective water and lipid suppression was performed with the volume-of-interest covering the enlarged lymph node and adjacent lipid tissue showing choline only inside the lymph node. Histopathology obtained from both the prostate and the lymph node revealed prostate cancer presence. Thus, this study described the first performance of ^{1}H-MRSI at 3T using only external surface coils, both in the prostate as well as an enlarged lymph node.

Chapter 8 presented the feasibility and accuracy of localizing prostate cancer with 3T 3D-^{1}H-MRSI using only external radiofrequency surface coils in a cohort of 45 men with biopsy-proved prostate cancer that subsequently underwent radical prostatectomy. A 3D water- and lipid-suppressed point-resolved spectroscopy pulse sequence was performed of the entire prostate (TR/TE: 750/145 ms; acquisition bandwith: 1250 Hz; 512 spectral data points; voxel size: 7 x 7 x 7 mm^3). On the basis of the prostatectomy specimens and blinded to the spectra, per patient 1-4 voxels were matched and classified into healthy peripheral zone, central gland, periurethral zone, and cancer tissue. Cancer voxels were classified according to cancer size and the certainty of matching histopathologic findings with MR images. After visual inspection of automated fitting of classified voxels, the choline plus

creatine-to-citrate (Cho+ Cr/Cit) ratio was calculated for all tissues. A median of 82% of the classified voxels per patient was used in the analysis. Mean Cho+Cr/Cit ratios for healthy tissues were 0.22 for peripheral zone, 0.34 for central gland, and 0.36 for the periurethral area; all were significantly different from that of cancer (1.3). The AUC for discrimination of probable and definite cancer tissue from healthy tissue for the peripheral zone (0.84) was significantly higher than that for the central gland (0.69). Thereby, this study demonstrated that 3T 3D-^{1}H-MRSI using only external coils is feasible and achieves high accuracies in differentiating cancer from healthy prostatic tissue.

Chapter 9 described a prospective study in which 18 men with biopsy-proved prostate cancer underwent 3T 3D ^{1}H-MRSI of the prostate both without and with an ERC prior to radical prostatectomy. The voxel resolution with a BAC and an ERC were 7 x 7 x 7 mm and 6 x 6 x 6 mm, respectively (for both the scanning parameters were TR/TE: 750/145 ms; acquisition bandwidth: 1250 Hz; total acquisition time: 9 minutes). Semi-automatic voxel postprocessing resulted in a Cho+Cr/Cit ratio for each voxel. Each prostate was divided into 14 regions of interest (ROIs). Four readers with varying levels of experience individually scored all imaging sets separately and determined the presence of cancer based on predefined ratio cut-offs using a five-point scale for each segment. Whole mount section histopathology was the standard of reference. Significantly more ROIs were non-ratable with ^{1}H-MRSI without an ERC compared with ^{1}H-MRSI with an ERC. For the more experienced readers ^{1}H-MRSI with an ERC had a high specificity (82-92%), but a low sensitivity (20-57%). For the novice reader, ERC ^{1}H-MRSI had a high sensitivity (80%) and a low specificity (34%). For all readers, the negative predictive values were high (82-89%), whereas the positive predictive values were low (20-45%) for both imaging with and without an ERC. Prostate cancer localization with the use of an ERC had a significantly higher AUC (0.68) than without the use of an ERC (0.63). Thus, it was shown that usage of the ERC with 3T ^{1}H-MRSI resulted in a significantly higher accuracy of localizing prostate cancer.

Chapter 10 reflected a selection of the chapter of the 2007 Dutch comprehensive cancer centers (CBO) guideline regarding the use of imaging in prostate cancer diagnosis. The localization of prostate cancer with MR imaging was deemed significantly superior compared with digital rectal examination and biopsy. It was advised to perform an MR imaging scan using an endorectal coil in high-risk patients with negative TRUS biopsies prior to subsequent further biopsies. 3T ERC improves sensitivity of local staging compared with 1.5T. The suboptimal availability of ERC MR imaging in the Netherlands was still a concern. For the identification of the exact location of the cancer within the prostate gland for radiation therapy purposes, MR imaging was deemed the modality of choice.

CONCLUSIONS

The role of MR imaging in the initial diagnosis and local staging of prostate cancer is increasing. By using MR imaging techniques, one is able to provide more personalized medicine and, subsequently, to present each prostate cancer patient with his own optimal treatment plan.

An overview of the current MR imaging techniques and literature available was given. Thereafter, the possibilities of prostate MR imaging at 3T using an endorectal coil were examined. An early study demonstrated the feasibility of determining the local disease stage with an endorectal coil using predefined criteria for extraprostatic extension, obtaining both a high sensitivity and specificity for determining the exact local disease stage. A direct comparison between imaging without and with an endorectal coil at 3T showed a significantly higher accuracy with endorectal coil imaging in exactly localizing prostate cancer within the prostate as well as in assessing the local disease stage. Minimal capsular penetration could be detected only using an endorectal coil.

By obtaining imaging with and without an endorectal coil at 3T, it was shown that the introduction of a coil significantly changed the prostate shape, particularly the anteroposterior diameter, as well as the determined prostate volume. This raised important concerns for radiation therapy planning based on MR imaging scans using an endorectal coil.

Using histopathologic confirmation, it was demonstrated that the ^{1}H-MRSI technique at 3T was feasible when solely using external coils. This was first demonstrated in a case report in which spectroscopic imaging was performed to detect prostate cancer in both recurrent disease in the prostate and metastatic disease in a pelvic lymph node. Secondly, in a large preprostatectomy patient cohort it was shown that the technique had a high accuracy of differentiating cancer from healthy prostatic tissue. Lastly, in a preprostatectomy patient cohort, it was demonstrated that ^{1}H-MRSI with an ERC significantly increased the localization accuracy compared with using only external coils.

The abovementioned more central role of MR imaging was reflected in a number of recommendations in the 2007 Dutch comprehensive cancer centres (CBO) prostate cancer guideline.

Thus, using an endorectal coil at 3T was feasible and significantly increased prostate cancer localization and local staging sensitivity. The changes in prostate shape by introduction of the coil are an important concern for exact radiation therapy planning. While proton spectroscopic imaging at 3T using solely external coil is feasible, usage of the endorectal coil significantly increased the localization accuracy.

SAMENVATTING EN CONCLUSIES

In **Hoofdstuk 2** werd een systematische review van de recente literatuur omtrent de beeldvormingsmodaliteiten voor het detecteren en lokaliseren van prostaatkanker uitgevoerd. Om de zorg rond prostaatkanker voor wat betreft de diagnose te optimaliseren kan beeldvorming een belangrijke rol spelen. In de algemene (screenings)populatie kan transrectale echografie (TRUS), in het bijzonder met intraveneus contrastmiddel, uitstekend de biopsienaald richting een verdacht gebied in de prostaat leiden. CT-scans behoren geen rol meer te spelen bij prostaatkankerdetectie of -lokalisatie. Door zijn hoge wekedelencontrast heeft MRI met functionele technieken zoals diffusiegewogen imaging (DWI), proton spectroscopie (^{1}H-MRSI) en dynamische contrastaankleuring analyse (DCE) een hoge sensitiviteit en specificiteit voor de detectie en lokalisatie van prostaatkanker. Dit is nog uitgesprokener bij patiënten met eerdere negatieve TRUS-geleide biopten. Watermolecule diffusie restrictie aangetoond middels DWI kan biopten geleiden en differentiëren tussen laag- en hooggradige prostaatkanker. Een veelbelovende recente ontwikkeling is het verrichten van prostaatbiopten in een MRI-scanner. FDG-PET-scans hebben een relatief lage accuratesse voor het lokaliseren van prostaatkanker. Gebruik van 11C-choline als tracer verhoogd deze accuratesse enigszins. Vervolgens werd een protocol voor het optimaal toepassen van radiologische beeldvorming gepresenteerd. Vergelijking van dit schema met de richtlijnen van de Europese en Amerikaanse urologieverenigingen toonde dat MRI hierin niet genoemd werd voor prostaatkanker lokalisatie.

In **Hoofdstuk 3** werd een systematische review van de literatuur over beeldvormingsmodaliteiten voor wat betreft stadiëring van prostaatkanker uitgevoerd. Botscintigrafie was de sensitiefste methode om botmetastasen te detecteren. MRI is echter een veelbelovende techniek voor de evaluatie van het axiale skelet, met als voordeel de mogelijke detectie van metastasen in andere organen. Voor stadiëring van lymfeklieren met CT-scan of MRI-scan is de grootte en vorm van een lymfeklier nog steeds de enige leidraad. Lymfeklierspecifieke MRI-contrastmiddelen hebben in een preklinische setting al hoge accuratesse vertoond. Hoewel TRUS een makkelijk beschikbare modaliteit is voor de bepaling van het lokale ziektestadium, bleek MRI met een endorectal spoel (ERC) een hogere accuratesse te hebben. CT-scans dienen niet gebruikt te worden voor de lokale stadiëring van prostaatkanker.

In **Hoofdstuk 4**, werd een prospectieve studie beschreven van 32 mannen met biopsie bewezen prostaatkanker die een T2-gewogen hoge-spatiële-resolutie 3T MRI met ERC ondergingen gevolgd door radicale prostatectomie. Alle beelden werden geëvalueerd door drie radiologen (twee ervaren en een derde minder ervaren radioloog) met betrekking tot de lokale ziekte-uitbreiding, d.w.z. extracapsulaire uitbreiding en zaadblaasjes invasie. Criteria welke duidden op lokaal uitgebreide kanker waren: asymmetrie van de neurovasculaire bundel, obliteratie van de rectoprostatische hoek, irregulaire bulging van de prostaatcontour,

tumor signaal intensiteit in het periprostatische vet, duidelijke extracapsulaire tumor en abnormaal asymmetrisch lage signaal intensiteit in de zaadblaasjes. Whole-mount-sectie histopathologie was de gouden standaard. De accuratesse, sensitiviteit en specificiteit van lokale stadiëring waren respectievelijk 94%, 88% en 96% voor beide ervaren radiologen, en 81%, 50%, en 92% voor de minder ervaren radioloog. Er was een substantiële overeenkomst tussen beider ervaren readers (0,42–0,79) en matige overeenkomst tussen de minder ervaren reader en de ervaren readers met betrekking tot alle criteria voor extracapsulaire uitbreiding. Twee van de drie casus met minimale extracapsulaire uitbreiding werden gedetecteerd door beide ervaren radiologen. Deze studie toonde aan dat 3T MRI met een endorectale spoel mogelijk was om prostaatkanker accuraat te stadiëren.

Hoofdstuk 5 bevatte een prospectieve studie van een ander cohort van 46 mannen met biopsie bewezen prostaatkanker die een 3T T2-gewogen MRI ondergingen met zowel een body-array coil (BAC) (voxel grootte: 0,43 x 0,43 x 4,0 mm) en een ERC (voxelgrootte: 0,26 x 0,26 x 2,5 mm) voorafgaand aan radicale prostatectomie. Vier radiologen met verschillende ervaringsniveaus evalueerden alle datasets onafhankelijk van elkaar. Tien beeldkwaliteit karakteristieken gerelateerd aan prostaatkankerlokalisatie en -stadiëring (onderscheid tussen perifere en centrale zone, zichtbaarheid van de perifere en centrale zone zelf, waarneembaarheid van de vermeende laesie, visualisatie van de interne architectuur van de centrale zone, afgrensbaarheid van het prostaatkapsel, visualisatie van de neurovasulaire bundel en de rectoprostatische hoek en de algehele beeldkwaliteit) werden gescoord op een vijfpuntsschaal. Vervolgens werd de aanwezigheid van prostaatkanker in de gehele prostaat, verdeeld in 14 segmenten, aangegeven op een vijfpuntswaarschijnlijkheidsschaal. Als laatste werd het lokale ziektestadium als orgaanbegrensd of lokaal uitgebreid aangegeven op een vijfpuntswaarschijnlijkheidsschaal. Whole-mount-sectie histopathologie was de gouden standaard. Er waren significant meer bewegingsartefacten aanwezig bij onderzoek met een ERC. Alle andere beeldkwaliteit karakteristieken verbeterden significant met een ERC. De area under the curve (AUC) voor de lokalisatie van prostaatkanker nam significant toe van 0,62 naar 0,68 met een ERC. Tevens verbeterden de AUCs voor lokale stadiëring alsook de sensitiviteit voor detectie van lokaal uitgebreide ziekte van de ervaren readers van 7% naar 73-80%, terwijl een hoge specificiteit van 97-100% werd behouden. Extracapsulaire uitbreiding tot 0,5 mm gevonden bij pathologie kon slechts met ERC beeldvorming accuraat worden gedetecteerd. Derhalve toonde deze studie aan dat beeldvorming met een endorectale spoel betere resultaten opleverde dan met slechts externe spoelen wat betreft beeldkwaliteit, prostaatkankerlokalisatie en -stadiëring.

Hoofdstuk 6 besloeg een studie van 44 opeenvolgende mannen met biopsie bewezen prostaatkanker die afzonderlijke T2-gewogen MRI-onderzoeken in drie richtingen op 3T met een BAC en een opgeblazen ERC ondergingen. Prospectief evalueerden twee ervaren readers onafhankelijk beide data sets in willekeurige volgorde. De maximale voor achterwaarts,

rechts-links en craniocaudale prostaatdiameters werden gemeten met BAC en met ERC. Vervolgens werd een contour getrokken rond de gehele prostaat en de perifere zone op elke plak. Hieruit werd het volume van de totale prostaat, perifere zone en transitie zone bepaald voor en na introductie van de ERC. Ten gevolge van de ERC veranderde de prostaatvorm significant in alle drie richtingen, met gemiddelde veranderingen in de voor achterwaartse, rechts-links en craniocaudale diameters van 15,7% (5,5 mm), 7,7% (3,5 mm) en 6,3% (2,2 mm), respectievelijk. Na introductie van de ERC nam het gemiddelde totale volume van de prostaat, de perifere zone en de transitie zone significant af met respectievelijk 17,9% (8,3 cm^3), 21,6% (4,8 cm^3) en 14,2% (3,4 cm^3). De gemiddelde voor achterwaartse diameter werd gereduceerd met ongeveer één-zesde en het gemiddelde totale prostaat volume nam af met circa 18%. Deze studie toonde dat de ERC significante veranderingen in de prostaat induceert welke in acht dienen te worden genomen wanneer een MRI-scan met ERC wordt gebruikt voor fusie met CT voor radiotherapie planning.

In **Hoofdstuk 7** werd een nieuwe ^{1}H-MRSI techniek op 3T met gebruikmaking van alleen externe spoelen beschreven en toegepast in zowel de prostaat als een vergrote lymfeklier. Een 77-jarige man onderging oorspronkelijk externe radiotherapie voor een T3bN0M0 prostaatkanker. Meer dan twee jaar hierna onderging hij nogmaals een MRI-scan vanwege een stijgend PSA-niveau. Driedimensionale ^{1}H-MRSI middels een combinatie van externe oppervlaktespoelen (TR/TE: 750/145 ms; acquisitie bandbreedte: 1250 Hz; 512 spectrale data punten; FOV: 84 x 70 x 70; matrix grootte: 12 x 10 x 10; aantal gewogen gemiddelden: 6; 7 saturatie banden; voxel grootte: 7 x 7 x 7 mm^3) toonde hoge choline niveaus in de gehele prostaat, duidend op recidief ziekte. Tevens werd een enkele vergrote lymfeklier in het kleine bekken waargenomen. Een single voxel echo time averaged point resolved spectroscopie sequentie met het voxel gepositioneerd in de lymfeklier werd uitgevoerd (TR 1500 ms, TE 136 tot 272, 256 averages, voxel grootte: 15 x 17 x 13 mm^3) en toonde een choline piek in het spectrum. Om de lokatie van de choline in de lymfeklier te valideren werd een 3-dimensionale ^{1}H-MRSI meting verricht (TR/TE: 1500/100 ms; FOV: 100 x 100 x 100 mm^3; matrix grootte: 10 x 10 x 10) met dual frequency selectieve water- en vetonderdrukking waarbij het volume van interesse de vergrote lymfeklier en omgevend vetweefsel was. Deze toonde de aanwezigheid van choline in slechts de lymfeklier. Histopathologie werd verkregen uit zowel de prostaat als de lymfeklier en toonde in beide de aanwezigheid van prostaatkanker. Hiermee beschreef deze studie als eerste ^{1}H-MRSI met alleen externe spoelen bij 3T in zowel de prostaat als een vergrote intra-abdominale lymfeklier.

Hoofdstuk 8 toonde de mogelijkheid en de accuratesse van het lokaliseren van prostaatkanker met 3T 3D-^{1}H-MRSI met alleen radiofrequentie oppervlakte spoelen in een cohort van 45 mannen met biopsie bewezen prostaatkanker die vervolgens een radicale prostatectomie ondergingen. Een 3D water- en vetonderdrukte point-resolved spectroscopy pulse sequence werd uitgevoerd op de gehele prostaat (TR/TE: 750/145 ms; acquisitie bandbreedte: 1250

Hz; 512 spectrale data punten; voxel grootte: 7 x 7 x 7 mm^3). Gebaseerd op de prostatectomie specimina en geblindeerd voor de spectra, werden per patiënt 1-4 voxels op de 3D-^{1}H-MRSI gematched en geclassificeerd voor gezonde perifere zone, transitiezone, peri-urethraal weefsel en kankerweefsel. Kankervoxels werden geclassificeerd naar kankergrootte en zekerheid van matching van 3D-^{1}H-MRSI met histopathologische bevindingen. Na visuele inspectie van geautomatiseerde fitting van geclassificeerde voxels werden de choline plus creatine-gedeeld door citraat (Cho+ Cr/Cit) ratio's berekend voor alle weefsels. Mediaan kon 82% van de geclassificeerde voxels per patiënt worden gebruikt voor de analyse. De gemiddelde Cho+Cr/Cit ratio's voor gezond weefsel waren 0,22 voor perifere zone, 0,34 voor de transitiezone en 0,36 voor peri-urethraal weefsel; alle verschilden significant met dat van kanker (1,3). De AUC voor het onderscheid tussen waarschijnlijk en zeker kankerweefsel en gezond weefsel voor de perifere zone (0,84) was significant hoger dan dat van de transitiezone (0,69). Derhalve toonde deze studie aan dat 3T 3D-^{1}H-MRSI met alleen externe spoelen mogelijk was en hoge accuratesse had om kankerweefsel te onderscheiden van gezond prostaatweefsel.

In **Hoofdstuk 9** ondergingen 18 mannen met biopsie bewezen prostaatkanker een 3T 3D-^{1}H-MRSI-onderzoek van de prostaat zowel zonder als met een ERC voorafgaand aan radicale prostatectomie. De voxelresolutie met een BAC en een ERC waren 7 x 7 x 7 mm en 6 x 6 x 6 mm, respectievelijk (voor beide waren de scanparameters TR/TE: 750/145 ms; acquisitie bandbreedte: 1250 Hz; totale scantijd: 9 minuten). Semi-automatische voxel postprocessing resulteerde in een Cho+Cr/Cit ratio voor elk voxel. Iedere prostaat werd verdeeld in 14 gebieden van interesse (ROI's). Elk van de vier readers met verschillende ervaringsniveaus scoorden alle beeldensets apart en bepaalden de aanwezigheid van kanker op basis van een vooraf vastgestelde afkapwaarden van de ratio op een vijfpuntsschaal voor elk segment. Whole-mount-sectie histopathologie was de gouden standaard. Significant meer ROI's waren niet te beoordelen bij ^{1}H-MRSI zonder een ERC vergeleken met ^{1}H-MRSI met een ERC. Voor de ervaren readers had ^{1}H-MRSI met een ERC een hoge specificiteit (82-92%) maar een lage sensitiviteit (20-57%). Voor de onervaren reader had ERC ^{1}H-MRSI een hoge sensitiviteit (80%) maar een lage specificiteit (34%). Voor alle readers waren de negatief voorspellende waarden hoog (82-89%) en de positief voorspellende waarden laag (20-45%), zowel voor beeldvorming zonder en met een ERC. Prostaatkankerlokalisatie met een ERC had een significant hogere AUC (0,68) dan beeldvorming zonder een ERC (0,63). Hiermee werd aangetoond dat gebruik van een ERC bij 3T ^{1}H-MRSI de lokalisatie van prostaatkanker significant verbeterde.

Hoofdstuk 10 bevat een hoofdstuk van de landelijke CBO-richtlijn Prostaatcarcinoom 2007 met betrekking tot het gebruik van beeldvorming bij prostaatkankerdiagnostiek. De lokalisatie van prostaatkanker met MRI werd als significant beter gezien vergeleken met rectaal toucher en biopsie. Er werd geadviseerd een MRI-scan met ERC te verrichten bij

patiënten met een hoog risico op prostaatkanker na negatieve TRUS-biopsie voorafgaand aan verdere biopten. 3T ERC verbetert de sensitiviteit van de lokale stadiëring vergeleken met 1.5T. De suboptimale beschikbaarheid van ERC MRI in Nederland was een reden van zorg. Voor de identificatie van de exacte lokalisatie van kanker in de prostaat voor radiotherapie werd MRI aangewezen als de modaliteit van keuze.

CONCLUSIES

De rol van MRI bij de initiële diagnose en lokale stadiëring van prostaatkanker neemt steeds verder toe. Door het gebruik van MRI-technieken kan men betere *personalized medicine* toepassen en vervolgens elke prostaatkankerpatiënt zijn individuele behandelplan toewijzen.

Er werd een overzicht van de huidige MRI-technieken en beschikbare literatuur gegeven. Vervolgens werden de mogelijkheden van prostaat MRI bij 3T met een endorectale spoel onderzocht. Een vroege studie toonde de mogelijkheid van het accuraat bepalen van het lokale ziektestadium middels een endorectal spoel bij gebruikmaking van vooraf gedefinieerde criteria voor extraprostatische uitbreiding. Hiermee werden zowel een hoge sensitiviteit als specificiteit behaald. Een directe vergelijking tussen beeldvorming zonder en met een endorectale spoel bij 3T toonde een significant hogere accuratesse van endorectale spoel beeldvorming bij het lokaliseren van prostaatkanker en het bepalen van het lokale ziektestadium. Minimale kapselpenetratie kon slecht worden gedetecteerd met beeldvorming met een endorectale spoel.

Beeldvorming zonder en met een endorectale spoel bij 3T liet zien dat het gebruik van een endorectale spoel de prostaatvorm significant veranderde, met name de voor-achterwaartse diameter, alsook het prostaatvolume. Hiermee werd aangetoond dat het gebruik van de endorectale spoel consequenties heeft voor de planning van radiotherapie op basis van deze MRI-beelden.

Met histopathologische bevestiging werd aangetoond dat ^{1}H-MRSI bij 3T met alleen externe spoelen mogelijk was. In een casus reportage werd de mogelijkheid van prostaatkankerdetectie ^{1}H-MRSI om in zowel de prostaat als in een vergrote metastatische lymfeklier in het kleine bekken bewezen. Vervolgens werd in een patiëntencohort aangetoond dat deze techniek een hoge accuratesse had voor het onderscheiden van prostaatkanker van gezond prostaatweefsel. Tevens werd in een patiëntencohort gedemonstreerd dat ^{1}H-MRSI met een endorectale spoel de accuratesse van de prostaatkankerlokalisatie significant verbeterde.

De hierboven vastgestelde toegenomen rol van MRI bij prostaatkankerdiagnostiek werd gereflecteerd in een aantal aanbevelingen in de CBO-richtlijn Prostaatcarcinoom uit 2007.

Aldus werd in dit proefschrift aangetoond dat het gebruik van een endorectale spoel bij een veldsterkte van 3T mogelijk was en dat dit een significante verbetering gaf van de prostaatkankerlokalisatie en de lokale stadiëring. De veranderingen van de prostaatvorm door het gebruik van de spoel zijn van belang voor de exacte planning van radiotherapie op basis van deze scans. Hoewel gebruik van ^{1}H-MRSI bij 3T met alleen externe spoelen mogelijk is, wordt de lokalisatie accuratesse significant verbeterd door het gebruik van de endorectale spoel.

CHAPTER 12

Discussion

The use of the endorectal coil at 3T has been a widely debated subject due its many advantages as well as disadvantages.

A drawback of the use of an endorectal coil is the more invasive nature of the examination since one introduces a foreign object into a body cavity, causing at least some discomfort to the patient. In a number of countries, this action in male patients is deemed inapropriate, increasing the resistance to using the coil. When applied, contraction of the sphincter musculature may cause some movement artifacts in the images. This may be counteracted by applying bowel motion suppression drugs. Application of the coil will also lengthen the examination time due to the time needed for its introduction and the necessity for checking its correct position prior to starting the actual exam. For hospital managers this may be their argument against its usage as this will descrease the number of patients that can be scanned within the finitesimal scanner time. For radiation oncologists the treatment planning and the actual treatment itself is normally performed without an endorectal balloon. As outlined in this thesis, the prostate shape changes markedly with the introduction of the endorectal coil. Thus, alignment of the endorectal MR imaging scan performed with an endorectal coil and the planning CT scan without an endorectal balloon may be troublesome regarding the delineation of both the prostate as well as the delineation of the prostate cancer focus.

However, on the opposite, this thesis has established a number of advantages of using the endorectal coil. The main advantage is the higher resolution that is obtainable with the coil. For patients that are enlisted for radical prostatectomy, it was proven to be more sensitive in detecting both the presence as well as the exact location at which capsular penetration was observed. In case of extensive extraprostatic spread, the patient may chose to change the treatment strategy from surgery to radiation treatment. If extracapsular extension is small or if assessed as possibly present, the urologist may be forewarned to obtaining negative surgical margins at the exact site of perceived capsular penetration by resecting with a wider margin or sacrificing the neurovascular bundle on one side of the prostate. The higher resolution may also allow for more accurate local primary or salvage possibilities as an optimal delineation of the cancer focus allows for smaller target volumes, which is particularly helpful in patients that have received prior radiation treatment.

For MR spectroscopic imaging, it was demonstrated that imaging using solely external coil was feasible in both an enlarged lymph node as well as within the prostate itself. Since this part of the MR examination consumes a relatively long part of the exam, it could be argued that this may be performed without an endorectal coil. However, the increased localization accuracy with an endorectal coil may provide more certain cancer localization, particularly in establishing the site of the most aggressive cancer focus.

Lastly, it may be argued that for the special skills for and knowledge of endorectal coil imaging, its use could be restricted to only a number of centers. However, in displaying greater detail, use of the coil may very well aid less experienced readers.

Future clinical use of MR magnets with field strengths higher than 3T may possibly render details which possibly could compete with the use of the endorectal coil. However, more work is needed before this can be used in a clinical setting.

PhD portfolio

PHD PORTFOLIO – SUMMARY OF PHD TRAINING AND PRESENTATIONS

In-depth courses

- Abdominal Radiology Course 2006 to 2010
- ISMRM Weekend Educational Course 2005 to 2007, 2012
- ESMRMB Basic Course on MRI 2004

Guideline and consensus meetings participations

2009 Royal College of Surgeons' European Consensus Meeting: Creation of a Scoring System for the Interpretation of Diagnostic Prostate MRI (London, UK)

2006 Dutch Guideline Committee on Prostate Cancer (Utrecht, NL)

Invited lectures

2008 Dutch Toshiba User Dag, "Contrast-echografie van de prostaat" (Zoetermeer, NL)

2008 GlaxoSmithKline "State of the art Urology" symposium: Systematische versus contrast-geleide echografische prostaatbiopsie (Vught, NL)

2007 GlaxoSmithKline "State of the art Urology" symposium: Mogelijkheden van MRI bij prostaatkanker (Garderen, NL)

2007 GlaxoSmithKline "State of the art Urology" symposium: Systematische versus contrast-geleide echografische prostaatbiopsie (Apeldoorn, NL)

2005 "New Developments in Prostate Cancer MR". Diagnostik des Prostatakarzinoms: Expertenmeeting Aachen (Aachen, Germany)

2005 Multidisciplinary symposium: Prostate cancer. "Prostate ultrasound – for urologists only?" ICIS 2005 (Amsterdam, NL)

2005 "Echografie van de prostaat met contrast". Symposium echografie, Nederlandse Vereniging Medische Beeldvorming en Radiotherapie (Ede, NL)

Attended the following international conferences, at which the author gave over 25 presentations and workshops:

Abdominal radiology course (ARC): 2006-2010, 2013
European Association of Urology (EAU): 2007
European Congress of Radiology (ECR): 2005-2008
European Multidisciplinary Meeting on Urological Cancers (EMUC): 2007
European Society of Urogenital Radiology (ESUR): 2005-2008
International Cancer Imaging Society (ICIS): 2005
International Society of MR in Medicine (ISMRM): 2005-2009, 2012, 2014
Radiological Society of North America (RSNA): 2005-2010, 2012

Dankwoord

Promotores

Prof. dr. J.O. Barentsz – Beste Jelle, het was een voorrecht om al die jaren met je te hebben mogen werken. Jouw voorliefde voor de oncologische radiologie is mij altijd een voorbeeld geweest. Bedankt dat ik op zoveel (prachtige) plekken op de wereld onze onderzoeksresultaten voor het voetlicht mocht brengen. Dank voor de energie die je al die jaren richting mij hebt uitgestraald, ook in tijden dat het wat minder ging.

Prof. dr. J.A. Witjes – Beste Fred, met name in de beginjaren hebben we wekelijks rond de tafel gezeten. Op jouw afdeling heb ik de kunst van de prostaatechografie mogen leren. Je bent recht door zee en weet op directe doch uiterst charmante wijze snel de kern van de zaak te becommentariëren. Bedankt dat je altijd op de bal en nooit op de man speelt. Dank voor je immer kritische blik.

Co-promotores

Dr. J.J. Fütterer – Beste Jurgen, ik mocht jouw plaats innemen in de prostaatwetenschap toen jij in opleiding ging. We bleken meer dan alleen krullen en een bril gemeenschappelijk te hebben. Jouw onuitputtelijk drive en uitmuntende onderzoekskwaliteiten hebben mij altijd tot het uiterste gestimuleerd. Je 'snelle Jurgen' techniek was een prima combinatie met mijn aanpak, getuige ook onze vele publicaties samen. Onze drang het onderzoek te presenteren (lees ook: reislust) bracht ons naar de meest uiteenlopende plekken op deze aardbol. Gebleken is dat over goede wijn en steak het makkelijk vriendschap sluiten is. Dank voor je steun gedurende al die jaren.

Dr. T.W.J. Scheenen – Beste Tom, vele uren hebben we samen patiënten gescand, eerst in het F.C. Donders Centrum en later op P-Oost. Deze veelal avondlijke uren in een verlaten pand schepten een hechte band. Het hangfauteuil dat zo lang op je kamer stond was een heerlijke plek om even bij te praten over van alles en nog wat. Vaak ben ik bij je langsgekomen als ik weer eens iets niet snapte op MRI-technisch gebied. Jouw wetenschappelijke achtergrond was een welkome aanvulling op mijn wat meer klinisch georiënteerde blik op onderzoek. Als een paper langs jou was gekomen, wist je dat het goed zat. Zie dat maar als het grootste compliment dat ik je kan geven. Dank voor je open en nietsontziende kritiek.

Paranimfen

Drs. D.R. Kool en drs. H. Toonen – Beste Digna en Hanneke, gedurende onze Radboudjaren hebben we door dik en dun een mooie vriendschap opgebouwd. Digna, je bent niet alleen

de beste opleider die ik heb gehad maar ook een geweldig mens. Hanneke, de ontelbare uren die we samen doorbrachten op het werk en in de diverse kroegen en eetcafé's van Nijmegen waren onbeschrijflijk waardevol. Ik ben trots dat jullie mijn paranimfen willen zijn. Dank voor jullie vriendschap.

Radiologie

Prof. dr. A. Heerschap – Beste Arend, voor mij was jij op de afdeling samen met Tom degene die werkelijk wist hoe een MRI-scan nou echt werkte. In onze papers samen heb je elke keer dat ik de voorlopige versie opstuurde multiple kritische noten en punten op de i geplaatst, waardoor het telkens toch niet de laatste versie werd. Je woorden "je moet alleen iets insturen waar je trots op kunt zijn", zijn mij tot op de dag van vandaag bijgebleven. Dank voor je kennis en oprechtheid.
Dr. T. Hambrock – Beste Thomas, als mijn officieuze opvolger heb ik je mogen zien groeien in het onderzoek. Dank voor je hulp bij het scannen en scoren van patiënten. Onze tijd samen op de kamer was plezierig. Het feit dat de rommel bij jou op het bureau toch altijd nog groter was dan op die van mij, was altijd erg geruststellend. Bedankt voor je tomeloze inzet.
Ondersteuning – Vanuit het secretariaat wil ik alle secretaresses en met name Claudia Nikiforakis-Pronk, Marijke Hogenkamp en Manita Verhoeven bedanken voor al die kleine zaken die jullie hebben opgelost. Al het kleine bij elkaar was desalniettemin een grote kluif. Bedankt voor jullie hulp bij het inplannen van patiënten!
Laborantenteam (met name, maar niet uitsluitend, Miranda Fütterer, Richard en Jolanda) – Eerst leerde ik een aantal van jullie kennen op het F.C. Donderscentrum tijdens de klinische delen van het programma aldaar. Daarna op P-Oost en tijdens de opleiding heb ik jullie nog beter leren kennen. Zonder jullie kunnen wij het niet. Prachtige apparatuur is één ding, schitterende mensen zijn van groter belang. Dank voor jullie hulp!

Overige disciplines

Prof. dr. L.A.L.M. Kiemeney – Beste Bart, bij mijn allereerste review schreef je (toen alle andere auteurs het stuk al hadden goedgekeurd) na het doorgenomen te hebben op het titelblad: "je methode klopt niet". Ik wist: dit is de juiste man! Sindsdien heb je meegewerkt en -gedacht aan meerdere van mijn artikelen. Ik heb je leren kennen als een bijzonder intelligent persoon en iemand op wie je kunt bouwen. Dank voor je nimmer aflatende, opbouwend kritische blik!
Drs. B.C. Knipscheer – Beste Ben, bedankt dat je de waarde van ons onderzoek voor jouw patiënten met betrekking tot de laparoscopische radicale prostatectomie zo doortastend hebt ingezien.

Dr. C.A. Hulsbergen-v.d. Kaa – Beste Christina, zo vaak heb ik je te weinig genoemd en bedankt voor topkwaliteit waarop jij de prostatectomiepreparaten analyseerde en ons visueel terugrapporteerde. Deze zijn van wereldklasse! Onze studies hadden zonder jou niet kunnen plaatsvinden. Dank voor je professionaliteit!
Dr. E.J.N.Th. van Lin – Beste Emile, mede dankzij jouw tomeloze energie hebben we samen twee artikelen geschreven. Dank voor je eindeloze inzet!

Life

Mijn ouders – Bedankt dat jullie mij altijd gesteund hebben. Zonder jullie stond ik hier niet. Dank voor alle liefde!

Lieve Kim – Tijdens de mooiste periode van mijn assistentschap mocht ik jou ontmoeten. Het bloeide uit tot een schitterend samen zijn. Bedankt voor al je steun, op zoveel vlakken!

List of publications

Full papers

Fütterer JJ, **Heijmink SWTPJ**, Scheenen TWJ, Jager GJ, Hulsbergen-Van de Kaa CA, Witjes JA, Barentsz JO. Local staging of prostate cancer using 3T endorectal coil MR imaging – Early Experience. *Radiology 2006*;238(1):184-191**.**

Heijmink SWTPJ, Moerkerk H van, Kiemeney LALM, Witjes JA, Frauscher F, Barentsz JO. A comparison of the diagnostic performance of systematic versus ultrasound-guided biopsies of prostate cancer. Eur Radiol 2006;16(4):927-938.

Lin ENJTh van, Fütterer JJ, **Heijmink SWTPJ**, Vight LP van der, Hoffmann AL, Kollenburg P van, Huisman HJ, Scheenen TWJ, Witjes JA, Leer JW, Barentsz JO, Visser AG. IMRT Boost Dose Planning on Dominant Intra-Prostatic Lesions: Gold Marker Based 3D Fusion of CT with Dynamic Contrast-Enhanced and 1H-Spectroscopic MR Imaging. *Int J Radiat Oncol Biol Phys 2006*;65(1):291-303.

Fütterer JJ, **Heijmink SWTPJ**, Scheenen TWJ, Veltman J, Huisman HJ, Vos P, Hulsbergen-Van de Kaa CA, Witjes JA, Krabbe PFM, Heerschap A, Barentsz JO. Prostate cancer localization with dynamic contrast-enhanced MR imaging and proton MR spectroscopic imaging. *Radiology 2006*;241(2): 449–458.

Moerkerk H van, **Heijmink SWTPJ**, Barentsz JO, Witjes JA. Computerized 3D localization of prostate cancer using contrast-enhanced power Doppler and clustering analysis. *Eur Urol 2006*;50(4):762-769.

Fütterer JJ, Scheenen TWJ, **Heijmink SWTPJ**, Hulsbergen-Van de Kaa CA, Heerschap A, Barentsz JO. Standardized Threshold Approach using Three-Dimensional Proton MR Spectroscopic Imaging in Prostate Cancer Localization of the Entire Prostate. *Invest Radiol 2007*;42(2):116-122.

Heijmink SWTPJ, Fütterer JJ, Hambrock T, Takahashi S, Scheenen TWJ, Huisman HJ, Hulsbergen-Van de Kaa CA, Knipscheer BC, Kiemeney LALM, Witjes JA, Barentsz JO. Body Array versus Endorectal Coil MR Imaging of Prostate Cancer at 3 Tesla: Comparison of Image Quality, Localization, and Staging Performance with Whole-Mount Section Histopathology. *Radiology 2007*;244(1):184-195.

Heijmink SWTPJ, Scheenen TWJ, Fütterer JJ, Klomp DW, Heesakkers RAM, Hulsbergen-van de Kaa CA, Lin ENThJ van, Heerschap A, Barentsz JO. Prostate and Lymph Node MR Spectroscopic Imaging with External Array Coils at 3T to Detect Recurrent Prostate Cancer after Radiation Therapy: a Technical Note. *Invest Radiol 2007*;42(6)420-7.

Heijmink SWTPJ, Barentsz JO. Contrast-enhanced versus Systematic Transrectal Ultrasound-guided Prostate Cancer Detection: an Overview of Techniques and a Systematic Review. *Eur J Radiol 2007*;63(3):310-6.

Scheenen TWJ, **Heijmink SWTPJ**, Roell S, Hulsbergen-Van de Kaa CA, Knipscheer BC, Witjes JA, Barentsz JO, Heerschap A. Fast non-invasive 3D proton-MR Spectroscopic Imaging of the Human Prostate at 3 Tesla without an Endorectal Coil. *Radiology 2007*;245(2):507-16.

Fütterer JJ, **Heijmink SWTPJ**, Spermon JR. Imaging the Male Reproductive Tract, Current Trends and Future Directions. *Radiol Clin N Am* 2008;46(1):133-47.

Fütterer JJ, Barentsz JO, **Heijmink SWTPJ**.Value of 3-T magnetic resonance imaging in local staging of prostate cancer. *Top Magn Reson Imaging* 2008;19(6):285-9.

Heijmink SWTPJ, Scheenen TWJ, Lin EJNTh van, Visser AG, Kiemeney LALM, Witjes JA, Barentsz JO. Changes in Prostate Shape and Volume and Their Implications for Radiation Therapy after the Introduction of an Endorectal Balloon as Determined by MR Imaging at 3 Tesla. *Int J Radiat Oncol Biol Phys 2009*; 73(5):1446-53.

Fütterer JJ, Barentsz JO, **Heijmink SWTPJ**. Imaging modalities for prostate cancer. *Expert Rev Anticancer Ther 2009*;9(7):923-37.

Dickinson L, Ahmed HU, Allen C, Barentsz JO, Carey B, Fütterer JJ, **Heijmink SW**, Hoskin PJ, Kirkham A, Padhani AR, Persad R, Puech P, Punwani S, Sohaib AS, Tombal B, Villers A, Meulen J van der, Emberton M. Magnetic Resonance Imaging for the Detection, Localisation, and Characterisation of Prostate Cancer: Recommendations from a European Consensus Meeting. *Eur Urol* 2011;59(4):477-494.

Yakar D, **Heijmink SWTPJ**, Hulsbergen-van de Kaa CA, Huisman HJ, Barentsz JO, Fütterer JJ, Scheenen TWJ. Initial Results of 3-Dimensional 1H-Magnetic Resonance Spectroscopic Imaging in the Localization of Prostate Cancer at 3 Tesla: Should We Use an Endorectal Coil? *Invest Radiol* 2011;46(5):301-6.

Heijmink SWTPJ, Fütterer JJ, Strum SS, Oyen WJG, Frauscher F, Witjes JA, Barentsz JO. State-of-the-art uroradiologic imaging in the diagnosis of prostate cancer. *Acta Oncologica* 2011; 50(S1):25-38.

Prostate cancer: multiparametric MR imaging for detection, localization, and staging. Hoeks CM, Barentsz JO, Hambrock T, Yakar D, Somford DM, **Heijmink SW**, Scheenen TW, Vos PC, Huisman H, van Oort IM, Witjes JA, Heerschap A, Fütterer JJ. **Radiology** 2011;261(1):46-66.

Neue Ultraschalltechnologien für die Diagnostik des Prostatakarzinoms. [New ultrasound technologies for the diagnostics of prostate cancer]. De Zordo T, Ladurner M, Horninger W, Heijmink SW, Jaschke W, Aigner F, Frauscher F. **Radiologe** 2011;51(11):938, 940-6.

Scoring systems used for the interpretation and reporting of multiparametric MRI for prostate cancer detection, localization, and characterization: Could standardization lead to improved utilization of imaging within the diagnostic pathway? Dickinson L, Ahmed HU, Allen C, Barentsz JO, Carey B, Futterer JJ, **Heijmink SW**, Hoskin P, Kirkham AP, Padhani AR, Persad R, Puech P, Punwani S, Sohaib A, Tombal B, Villers A, Emberton M. *J Magn Reson Imaging* 2013;37(1):48-58.

Clinical applications of multiparametric MRI within the prostate cancer diagnostic pathway. Dickinson L, Ahmed HU, Allen C, Barentsz JO, Carey B, Futterer JJ, **Heijmink SW**, Hoskin P, Kirkham AP, Padhani AR, Raj Persad ChM, van der Meulen J, Villers A, Emberton M; PREDICT Consensus Panel. *Urol Oncol* 2013;31(3):281-4.

MRI en active surveillance voor laagrisicoprostaatkanker. Van den Bergh RCN, Meijer RP, **Heijmink SW**, Van der Poel HG. *Tijdschrift voor urologie* 2014;4(8):185-91.

Prostate tumor delineation using multiparametric magnetic resonance imaging: inter-observer variability and pathology validation. Steenbergen P, Haustermans K, Lerut E, Oyen R, De Wever L, Berg L van den, Kerkmeijer LGW, Pameijer FA, Veldhuis WB, Van der Voort van Zyp JRN, Pos FJ, **Heijmink SW**, Kalisvaart R, Teertstra HJ, Dinh CV, Ghobadi G, Van der Heide UA. *Radiother Oncol 2015*; in press; http://dx.doi.org/10.1016/j.radonc.2015.04.012.

Book chapters

First author of the chapter on prostatitis and second author of chapter on prostate cancer in “Encyclopedic Reference of Imaging”, Editor-in-Chief: Prof. A. L. Baert. Springer-Verlag: Published.

Fütterer JJ, **Heijmink SWTPJ**, Jager GJ. Chapter 5.2 Local Staging of Prostate Cancer. Editor: Prof. J.O. Barentsz. Springer Verlag, In press.

Heijmink SWTPJ, Jong IJ de, Hulsbergen-v.d. Kaa CA, Barentsz JO. Dutch guidelines on prostate cancer: Diagnosis and staging by radiologic imaging. Development of guidelines on prostate cancer, Comprehensive Cancer Centres (IKC), The Netherlands. Approved Guideline, published 2007.

Heijmink SWTPJ, Fütterer JJ. Chapter 16.10 "CT en MRI". In: Handboek prostaataandoeningen. Editors: Boon TA, Bosch JLHR, Poppel HPAM van, Witjes JA. Publisher: De Tijdstroom. Published, March 2009.

Fütterer JJ, **Heijmink SWTPJ**. Book chapter Imaging Urological Cancers. In press.

Heijmink SWTPJ, Barentsz JO. Co-authors of the book chapter "Beeldvorming oncologie". Leerboek Oncologie. Editors: Van de Velde, Kieken, Vermorken.

Poster publications

(Co-)author of 13 posters presented at various international conferences.

Published abstracts

(Co-)author of over 40 abstracts presented at numerous international conferences.

Curriculum Vitae

Stijn Wilhelmus Theodorus Petrus Johannes Heijmink werd op 15 april 1978 geboren in het Academisch Ziekenhuis te Nijmegen. In 1996 deed hij eindexamen aan het Stedelijk Gymnasium Nijmegen en begon hij zijn studie aan de Katholieke Universiteit Nijmegen. Achtereenvolgens behaalde hij aldaar in 1997 de propedeuse Biomedische Gezondheidswetenschappen cum laude, in 1998 de propedeuse Geneeskunde cum laude, in 2001 het doctoraalexamen Geneeskunde cum laude en na de coschappen doorlopen te hebben in 2003 het artsexamen. De bezielde passie van het overbrengen van kennis in de beeldvorming op andere clinici waarmee hij bij de afdelingsleiding van de afdeling radiologie tijdens zijn coschappen in aanraking kwam, deed hem besluiten zich te specialiseren in dit specialisme. Allereerst begon hij in 2003 als arts-onderzoeker bij prof. dr. Barentsz op de afdeling radiologie van het UMC St. Radboud met onderzoek naar beeldvorming van prostaatkanker middels MRI, waarvan het voorliggende proefschrift het resultaat werd. In 2005 begon hij op diezelfde afdeling aan de opleiding tot radioloog, welke hij in 2011 op de afdeling radiologie van ziekenhuis Rijnstate te Arnhem afsloot. Sindsdien is hij werkzaam als radioloog in het Antoni van Leeuwenhoek - Nederlands Kanker Instituut te Amsterdam met als speciaal aandachtsgebied oncologische beeldvorming middels MRI, in het bijzonder van prostaatkanker.

ISBN/EAN: 978-90-9029032-4